INSTITUTE OF PHOTONIC SCIENCES (ICFO)

Correlates of cerebral vasoreactivity measured by non-invasive diffuse optical measurements as biomarkers of brain injury risk

by

Clara Gregori Pla

Supervisor: Prof. Turgut Durduran

A thesis submitted in partial fulfillment for the degree of Doctor of Philosophy

Castelldefels, January 2019

"-Would you tell me, please, which way I ought to go from here?-, said Alice.
-That depends a good deal on where you want to get to- said the Cat.
-I don't much care where-, said Alice.
-Then it doesn't matter which way you go-, said the Cat.
-so long as I get SOMEWHERE,- Alice added as an explanation.
-Oh, you're sure to do that-, said the Cat, -if you only walk long enough.-"

Lewis Carroll (from *Alice in Wonderland*)

Dedicated to Nu, mare and pare

Abstract

I have used and developed a practical new platform in the clinics for the non-invasive estimation of cerebral hemodynamics. The platform combines two diffuse optical techniques: near-infrared spectroscopy and diffuse correlation spectroscopy.

To study patients at a high risk of cerebrovascular accidents, and those who have recently suffered an ischemic stroke, several protocols were devised and carried out. This set of multi-disciplinary studies was performed in close collaboration with the Stroke Unit and the Sleep Unit at Hospital de la Santa Creu i Sant Pau (Barcelona, Spain) with the ultimate goal to identify new biomarkers for the assessment of cerebral autoregulation and cerebral vasoreactivity, and, ultimately, cerebral well-being.

The bulk of the studies on these patients focused on the investigation of microvascular cerebral physiology in response to a non-invasive and benign challenge, without the need of patient collaboration nor any additional equipment. This challenge involved an alteration of the patient head-of-bed positioning. Interestingly, the head-of-bed challenge with the measurement of microvascular cerebral blood flow has been shown as a potential protocol to tell us about the status of cerebral autoregulation in these patients. This in turn was shown to track impairments over time, and the patients' response to treatments, and to predict long-term outcome.

Overall, this thesis pushes the limits of the clinical translation of hybrid diffuse optics, paving the way for new clinical applications at the point-of-care and in the neurocritical care.

Resum

En aquest treball he utilitzat i desenvolupat una nova plataforma d'ús clínic per a l'estimació no invasiva de l'hemodinàmica de teixits que combina dues tècniques híbrides d'òptica difusa: l'espectroscòpia de l'infraroig proper i l'espectroscòpia de correlació difusa.

S'han ideat i dut a terme diferents protocols per estudiar pacients amb un alt risc d'accidents cerebrovasculars i pacients que han patit recentment un accident cerebrovascular isquèmic. Aquest conjunt d'estudis multidisciplinars s'han pogut dur a terme gràcies a l'estreta col·laboració amb la Unitat d'Ictus i la Unitat de Trastorns Respiratoris del Son de l'Hospital de la Santa Creu i Sant Pau (Barcelona, Espanya), amb la finalitat d'identificar nous biomarcadors per a l'avaluació del funcionament de l'autoregulació cerebral i la vasorreactivitat cerebral, i globalment, del bon funcionament cerebral.

Aquests estudis s'han centrat en la investigació de la fisiologia cerebral microvascular en resposta a un estímul no invasiu, sense la necessitat de la col·laboració dels pacients, ni tampoc de cap material addicional; aquest estímul és un simple canvi de posició de la capçalera del llit. Curiosament, el dit canvi de posició de la capçalera del llit, juntament amb la mesura del flux sanguini cerebral de la microvasculatura, han demostrat ser un protocol amb potencial per aportar informació sobre l'estat de l'autoregulació cerebral. A més a més, a través d'aquest protocol s'han pogut estudiar l'estat del benestar cerebral al llarg del temps, els canvis deguts possiblement al tractament, així com les correlacions amb el pronòstic d'aquests pacients.

En resum, aquesta tesi amplia els límits de l'òptica difusa, obrint camí a noves aplicacions clíniques en els hospitals.

Acknowledgements

Of course, this thesis would not have been possible with the endless help of Professor Turgut Durduran. His advice, constructive criticism and a wise perceptive to see beyond the results has made me grow up enormously as a researcher. I really appreciate all the advices received.

Translational research requires open collaboration. This work would not have been possible without the collaborators at Hospital de la Santa Creu i Sant Pau, your help and fruitful discussions have been essential for building up our little contribution to science. Thanks Raquel, Mercè, Pol, Joan, Ana, and others. Also, thanks Isabel, from Centre de Recerca Matemàtica.

It is a great pleasure for me to acknowledge all the people who have supported me with their love and helped me to get to reach the end of my PhD. Definitely my family is at the top of my list, with my sister-Always-there, my parents and Charlie.

I share the credit of my work with all my colleagues and friends in the Medical Optics group: Jordi, Johannes, Giacomo, Luca, Maria, Xavier, Claudia, Stella, Federica, Ameer, Giuseppe, Tanja, Ernesto, Miguel, Claus, Igor, Peyman, Martina, Marco, Lorenzo, Lisa, Jonas, Susanna, Víctor, Pablo and Parisa. Also, to David Busch, who made an inflexion point in my research career during his visit.

Also, I want to dedicate this work to my friends and family from Barcelona, Agramunt, and la Vall d'Àger. I do not list your names here but I am grateful to have all of you in my life.

Contents

List of Figures

List of Tables

Glossary

μ_s	Scattering Coefficient.
μ_s'	Reduced Scattering Coefficient, $\mu_s' = \mu_s(1-g)$.
φ	Scattering Angle.
μ_a	Absorption Coefficient.
α	Fraction of photon scattering events that occur from moving particles in the medium.
g	Mean Cosine of Photon Scattering.
G_1	Electric Field Temporal Autocorrelation Function.
ν	Speed of Light in Tissue or Turbid Medium.
Δ**rCBF**	Relative Cerebral Blood Flow Changes.
Δ**HR**	Heart Rate Changes.
Δ**HbO**$_2$	Oxy-Hemoglobin Concentration Changes.
Δ**Hb**	Deoxy-Hemoglobin Concentration Changes.
Δ**THC**	Total Hemoglobin Concentration Changes.
ℓ_{tr}	Transport Mean Free Path, $\ell_{tr} \approx 1/\mu_s'$.
ω	Laser/Source Modulation Frequency.
$\langle \Delta r^2(\tau) \rangle$	The mean-square displacement in time τ of the scattering particles (e.g. red blood cells).
D	Photon Diffusion Coefficient.

D_b Effective Diffusion Coefficient.

ϵ_i Extinction Coefficient.

c_i Concentration of the i^{th} chromophore.

k Complex Wave-Number of Diffuse Photon Density Waves.

n Index of Refraction.

g_1 Normalized Electric Field Temporal Autocorrelation Function.

g_2 Normalized Intensity Temporal Autocorrelation Function.

ϕ Photon Fluence Rate.

ρ Source-Detector Separation on a Plane.

R_{eff} The effective reflection coefficient to account for the index mismatch between tissue and air.

ACA Anterior Cerebral Artery.

ACZ Acetazolamide.

AHI Apnea-Hypopnea Index.

AHT Arterial Hypertension.

AIS Acute Ischemic Stroke.

ASPECTS Alberta Stroke Program Early Computed Tomography Score.

ASV Adaptive Servoventilation.

BDS Breathing Disorders.

BFI Blood Flow Index estimated by DCS (i.e., αD_b).

BHI Breath-Hold Index.

BMI Body Mass Index.

CAR Cerebral Autoregulation.

CBF Cerebral Blood Flow.

CBFV Cerebral Blood Flow Velocity.

$CMRO_2$ Cerebral Metabolic Rate of Oxygen.

CPAP Continuous Positive Air Pressure.

CPP Cerebral Perfusion Pressure.

CT Computed Tomography.

CT90 % of measured night sleep time when arterial oxygen saturation is lower than 90%.

CVR Cerebral Vasoreactivity.

CVR_i Cerebral Vasoreactivity Index.

CW NIRS-DOS Continuous-Wave Near-Infrared Spectroscopy.

DAQ Data Acquisition Card.

DCS Diffuse Correlation Spectroscopy.

ΔSpO_2 Arterial Oxygen Saturation Changes.

DLP Dyslipidemia.

DM Diabetes Mellitus.

DPDWs Diffuse Photon Density Waves.

DPF Differential Pathlength Factor.

DWS Diffusing Wave Spectroscopy.

ECG Electroencephalography.

EEG Electrocardiography.

FD NIRS-DOS Frequency-Domain Near-Infrared Spectroscopy.

Hb Deoxy-Hemoglobin Concentration.

HbO_2 Oxy-Hemoglobin Concentration.

HOB Head-of-Bed.

HR Heart Rate.

ICA Internal Carotid Artery.

LED Light-Emitting Diode.

MAP Mean Arterial Pressure.

MCA Middle Cerebral Artery.

MRI Magnetic Resonance Imaging.

mRS Modified Rankin Scale.

NIHSS National Institute of Health Stroke Scale.

NIRS-DOS Near-Infrared Diffuse Optical Spectroscopy.

OD Opical Density.

ODI4 Number of times where arterial oxygen saturation decreases 4% due to an apnea or hypopnea.

OSA Obstructive Sleep Apnea.

pCO_2 Partial Pressure of Carbon Dioxide.

PSG Polysomnography.

r_s Source Position.

rtPA Recombinant Tissue Plasminogen Activator.

S Source Term.

SpO_2 Arterial Oxygen Saturation.

StO_2 Tissue Blood Oxygen Saturation.

τ Delay Time.

TCD Transcranial Doppler Ultrasound.

THC Total Hemoglobin Concentration.

TOAST Trial of Org 10 172 in Acute Stroke Treatment.

TRS NIRS-DOS Time-Resolved Near-Infrared Spectroscopy.

TTL Transistor-Transistor Logic.

U Photon Fluence Rate; expressed in the frequency-domain.

Part I

Introduction and theoretical background

Chapter 1

Introduction

"Cogito, ergo sum/I think, therefore I am" [René Descartes (1596-1650)]. Different human civilizations have realized that the brain distinguishes the *homo sapiens* from the rest of the animal species. This complex organ not only lets us cry and laugh, but also lets us solve difficult algorithms in a unique way. Therefore, with all the passion my brain can offer, I did my best to characterize this organ by measuring cerebral hemodynamics using light.

Even though the brain is only 2% of the body weight, it stands for 20% of body metabolism and 14% of blood flow [1]. This tells us about the relevance of the proper supply of oxygen and glucose, as the nutrients to sustain this metabolic demand to this critical organ of our body. For instance, a short interruption of the cerebral blood flow (CBF) can lead to fainting, while a longer shortage may lead to more severe and deadly conditions such as ischemic stroke [2–4].

Indeed, CBF is an important biomarker about the cerebral well-being. Nowadays, different techniques are available for monitoring CBF and the state of the cerebral autoregulation (CAR; the ability to maintain a constant cerebral blood flow despite changes in cerebral perfusion pressure) and the cerebral vasoreactivity (CVR; the response to a stimulus that dilates or contracts the cerebral vasculature). However, some of them are expensive, their availability is limited in the clinics, others are invasive or require exposure to ionizing radiation [5, 6].

An optimal technique for monitoring the cerebral hemodynamics that is portable, non-invasive, continuous, able to measure at the point-of-care, and relatively inexpensive is desired and none of the potential candidates are yet clinically accepted.

Transcranial Doppler ultrasound (TCD), with the measurement of the CBF velocity, fulfills many of these requirements. However, arteries cannot be insonated in part of the population due to the skull anatomy, and the estimation of the blood flow can be erroneous due to difficulties in estimating the artery diameter [4]. In the last decade, diffuse correlation spectroscopy (DCS) has been proven to be a valid non-invasive transcranial optical method for measuring microvascular cortical CBF [5, 7]. It has been validated against other measures of CBF such as phase contrast-magnetic resonance imaging, arterial-spin labeled-magnetic resonance imaging, xenon computed-tomography, oxygen-15 water positron emission tomography, contrast-enhanced time-resolved near-infrared spectroscopy and TCD [7–15].

In this work, DCS is combined with near-infrared diffuse optical spectroscopy (NIRS-DOS), a more established technique that uses wavelength-dependent light attenuation to measure oxy-hemoglobin concentration (HbO_2), deoxy-hemoglobin concentration (Hb), total hemoglobin concentration (THC) and tissue blood oxygen saturation (StO_2). Relevantly, prior work has shown that this hybrid DCS/ NIRS-DOS optical monitor is capable of detecting cerebral hemodynamic changes [7, 16–20].

Diffuse correlation spectroscopy is sensitive to signals from the brain, but also contains scalp and skull contributions [21–23]. However, a brain-to-scalp sensitivity of 45% is found approximately, which is greater than the 10% sensitivity found by NIRS-DOS [24]. Overall, even though the measurements contain extracerebral contributions, we can say that a relevant contribution is due to the brain as shown by earlier studies [7–11, 24]. Moreover, DCS studies are mainly limited to the frontal lobes; however, they have been shown to be an important area of measurement for the questions addressed in this thesis when looking, for instance, at the CVR with other techniques [25].

It is well known that there are different control mechanisms in the reactivity of the cerebral microcirculation. The main control mechanisms of the CBF are the CBF changes due to changes on the arterial partial pressure of carbon dioxide, followed by the cerebral autoregulation mechanisms [26]. Other mechanisms that exist but that are less studied are the CBF changes due to changes on the arterial partial pressure of oxygen, and other modulating mechanisms such as neural phenomena or the effect of molecular biomarkers [27, 28]. In this thesis, the individual effect of the different CBF control mechanisms is not differentiated. Instead, the

goal of diffuse optics in these studies is to detect relative cerebral hemodynamic changes caused by different pathological phenomena (such as obstructive apneas) and challenges (such as head-of-bed position changes, acetazolamide injection and breath-hold), without going into the details of the ultimate physiological cause responsible for the changes in the cerebral hemodynamics of the individuals studied.

My PhD is motivated mainly by the application of the above-mentioned diffuse optical techniques for studies of neurovascular pathologies to obtain new information about the cerebral well-being of these patients, with the end goal of enhancing the efficiency of their management and treatments to improve the outcome. In order to do this, I have focused on the implementation of the two mentioned diffuse optical techniques, DCS and NIRS-DOS, in order to assess frontal cortical cerebral microvascular hemodynamics at the point-of-care in the clinics. In this work, these techniques have been pushed to study different protocols on patients with risk of stroke, which suffer from obstructive sleep apnea and internal carotid artery stenosis, and also patients who suffered from a stroke event. Further clarification of the different studies according to their risk of stroke is illustrated in Figure 1.1.

1.1 Goals and hypotheses

The overall theme of this thesis is the combination of diffuse optical techniques for the simultaneous, non-invasive and continuous estimation of microvascular cerebral hemodynamics in several clinical scenarios with the following goals and hypotheses:

- Goal I: Investigation of head-of-bed position changes and the associated cerebral hemodynamics response in controls and in patients with different pathologies.

  Hypotheses:

  1. The blood flow response to an orthostatic challenge in obstructive sleep apnea patients correlates to the severity of the syndrome. See Chapter 5.
     - The blood flow response to an orthostatic challenge in obstructive sleep apnea patients after long-term treatment is similar to healthy subjects.

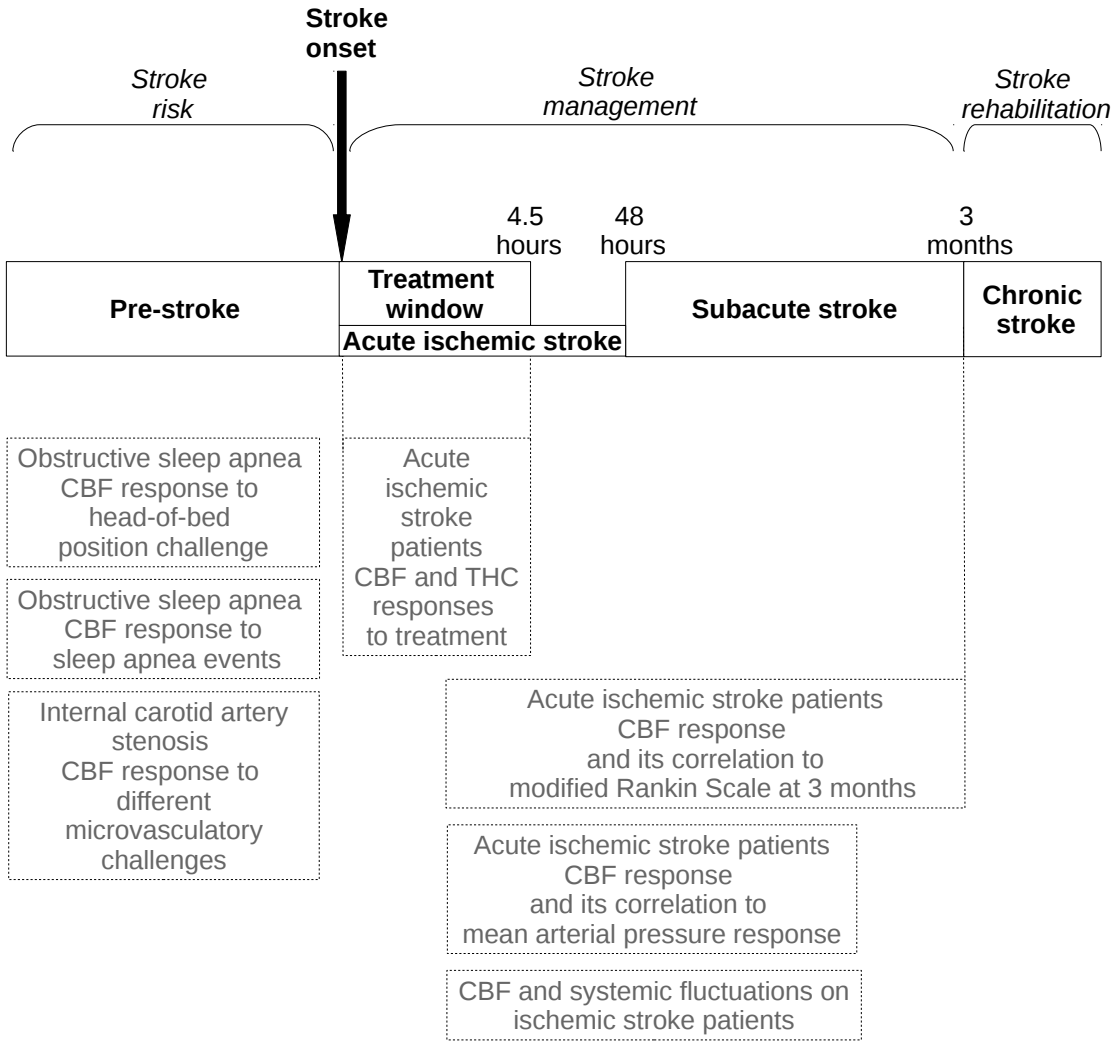

FIGURE 1.1: Schematic of the different clinical studies according the degree of risk of stroke and also to the stroke condition. CBF, cerebral blood flow; THC, total hemoglobin concentration.

2. The orthostatic challenge can be an alternative protocol to acetazolamide injection and breath-hold index challenges in order to derive a biomarker of cerebral vasoreactivity in evaluating the effects of internal artery carotid stenosis. See Chapter 7.

3. The blood flow response to an orthostatic challenge in ischemic stroke patients correlates with the clinical outcome at three months from the stroke onset. See Chapter 9.

4. The blood flow response to an orthostatic challenge in ischemic stroke patients correlates with the mean arterial pressure response to the same orthostatic challenge. See Chapter 10.

- Goal II: Monitoring of the microvascular cerebral hemodynamics during apneas and hypopneas during night sleep in obstructive sleep apnea patients. See Chapter 6.

  Hypothesis:

  1. Diffuse correlation spectroscopy is able to characterize the microvascular CBF response to each apnea event with a sufficient contrast-to-noise ratio to reveal its dynamics.

- Goal III: Enlarging a study of employment of diffuse optics on the emergency unit for ischemic stroke. See Chapter 8.

  Hypotheses:

  1. Hybrid diffuse optics can reliably be employed in the emergency unit environment and utilized during treatment and intensive care.
  2. Hybrid diffuse optics show a change during to the restoration of the microvascular cerebral hemodynamics due to the recanalization therapy after ischemic stroke.

- Goal IV: Investigation on unexpected periodic changes of cerebral hemodynamics in acute ichemic stroke patients. See Chapter 11.

  Hypothesis:

  1. The unexpected cerebral hemodynamic fluctuations are associated to apneic and hypopneic event.

1.2 Thesis outline

This thesis is organized in four parts. The first part aims to give a general understanding of diffuse optics. The second part aims to present the experimental setup that was designed, built and/or used in the third part, which contains the different *in-vivo* studies performed. Finally, the fourth part summarizes and concludes this work.

Chapter 3 focuses on the basis of light transport in biological tissues, presents the photon diffusion equation, the correlation diffusion equation and also their solutions for a semi-infinite geometry. These have been used to model the experimental

results in the measurements presented in this work. The optical instrumentation used in this work is presented in Chapter 4. It also contains my contributions to the design of a compact, next generation, instrumentation to be used in the future studies.

Chapter 5 presents *in-vivo* data focusing on CBF after a head-of-bed orthostatic challenge on severe obstructive sleep apnea patients before and after long-term treatment. Also, considering the patients recruited with the highest degree of severity, Chapter 6 shows polysomnographic and diffuse optical results from night sleep measurements in this cohort. Understanding the microvascular cerebral hemodynamics of these patients may help us to understand the alteration on the CAR that they suffer and its link to their risk of stroke (Figure 1.1).

Chapter 7 presents *in-vivo* data focusing on CBF and cerebral blood flow velocity on internal carotid artery stenosis patients in order to compare the existing acetazolamide injection and breath-hold index challenges to the head-of-bed orthostatic challenge. And also, to compare DCS versus the existing TCD technique used for checking an alternative biomarker to the cerebral vasoreactivity and autoregulation of these patients in the clinics. Similarly to OSA patients, these are also patients with a high risk of stroke (depicted in Figure 1.1), and cerebral hemodynamics may add clinical information to be related to this risk.

Chapter 8 presents *in-vivo* data focusing on CBF, total hemoglobin, and oxy- and deoxy-hemoglobin concentration changes on ischemic stroke patients during the time window for treatment on the first 4.5 hours after stroke onset. Continuous data from the emergency unit during the crucial recanalization theraphy is presented, opening the door towards the potential application of diffuse optics in real time monitoring of the recanalization.

Chapter 9 presents *in-vivo* data focusing on CBF on ischemic stroke patients after a head-of-bed orthostatic challenge in order to seek for an easy-to-do biomarker test related to the cerebral well-being of these patients during the first days after stroke. Associations between these results with outcome of stroke and other clinical variables are tested. Furthermore, this data is aggregated to two other datasets of different studies to further study the head-of-bed challenge in Chapter 10.

Finally, Chapter 11 presents *in-vivo* data focusing on continuous CBF, heart rate, arterial oxygen saturation and other respiratory parameters on acute ischemic stroke patients with possible breathing disorders. If apneas and hypopneas provoke

the cerebral microvasculature parameters to fluctuate during the first days after stroke, this could be detrimental for these patients where cerebral perfusion is aimed to be maximized.

In the last Chapter, the final conclusions are drawn.

Chapter 2

Cerebral blood flow regulation

2.1 Primary mechanisms involved in the cerebral blood flow regulation

The brain is one of the most complex organs of our body. It is also a very delicate organ. For example, even a brief (minutes) period of lack of sufficient oxygen to a specific part of the brain (e.g. such as during an ischemic stroke) may cause an irreversible damage. In order to protect the brain, and of particular interest to this work, there are complex mechanisms to regulate cerebral blood flow (CBF), which are primary mechanism to supply oxygen and other nutrients. In other words, the body aims to keep CBF constant in response to different challenges or to increase it sufficiently to meet increasing demands. The impairment of cerebral blood flow regulation of the cerebrovascular bed is quite common in several pathologies such as the acute phase of the severe traumatic brain injury, ischemic stroke or in other cerebrovascular diseases [4, 26]. These abnormalities are hard to characterize in the clinic -one of the motivations of this thesis work- but are hypothesized to play an important role in the physiopathology of these entities. A better understanding of and the ability to routinely evaluate the cerebral blood flow regulation of these patients could improve the diagnosis and management of these pathologies.

The level of CBF sets the amount of oxygen and nutrients to the brain and it is mediated by different mechanisms involved in the CBF control and regulation. Two mechanisms of interest in this work are the metabolic regulation response and the myogenic response. The metabolic regulation response consists on setting the

adequate level of CBF in order to regulate the oxygen demand of the brain dynamically, locally or globally. The myogenic response of the cerebrovascular bed refers to the response of the vasculature to changes in cerebral perfusion pressure, which is defined as the cerebral autoregulation (CAR) (see Figure 2.1). Additionally, the vessels will dilate or contract to maintain a constant CBF in response to a vasodilatory stimulus, this is due to cerebral vasoreactivity (CVR). The CVR is not only used in the myogenic response, but also it is one of the end-point regulatory mechanisms for the metabolic response. [4, 29, 30] In general, CVR is defined as the response to a stimulus (changes in cerebral perfusion pressure (CPP), changes in arterial partial pressure of carbon dioxide (pCO_2), acetazolamide injection, etc.) that dilates or contracts the cerebral vasculature [4].

2.2 Cerebral autoregulation

Nowadays, it is accepted that, in non-pathological conditions, the steady-state CBF is kept constant between two values of CPP, which is the difference between the arterial pressure and the intracranial pressure, even when the CPP may vary [4]. In this work, a non-invasive, easy-to-perform and mild challenge consisting on changing the head-of-bed (HOB) position has been studied under many conditions. This orthostatic challenge could be a biomarker related to CAR. This challenge is tackled in Chapters 5, 7, 9 and 10.

2.3 Secondary cerebral vasoreactivity to changes on the arterial partial pressure of carbon dioxide

The most common stimulus that is known to be a very potent driver of CVR is carbon dioxide. The pCO_2 provokes a strong vasodilatory response when increased (i.e. during a hypercapnia) and the reverse, a vasoconstriction, when reduced (i.e. during a hypocapnia). Several authors have established that in baseline pCO_2 values of 40 mmHg, the vascular response to a change of 1 mmHg in pCO_2 is about 2-4 % in CBF (albeit with some variations with some authors suggesting even larger changes)[27, 32, 33]. While we do not explicitly induce pCO_2 changes

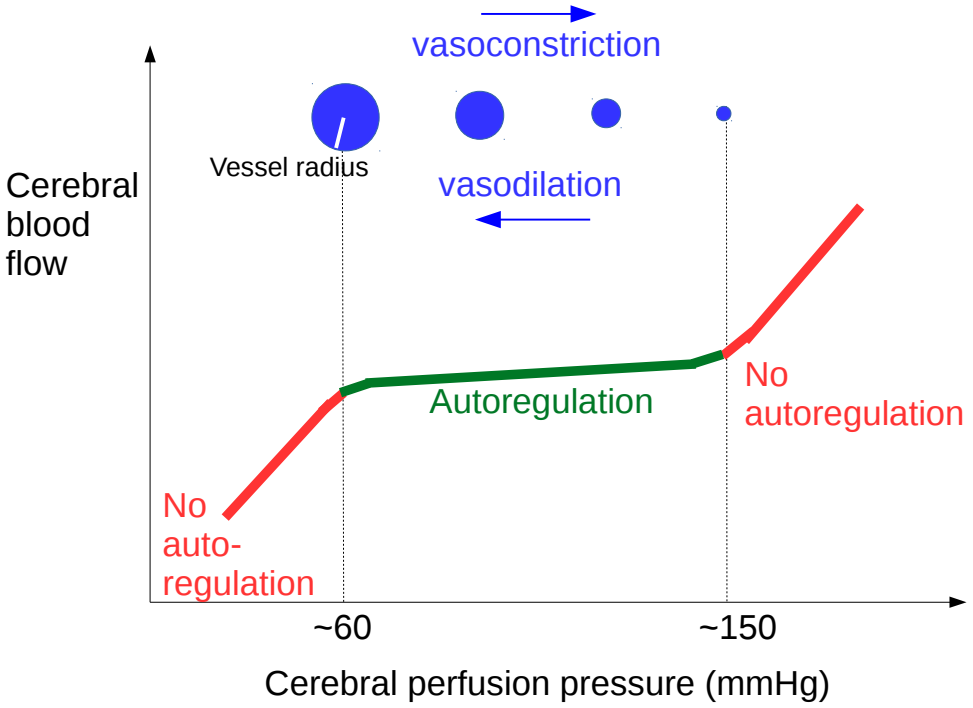

FIGURE 2.1: Diagram of cerebral autoregulation. The change in the vascular diameter in response to changes in cerebral perfusion pressure is the main mechanism that guides cerebral autoregulation to keep a constant cerebral blood [30, 31].

in this thesis, some of the conditions that we have investigated may have been driven by those, e.g. those in Chapters 6, 7 and 11.

2.4 Study of the cerebral vasodilatory reservoir through acetazolamide injection

The most common stimulus to study the well-being/reservoir of the CVR in our hospital settings (Hospital de la Santa Creu i Sant Pau, Spain) is acetazolamide. Acetazolamide (ACZ) is another chemical stimulator which is injected to measure the maximal vasodilation capacity [34, 35]. ACZ is a selective inhibitor of the enzyme carbonic anhydrase (EC 4.2.1.1). Figure 2.2 shows a cerebral blood flow change through the ACZ vasoreactivity stimulus measured with diffuse correlation spectroscopy. This stimulus has been used to test the CVR as shown in Chapters 5 and 7.

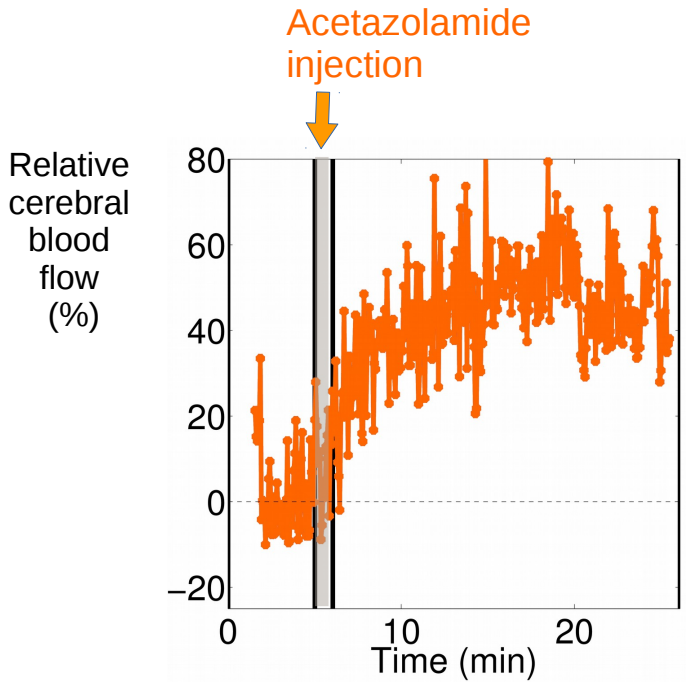

FIGURE 2.2: Microvascular cerebral blood flow response to acetazolamide injection as a vasoreactivity stimulus. This is a representative result of one patient from the study described in Chapter 7. The gray area indicates the duration of the injection.

Chapter 3

Theoretical background

3.1 Diffuse light in tissues

In the prehistorical times light became an important tool for the daily survival. Our ancestors used the light of the fire to get warm during the cold days, to cook the raw meat, to enable their eyes to see what was happening around them, etc. Nowadays, more and more applications with light are found to improve our lives due to its unique properties. For the purpose of this thesis, two main physical processes of light are considered: absorption and scattering. Regarding the first concept, light is absorbed (decreases intensity) when its wavelength coincides with a material resonance. About the second, light is scattered, in general terms, when is forced to deviate from a straight trajectory. Both concepts are wavelength dependent.

The propagation of the photons in tissues in our range of interest (650-950 nm) is mainly affected by scattering but also by absorption. In order to understand this propagation, there are some concepts that are important to understand: the scattering length is the average distance a photon needs to travel before it scatters and its reciprocal is named scattering coefficient (μ_s). The transport mean-free path (ℓ_{tr}) is the average distance a photon needs to travel before their direction is randomized, and its approximated reciprocal is called the reduced scattering coefficient (μ'_s), defined by $\mu'_s \equiv (1-g)\mu_s$, where $g \equiv \langle cos(\varphi) \rangle$ (φ is the scattering angle); the closer g is to unity, the more probable it is for a photon to be scattered in the forward direction. Finally, the absorption length is the average distance traveled by a photon before it is absorbed and its reciprocal is the absorption

coefficient (μ_a). The presented coefficients μ_s, μ'_s and μ_a are depicted in Figure 3.1, where common light-tissue interactions processes are shown.

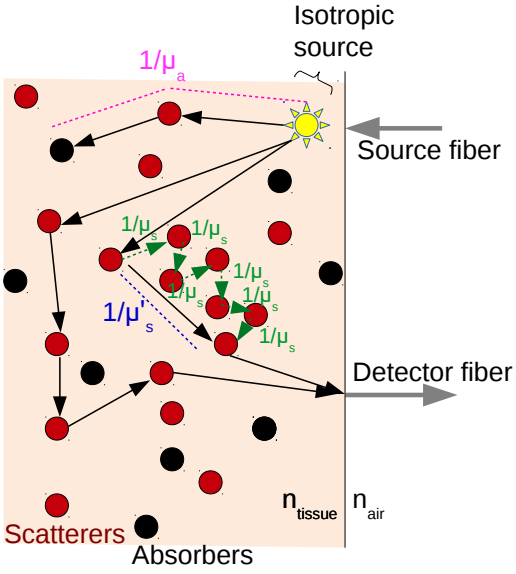

FIGURE 3.1: Schematic of main light-tissue (i.e. biological tissue) interaction processes of interest. Photons in a turbid medium interact with scatterers (red circles) or absorbers (black circles). μ_a, absorption coefficient; μ_s, scattering coefficient; μ'_s, reduced scattering coefficient; n, index of refraction.

The validity of the model used to explain how the light diffuses in tissues lies on the fulfillment of several properties. One of these properties is that radiance needs to be nearly isotropic. This condition is fulfilled when (1) $\mu'_s \gg \mu_a$ and (2) the distances traveled by photons within the medium are large relative to ℓ_{tr}. Other assumptions are to have an isotropic source and slow temporal flux variations [36].

With all these mentioned assumptions, we can describe the photon fluence rate (Φ) by the photon diffusion equation [37, 38]:

$$\nabla \cdot (D(\boldsymbol{\rho})\nabla\Phi(\boldsymbol{\rho},t)) - \nu\mu_a(\boldsymbol{\rho})\Phi(\boldsymbol{\rho},t) - \frac{\partial\Phi(\boldsymbol{\rho},t)}{\partial t} = -\nu S(r_s - \boldsymbol{\rho},t) \tag{3.1}$$

In equation 3.1, ν is the speed of light in the medium (cm/s), $D(\boldsymbol{\rho}) = \dfrac{\nu}{3(\mu_a(\boldsymbol{\rho}) + \mu'_s(\boldsymbol{\rho}))}$ is the photon diffusion coefficient (cm^2/s) at position $\boldsymbol{\rho}$, $U(\boldsymbol{\rho}, t)$ is the photon fluence rate (Wcm^{-2}) at position $\boldsymbol{\rho}$ and time t, $S(\boldsymbol{\rho}, t)$ is the source term (Wcm^{-3})) and r_s is the source position.

3.1.1 Three main source types

Different source types can be used to study medium properties (i.e. the absorption (μ_a) and the reduced scattering coefficient (μ_s')) using near-infrared light (650 - 950 nm). Each source type is used in a different near-infrared method, which provides different levels of information. The three different types of sources and methods of interest in this work for diffuse optics are illustrated in Figure 3.2.

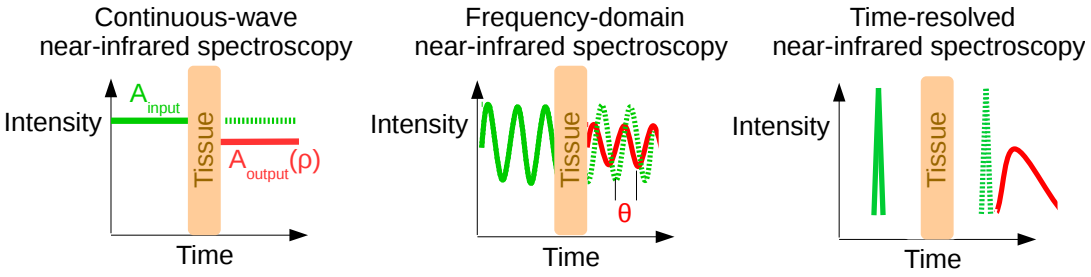

FIGURE 3.2: Three different types of sources and methods used in diffuse optics in: [Left] continuous-wave near-infrared spectroscopy (CW NIRS-DOS), [middle] frequency-domain near-infrared spectroscopy (FD NIRS-DOS) and [right] time-resolved near-infrared spectroscopy (TRS NIRS-DOS). The incident light is depicted in green and the detected light out from the tissue is depicted in red.

Continuous-wave near-infrared spectroscopy (CW NIRS-DOS) is the simplest and cheapest method that measures the intensity drop at a specific distance (ρ) from the source. A_{input} is the intensity of the incident light injected into the tissue, it is attenuated by the medium. The A_{output} is the detected attenuated intensity. CW NIRS-DOS can provide absolute μ_a and μ_s' values with the least information content per source-detector pair [39, 40] compared to the following spectroscopy techniques.

If the light source is sinusoidally modulated in intensity (∼100 MHz), not only the attenuation of the light is measured to derive the optical properties, but also the phase shift ($\nabla\theta$) between the incident and detected light introduced in the diffusive medium is measured. This technique is called frequency-domain near-infrared spectroscopy (FD NIRS-DOS) [41–44].

The third technique to list is the time-resolved near-infrared spectroscopy (TRS NIRS-DOS). TRS NIRS-DOS sends a narrow pulse (∼ ps) to the tissue, which broadens in time due to multiple scattering events inside the tissue. These time domain measurements use the distribution of photon travel times to derive the absolute values of μ_a and μ_s' [45–49] with the most information content per source-detector pair among the other presented methods.

3.1.2 Diffuse photon density waves

This section focuses on the particular case when the light source is sinusoidally modulated at ∼100 MHz (it is called frequency-domain, as presented previously) in the near-infrared spectra (650 - 950 nm).

When a source S in a turbid medium is intensity modulated (with components S_{dc} -the mean offset- and S_{ac} -the amplitude fluctuated of the dc-, where $S(r_s - \boldsymbol{\rho}, t) = S_{dc}(r_s - \boldsymbol{\rho}) + S_{ac}(r_s - \boldsymbol{\rho})e^{iwt}$), and the photon fluence rate oscillating at the same angular frequency is selected, the ac contribution obtained has this general form:

$$\phi_{ac}(\boldsymbol{\rho}, t) = U(\boldsymbol{\rho})e^{iwt} \tag{3.2}$$

where ω is the laser/source modulation frequency.

This traveling disturbance of the light energy density is called a diffuse photon density wave [44, 50].

Combining equation 3.2 and the diffusion equation (equation 3.1), we obtain:

$$\nabla \cdot (D(\boldsymbol{\rho})\nabla U(\boldsymbol{\rho})) - (\nu\mu_a(\boldsymbol{\rho}) - iw)U(\boldsymbol{\rho}) = -\nu S_{ac}(\boldsymbol{\rho}) \tag{3.3}$$

Since, for this work, the medium (i.e. the brain) is approximated to be homogeneous, then, the equation 3.3 simplifies to [5]:

$$(\nabla^2 - k^2)U(\boldsymbol{\rho}) = -\frac{\nu}{D}S_{ac}(\boldsymbol{\rho}) \tag{3.4}$$

Solving the previous equation 3.4, the photon fluence rate of diffuse photon density waves (DPDWs) in the frequency-domain in an infinite geometry is [5]:

$$U(\boldsymbol{\rho}) = \frac{\nu S_{ac}}{4\pi D\rho}e^{-k\rho} \tag{3.5}$$

where, $\rho = |\boldsymbol{\rho}|$, k is a complex wavevector $k = k_r + ik_i$, and k_r and k_i are:

$$k_r = (\frac{\nu\mu_a}{2D})^{1/2}[(1 + [\frac{w}{\nu\mu_a}]^2)^{1/2} + 1]^{1/2} \tag{3.6}$$

$$k_i = -(\frac{\nu\mu_a}{2D})^{1/2}[(1 + [\frac{w}{\nu\mu_a}]^2)^{1/2} - 1]^{1/2} \tag{3.7}$$

From equations 3.6 and 3.7 it can be noted that the DPDW wavelength is related to the absorption coefficient (μ_a) of the medium, and it is inversely related to the reduced scattering coefficient (μ_s'), to the ratio of index of refraction to the outside (n_{air}, in this study) and to the modulation frequency (w). Consequently, when DPDW propagates in the medium, its amplitude decreases due to absorption and its phase increases due to multiple scattering; where these mentioned decreases and increases depend on the properties of the medium. Moreover, DPDWs have been demonstrated to exhibit not only absorption and scattering, but also several familiar wave-like properties including diffraction, refraction, interference and dispersion [50–52].

3.1.3 Solving the diffusion equation

In order to solve the diffusion equation the brain is approximated to a planar interface (i.e., the forehead), where a semi-infinite turbid tissue (i.e., the brain) is bounded in the other half-space by air. Cylindrical symmetry will be used to specify position, i.e., $\boldsymbol{\rho} = (\rho, z)$.

Also, the method of images is used in the process of solving the diffusion equation. This method consists on using an extrapolated zero boundary condition by introducing a negative image point source at $z_s = (2z_b + l_{tr})$ as shown in Figure 3.3. For this method, the fluence rate curve is approximated by its tangent line at $z = 0$, and the photon fluence rate is approximated to be equal to zero ($\phi = 0$ intercept of this curve is found at $z = -z_b$).

Then, the Green's function for a semi-infinite geometry is used to find the following Green's function solution of the diffusion equation:

$$G([\rho, z]) = \frac{1}{4\pi}[\frac{e^{-kr_1}}{r_1} - \frac{e^{-kr_b}}{r_b}] \tag{3.8}$$

$r_1 = \sqrt{\rho^2 - (z - l_{tr})^2}$

$r_b = \sqrt{\rho^2 + (l_{tr} + z + 2z_b)^2}$

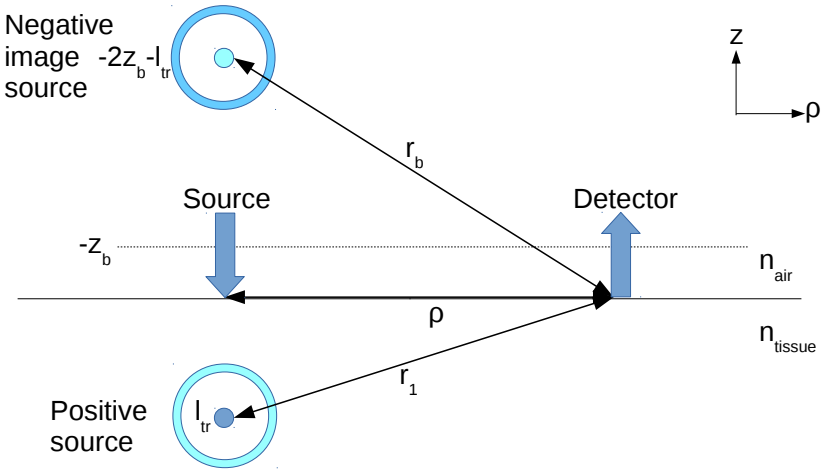

FIGURE 3.3: In the extrapolated zero boundary condition described here, the isotropic nature of the source is modeled for a semi-infinite geometry by an isotropic light source at z = l_{tr} inside the tissue medium (refractive index n_{tissue}) and a negative isotropic image source at z=-2z_b-l_{tr} above the medium (refractive index n_{tissue}). The source-detector distance (ρ) is located at the medium interface (z=0). Illustration inspired by [53].

$z_b = 2l_{tr}\dfrac{1+R_{eff}}{1-Reff}$, it is the extrapolated zero boundary distance perpendicular to the boundary.

$R_{eff} = \dfrac{-1.440}{n^2} + \dfrac{0.710}{n} + 0.668 + 0.00636n$; it is the approximated effective reflection coefficient to account for the index mismatch between tissue and air, where $n = \dfrac{n_{tissue}}{n_{air}}$, it is the ratio of the index of refraction of inside and outside media (corresponding to air, in general).

$k = \sqrt{\dfrac{\nu\mu_a - iw}{D}}$

If the approximation $\rho \gg (l_{tr} + 2z_b)$ is fulfilled, the photon fluence rate can be fitted (equation 3.8) and the exact solution found at z=0 is:

$$U(\rho) \approx \frac{A_0 e^{-k_r\rho}}{\rho^2}(e^{i(-k_i\rho+\theta_0)}) = A(\rho)e^{i\theta(\rho)} \tag{3.9}$$

Where $ln(\rho^2 A(\rho))$ and $\theta(\rho)$ depend linearly on ρ:

$$ln(\rho^2 A(\rho)) = k_r\rho + lnA_0 \tag{3.10}$$

$$\theta(\rho) = -k_i\rho + \theta_0 \tag{3.11}$$

Since the absolute value of the photon fluence rate corresponds to the amplitude and the angle contribution corresponds to the detected phase, then, μ_a and μ_s' can be calculated with the equations 3.10 and 3.11 after measuring amplitude and phase by FD NIRS-DOS.

Even though FD NIRS-DOS was part of the optical platform, the studies that have utilized it and their analysis have not made it into this dissertation.

3.1.4 Tissue chromophore concentrations

In diffuse optics the light of interest is the near-infrared light (650 - 950 nm), and the primary tissue chromophores within biological tissue are deoxy-hemoglobin, oxy-hemoglobin, water and lipids concentrations.

The tissue absorption depends directly on the concentration of tissue chromophores in the following way:

$$\mu_a(\lambda) = \sum_i^N \epsilon_i(\lambda) c_i \tag{3.12}$$

Where $\epsilon_i(\lambda)$ (cm^2/mol) is the wavelength-dependent extinction coefficient of each chromophore for absorption obtained from the literature [54] ($\epsilon_{i,absorption} = e \cdot \epsilon_{i,absorbance}$), c_i (mol/cm^3) is the concentration of each chromophore, and N is the total number of chromophores that are summed. As a note, in general, the literature refers to the concept of absorbance, instead of the concept of absorption, where absorbance is defined as:

$$Absorbance = -\ln \frac{A(r_d, t)}{A(r_d, t=0)} \cdot \frac{1}{\rho} \tag{3.13}$$

where $A(r_d,t)$ is the photon fluence rate amplitude at a time t and a r_d position of the detector.

Using equation 3.12, deoxy-hemoglobin concentration (Hb) and oxy-hemoglobin concentration (HbO_2) can be calculated using the well-known spectra (Figure 3.4)

of these molecules [55]. From these concentrations, two important biomarkers in medicine [56] can be found; the total hemoglobin concentration (THC) and the tissue blood oxygen saturation (StO_2).

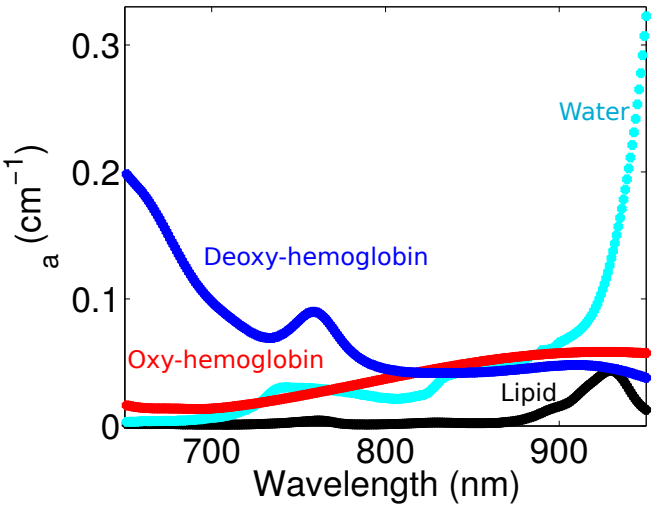

FIGURE 3.4: Absorption spectra of major tissue chromophores over the so-called "physiological window" in the near-infrared (650 - 950 nm) where water and hemoglobin concentration absorption are relatively low. Light can penetrate several centimeters in the tissue in this part of the spectrum.

Where THC is calculated by:

$$THC = HbO_2 + Hb. \tag{3.14}$$

and StO_2 is calculated by:

$$StO_2 = \frac{HbO_2}{HbO_2 + Hb} 100 \tag{3.15}$$

3.1.4.1 The differential pathlength approach

In some contexts/studies, the temporal variation of quantities such as oxy-hemoglobin and deoxy-hemoglobin concentrations, respect to a defined perturbation, provide valuable information; so, absolute values are not required. In these cases, a simple differential pathlength method can be used to calculate oxy-hemoglobin and deoxy-hemoglobin concentration changes considering only the intensity of the detected light.

This method relates temporal changes in the optical density (OD), OD = ln(10)· $Absorbance \cdot \rho$ = -ln(A(r_d, t)/A(r_d)), to changes in chromophore concentrations

[57–59]. Where, A($_d$,t) corresponds to the photon fluence rate amplitude at a time t and a r_d position of the detector.

After truncating the Taylor series expansion of the optical density for a given source-detector separation ρ to the first order in μ_a and μ_s', a modified Beer-Lambert law can be approximated:

$$\Delta OD(\lambda, t) \approx \sum_i (\epsilon_i(\lambda)\Delta c_i(t))DPF(\lambda)\rho \tag{3.16}$$

Here, the differential pathlength factor (DPF), which is the mean pathlength traveled by photons between reference and output detectors, is obtained from the literature [54].

The DPF approach has been used in part of this work presented in this thesis in data collected from a CW NIRS-DOS device.

3.2 Diffuse correlation spectroscopy

Diffuse correlation spectroscopy (DCS) measures the temporal speckle fluctuations of the scattered light and it is sensitive to the motions of the main moving scatterers in the tissue, the red blood cells [5, 7, 8, 60]. But, first of all, what is this concept that DCS measures?

3.2.1 Speckle concept

A surface is typically rough in the wavelength scale, and, when coherent light shines on it, it scatters at different points and generates a granular pattern [61], a visible interference pattern called speckle pattern. Similarly, when coherent laser light travels through diffuse media composed by particles in suspension like biological tissues, light is scattered by the different particles at random directions and interferes constructively and destructively creating the speckle pattern.

The bright spots (constructive interference) correspond to positions in space in which the scattered light from the surface or by some particles inside the medium arrives in phase. On the other hand, the dark spots correspond to positions where

destructive interference takes place because the scattered light arrives out of phase, as it is depicted in Figure 3.5.

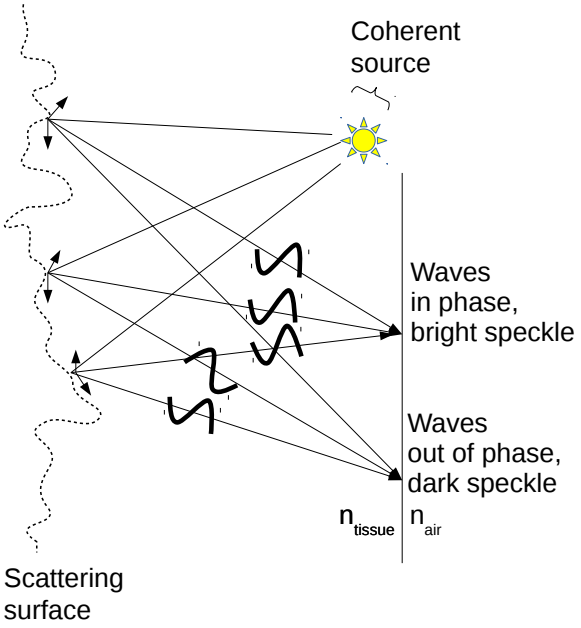

FIGURE 3.5: Schematic of an example of generation of speckles. Illustration inspired by [62].

Moreover, if some of the scattering particles are in movement, the scattered electrical wave arrives with a different optical phase to a point X, modifying the interference pattern.

As mentioned, in tissue, the main moving scatterers are the red blood cells. DCS technique measures the variation over time of a single speckle attributed to red blood cells motion and by means of some statistical functions further introduced, these temporal speckle fluctuations have been found to be proportional to the microvascular blood flow [63–66].

Other than presenting the concept of a speckle, it is also relevant to introduce two main regimes for defining DCS. These two regimes are dependent on whether photons experiment a single scattering event or whether they propagate into the medium through multiple scattering events.

3.2.2 Dynamic light single scattering

The dynamic light scattering technique measures the motions of the scatterers. If long coherence light is shone onto a solution with diluted particles, each single

particle develops a dipole which emits scattered light in an isotropical way. Since all particles in a liquid are in motion, the phases of the dipole electromagnetic fields fluctuate. [67–69]

The randomly distributed particles will create random differences in the optical pathlengths that will create interference patterns. But only the constructive interferences will be observed in the detector as bright spots.

Relevantly, one can measure these bright spots by a fixed detector, as it is shown in Figure 3.6. From these measured intensity fluctuations, the normalized intensity temporal autocorrelation function can be calculated (g_2):

$$g_2(\rho, \tau, t) \equiv \frac{\langle I(\rho, t) I(\rho, t+\tau) \rangle}{\langle I(t) \rangle^2} \tag{3.17}$$

where τ is the delay time.

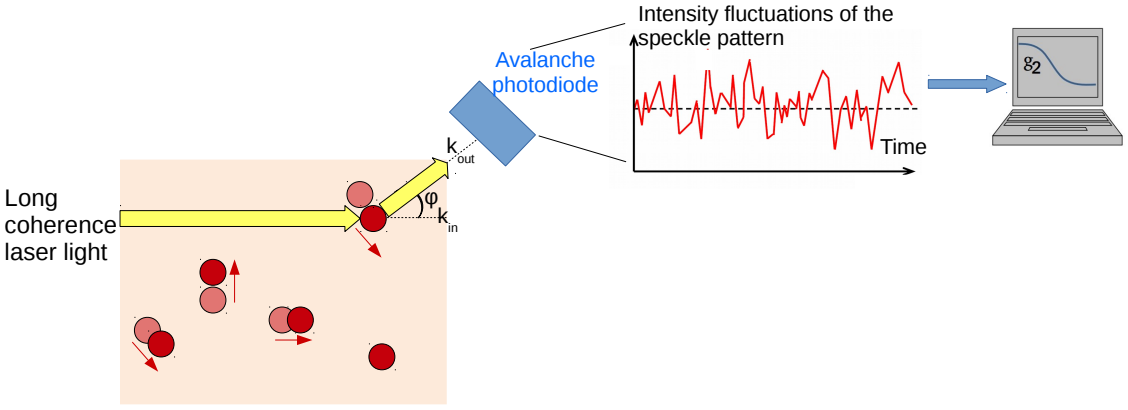

FIGURE 3.6: Schematic of a single scattering experiment. The scattered light is collected in a detector placed at an angle φ respect to the incident laser light beam.

These intensity fluctuations can be measured, as mentioned, but we cannot measure the full electromagnetic fields. Instead, we can model the normalized electric field autocorrelation function (g_1) as [5, 70, 71]:

$$g_1(\rho, \tau, t) \equiv \frac{\langle E^*(t) \cdot E(t+\tau) \rangle}{\langle |E(t)|^2 \rangle} = e^{\frac{i2\pi\tau}{\lambda}} e^{\frac{-q^2 \langle \Delta r^2(\tau) \rangle}{6}} \tag{3.18}$$

λ is the wavelength in the medium of the incident light, q is the scattered wavevector representing the difference between output (k_{out}) and input (k_{in}) wavevectors, $\langle \Delta r^2(\tau) \rangle$ is the mean-square particle displacement in time τ, and brackets $\langle\ \rangle$ represent ensemble averages.

Since, as mentioned, the modeling is done for the electric field autocorrelation function, a link between g_1 and g_2 is needed to relate the measured intensity fluctuations to the electromagnetic fields generated. This link is the Siegert relation [71]:

$$g_2(\tau) = 1 + \beta |g_1(\tau)|^2, \tag{3.19}$$

β is a constant determined primarily by the source and the collection of optics of the experiment [71], thus β can be measured from experimental data from the g_2 when τ is near to zero.

Some recent advances on diffuse optics have enabled to measure g_1 directly without relying on the Siegert relation from the simultaneous measurement of multiple speckles, and to be able to measure not only the blood blow index, but also scattering and absorption at the same time [72, 73]. This technique is called interference diffuse correlation spectroscopy/interference diffusing wave spectroscopy. However, so far, it has different drawbacks with respect to DCS, including worse signal-to-noise ratio, complex source and detector requirements, and comes at a higher cost. Further work my enable its introduction to clinical research.

3.2.3 Dynamic light multiple scattering

However, photons may experience many scattering events before they exit a turbid media (such as tissue) in the near-infrared spectra (650 - 950 nm), as it is shown in Figure 3.7.

DCS is based on pioneering work on diffusing wave spectroscopy (DWS) [65, 74, 75], which is based on the same physics as DCS but did not employ the correlation transport theory or the correlation diffusion approximation to it, which has been critical for the introduction of DCS for biomedical use [5, 63, 64].

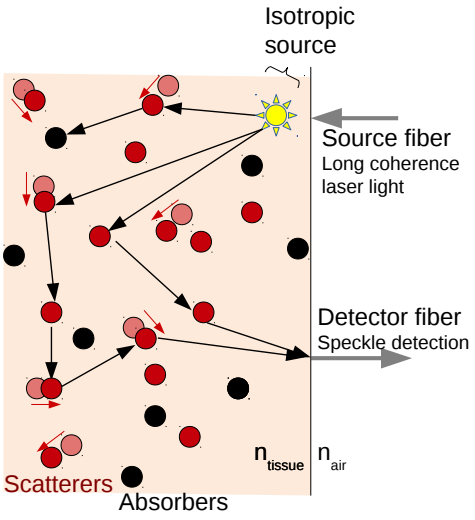

FIGURE 3.7: Schematic of the photon path during multiscattering events in the reflection geometry. The photons reach the detector after experiencing multiple scattering events.

In practice, and relevant to this work, it has been found that the Brownian motion, $\langle \Delta r^2(\tau) \rangle = 6D_b\ \tau$, fits the observed correlation decay curves in the detector in the tissue (i.e. in the brain) [12, 15, 17, 76–79]; where D_b is the effective diffusion coefficient. But D_b is of orders of magnitude larger than the traditional thermal Brownian diffusion coefficient of red blood cells [80]. Relevantly, it has been demonstrated in several DCS measurements that the fitted parameter αD_b, where α represents the fraction of photon scattering events that occur from moving particles in the medium, correlates well with blood flow values measured by other modalities [12, 13, 15–17, 76–78, 81–85]. This parameter αD_b has been defined as the blood flow index (BFI). The BFI is not a measure of absolute blood flow, but its relative change has been shown to be a measure of relative change in blood flow. Interestingly, a last study [86] provides experimental evidence that BFI is mainly sensitive to the shear-induced diffusion of red blood cells, proving right the validity of our diffusion model as a measure of blood blow.

Finally, in order to find the desired BFI (in order to fit for $\alpha \mathrm{D}_b$), equations 3.17 and 3.19 are used together with the Green's function solution of the correlation diffusion equation for semi-infinite boundary conditions (as brain has been approximated to) [5], G_1:

$$G_1(\rho, \tau) = \frac{3\mu_s'}{4\pi}\left[\frac{e^{-K(\tau)r_1}}{r_1} - \frac{e^{-K(\tau)r_b}}{r_b}\right] \tag{3.20}$$

With

$$K(\tau) = \sqrt{3\mu_a\mu_s' + 6{\mu_s'}^2\kappa^2\alpha D_b\tau} \tag{3.21}$$

κ is the wave-number of light in the medium $= \dfrac{2\pi}{\lambda}$.

Part II

Diffuse optical instrumentation

Chapter 4

Diffuse optical instrumentation

In the previous chapter, the different techniques used in this work have been presented. These are diffuse correlation spectroscopy (DCS), which is an emerging technique that can measure microvascular blood flow; and continuous-wave near-infrared spectroscopy (CW NIRS-DOS). This chapter aims to present the instrumentation used in the different *in vivo* studies, and also, to present the instrumentation designed and built for improving the setup of future studies. Depending on the characteristics of the experimental design and protocol, the DCS module (Chapters 5, 9, 10, 6, 7 and 11), or the combination of DCS and CW NIRS-DOS (Chapter 8) have been used in the different clinical studies.

4.1 The diffuse optical multidevice used in our studies

The portable cart present in the clinics (Figure 4.1) includes these mentioned techniques. This allows us to be flexible when running different protocols during the same period of time. In order to achieve this flexibility, hardware and software have been modified to easily choose the desired combination of techniques.

4.1.1 Diffuse correlation spectroscopy

The main components of the DCS consist of two lasers (for bilateral illumination), two units (for bilateral collection of light) of four detectors, a correlator, and a custom made data acquisition card as shown in Figure 4.1.

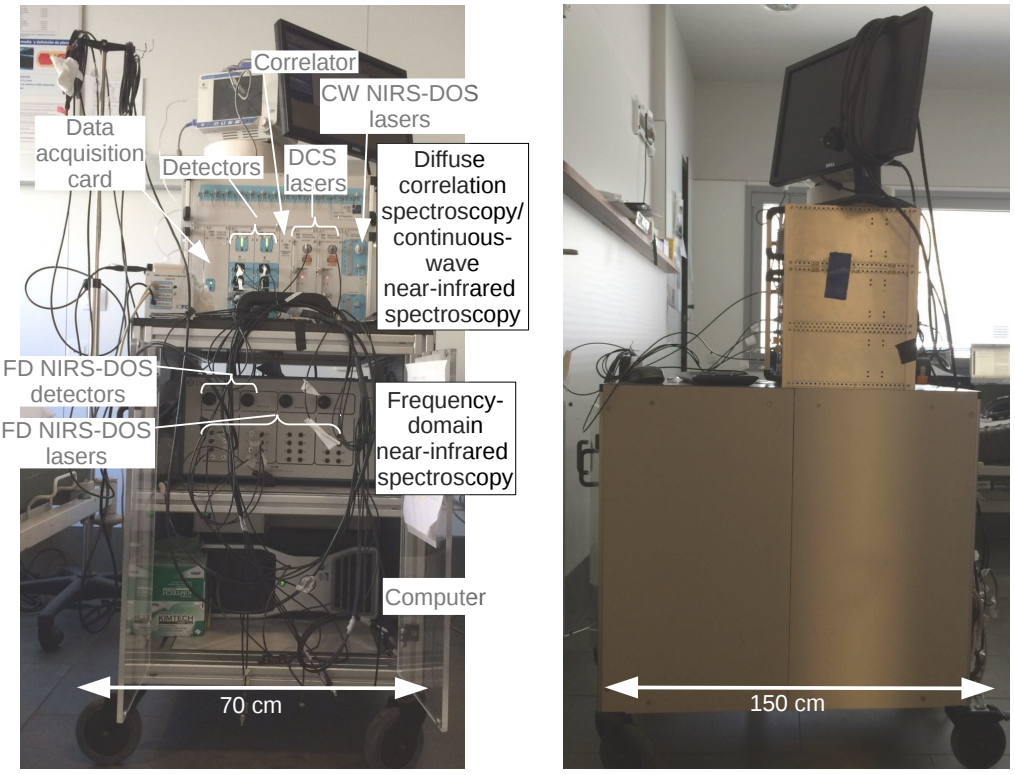

FIGURE 4.1: The diffuse optical multidevice (front view (left) and lateral view (right)) present in the clinics. On the top of the cart, a module including diffuse correlation spectroscopy (DCS) and a continuous-wave near-infrared spectroscopy (CW NIRS-DOS) device can be found. Inside the cart, a commercial frequency-domain near-infrared spectroscopy (FD NIRS-DOS) device that can work independently or together with the previous module is found. All techniques are controlled by a single computer. The spectroscopy techniques are labeled in black, and the main components of each device are labeled in grey.

The DCS lasers are mode-hope free, long-coherence-length (>15 m), continuous-wave, solid state lasers at 785 nm (DL785-120-SO, 120 mw, CrystaLaser, Reno, USA). The long-coherence-length fulfills the need to be longer than the spread of the pathlength distribution of the photon trajectories through tissue. Apart from being within the physiological window, this wavelength of 785 nm is close to the isosbestic point (the wavelength at which Hb and HbO_2 spectra cross each other), thus we are less sensitive to the differences in the variation of both Hb and HbO_2 measured with NIRS-DOS. The laser light is delivered to the tissue through a multimode fiber with a core diameter of ~ 200 μm (numerical aperture

of 0.22). Even though the lasers used are longitudinal and transverse mode lasers, light scatters within the tissue creating an interference pattern; considering this and also taking into account that multi-mode fibers have been used to deliver the light into the tissue, the incoming light at the detector no longer has a single mode. However, by using a single-mode optic fiber in the detection path, a single mode can be sensed in the detector. DCS uses two bundles of four-single mode fibers (one bundle for each cerebral hemisphere, and one single mode fiber for each single detector) of ~ 5 μm core diameters, embedded together with the mentioned multimode fiber in different home-made or custom made probes that are adapted to each different protocol. For this work, in general, a source-detector separation of 2.5 cm has been used, which has been found to be a good compromise and was validated in numerous studies [7, 8, 24]. The probes for each clinical study are presented in the incoming chapters.

Two units of four-single photon counting avalanche photodiodes are used as detectors (SPCM-AQRH-14-FC, Perkin Elmer, Waltham, USA), one unit for each cerebral hemisphere. As mentioned, only single modes will arrive at the detector. Because of this, a big sensing area does not add a relevant benefit, instead, quantum efficiency influences the light detection. For these reasons mentioned, single photon counting avalanche photodiodes are used in the detection system, which are avalanche photodiodes that work in the Geiger Mode and incorporate the electronics to transform the photocurrent into digital pulses. In this work, four single-mode fibers (each one connected to one single detector) are embedded in one probe to maximize the signal-to-noise ratio of a single measurement location. As mentioned, a total of two probes are used for considering bilateral measurements. The final transistor-transistor logic (TTL) signal generated by these detectors, every time that a photon is detected, is sent to a digital correlator (Flex05-8 ch, Correlator.com, Bridgewater, USA).

The normalized intensity temporal autocorrelation functions (g_2) (Section 3.2.2 in Chapter 3) are calculated in real-time by the digital correlator for each detector channel. Once the acquisition time has passed, the calculated g_2 is saved by the software on a text file and a new measurement starts. The acquisition time has been chosen to be from 1 to 3 seconds depending on the study and/or on the subject in order to obtain an acceptable signal-to-noise ratio. All components are controlled by an adapted Visual Basic software through a custom made data

acquisition card that basically sends and receives TTL signals to allow or cease the activity of the different electronic components.

4.1.2 Continuous-wave near-infrared spectroscopy

The main components of the CW NIRS-DOS are two lasers, two units of the same four-array of detectors shared with DCS, and a custom made data acquisition card also shared with DCS.

The two lasers are diode lasers of 690 and 830 nm of wavelength (∼50 mW) from the company OZ Optics (Ottawa, Canada), driven by a laser driver board and the temperature controller board developed by the Electronical Workshop at ICFO. The laser light of these two lasers is delivered in turns (by a laser switch (FSM-1X9, Piezosystem Jena GmbH, Jena, Germany)) to the tissue through a multimode fiber with a core diameter of $\sim$ 400 μm (numerical aperture of 0.22). For simplicity of the setup and in expense of the signal-to-noise ratio, the same single-mode detector fibers used for DCS are also used for the CW NIRS-DOS in this device for light collection, as well as the same single photon counting avalanche photodiodes are used as detectors (SPCM-AQRH-14-FC, Perkin Elmer), again, with one channel for each single mode fiber and four channels for each cerebral hemisphere. These fibers have been embedded together with the DCS source fibers in different home-made or custom made probes depending on the study. Again, the TTL signals generated are sent to the digital correlator, and the number of counts per second measured are saved on a text file.

4.1.3 Frequency-domain near-infrared spectroscopy

A commercial FD NIRS-DOS spectrometer (Imagent, ISS, Champaign, USA) has also been used in our clinical studies. The unit is customized to be able to use a maximum of fifteen laser sources at three different wavelengths, which are intensity modulated at 110 MHz. Two photo multipliers, one for each cerebral hemisphere, are used to collect the light in the reflection geometry. The minimum acquisition time for the FD NIRS-DOS is 0.1 seconds; however, in the studies performed (not presented in this thesis), it was always combined with DCS and the final acquisition time was in the order of seconds. Input and output TTL signals have been custom added in order to control the device through the Visual Basic DCS

software, which allows FD NIRS-DOS and DCS to run in turns or at the same time.

4.2 A new compact diffuse optical hybrid device

The combination of the previous units provides not only continuous CBF, but also continuous Hb and HbO_2 absolute values or relative changes. However, the combination of the DCS with the mentioned CW NIRS-DOS or FD NIRS-DOS units has one simple but significant problem: the size. These combinations cannot fit in the crowded-with-gadgets emergency unit of the hospital. Because of this, a new compact device (as shown in Figure 4.2) has been designed and built with the help of the students Maria Garcia and Xavier Casas. The device is divided in two main parts, which are an enclosure and a stand set on top of it. The stand includes free-rotating wheels to allow the total mobility of the entire device, each one with its corresponding brake, and also a fiber holder. The height has been set in order to have the suitable distance at which to work with the computer.

Besides its (relative) compactness, another particularity of this device is that data from both hemispheres of the brain can be recorded simultaneously and, this data is analyzed on real-time by a new Java based software (work of Ameer Ghouse) allowing the blood flow index to be shown on the screen on real time for each hemisphere separately.

The main components that conform this device have already been described previously (Section 4.1). Moreover, further electronic components are also presented in this section.

The compact device contains six continuous wave lasers of three different wavelenghts: two units at 785 nm for the DCS technique (DL785-070-SO, 70 mW, CrystaLaser, Reno, USA), and two custom made units at 690 nm ($\sim$50 mW) and two at 830 nm ($\sim$50 mW) (custom made by the Electronical Workshop at ICFO, by using laser diodes from OZ Optics, Ottawa, Canada) for the CW NIRS-DOS technique. All six lasers are computer controlled by a data acquisition card (DAQ; USB-6341 National Instruments DAQ, Austin, USA). Moreover, for safety reasons, a control board mediates the TTL signals from the DAQ to the lasers and it also monitors six (one for each laser) bicolour light-emitting diodes (LEDs; as explained in Section 4.2.1). The different lasers of different wavelengths work

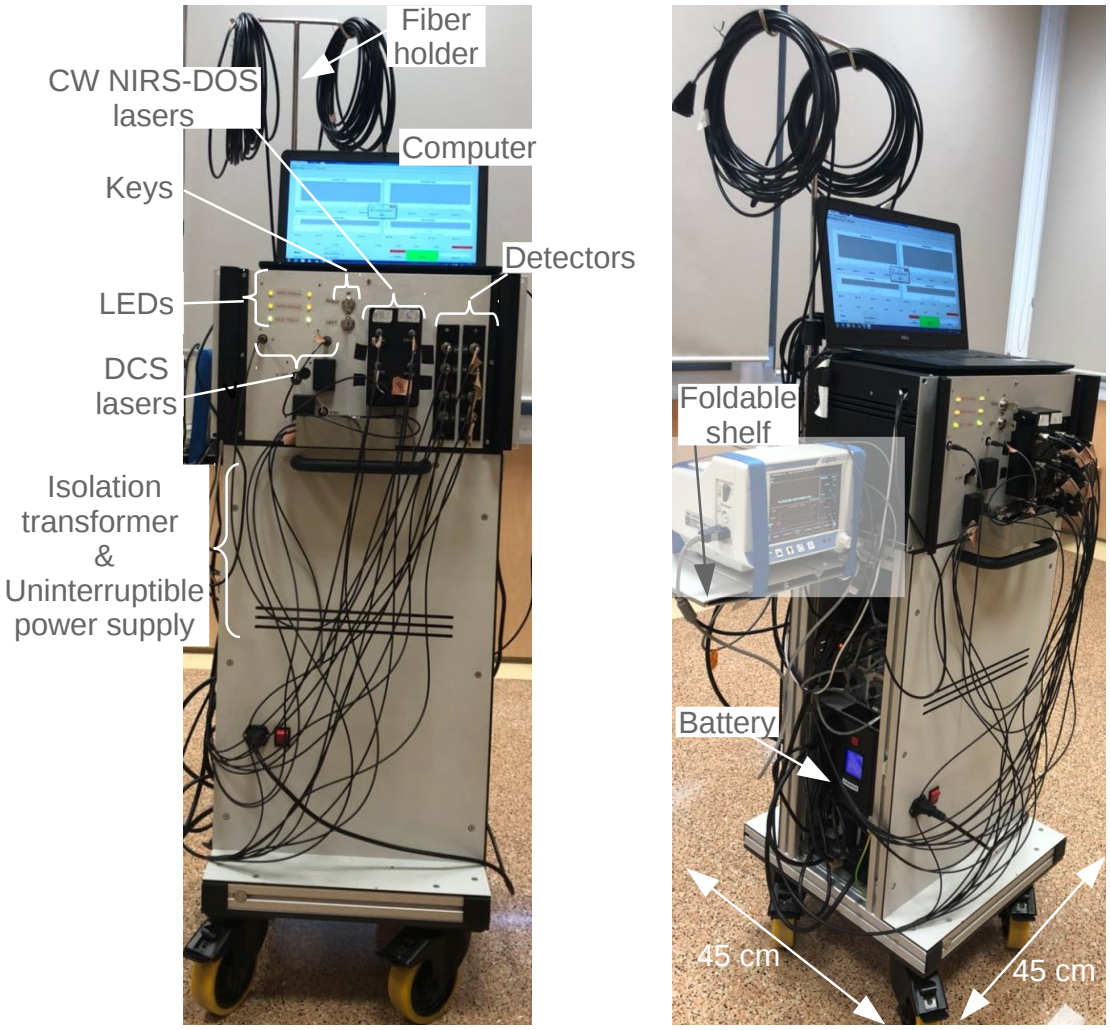

FIGURE 4.2: The new compact diffuse optical hybrid device. The enclosure contains the six lasers, the two modules with two units of four detectors each, the correlator, the control board and the data acquisition card. The stand contains the isolation transformer, the power box and the uninterruptible power supply. DCS, diffuse correlation spectroscopy; CW NIRS-DOS, continuous-wave near-infrared spectroscopy.

in turns, while the two lasers with the same wavelength can be shone bilaterally. Further clarification of the protocol for the operation of the lasers for each technique is shown in Figure 4.3. Due to TTL communication signals, the minimum acquisition time is six seconds even though nine seconds was used for the first tests, including the three different laser wavelengths present in the device. During the acquisition time, the TTL signals sensed in the detectors are sent to the correlator (Flex05-8 ch, Correlator.com, Bridgewater, USA), which provides the normalized intensity auto-correlation function, $g_2(\tau)$, and the number of counts per second, as explained in Chapter 3, and, are all finally stored on a text file. In addition, the DAQ reads the analogue signals of the photodiodes from the NIRS-DOS lasers, which are then stored in a second text file (as explained in section 4.2.1).

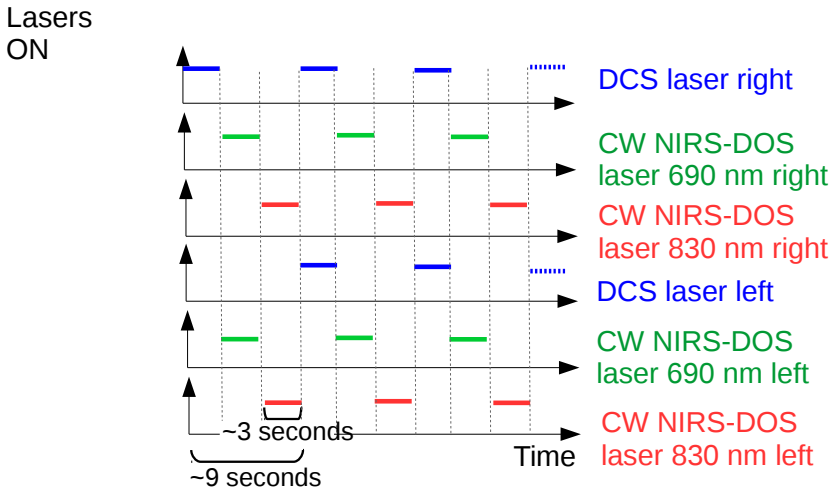

FIGURE 4.3: The protocol for the operation of the lasers of the new compact diffuse optical hybrid device.

An uninterruptible power supply (K-LCD 1200, Protec-Sai, Barcelona, Spain) enables to power supply the device during $\sim$ 10 minutes at 1200 VA during a power cut from the power source. The uninterruptible power supply is placed between an isolation transformer (Reomed 600, REO Inductive Components, Berlin, Germany) and the power source. The main function of an isolation transformer is to provide electrical power to the powered devices while isolating them from the power source. This isolation transformer unit contains nine outlets which deliver 230 V each and 1000 VA of power.

The diagram shown in Figure 4.4 describes the main connections between the different elements of the compact device. The components that directly require 230 V are plugged directly in the isolation transformer, while the rest of them are plugged in a power box, which provides voltages of 5.5, 6.5 and 12 V.

In the front panel, the device incorporates four independent key switches to control the state of the six lasers. One position corresponds to the open switch state where the laser cannot emit light, and the other position corresponds to the close switch state where the laser is able to be on threshold or on ON mode (depending on the TTL signal from the control board). The DCS lasers already incorporate a key, then, no further action has been required. For the NIRS-DOS lasers, the four CW NIRS-DOS lasers have been designed to be controlled by two keys, one for each cerebral hemisphere for safety reasons.

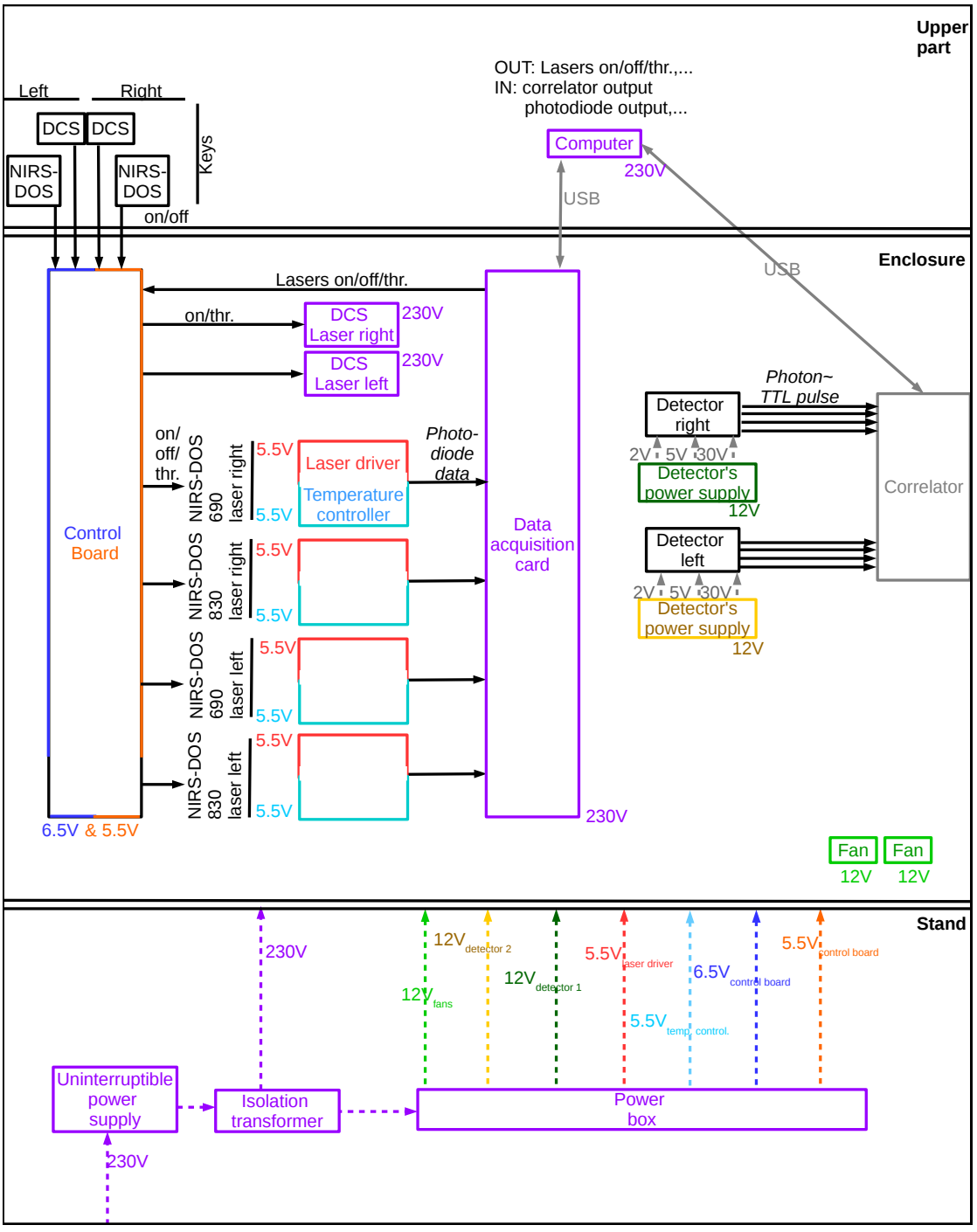

FIGURE 4.4: General diagram of the components and the electronic connections in the compact device. Three divisions are shown, the upper part of the device, the enclosure and the stand. Different colors depict different power supplies. DCS, diffuse correlation spectroscopy; NIRS-DOS, near-infrared spectroscopy-diffuse optical spectroscopy; TTL, transistor-transistor logic; thr., threshold.

Inputs		Outputs	
Key	DAQ signal send by the computer	Laser ON	LED
0	0	0	OFF
0	1	0	OFF
1	0	0	OFF
1	1	1	Green

TABLE 4.1: Diagram of transistor-transistor logic inputs and outputs for diffuse correlation spectroscopy by the control board. DAQ, data acquisition card; LED, light-emitting diode.

4.2.1 Description of the custom made electronic components

Control board: smart switch and LEDs monitoring

For safety reasons, the ability of switching on and off the lasers by an external key (one for each technique and cerebral hemisphere) is needed. Therefore, a control board has been designed and implemented in the new compact device. This control board receives different inputs from the DAQ card indicating which laser needs to be controlled (ON or OFF -for all lasers-, or on threshold -only for the CW NIRS-DOS lasers-). As outputs, the control board sends TTLs to the different lasers to power or set them on threshold state (only for the case of CW NIRS-DOS lasers) and enable them (set them to the ON state -for the case of all lasers-). It can also cut the power supply of the CW NIRS-DOS lasers. As a clarification, DCS lasers are on threshold as long as they are powered (and with the key ON), so the control board is only in charge of setting them on the ON state. Moreover, different LEDS (one for each laser), controlled by the control board, visually show if CW NIRS-DOS lasers are OFF (LEDS OFF), on threshold (LEDS in orange) or ON (LEDS in green). For the DCS, two LEDS (one for each hemisphere) show if the lasers are OFF or on threshold (LEDS OFF) or ON (LEDS in green). See Tables 4.1 and 4.2 for clarification of the input and output signals of the control board for both spectroscopy techniques.

Inputs		Outputs			
Key	DAQ signal send by the computer	Threshold	Laser ON	Power the laser	LED
0	0	0	0	0	OFF
0	1	0	0	0	OFF
1	0	1	0	1	Orange
1	1	0	1	1	Green

TABLE 4.2: Diagram of transistor-transistor logic inputs and outputs for continuous-wave near-infrared spectroscopy by the control board. DAQ, data acquisition card; LED, light-emitting diode.

Continuous-wave near-infrared spectroscopy lasers

The Electronic Workshop at ICFO designed and built under our supervision the electronics behind the four laser diodes (OZ Optics, Ottawa, Canada); two for each hemisphere. Two lasers diodes correspond to a wavelength of 690 nm and the other two of 830 nm, as mentioned previously. All lasers were set to emit around 30 μW of power when the working current was set at its threshold; while at the ON state, they were set to emit around 50 mW (as stated as the working power in the data sheet).

Each of the laser diodes was connected to two different boards: the driver laser board and the temperature controller board. The functions of these boards are to power supply the laser and to control the temperature at which it works by maintaining constant the working current, respectively. The driver laser board incorporates a transimpedance amplifier to filter, amplify and transform the photocurrent sensed by the photodiode to voltage. This voltage is an output parameter read in the data acquisition card. The temperature controller board implements a proportional integral control, which controls the Peltier by considering as a reference the temperature sensed by an negative temperature coefficient thermistor. Moreover, a second thermistor checks the temperature of the atmosphere.

Detector's power supply

The detectors require a set of voltages to be powered up. These detectors are working in the Geiger mode, so a high reverse voltage is needed to create the wide space charge region and to work over the breakdown voltage. According to the

specifications, in this case, the breakdown voltage is 30 ± 1 V. Moreover, in order to reduce the dark count rate to the minimal threshold, the detectors incorporate a temperature controller with a required voltage of 2 ± 0.05 V. Finally, 5 ± 0.25 V are needed to to transform the photocurrent into TTLs that will be sent to the correlator.

In order to simplify this set of power supplies, a printed circuit board was custom designed (HemoPhotonics S.L., Castelldefels, Spain) to transform a single input of 12 V into 2 V, 5 V and 30 V. Moreover, each power board (two units are included due to bilateral monitoring) includes four independent connectors in order to deliver the TTLs obtained from the four channels (each detector unit has four single detector photodiodes) to the correlator.

Power box

The power box is a solution to encapsulate the commuted power supplies required by the elements which need different voltages than 230 V to work. It contains five different sources needed in the device. The front panel includes a switch for every single source as well as a general switch. Additionally, each power source is protected with a fuse.

As mentioned previously, each CW NIRS-DOS laser contains a laser driver board and a temperature controller board that need 5.5 V at 1 A to properly work. Since the Peltier of the temperature controller board with its electronics typically induces relevant quantities of noise in the circuit, the two laser driver boards are powered by the same power supply, but by a different power supply from the two temperature controller boards.

A power supply of 12 V at 1.3 A is used for the two fans that ventilate the enclosure. And also two different 12 V power supplies are used for the detectors working at 4.2 A. Again, the main reason is that the fans also introduce significant noise in the circuit [87], therefore, the detectors need to be isolated from this source of noise.

4.2.2 Validating the components by phantom and *in vivo* measurements

Lasers

In order to validate the proper functionality of the lasers, the power stability was checked over time. First, a setup consisting of the laser to be tested, a multi-mode fiber, and a powermeter were used to check the power stability. A second test was considered in order to check the lasers together with the rest of the components. The setup of this second test consisted of the laser to be tested, a multi-mode fiber ending on a probe placed on the surface of a phantom made of water and lipofundin [88] (μ_a = 0.1 cm^{-1} and $\mu_s^{'}$=10 cm^{-1}), a single-mode fiber placed on the probe at a specific separation from the multi-mode fiber and connected to the detection system, the detection system consisting of one single avalanche photodiode detector and, finally, a correlator. This whole setup was covered with a black fabric to minimize the contributions from the ambient light. The probe was placed on the surface of the phantom -not inside the phantom- to mimic the semi-infinite geometry of the subject's frontal lobes to be measured in the clinics. Figure 4.5 shows the setup.

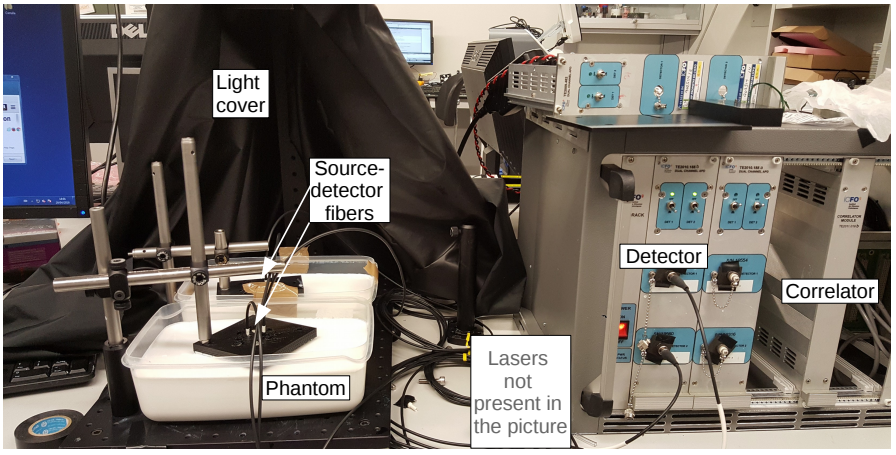

FIGURE 4.5: Setup for measuring the stability of the lasers. The setup consists of the laser to be tested, source and detector fibers, a phantom made of water and lipofundin, a detector and a correlator. Photograph courtesy of M. Garcia.

Continuous-wave near-infrared spectroscopy laser

The information of interest from the CW NIRS-DOS lasers is the number of counts per second saved through the correlator. Once the output power of the laser was

found to be stable by a powermeter during the first test, the number of counts per second were measured during a whole night ($\sim$ 16 hours) in the second test mentioned previously. Figure 4.6 shows the successful results of these tests for the left hemisphere lasers. Similar results were obtained for the right hemisphere lasers. The top figure shows the variation over time of the number of counts per second sensed on the surface of the phantom. In all lasers, the standard deviation was not higher than 2 kHz. About the photodiode signal output, despite the few observed peaks, both voltages varied in a range of 10-20 mV, which in power is equal to 0.3-0.6 mW, being insignificant. This equivalence was calculated by incorporating a potentiometer to tune both the threshold and the current, and, by plugging the photodiode voltage into an oscilloscope and the optical fiber into a powermeter.

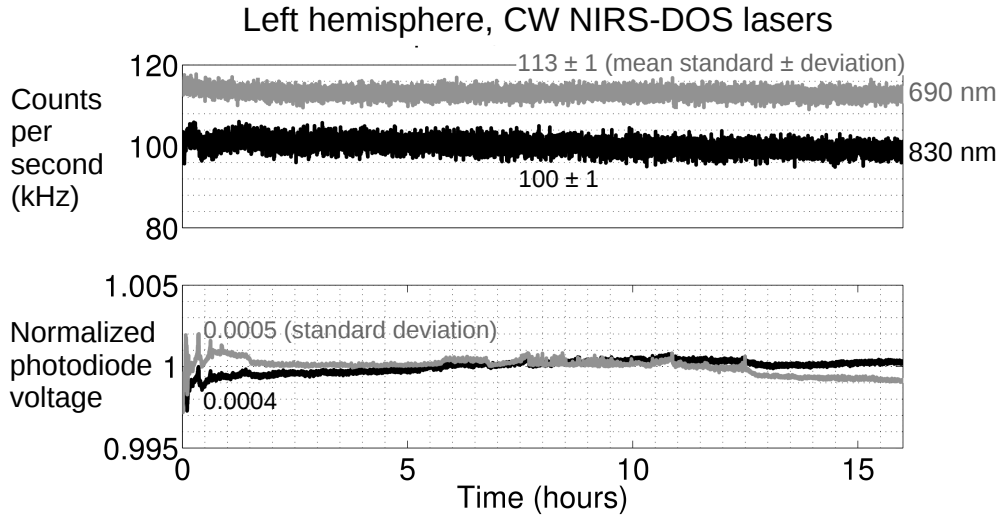

FIGURE 4.6: Stability test for the left continuous-wave near-infrared spectroscopy (CW NIRS-DOS) lasers during a whole night (grey for the 690 nm and black for the 830 nm): the top plot shows the number of counts per second sensed on the surface on the phantom over time; the bottom plot shows the normalized voltage of the photodiode of each laser. Source-detectors separation of 2.4 cm.

Diffuse correlation spectroscopy laser

Regarding the DCS lasers, the output power of the lasers was found to be stable by a powermeter during the first test. During the second test, in which lasers (one by one) were checked together with the rest of the components on a liquid phantom, the β parameter was stable in both lasers below the maximum expected value at 0.5. Also, the number of counts per second detected over time was stable

as expected (see Figure 4.7 for the results of the left hemisphere laser). Similar results were obtained for both lasers. The fluctuations on the relative flow did not exceed, in general, the 5%. Few spontaneous single drops on beta were observed during seven hours of measurements in both lasers, but no further actions have been taken.

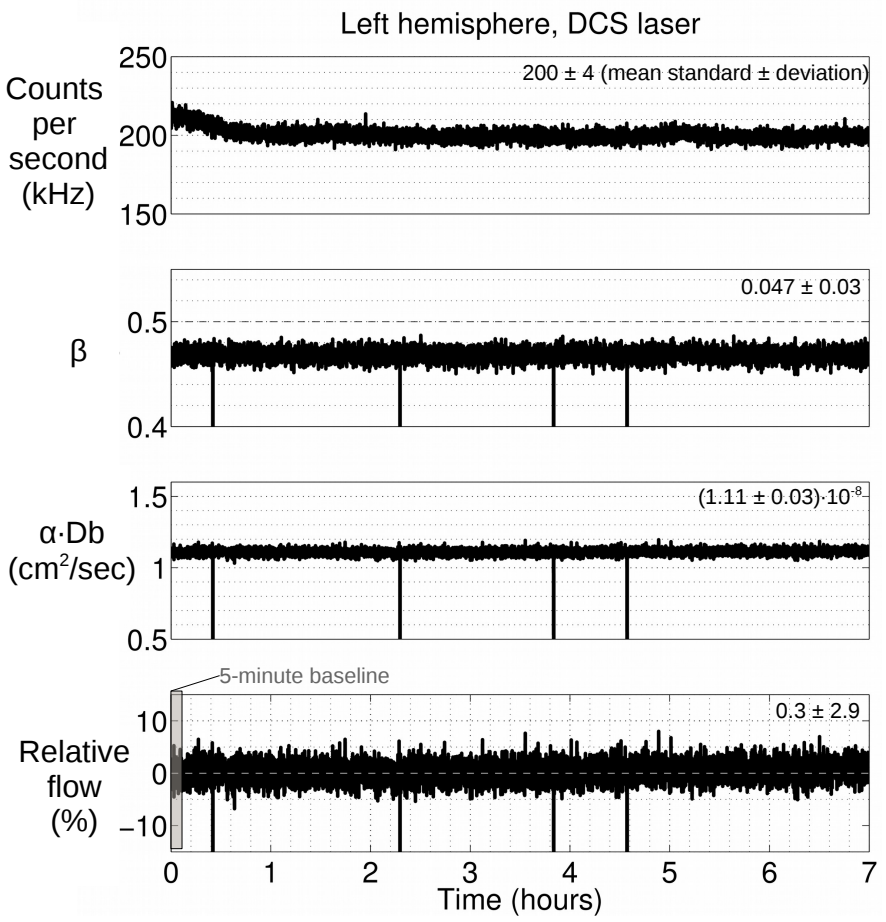

FIGURE 4.7: Stability test for the left diffuse correlations spectroscopy (DCS) laser. Number of counts per second and β stability for the DCS laser shining light at 85 mW are shown. All day long experiment. The values of fitted product of the fraction of photon scattering events per the particle diffusion coefficient (αD_b) and relative flow over the time have been calculated over lipofundin phantoms in order to quantify the degree of background noise. Source-detectors separation of 2.4 cm.

Testing the detection unit

The procedure for testing the detection system consists of two parts. First, the detector power supply have to be tested with a tester board which simulates the resistance of the detector in order to confirm that the delivered voltages are within the acceptable ranges. Second, once the detector power supply has been validated,

it is used to test the dark count rate of the detectors compared with the values provided by the manufacturer. These last measured values define the level of noise of the detector.

On the tester board, the voltages provided by the detector power supply were tested as shown on Table 4.3 for the left power supply. Even though the value of 2 V was slightly below the manufacturer's limits when the tester board was plugged in, no actions have been taken about this result. In any case, no unexpected results have been further found. Similar results were obtained for the right detector power supply.

Voltage to test	No tester board	With the tester board
2 V	2.001 V	1.917 V
5 V	4.971 V	4.941 V
30 V	30.21 V	30.210 V

TABLE 4.3: Results from the left detectors' power supply. The measurements were performed in each test point of the tester board.

Once the detector power supplies were tested, these were also tested together with each detector unit enclosed into a black box for this purpose. The output TTLs sent by each avalanche photodiode (four in total in each unit) after detecting a single photon were read by the oscilloscope in order to count the pulses with the counter function. Table 4.4 summarizes the measured dark count rate values. The numbers have been obtained by making an average of ten recorded values using the segmented mode of the oscilloscope over 30 different segments of 2 μs (the pulse width is 25 ns). Note that in the left module, values for channel 0 and channel 2 exceed the maximal range, but no further action has been taken. Note that the number of counts per second of the measurements are in a range between 20-150 kHz. Therefore, a dark count rate of 500 Hz only implies 1-7.5% of extra noise.

Detector channel		0 (Hz)	1 (Hz)	2 (Hz)	3 (Hz)
Right detector	Expected	266	341	295	439
	Obtained	268	496	311	453
Left detector	Expected	356	424	333	319
	Obtained	576	374	619	305

TABLE 4.4: Detectors' dark count rate of the two detectors used in the new compact device.

Once the different components were validated, the complete device was further tested before being used in the clinics. An arm cuff measurement is shown below

to prove the robustness of the device. Furthermore, a head-of-bed position manipulation change protocol is also shown to prove the simultaneous bilateral recording of the device on the frontal lobes.

Arm cuff measurement

The arm cuff test is one simple experiment that can be performed in the laboratory settings. A blood pressure cuff was placed around the arm bicep and an optical probe with source and detectors fibers for DCS and CW NIRS-DOS was placed over the wrist flexors (see Figure 4.8). The source-detector separation for all three lasers was 2.5 cm.

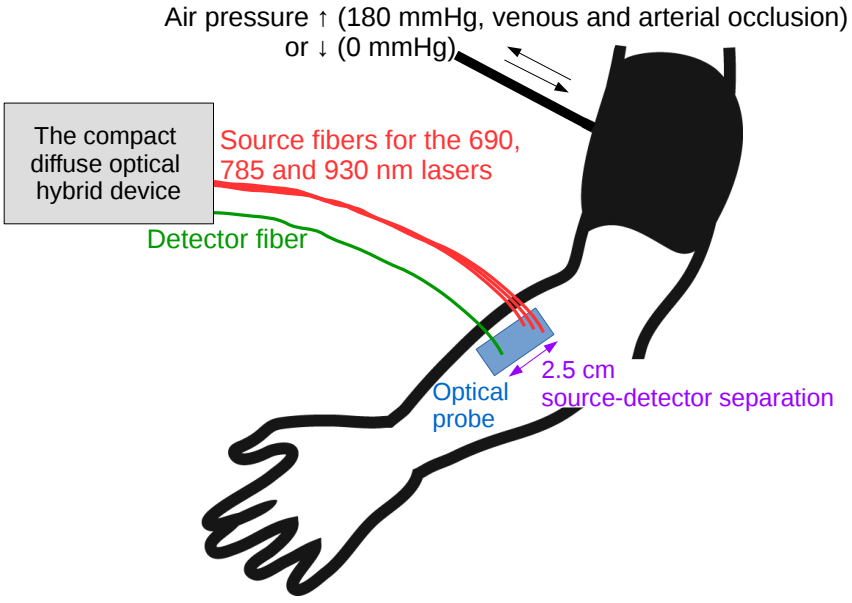

FIGURE 4.8: Blood pressure cuff occlusion setup. Figure adapted from https://catalog.niddk.nih.gov.

The protocol consisted of three minutes of baseline measurements, a quick increase of pressure up to 180 mmHg inside the arm cuff to simulate an arm tourniquet for five minutes, a quick release of the air inside the cuff, and finally, a recovery period for five minutes. The DCS collected data for three seconds, followed by the 690 nm CW NIRS-DOS laser for three seconds, and finally, the 830 nm CW NIRS-DOS laser collected data for the three last seconds. Summing it up, the hemodynamics data was acquired every nine seconds.

The results for the blood flow and Hb and HbO_2 are shown in Figure 4.9. The results are in agreement with the bibliography [89]. As expected, the blood flow drops during the arm cuffed period, and, right after the air release, an expected peak is observed just at the beginning of the recovery period. According to it, the HbO_2 is found to decrease during the arm cuffed period while the Hb increases. As expected, HbO_2 increases and Hb decreases after the release of the air inside the cuff.

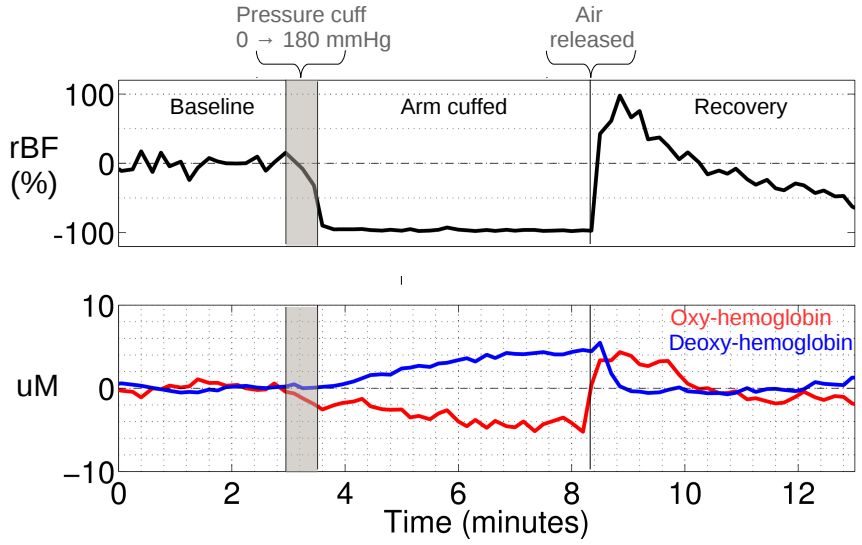

FIGURE 4.9: Hemodynamics results from the pressure cuff occlusion. rBF, relative blood flow.

Head-of-bed position changes

Another protocol to test the device should measure simultaneous, bilateral cerebral hemodynamics on the forehead as it is expected in the clinics. Since the head-of-bed challenge is the most recurrent protocol in this work, it was chosen to be the next validation protocol for the device.

The protocol consisted of five minutes of baseline measurements at supine position, a quick increase of the head-of-bed position to 30°, five minutes at 30°, a quick decrease of the head-of-bed position back to the supine position, and finally, five minutes at this last supine position. See Figure 4.10 for the visualization of the protocol and for one representative example for the blood flow and total hemoglobin concentration results. As expected, Figure 4.10 shows that the blood flow and the total hemoglobin concentration were lower in the elevated head-of-bed

position, and, when the supine position was restored, the two cerebral hemodynamic variables increased. Again, the cerebral hemodynamics data was acquired every nine seconds as for the arm cuff measurement.

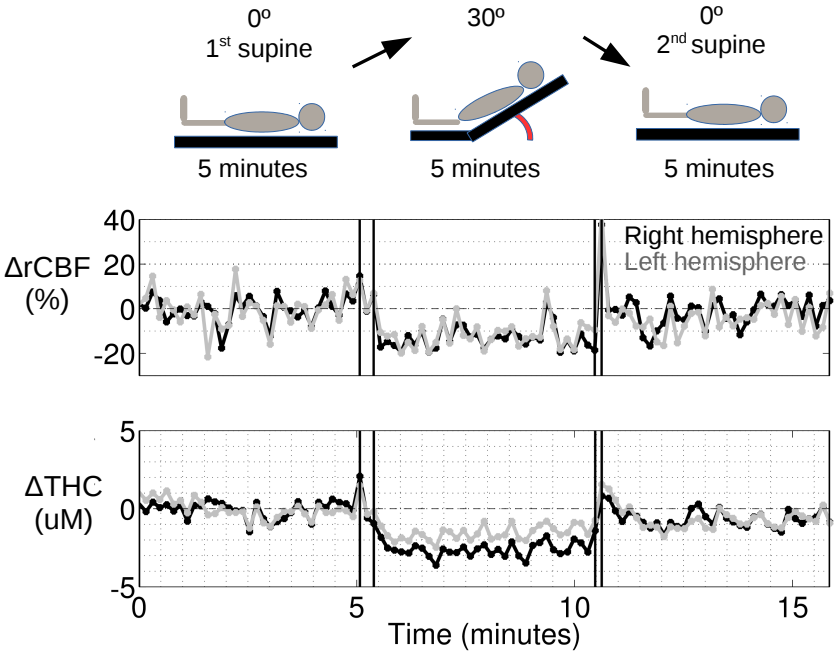

FIGURE 4.10: Frontal cerebral hemodynamics protocol (top) and results (bottom) from a representative example for the head-of-bed position challenge. ΔrCBF, relative cerebral blood flow changes; ΔTHC, total hemoglobin concentration changes.

The presented tests have been repeated to ensure a proper functionality of the device.

Part III

In-vivo clinical studies

Chapter 5

Cerebral vasoreactivity in response to a head-of-bed position challenge is altered in patients with moderate and severe obstructive sleep apnea

Hypotheses:

-The blood flow response to an orthostatic challenge in obstructive sleep apnea patients correlates to the severity of the syndrome.

-The blood flow response to an orthostatic challenge in obstructive sleep apnea patients after long-term treatment is similar to healthy subjects.

5.1 Introduction

Obstructive sleep apnea (OSA) is a highly prevalent disorder associated with sleepiness [90, 91], neurocognitive impairment, cardiovascular and cerebrovascular disease [92–95], and increased morbidity and mortality [96, 97]. Strong evidence indicates that it is an independent risk factor for ischemic stroke (with a frequency

in stroke of 30% to 80% [98–101]), including both longer time and poorer functional outcome from rehabilitation after ischemic stroke, and an increased risk of recurrence and mortality [102, 103]. The mechanisms responsible for those effects remain partly unknown. It is, however, known that repeated episodes of hypoxia-reoxygenation and increased sympathetic activity can activate different pathogenic pathways leading to oxidative stress, endothelial dysfunction, hypercoagulability and insulin resistance, which promote atherogenesis [104–107]. OSA, hence, alters the basic control mechanisms for regulating cerebral blood flow (CBF) by decreasing resting CBF, impairing autoregulation and reducing cerebrovascular reserve capacity [108]. A blunted cerebrovascular reactivity, typically defined as the CBF change in response to a vasoactive stimulus such as hypercapnia, hypoxia or breath-hold has been described in patients with OSA [109–111]. An impaired compensatory response to cerebral hypoperfusion secondary to orthostatic hypotension has also been described [112]. These alterations to normal cerebrovascular control interfere with brain function and render the brain more vulnerable to ischemic events as brain tissue is particularly sensitive to hypoxic damage and rapid reperfusion.

There are several techniques for monitoring the state of cerebral vasoreactivity (CVR; autoregulatory response to a stimulus that dilates or contracts the cerebral vasculature) in patients. However, many of these techniques are expensive, have limited availability and some are invasive and require exposure to ionizing radiation [5, 113–116]. An optimal technique for hemodynamic monitoring which is non-invasive, portable, continuous, able to measure at the point-of-care or at the bedside, and relatively inexpensive is still not present in the clinics. Recently, diffuse correlation spectroscopy (DCS) has been used to study the cerebral hemodynamic response derived from different stimulus such as acetazolamide injection in different studies [83, 117] (Chapter 7), hypercapnia [111], visual and motor stimulation [7], and orthostatic stress in a head-of-bed manipulation protocol by different authors [117–123] (Chapters 7, 9 and 10).

The key result, relevant to this work, from these mentioned studies that measured CBF response to a mild orthostatic head-of-bed challenge, is that DCS is able to observe altered CVR in the brain cortex affected by different conditions such as ischemic stroke.

Igor Blanco, in his thesis [124], assumed that DCS allows us to assess microvascular CBF at bedside in a safe and well-tolerated manner and that DCS is suitable for

studying CVR impairments of the frontal cortex in OSA syndrome. This allowed to hypothesize that, compared with non-OSA subjects, patients with OSA would have an altered microvascular cerebral flow response to a mild orthostatic head-of-bed challenge. It was also hypothesized that this impairment is related to OSA severity.

Finally, for this thesis, we were motivated by the fact that some studies have detected an improvement of the impaired cerebrovascular reactivity response after treatment with continuous positive airway pressure (CPAP) [110, 125, 126]. This allowed us to hypothesize that the CVR impairment as measured by DCS on the frontal lobes could be ameliorated by long-term CPAP treatment.

For this purpose, we used DCS to study cerebral hemodynamic responses to a head-of-bed position change in a group of patients with OSA with different levels of severity, and compared their cerebral hemodynamics to a control group of healthy subjects as shown in [124]. In addition, for this thesis, the effect of CPAP on brain hemodynamic changes was evaluated in a subgroup of patients with severe OSA after two years of CPAP treatment. And finally, a severe OSA patient was measured before and after the CPAP treatment up-to five times to learn more about an unexpected paradoxical (no change or change in the opposite expected direction) CBF response to the head-of-bed position challenge found after around two years of CPAP treatment. Partial results of this study are published in Gregori-Pla *et al* [127] and in Igor Blanco's thesis [124].

5.2 Materials and methods

5.2.1 Study design and participants

This study was conducted at a referral Sleep Unit (Department of Respiratory Medicine, Hospital de la Santa Creu i Sant Pau) in Barcelona, Spain. The study protocol was approved by the Ethical Committee of Clinical Investigation of Sanitary Health Management of the Hospital de la Santa Creu i Sant Pau (EC/11/001/1166). All participants gave their written informed consent. Two groups of subjects were enrolled: patients with OSA syndrome with an apnea-hypopnea index (AHI) ≥ 5, and healthy controls (AHI < 5). OSA severity was classified in two levels based on AHI (moderate and severe ≥ 15, and mild > 5 to

14.9 events/hour). Exclusion criteria were: being older than 80 years, receiving or having previously received CPAP treatment, presence of chronic obstructive pulmonary or neuromuscular diseases, previous ischemic stroke, and refusal to participate in the study. Anthropometric characteristics were obtained for all participants. A pre-established questionnaire was used to collect demographic variables including medical history, cardiovascular risk factors and current medication. Subjects were instructed to avoid caffeinated or alcoholic beverages during the hours prior to the study. Diagnosis of arterial hypertension (AHT) was established according to European Society of Hypertension/European Society of Cardiology criteria [128]. In a subgroup of patients with severe OSA (AHI > 30), the measurements were repeated after around two years of CPAP treatment.

5.2.2 Sleep studies

OSA diagnosis was performed by conventional full polysomnography (Siesta, Compumedics, Melbourne, Australia) or respiratory polygraphy (Embletta, Natus Medical, Middleton, USA) including, at least, the following parameters: oronasal flow (thermistor and nasal cannula), thoracoabdominal movements and pulse oximetry. The respiratory events included in the calculation of the AHI were defined according to the Spanish Sleep group [129] and the American Sleep Disorders Association guidelines [130]. The extent of self-reported sleepiness/drowsiness was analyzed using the Spanish version of the Epworth scale [131].

5.2.3 Continuous positive airway pressure titration and compliance

All patients with severe OSA received CPAP treatment [129] after the study onset and part of these severe patients were measured with our protocol again after around two years of treatment. CPAP titration was performed by an overnight polysomnography with manual CPAP titration or by autotitration devices [132]. Objective treatment compliance was determined by dividing the number of hours recorded by the CPAP devices built-in hour meter by all the nights of the treatment period. Patients with an average use time of less than four hours per night were considered non-compliant.

5.2.4 Optical methods and instrumentation

We have used the DCS unit of the hybrid device described in Section 4.1.1. A custom probe consisting of a detector fibre set at 2.4 cm from a source fibre, providing information about the cerebral cortex hemodynamics, was placed centered on the right forehead avoiding the sinuses (Figure 5.1). As mentioned, we have assumed that cerebral hemodynamic changes due to orthostatic stress are global in patients without cerebrovascular disease [118]. The microvascular blood flow index was measured continuously with a three second temporal resolution during the study.

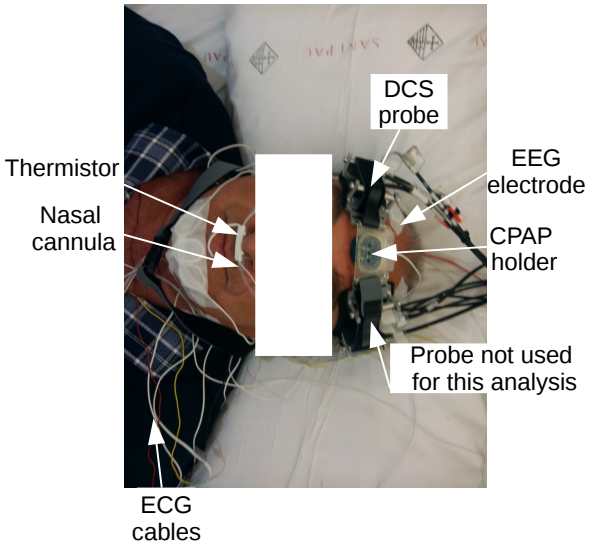

FIGURE 5.1: The optical probes for each technique (the left probe data provided no DCS information, so it is not used for this analysis) and some of the polysomnographic sensors. DCS, diffuse correlation spectroscopy; EEG, electroencephalography; CPAP, continuous positive airway pressure and ECG, electrocardiography.

For the case study with a paradoxical CBF response measured in this work, not only the microvasculature cerebral blood was measured continuously by DCS, but also the macrovasculature was measured continuously by a transcranial Doppler ultrasound (TCD) system DWL MultiDop-T digital (DWL Elektronische Systeme GmbH, Singen, Germany). Figure 5.2 shows the two optical probes placed on the forehead bilaterally on both hemispheres, as lateral as possible trying to avoid the sinuses, as well as the TCD probes. The source-detector separation of the probes was 2.5 cm. The optical data were obtained every three seconds where TCD data were obtained simultaneously every 0.1 seconds during the measurement.

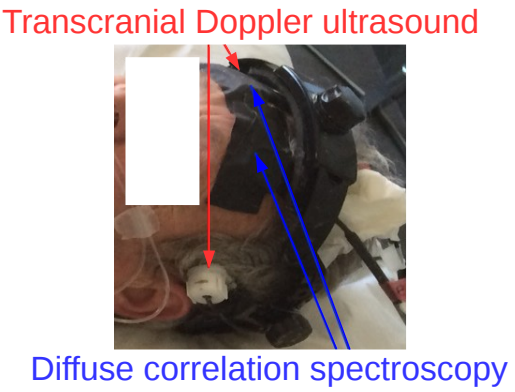

FIGURE 5.2: The placement of the optical probes and the transcranial Doppler ultrasound probes bilaterally on the forehead for the case study with a paradoxical response.

5.2.5 Head-of-bed protocol

We have used a head-of-bed position change as a mild orthostatic challenge to induce CBF changes [117–123, 133, 134] (as in Chapters 7, 9 and 10). This protocol involved changing the head-of-bed angle from the supine baseline (0°) to 30° elevation and back to the initial supine position (0°). Figure 5.3 illustrates the protocol.

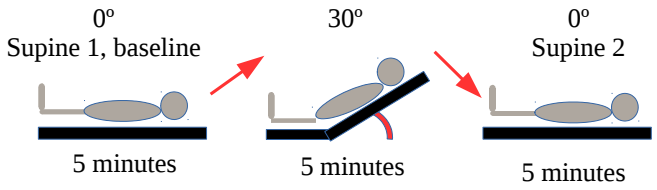

FIGURE 5.3: The protocol of the different head-of-bed position changes.

First, the subjects were asked to lie on a motorized movable bed to place and fix the optical probe on their foreheads. The protocol was started after about thirty minutes of preparation. During the experiment, the subjects were kept for five minutes in each head-of-bed position. The transitions between head-of-bed positions lasted a maximum of thirty seconds. The relative CBF (ΔrCBF) changes for each position were obtained by normalizing the continuous blood flow index obtained for each position with the mean blood flow index corresponding to the initial supine position, and averaging the normalized values corresponding to each position. To avoid bed movement artifacts, the first minute and the last minute for each position were excluded in the analysis. ΔrCBF response to the change from

the supine position to 30° is represented as $\Delta\text{rCBF}_{\text{supine}_1 \text{ to } 30°}$. ΔrCBF response when tilting back to the initial supine position considering the baseline as the initial supine position is represented as $\Delta\text{rCBF}_{\text{supine}_1 \text{ to supine}_2}$. All measurements were performed during the daytime.

5.2.6 Acetazolamide injection

One standard way to evaluate the cerebral well-being is to measure the maximal vasodilation/vasoconstriction capacity, the CVR, of the cerebral arterioles to a chemical stimuli using acetazolamide (ACZ) [34, 35]. ACZ is a selective inhibitor of the enzyme carbonic anhydrase (EC 4.2.1.1). For one case study with a paradoxical CBF response, the acetazolamide injection was used test the CVR of this patient. We have used ACZ (1g/10ml saline) as the stimulus for this CVR assessment.

5.2.7 Statistical analysis

We have expressed quantitative variables as a median and an interquartile range (median (Q1, Q3)), and categorical variables as number of cases and percentages (cases (percentages)). The Shapiro-Wilk test was used to assess for normality. The Kruskal-Wallis test (for quantitative dependent variables) or the chi-squared test (for categorical dependent variables) were used with three-way pairwise comparisons with a Bonferroni correction. The Wilcoxon signed-rank test was used to assess the differences within the same group or to check if a response was different from zero. The Wilcoxon rank-sum test (for quantitative variables) or the chi-squared (for categorical variables) test were used to assess the differences between two groups. Spearman correlation was used to assess the correlation between quantitative variables. A multiple linear model (in a forward stepwise way) was used to linearly model the relationship between a dependent variable and the different quantitative and categorical variables. $p < 0.05$ was considered as the threshold for rejection of the null hypothesis for all statistical tests. All statistical analyses were performed with R [135] using the "PMCMR" [136] package.

5.3 Results

5.3.1 Baseline characteristics

A cohort of eighty-two (n = 82) subjects conformed the population of this study. Sixty-eight (n = 68) patients with OSA (forty moderate and severe, and twenty-eight mild) and fourteen control subjects were recruited. Full polysomnography was performed on thirty-two subjects (39%) and respiratory polygraphy on fifty subjects (61%). These measurements before the CPAP treatment were performed mainly by Igor Blanco, but also by the author of this thesis.

Table 5.1 contains the demographics, clinical characteristics and sleep study results of the included subjects. Patients with moderate and severe OSA were older than the control group and more obese than both the patients with mild OSA and the controls. Gender distribution was different between groups, but pairwise comparisons with a Bonferroni correction did not provide evidence between which groups significant differences existed. Smoking, diabetes and dyslipidemia were similar among the three groups.

	Control (n=14)	Mild (n=28)	Moderate and severe (n=40)	p	Total (n=82)
Age (y.)	52.5 (40, 56)	53.5 (47.5, 61)	57 (50, 62)	0.040*[a]	54 (48, 62)
Males, n (%)	5 (36)	18 (64)	30 (75)	0.030*	53 (65)
BMI (kg/cm^2)	24 (23, 26)	28 (25, 30)	31.5 (28, 35)	< 0.001*[b]	29 (25, 33)
Epworth	7 (5, 9)	12 (8, 15)	11 (7, 14.5)	0.040*[c]	10 (6, 14)
AHT, n (%)	0 (0)	2 (7)	22 (55)	< 0.001*[b]	20 (24)
Smoker, n (%)	5 (36)	17 (61)	18 (45)	0.325	49 (60)
Diabetes, n (%)	0 (0)	3 (11)	9 (22.5)	0.094	11 (13)
Dyslipidemia, n (%)	2 (14)	5 (18)	9 (22.5)	0.440	18 (22)
AHI (n./hour)	2 (1, 4)	9 (7, 12)	48.5 (21, 78)	< 0.001*[d]	14.5 (6, 47)
Mean SpO_2 (%)	95.5 (95, 96)	95 (94, 96.5)	93 (92, 95)	< 0.001*[b]	94 (93, 96)
CT90 (%)	0 (0, 0)	0 (0, 0.3)	10 (3, 23)	< 0.001*[b]	0.4 (0, 11)
ODI4 (%)	1 (0, 3)	5 (3, 10)	44 (19, 71)	< 0.001*[b]	11 (3.5, 43)

TABLE 5.1: Demographics, clinical characteristics (top) and sleep study results (bottom). Data shown as median (interquartile range) or number of cases (percentages). Symbols indicate a statistically significant difference between the different groups ($*$), the moderate and severe group with OSA versus the control group (^{a}), the moderate and severe group with OSA versus the other groups (^{b}), the control group versus the mild group with OSA (^{c}), and all the groups pairwise (^{d}). BMI, body mass index; AHT, arterial hypertension; AHI, apnea-hypopnea index; SpO_2, arterial oxygen saturation; CT90, % of measured night sleep time when arterial oxygen saturation is lower than 90%; ODI4, number of times where arterial oxygen saturation decreases 4% due to an apnea or hypopnea; OSA, obstructive sleep apnea.

None of the control subjects were receiving chronic medications. Patients with OSA, on the other hand, were receiving chronic medications (the majority being anti-hypertensive); five received calcium channel blockers, eight angiotensin-converting enzyme inhibitor, six beta blockers, four diuretics, six angiotensin II receptor blockers, and two alopurinol.

Not all data (demographics, clinical characteristics, sleep study results and optical study results) was normally distributed. For consistency, we have opted to use statistical tests that are appropriate for non-normally distributed data.

5.3.2 Orthostatic cerebral blood flow challenge: patients versus the healthy control group

As shown in Figure 5.4, the category of the patients assigned according to OSA severity was not a statistically significant factor for ΔrCBF response to the change from the supine position to 30° ($p = 0.819$). In other words, all controls and patients showed a similar ΔrCBF response after the first HOB position change. However, when being tilted back to the supine position, the category of the patients identified according to the OSA severity was a statistically significant factor ($p = 0.004$). The control group ($p = 0.091$) and the group with mild OSA ($p = 0.227$) recovered to the initial baseline while the group with moderate and severe OSA presented a statistically significantly higher blood flow relative to the initial supine position ($p < 0.001$). The recovery response of the group with moderate and severe OSA was significantly different from that of the control group ($p = 0.003$), though the recovery response of the group with mild OSA was not significantly different from that of the control group ($p = 0.174$). These results are also extended in Igor Blanco's thesis [124].

5.3.3 Association between sleep study results, demographics, clinical characteristics, and the cerebrovascular response

No statistically significant correlations were found between $\Delta\text{rCBF}_{\text{supine}_1 \text{ to } 30°}$ and any of the sleep study results, demographics or clinical characteristics.

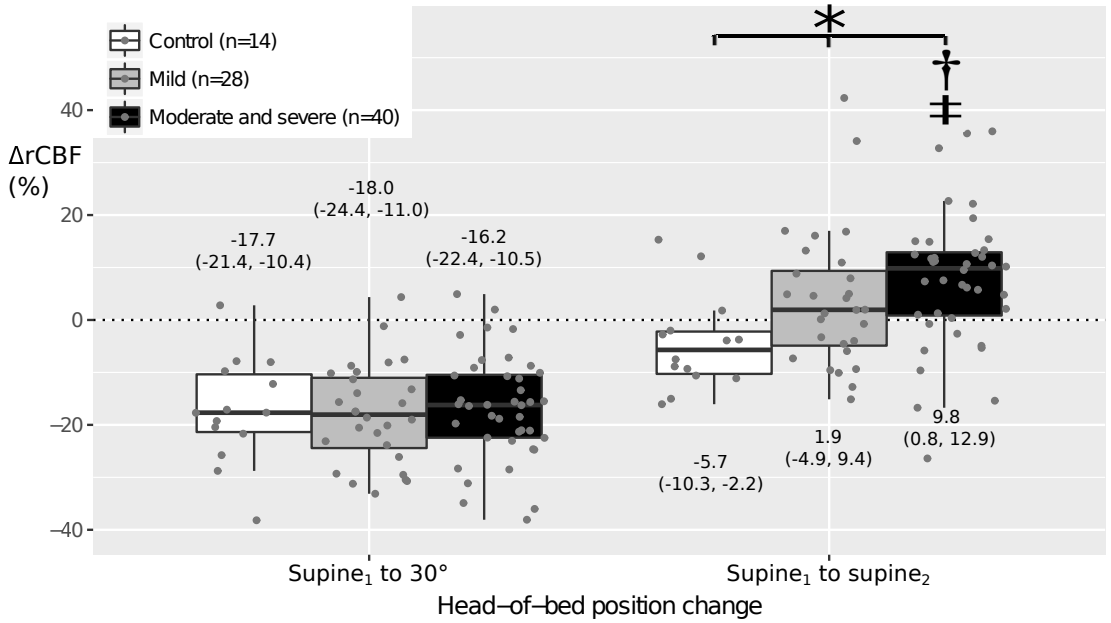

FIGURE 5.4: ΔrCBF response to orthostatic stress induced by a mild head-of-bed position change for the different OSA severity groups (moderate and severe, and mild) and the control group.

Measured mean data points for each patient and each head-of-bed position change, and classic boxplots for each group and each head-of-bed position change are shown. Labels show the median (interquartile range) for each group and each head-of-bed position change. Symbols indicate a statistically significant difference between the different groups (*), the group versus the control group (†), and the group versus the baseline (‡). ΔrCBF, relative cerebral blood flow; OSA, obstructive sleep apnea. This figure is published at [127], in which I have the copyright to the published content.

For all subjects measured, a positive statistically significant Spearman correlation ($p = 0.007$, Table 5.2) was found between $\Delta rCBF_{supine_1 \text{ to } supine_2}$ and AHI, and a negative significant correlation was found between $\Delta rCBF_{supine_1 \text{ to } supine_2}$ recovery and mean arterial oxygen saturation (SpO_2) sleep night value ($p = 0.002$). Other positive relevant correlations were between $\Delta rCBF_{supine_1 \text{ to } supine_2}$ and % of total sleep time with SpO_2 lower than 90% (CT90) ($p = 0.005$), $\Delta rCBF_{supine_1 \text{ to } supine_2}$ and 4% oxygen desaturation index (ODI4) ($p = 0.048$), and $\Delta rCBF_{supine_1 \text{ to } supine_2}$ and body mass index (BMI) ($p = 0.005$). Age was not significantly correlated to $\Delta rCBF_{supine_1 \text{ to } supine_2}$ ($\rho_{Spearman} = 0.15$, $p = 0.199$). Excluding the control group, only mean SpO_2 was found to be correlated to $\Delta rCBF_{supine_1 \text{ to } supine_2}$ ($\rho_{Spearman} =$ -0.28, $p = 0.023$).

$\rho_{Spearman}$ (p)	ΔrCBF$_{\text{supine}_1 \text{ to supine}_2}$ (%)	Mean SpO_2 (%)	AHI (n/hour)	ODI4 (%)	CT90 (%)
Mean SpO_2 (%)	-0.34 (0.002)				
AHI (n/hour)	0.30 (0.007)	-0.58 (<0.001)			
ODI4 (%)	0.22 (0.048)	-0.57 (<0.001)	0.92 (<0.001)		
CT90 (%)	0.31 (0.005)	-0.76 (<0.001)	0.85 (<0.001)	0.81 (<0.001)	
BMI (kg/cm^2)	0.31 (0.005)	-0.53 (<0.001)	0.57 (<0.001)	0.56 (<0.001)	0.59 (<0.001)

TABLE 5.2: Correlations with optical study results, sleep study results and demographics of all subjects measured. All correlations are statistically significant. Spearman correlations shown. ΔrCBF, relative cerebral blood flow; SpO_2, arterial oxygen saturation; AHI, apnea-hypopnea index; ODI4, number of times where arterial oxygen saturation decreases 4% due to an apnea or hypopnea; CT90, % of measured night sleep time when arterial oxygen saturation is lower than 90%; BMI, body mass index. This table is published at [127], in which I have the copyright to the published content.

When performing a multiple linear model with $\Delta rCBF_{supine_1 \text{ to } supine_2}$ as the dependent variable versus the different sleep study results, demographics and clinical characteristics as the independent variables, mean SpO_2 was the independent variable whose inclusion gave the most statistically significant improvement of the fit with r^2_{adj} (percentage of the response variable variation that is explained by a linear model) of 0.12 and a slope (β) of -2.02. No other secondary variables (AHI, natural logarithm of AHI, age, gender, smoking status, BMI, AHT, diabetes, dyslipidemia, CT90, ODI4 or Epworth scale) improved the model to a statistically significant extent. A second multiple linear model was performed excluding the control group. Again, a model with $\Delta rCBF_{supine_1 \text{ to } supine_2}$ as the dependent variable and mean SpO_2 as the independent variable was found with r^2_{adj} of 0.09 and a slope (β) of -1.71.

5.3.4 Cerebral vasoreactivity in obstructive sleep apnea patients after long-term continuous positive airway pressure treatment

Thirteen (n = 13) patients with severe OSA were recruited again after 2.3 (2.0, 2.4) years of CPAP treatment. All the patients that were recruited again had good CPAP treatment compliance of 6.8 (5.3, 7.0) hours per night. Mean CPAP pressure was 10 (8-10) mmHg. Their first use of CPAP corresponded with the day after the first optical measurement. The same protocol (the HOB position change) used in the first recruitment was performed again. The remaining patients treated with CPAP were excluded due to their refusal to participate in the second part of the study. None of the patients changed their condition with respect to diabetes, dyslipidemia or other relevant cardiovascular conditions (e.g. none had a stroke) during the CPAP treatment. The weight differences before the treatment and after two years were not statistically significant (p=0.787) either. One patient changed from being non-hypertensive to being hypertensive together with the start of hypertensive treatment.

Table 5.3 contains the pre-treatment demographics, clinical characteristics, and the sleep study results of the subgroup of patients with severe OSA recruited after two years of CPAP treatment compared to the rest of the group with severe OSA measured one time, and to the complete severe OSA group. No statistically significant differences between demographics, clinical characteristics, or sleep study

results were found. $\Delta rCBF_{supine_1 \text{ to } supine_2}$ was not statistically significantly different between the patients with severe OSA remeasured and the patients measured one time (p = 0.053).

	Severe OSA measured one time (n=15)	Severe OSA remeasured (n=13)	p	Severe OSA total (n=28)
Age (y.)	61 (53.5, 63)	57 (53, 63)	0.764	58 (53, 63.3)
Males, n (%)	12 (43)	10 (36)	0.871	22 (79)
BMI (kg/cm^2)	32 (30, 38)	33 (31, 36)	0.964	33 (30, 36)
AHT, n (%)	9 (32)	7 (25)	0.768	16 (57)
Epworth	11 (3,14)	14 (9, 15)	0.267	11.5 (7.5, 15)
AHI (n./hour)	75 (43, 92)	73 (47, 80)	1	73.5 (47, 87)
Mean SpO_2 (%)	93 (92, 94)	92 (90, 94)	0.273	93 (91, 94)
CT90 (%)	14 (9, 26)	23 (11, 38)	0.279	16 (9, 27)
ODI4 (%)	55 (36, 76)	69 (46, 74)	0.525	63.5 (41, 75)

TABLE 5.3: Pre-CPAP treatment demographics, clinical characteristics (top) and sleep study results (bottom) of the subgroup with severe OSA remeasured after two years of CPAP treatment, the subgroup with severe OSA measured one time, and all the group with severe OSA. Data shown as median (interquartile range) or number of cases (percentages). BMI, body mass index; AHT, arterial hypertension; AHI, apnea-hypopnea index; SpO_2, arterial oxygen saturation; CT90, % of measured night sleep time when arterial oxygen saturation is lower than 90%; ODI4, number of times where arterial oxygen saturation decreases 4% due to an apnea or hypopnea; OSA, obstructive sleep apnea; CPAP, continuous positive airway pressure treatment. This figure is published at [127], in which I have the copyright to the published content.

The $\Delta rCBF_{supine_1 \text{ to } 30^\circ}$ for the group with severe OSA remeasured was again similar to two years before (p = 0.893). Figure 5.5 shows, in contrast, that after a head-of-bed change from the supine position to 30° and back to the supine position, the magnitude of $\Delta rCBF_{supine_1 \text{ to } supine_2}$ changed significantly from the pre- to post-CPAP period (p = 0.047). The pre-CPAP group with severe OSA did not recover to the baseline (p = 0.001), while the post-CPAP group with severe OSA did (p = 0.094).

A full subject-wise representation of the demographics, sleep study results, clinical characteristics and optical study results of the severe patients measured before and after CPAP treatment can be found in the Appendix, Table 5.5.

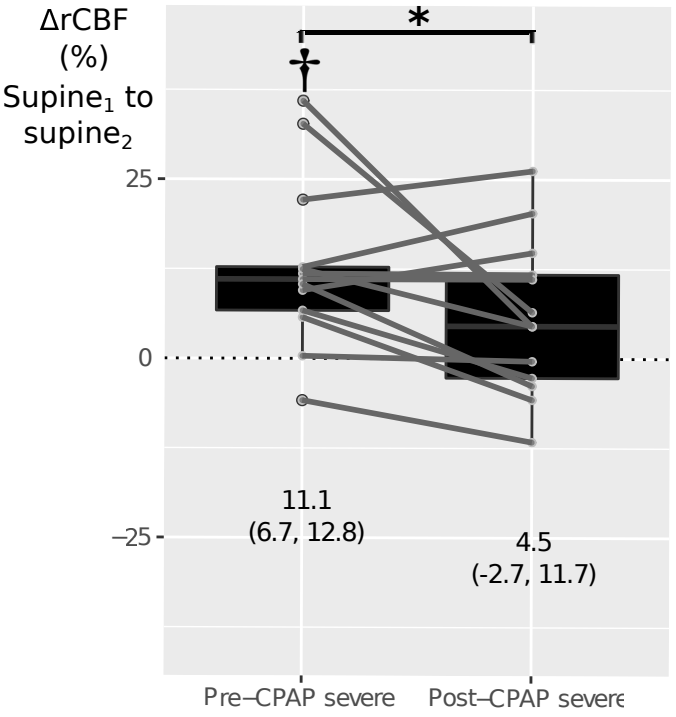

FIGURE 5.5: $\Delta rCBF_{supine_1 \text{ to } supine_2}$ recovery after a head-of-bed position change and back to the supine position in patients with severe OSA before and after long-term CPAP treatment. Measured mean data points and classic boxplots are shown. Median (interquartile range) are shown in labels. Symbols indicate a statistically significant difference between the mean ranks (*), and from the baseline (†). ΔrCBF, relative cerebral blood flow; CPAP, continuous positive airway pressure treatment. This figure is published at [127], in which I have the copyright to the published content.

5.4 Discussion

To the best of our knowledge this is the first study that evaluates the cerebral microcirculatory vasoreactivity in response to a mild orthostatic stress in patients with OSA. The main finding is the different response of the microvascular blood flow in patients with moderate and severe OSA as compared to patients with mild OSA and healthy control subjects. In patients with moderate and severe OSA the orthostatic challenge leads to an alteration of the supine CBF upon returning to the initial HOB supine position. We found that this alteration is related to OSA severity, AHI and mean SpO_2, and that long-term CPAP treatment ameliorates this alteration.

In our study with DCS, the amount of CBF change in response to a HOB from the supine position to 30° was similar for all subjects measured, and in agreement with

previous DCS studies. Edlow *et al* [118], in healthy patients, found a response of 18 (± 1.5)% (mean(standard error)) cerebral blood flow. In ischemic stroke patients in a similar protocol, Durduran *et al* [120] obtained a change of 30 (±7)% and 25 (±7)% in the ipsi- and contra-infarct hemispheres respectively, and Favilla *et al* [119] applying the same protocol, found a change of 17 (±4.6)% and 15 (±4.6)% in the ipsi- and contra-infarct hemispheres, respectively. Considering these studies with control subjects and stroke patients, Chapters 7, 9 and 10 from this thesis, and, the results presented in this Chapter including patients with OSA, a HOB change from the supine position to 30° may be a too mild challenge to be able to observe differences in the CVR of the brains of this population.

In our study $\Delta\text{rCBF}_{\text{supine}_1 \text{ to supine}_2}$ was different between cohorts grouped by OSA severity. Patients with moderate and severe OSA presented a significantly higher blood flow than the corresponding value at the initial supine position, while the controls and the patients with mild OSA did not. This result suggests that patients with OSA might need a longer time period than five minutes in each HOB position to stabilize their hemodynamic response. This is assuming that healthy cerebral auto-regulation would, given enough time, normalize the CBF. Urbano *et al* [112] measured (by TCD) the effect of a strong orthostatic challenge (standing to squatting position) in twenty-six patients with moderate or severe OSA and twenty-eight control subjects, and showed that patients with moderate or severe OSA presented an impaired compensatory response to a strong orthostatic challenge. While the degree of change was similar between the two groups, patients with OSA had a significantly slower rate of recovery of blood pressure, cerebral blood flow velocity and cerebro-vascular conductance than the control group. However, this study did not consider the correlation between OSA severity (AHI) and the recovery time. Even though there are differences in design and protocol, the results are in accordance with our findings, showing that patients with OSA might take a longer time than healthy subjects to recover cerebral blood flow to baseline after an orthostatic stress. This hypothesis needs to be checked in future studies in which patients should stay for longer periods of time in each HOB position. Unfortunately, this is a non-trivial set-up because of potential confounders since patients often do not comply well with protocols including long resting periods.

With a similar protocol but on internal carotid artery patients, $\Delta\text{rCBF}_{\text{supine}_1 \text{ to supine}_2}$ was found to correlate with ΔMAP only in the stenosed ($\geq$ 70%) hemisphere of

fourteen (n=14) unilateral stenosis patients, but not on the non-stenosed hemisphere [117] (Chapter 7). Again, $\Delta rCBFV_{supine_1 \text{ to } supine_2}$ was found to correlate with ΔMAP only in the ipsilesional hemisphere of twenty (n=20) ischemic stroke patients, but not on the contralesional hemisphere [122] (Chapter 10). Interestingly, this correlation was not observed by cerebral blood flow velocity by TCD. This result reinforces the idea that this correlation is due to damaged cerebral vasoreactivity, and also, that DCS during a HOB challenge may be superior to TCD to be able to measure the general well-being of the brain. All in all, these studies suggest that $\Delta rCBF_{supine_1 \text{ to } supine_2}$ carries information of the CVR well-being, which is damaged in these patients.

Other studies have looked at the CVR in patients with OSA with conflicting results. Busch *et al* [111], who also used DCS, found that children with OSA and snorers have a blunted CBF response to hypercapnia during wakefulness compared to a control group. Placidi *et al* [137] used a breath-holding test finding a reduction of CVR in a group of patients with severe OSA when compared to controls. In contrast to these two studies, Foster *et al* [138] and Ryan *et al* [139] did not detect differences in a small group of patients using other testing procedures for hypercapnia induced stimulation. Reichmuth *et al* [125] studied twenty patients with moderate and severe OSA and twenty controls, showing that cerebral vasodilation response to hypoxia and hypercapnia was smaller in patients versus controls. They also found that hypoxia induced vasodilation in the forearm, though not vasodilatation induced by hypercapnia, was attenuated in patients with OSA. Morgan *et al* [109] described a blunted cerebrovascular response to hyperoxic hypercapnia in a large sample of 373 participants from the Sleep Heart Health Study cohort. They observed a positive correlation between the mean level of arterial oxygen during sleep and vascular cerebral responsiveness to hypercapnia. In contrast, AHI was not statistically significantly associated with cerebrovascular carbon dioxide reactivity. Nasr *et al* [140] evaluated cerebral autoregulation (the arterial blood pressure-cerebral blood flow relationship) in patients with moderate OSA and age-matched control subjects. Cerebral autoregulation was impaired in patients with OSA during wakefulness with a strong relationship between the impairment and the number of apneas and hypopneas during sleep, suggesting that patients with the most severe OSA had the strongest alteration of cerebral autoregulation.

We have found significant correlations with $\Delta rCBF_{supine_1 \text{ to } supine_2}$ recovery and with both AHI and mean SpO_2, though mean SpO_2 was the best predictor when

performing a multiple linear model. Other tested predictors that did not improve this model were age, gender, smoking status, BMI, AHT, diabetes, dyslipidemia, CT90, ODI4 and Epworth scale. When considering only patients with OSA, a significant correlation with $\Delta \mathrm{rCBF}_{\mathrm{supine_1\ to\ supine_2}}$ recovery and mean SpO_2 was found again, and mean SpO_2 was the best predictor in the multiple linear model again. This result is in agreement with the hypothesis that the value of nocturnal saturation over the number of apneas and hypopneas better predicts the degree of endothelial impairment, which is one of the main factors involved in cerebral dysfunction in OSA [108]. In line with our results, other authors have described a significant correlation between cerebrovascular reactivity and nocturnal hypoxemia [110, 126].

Impaired CVR may imply impaired cerebral autoregulation, which, in turn, may contribute to the increased risk of stroke in patients with OSA through two physiopathological pathways: an increased vulnerability to drops in arterial blood pressure leading to ischemia in the brain, and, an excess of flow in vessels in the brain during surges in arterial blood pressure leading to capillary damage [141]. In addition, impaired cerebral autoregulation might contribute to the poorer neurological outcome that has been reported in stroke patients with associated OSA [102].

After around two years of CPAP treatment, thirteen patients with severe OSA were measured again and CVR was shown to have normalized. In general, no significant clinical parameters nor medication were changed during this period. Even though only a small group of patients was measured again, other studies support a recovery of CVR due to CPAP treatment. Reichmuth *et al* [125] found that hypoxic vasodilation improved after twelve months of CPAP treatment. Prilipko *et al* [126] in twenty-three patients with moderate or severe OSA using a breath-holding stimulus and functional magnetic resonance imaging, found that the CVR of the thalamus was increased after two months of CPAP treatment, while it decreased in patients with sham CPAP. Foster *et al* [110] recruited eight patients with severe OSA who went through isocapnic hypoxia. Cerebral blood flow velocity response was significantly lower in patients than in control subjects, though the response was similar between patients with OSA and controls after four-to-six weeks of CPAP treatment. Taken together, these results support the claim that OSA related impairment in cerebrovascular function is reversible, at least partly, with treatment.

5.4.1 A case study over long period for one patient with two following paradoxical responses after treatment

One of the severe OSA patients measured again after twenty-one months from CPAP treatment with good compliance presented an unexpected paradoxical behavior (no increase or decrease) after the HOB from supine to 30° as shown in Figure 5.6.

Due to the this unexpected finding after treatment (but not before), this patient was further measured up-to five times in total, where in the two measurements after treatment the response was paradoxical, but in the last two measurements the response to the HOB position challenge from supine to 30° was found to normalize (to decrease from baseline) as shown in Figure 5.7. Clinical characteristics and blood biomarkers were also collected to try to understand this paradoxical response. Interestingly, iron levels and red blood cell levels were lower than the levels expected in the same period as the paradoxical responses were found. Also, during this period, the patient suffered from a weight increase of seven kilograms. However, the relations with these mentioned findings, the treatment intaken for hypertension, diabetes and dyslipidemia, together with the paradoxical response remain unclear.

The demographic and clinical characteristics of the severe OSA patient with the paradoxical response are depicted in Table 5.4.

Age (years)	61
Gender	Male
AHT	Yes
Smoker	Ex-smoker
Diabetes	Yes
Dyslipidemia	Yes

TABLE 5.4: Demographic and clinical characteristics of the severe OSA patient with an unexpected paradoxical response. BMI, body mass index; AHT, arterial hypertension.

After the two following paradoxical responses, the ACZ challenge was performed in this patient to measure the cerebral vasoreactivity response of the cerebral blood flow velocity (CBFV) measured by TCD together with the microvascular CBF in the two hemispheres (not only in the right hemisphere as performed so far for this study). Interestingly, CBF showed a bilateral and symmetric (p=0.274) response, whereas the right CBFV response by TCD showed a higher response than the

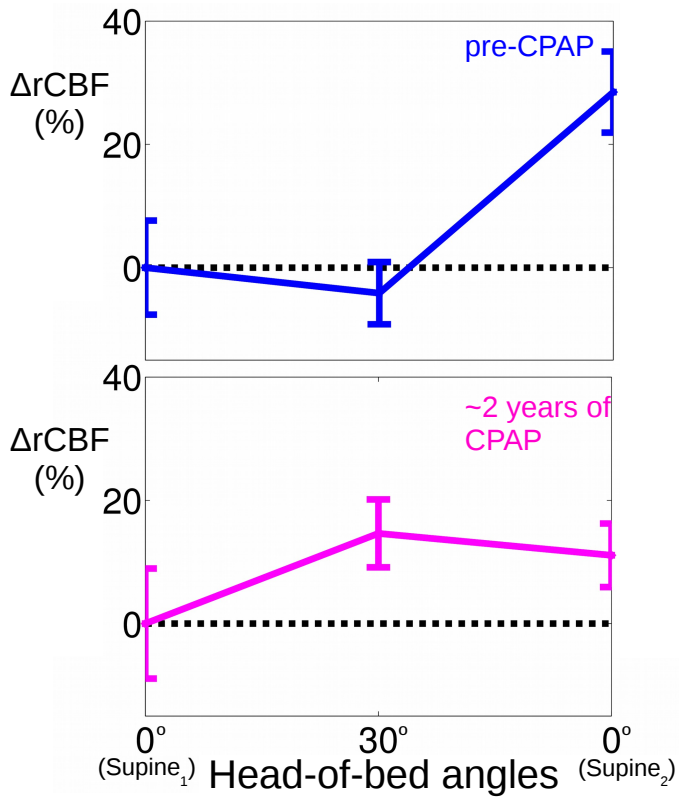

FIGURE 5.6: An expected (top) and paradoxical response (bottom) measured on a severe OSA patient before and after twenty-one months of continuous positive airway pressure (CPAP) treatment use. ΔrCBF, relative cerebral blood flow.

left CBFV response ($p<0.001$), and also, from both CBF responses ($p<0.001$) as shown in Figure 5.8. The mean of the last five minutes in all the measurements was statistically significantly different ($p<0.001$) from the baseline (considered as the five minutes before the injection). These results are interesting because the CBFV and CBF responses are not symmetric between hemispheres. It could be hypothesized that the left hemisphere does not autoregulate as well as the right hemisphere at the macrocirculation level, and moreover, that the CVR at the microcirculation level autoregulates properly. Relevantly, different studies [117, 119, 142] and also the results in Chapter 7 show that macrovascular CBFV responses and microvascular CBF responses (by DCS) are found to differ under pathological conditions.

Although the paradoxical response has long been described in around one quarter of patients with acute ischemic stroke and also in other types of brain injury, little is known about its pathophysiological mechanism and clinical implications [119, 120]. Paradoxical reactions may occur in healthy subjects and have been even interpreted as a normal physiologic response by some authors (from Ref.

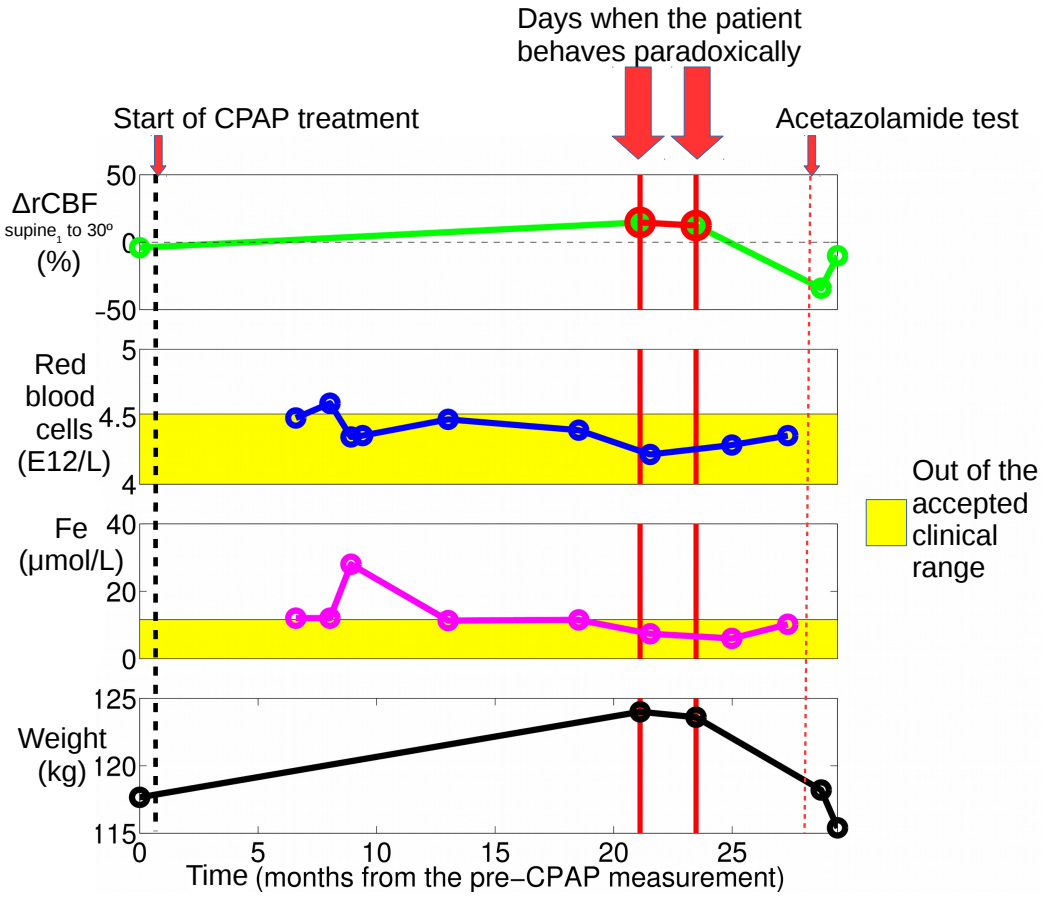

FIGURE 5.7: Clinical and blood sample characteristics out of the accepted clinical range along thirty months for the case study with a paradoxical response. Fe, iron; CBF, cerebral blood flow; CPAP, continuous positive airway pressure.

[118], unpublished observation, 2010). However, the higher incidence in brain-injured populations suggests that it most probably corresponds to a pathogenic mechanism, and moreover, the higher incidence of paradoxical responders with a worst functional outcome found in stroke patients in Chapter 9 reinforces this idea. Some authors have suggested a mechanism of excessive autoregulation of arterial vessels in response to maximal stimulation when cerebral perfusion pressure (CPP) changes abruptly due to a hyper-reactivity state to their sympathic and parasympathic receptors [143]. This would result in an excessive vasodilatation when CPP is reduced as a consequence of head-up tilt and an excessive vasoconstriction when CPP increases after HOB lowering. This "hyperautoregulation" or paradoxical rise in CBF as CPP drops has been demonstrated in experimental studies as a variation of the classic pattern of CBF-pressure autoregulatory curve [144].

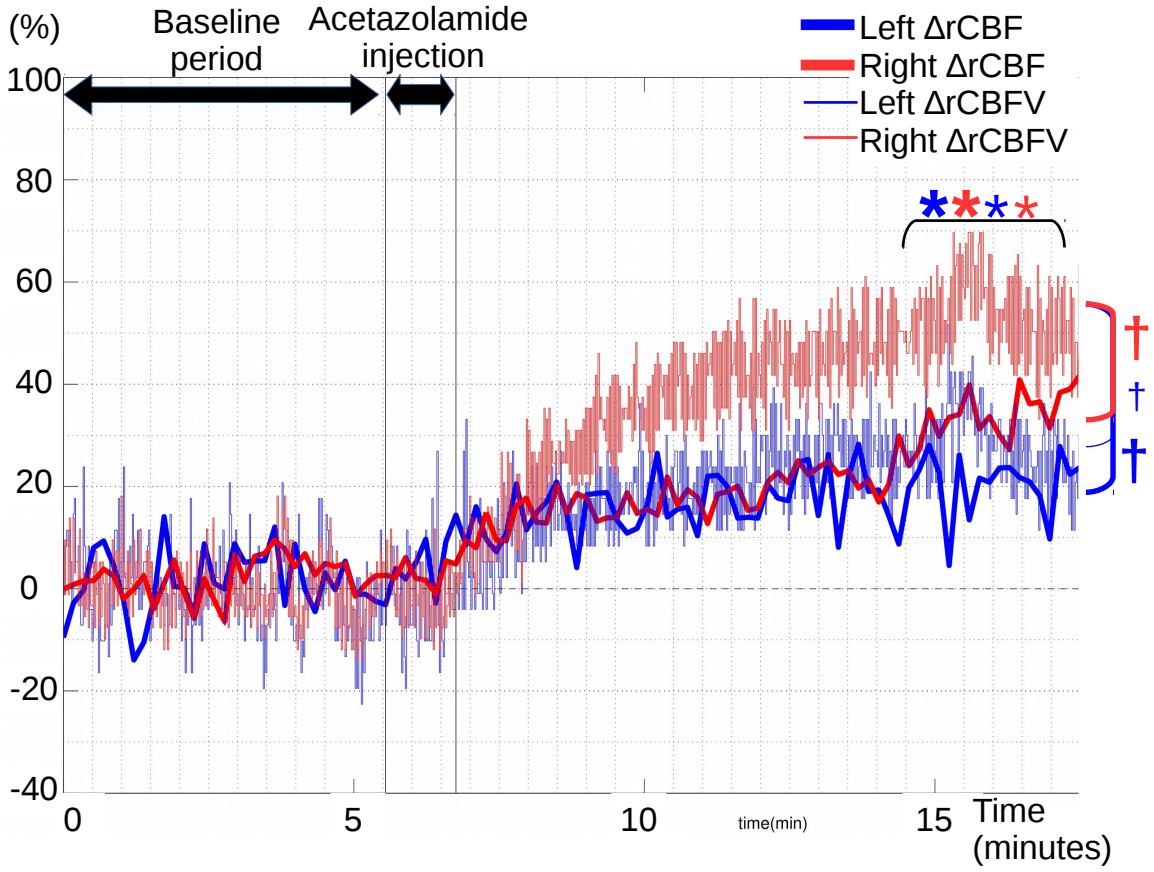

FIGURE 5.8: Simultaneous measurement of cerebral blood flow velocity (CBFV) and microvascular cerebral blood flow (CBF) during and after acetazolamide injection for one patient with a paradoxical response found. Symbols indicate a statistically significant response from baseline (∗) and from the right CBFV response (†).

5.4.2 Overall comments about the study

Our study has some potential limitations that should be taken in consideration. First, measurements were performed at different times during hospital working hours (74% of the patients in the afternoon) without considering the fact that it has been suggested that CVR diminishes in the morning in patients with OSA after the continuous stress of night hypoxemia and hypercapnia. In line with this, Placidi *et al* [137] found significantly lower values of breath-holding index in the morning than in the afternoon in patients with OSA by TCD. However, considering that the majority of moderate and severe subjects (70%) were measured in the afternoon, this factor is not expected to affect our results. This important aspect should be monitored in future studies.

Second, the study included patients with different OSA severity and control subjects that were not completely matched in demographics and clinical characteristics. In particular, BMI and AHT were significantly higher in patients with moderate and severe OSA. Chronic hypertension is involved independently in the production of reactive oxygen species, inflammation, endothelial dysfunction and vasodilatation impairment; therefore, the association of OSA, with a frequency in resistant hypertension of more than 80% [145], and hypertension could have an accumulative effect [146]. Considering that 91% of AHT subjects were patients with moderate and severe OSA, it is difficult to discriminate this effect in our dataset. Even though differences on age were found between OSA severity groups, Edlow *et al* [118] found no difference in $\Delta \text{rCBF}_{\text{supine}_1 \text{ to supine}_2}$ depending on age. In addition, while gender effect is not clear in our results, Edlow *et al* found it to be a significant effect. However, relevantly, when performing the multiple linear model for $\Delta \text{rCBF}_{\text{supine}_1 \text{ to supine}_2}$ as the dependent variable versus the different sleep study results, demographics, and clinical characteristics, only mean SpO_2 was identified as the best significant factor. Neither AHT, BMI, age nor gender improved the model. As mentioned previously, the same results were found when the analysis was only performed in patients with OSA.

Third, the partial pressure of carbon dioxide (PCO_2) was an unexplored relevant factor since the majority of the PCO_2 baseline values for the subjects included were not obtained. PCO_2 was not monitored during the orthostatic challenge. In any case, the literature shows that while hypoxemia is a factor that clearly modifies the cerebral autoregulation in patients with OSA, the results of the few studies that analyze cerebrovascular response to hypercapnia are contradictory [109, 112, 125]. The role of hypercapnia in the cerebrovascular response in patients with OSA needs to be investigated further in future studies.

Fourth, the use of respiratory polygraphy may underestimate the apnea or hypopnea index since the analysis does not distinguish between the awake and sleep periods, while polysomnography considers only the sleep periods. Moreover, respiratory polygraphy does not include respiratory events that lead to arousal without a significant desaturation of the arterial blood. This underestimation would not affect the patients currently labeled as being with severe OSA; instead, it would affect patients listed as moderate who should have been listed as being severe. However, since we have considered patients with moderate and severe OSA together for the analysis, this underestimation will not affect our main findings.

Finally, when looking at the CPAP effect, only a small group of patients, though with the strength of an excellent CPAP compliance, were reviewed. These results need to be confirmed in the near future in a large and clinically representative sample of patients with OSA. These results were published partly in Gregori-Pla *et al* [127] and in Igor Blanco's thesis [124].

5.4.3 Conclusions

In summary, this study shows an alteration of the cerebrovascular reactivity at the level of the microvasculature in response to a mild orthostatic challenge in patients with moderate and severe OSA. This impairment, which is dependent on OSA severity, is an important pathogenetic link between OSA and vascular disease. The alteration in vascular regulation could negatively impact tissue perfusion during acute episodes of apnea, and indicate a potential greater vulnerability of the cerebral vasculature to stroke injury. For this study we have used a non-invasive technique, DCS, which enables continuous bedside monitoring of CBF and, a mild orthostatic head-of-bed challenge. The orthostatic stress stimulus mimics a daily action without the need for pharmacological agents, hypoxemia or hypercapnia exposures, and with minimal patient collaboration. We propose that this stimulus together with diffuse correlation spectroscopy can be a relatively simple and easy biomarker protocol for identifying subclinical alterations of cerebrovascular reactivity. Chapters 7, 9 and 10 support this idea. Finally, we found that cerebral vasoreactivity may have been improved with CPAP treatment in a small group of highly compliant patients, suggesting that the impairment in cerebrovascular function may be reversible, at least in part, with treatment. Further studies will be needed to better define the importance of this finding.

5.5 Appendix

ID	Positional change	Male (yes=0)	Patient type	AHI (n./hour)	Mean SpO_2 (%)	ODI4 (%)	CT90 (%)	Smoking (current/ exsmoker=1)	Age (y.) pre-CPAP	Height (m)	Weight pre-CPAP (Kg)	Weight post-CPAP (Kg)	AHT pre-CPAP (yes=1)	AHT post-CPAP (yes=1)	DM (yes=1)	DLP (yes=1)	Time under treatment between measurements (y.)	Epworth pre-CPAP	Epworth post-CPAP	ΔrCBF (%) pre-CPAP	ΔrCBF (%) post-CPAP
3	0º to 30º	0	severe	99.5	92	73.7	22.8	0	63	1.59	94.00	84.80	1	1	1	0	2.5	15	2	-24.64	-18.48
3	30º to 0º	0	severe	99.5	92	73.7	22.8	0	63	1.59	94.00	84.80	1	1	1	0	2.5	15	2	32.74	6.48
5	0º to 30º	1	severe	74.2	94	78.4	10.8	1	54	1.76	86.20	83.00	1	1	0	0	2.4	7	0	-21.3	-28.91
5	30º to 0º	1	severe	74.2	94	78.4	10.8	1	54	1.76	86.20	83.00	1	1	0	0	2.4	7	0	0.36	-0.36
6	0º to 30º	1	severe	72.8	89	69.8	38	0	73	1.61	90.00	94.00	1	1	0	0	2.4	6	0	4.93	-15.93
6	30º to 0º	1	severe	72.8	89	69.8	38	0	73	1.61	90.00	94.00	1	1	0	0	2.4	6	0	9.52	14.77
8	0º to 30º	1	severe	91.1	86	88	58.6	1	49	1.81	152.00	154.80	0	0	0	0	2.5	23	6	-10.59	-13.74
8	30º to 0º	1	severe	91.1	86	88	58.6	1	49	1.81	152.00	154.80	0	0	0	0	2.5	23	6	10.39	-3.81
9	0º to 30º	0	severe	96.2	90	85.3	41.7	0	47	1.6	79.40	78.80	0	0	0	0	2.4	20	10	-7.64	-1.51
9	30º to 0º	0	severe	96.2	90	85.3	41.7	0	47	1.6	79.40	78.80	0	0	0	0	2.4	20	10	11.85	11.72
11	0º to 30º	1	severe	79.8	92	66.2	23.1	1	68	1.73	100.00	98.40	0	1	1	1	2.3	9	6	-16.17	-16.67
11	30º to 0º	1	severe	79.8	92	66.2	23.1	1	68	1.73	100.00	98.40	0	1	1	1	2.3	9	6	12.47	4.54
13	0º to 30º	1	severe	78.1	93	72.4	16.9	1	58	1.81	114.00	112.20	1	1	0	0	2.3	9	4	-28.33	-30.13
13	30º to 0º	1	severe	78.1	93	72.4	16.9	1	58	1.81	114.00	112.20	1	1	0	0	2.3	9	4	6.71	-2.69
25	0º to 30º	1	severe	46.1	96	45.9	5.2	1	57	1.65	89.00	100.00	1	1	0	1	1.7	15	8	-16.25	-10.09
25	30º to 0º	1	severe	46.1	96	45.9	5.2	1	57	1.65	89.00	100.00	1	1	0	1	1.7	15	8	22.15	26.2
27	0º to 30º	1	severe	71.2	86	70.5	58.3	1	53	1.58	89.00	90.00	1	1	0	1	2.0	23	13	-2.85	-8.1
27	30º to 0º	1	severe	71.2	86	70.5	58.3	1	53	1.58	89.00	90.00	1	1	0	1	2.0	23	13	35.96	4.51
30	0º to 30º	1	severe	34.2	91	35.4	18.7	1	57	1.78	98.20	104.60	1	1	0	1	2.0	15	8	-15.64	-2.52
30	30º to 0º	1	severe	34.2	91	35.4	18.7	1	57	1.78	98.20	104.60	1	1	0	1	2.0	15	8	12.76	20.29
33	0º to 30º	1	severe	46.5	94	42.6	8.6	0	47	1.79	82.00	83.40	0	0	0	0	2.0	11	5	-21.09	-20.87
33	30º to 0º	1	severe	46.5	94	42.6	8.6	0	47	1.79	82.00	83.40	0	0	0	0	2.0	11	5	5.75	-5.75
45	0º to 30º	0	severe	33.8	95	19.3	0.8	0	67	1.6	66.00	67.20	0	0	0	1	1.8	6	6	-31.14	-32.84
45	30º to 0º	0	severe	33.8	95	19.3	0.8	0	67	1.6	66.00	67.20	0	0	0	1	1.8	6	6	-5.83	-11.64
47	0º to 30º	1	severe	71.5	91	64	31.4	1	62	1.66	118.00	115.00	1	1	1	1	1.7	14	4	-1.73	14.62
47	30º to 0º	1	severe	71.5	91	64	31.4	1	62	1.66	118.00	115.00	1	1	1	1	1.7	14	4	11.06	11.08

TABLE 5.5: Demographics, sleep study results, clinical characteristics, and optical study results of the severe obstructive sleep apnea patients measured before and after continuous positive airway pressure treatment. AHI, apnea-hypopnea index; SpO_2, arterial oxygen saturation; ODI4, number of times where arterial oxygen saturation decreases 4% due to an apnea or hypopnea; CT90, % of measured night sleep time when arterial oxygen saturation is lower than 90%; CPAP, continuous positive airway pressure; AHT, arterial hypertension; DM, diabetes mellitus; DLP, dyslipidemia; ΔrCBF, relative cerebral blood flow.

Chapter 6

Characterization of the microvascular cerebral blood flow response to obstructive apneic events during night sleep

Hypothesis:
Diffuse correlation spectroscopy is able to characterize the microvascular CBF response to each apnea event with a sufficient contrast-to-noise ratio to reveal its dynamics.

6.1 Introduction

Obstructive sleep apnea (OSA) is defined, as in Chapter 5, by a repetitive interrupted breathing during sleep because of upper airway obstruction with simultaneous respiratory effort, terminated by arousals and, relevantly, in most cases accompanied by transient dips in arterial oxygen saturation. Symptoms of OSA include snoring, daytime sleepiness, morning headache, sexual dysfunction, fatigue, depression and behavioral disorders [147, 148]. OSA is also an independent predictor for cardiovascular disorders [97, 149–152] such as ischemic stroke. Relevant factors involved in these impairments are thought to be the repetitive intermittent hypoxemia, the sleep fragmentation, the increased sympathetic activity, and the periodic cerebral hemodynamic changes [105, 153, 154].

Previously, different works have studied the apnea-induced changes of the macrovascular cerebral blood flow velocity (CBFV) in the middle cerebral artery by transcranial Doppler ultrasound (TCD) [113, 155–158]. Interestingly, Bålfors *et al* [113] showed that CBFV and the mean arterial blood pressure showed a biphasic pattern consisting on a gradual increase close to the apnea end followed by a sudden decrease. However, TCD cannot measure the actual microvascular cerebral blood flow (CBF) in the brain. Furthermore, TCD can directly insonate only proximal vascular segments of large arteries and only indirectly provides information about more distal vascularity [159]. Also, few studies have also used microvascular cerebral blood oxygenation measured by near-infrared diffuse optical spectroscopy (NIRS-DOS) as a surrogate [160–163]. However, neither TCD nor NIRS-DOS can measure the microvascular cerebral blood flow (CBF) in the brain, which is a desirable parameter since it provides direct information about the health of the brain [164], is a key parameter to measure the oxygen metabolism [165–167] and acts as biomarker of cerebral autoregulation [168]. Because of this, we have used diffuse correlation spectroscopy (DCS), to measure microvascular, local CBF on the brain cortex of the frontal lobes at the bed-side non-invasively [5, 7]. Only one study attempted to measure night sleep changes by DCS in OSA patients [169] but individual apneic events could not be characterized, presumably due to technical limitations.

In this study, we have used a DCS device to characterize and evaluate the individual apnea-induced hemodynamic changes of the microvascular cerebral blood flow measured continuously in patients with severe OSA simultaneously using DCS and polysomnography. The results of this study are published in Zirak *et al* [170], in which I am the corresponding author.

6.2 Methods

This study was conducted at the Sleep Unit of the Department of Respiratory Medicine, Hospital de la Santa Creu i Sant Pau, Barcelona, Spain. The study protocol was approved by the local ethical committee (EC/11/001/1166). All participants gave their written informed consent.

The subjects were referred to a sleep study at the Sleep Unit because of being at a high risk of severe OSA according to the Epworth sleeping scale [131] results,

their clinical symptoms and the results of a previous home-use nocturnal pulse oximetry session [171].

The exclusion criteria were being older than 80 years, previous or current continuous positive air pressure (CPAP) treatment [129], chronic obstructive pulmonary or neuromuscular diseases, previous ischemic stroke, or refusal to participate in the study.

A pre-established questionnaire was used to collect demographic variables including their medical history, cardiovascular risk factors and current medications.

Patients were asked to arrive at the Sleep Unit at 19:00 on the study day. Caffeinated or alcoholic beverages were instructed to be avoided twenty-four hours previously to the measurement. Optical and PSG data was simultaneously acquired during the night sleep study.

The clinical technician fixed a CPAP mouth-nose mask to find the correct air pressure for preventing apneas if the obstructive apnea or hypopnea index (AHI; number of apneas and hypopneas per hour) was higher than 30 after about four hours of sleep. In other words, a split-night PSG was planned and for the subjects with split-night PSG, only the data recording of the first four hours of night sleep without CPAP was used for the analysis.

6.2.1 Overnight polysomnography

Polysomnography (Siesta Compumedics, Melbourne, Australia) sensors were wirelessly connected to the monitoring room. PSG included the recording of the oronasal flow (by a thermistor and a nasal cannula), the thoracic and abdominal movements (by a respiratory inductance plethysmography band), the heart rate (HR; by electrography chest leads and calculated from the electrocardiogram as described in [172]) and the arterial oxygen saturation (SpO_2), among other variables.

PSG data was post-processed by the sleep technicians according to the Spanish Sleep group recommendations [129]. Sleep technicians determined the start and end time points of each apneic event, identified the apnea types (i.e. obstructive apnea, hypopnea, mixed apnea, and central apnea) and calculated, among other parameters, the number of times where arterial oxygen saturation decreases 4%

due to an apnea or hypopnea (ODI4), % of measured night sleep time when arterial oxygen saturation is lower than 90% (CT90) and the AHI. From these variables, the diagnosis of OSA and the high degree of severity of these patients were confirmed or rejected after the recruitment. Due to the different pathophysiology of each type of apneic event, and for simplicity, only obstructive apneas were used for this analysis.

6.2.2 Determination of the cerebral blood flow

We have used the DCS unit of the hybrid device described in Section 4.1.1. The averaging time of the DCS measurement in each patient was adjusted from one to three seconds during the first minutes of the measurement in order to maximize the signal-to-noise ratio for the rest of the sleep measurement. In order to co-register the DCS data with the PSG variables, a transistor-transistor logic signal was generated through a digital output channel, which was fed into the PSG device and was used as a marker to synchronize DCS and the PSG variables.

The custom built optical probe was made of ninety-degree bent fibers of 2 mm of external diameter with a 2.5 cm source-detector separation. We have assumed that the hemodynamic changes in the brain are homogeneous bilaterally and, for patient comfort, we opted to fix a single DCS probe on the right forehead of the patient. The probe was located over the patient's forehead properly fixed to avoid the movement of the patient and allowing the implant/removal of the CPAP mask when necessary with the minimum possible effect on the optical measurement.

6.2.3 Group and individual analysis of cerebral blood flow, heart rate and arterial oxygen saturation apnea-induced changes

Each apneic event was characterized by the percent relative CBF change (ΔrCBF), defined as $\Delta rCBF = (\frac{BFI}{BFI_{bl}} - 1) \times 100$ where BFI_{bl} is the average of the cerebral BFI from thirty seconds before the apnea start up to thirty seconds after the apnea end. This choice for BFI_{bl} was meant to correct for slight changes in the probe position during the whole night of sleep and to account for the possible changes in the absolute CBF at different stages of sleep. A similar approach was taken to

systemic variables too, i.e. ΔrHR was defined as $\Delta rHR = (\frac{HR}{HR_{bl}} - 1) \times 100$, and ΔSpO_2 was defined as $\Delta SpO_2 = SpO_2 - SpO_{2bl}$.

In order to discard the CBF, HR and SpO_2 responses to obstructive apneic events with movement artifacts or with a low signal quality during the measurement, all responses were studied by developed methods for outlier detection [173, 174]. These allowed us to find the responses that presented higher or lower magnitude values than the majority or that exhibited a different time behavior. Each variable (CBF, HR or SpO_2) was analyzed independently. For instance, if the ΔrCBF response for one apnea was classified as an outlier, it did not imply that ΔrHR and/or ΔSpO_2 response for the same apnea were also classified as outliers. We expect that this will not cause any errors in the data analysis due to the large number of obstructive apneic events that were analyzed. The outlier detection procedure was implemented in R [135] using the "fda.usc" [174] package and the function "Outliergram" [173].

All the remaining apnea events for each variable (ΔrCBF, ΔrHR or ΔSpO_2) of all patients were averaged after removing the outliers from our database in order to visualize representative cerebral and systemic dynamics of obstructive apneas. The averaging was performed by selecting the start and the end of each obstructive apnea based on PSG measurements using the established criteria used in the clinics (see above), by calculating the ΔrCBF, ΔrHR or ΔSpO_2 traces for each apnea as explained previously, by aligning the data according to the start of each individual apnea, as illustrated in Figure 6.1 (left) and, finally, by grouping and averaging all obstructive apneas within a given range of apnea duration. Four groups were used according to apnea duration; apneas shorter than or equal to 15 seconds, apneas longer than 15 and up-to 30 seconds, apneas longer than 30 and up-to 45 seconds, and apneas longer than 45 and up-to 60 seconds. There were obstructive apneas of varying lengths in each group and, if an apnea was shorter than the full duration, it did not contribute to the remaining average. This grouping before averaging was performed since the apnea lengths vary from ten seconds up to around a minute and, even though this averaging is not perfect, grouping by duration allowed us to see more details of the apnea dynamics.

The present heterogeneity of the duration of apneas did not allow us to analyze the full duration of the single apnea induced ΔrCBF, ΔrHR or ΔSpO_2 changes. In order to do this, we have considered the apnea end as a pivot point to calculate each parameter. Also, the parameters associated to each obstructive apneic event

were considered as a function dependent on time (ΔrCBF(time), ΔrHR(time) and ΔSpO_2(time)), and then, the relative extrema of these functions along a specific time interval relative to the end of the apnea were calculated. The positive extrema are referenced as "peak" values, and the negative extrema as "drop" values. The time windows to find these extrema along the time dependent function were from -5 to 15 seconds for the first extremum on ΔrCBF (see Figure 6.1 as an example), from 0 to 15 seconds for the ΔrHR, and from 5 to 35 seconds for the ΔSpO_2. Moreover, in order to visualize the possible link between the hypoxemia present in these patients and the cerebral blood flow, also the second extremum that was outside this window was considered for ΔrCBF. These time windows were selected from the literature [113, 175] and also by visual observation of all apneas plotted together from -30 seconds to 60 seconds in order to include the majority of the peak/drop values. This analysis was performed with Matlab 2012a (Mathworks, MA, USA).

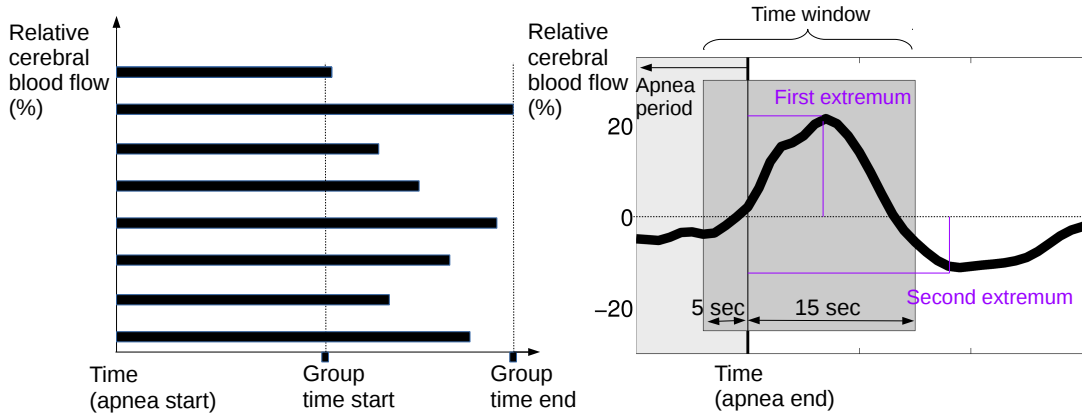

FIGURE 6.1: (Left) All individual obstructive apneas from the same duration group considering the start of the apnea as a pivot point. Apneas from the same duration group will be averaged for obtaining a canonical apnea shape for this duration group. (Right) Characterization of individual apneas, where the end of the apnea is considered as a pivot point. The light gray region indicates the apneic event. The dark gray region indicates the time window used to find the first extremum value. The first and second extrema are labeled in purple. This figure is published at [170], in which I have the copyright to the published content.

The association between the calculated ΔrCBF, ΔrHR and ΔSpO_2 extrema to apnea duration was analyzed by adjusting a linear mixed-effect model [176]. The patient identifier was the random factor, the apnea duration parameter was the fixed effect and the positive and negative extrema (previously defined as "peaks" and "drops") of the apnea time response on variables ΔrCBF, ΔrHR and ΔSpO_2

were the predictors. The linear mixed-effect analysis was carried out in the R programming language [176] using the "nlme" package. The associations between the calculated means of ΔrCBF, ΔrHR and ΔSpO_2 extrema responses for each patient with age, gender and body mass index (one by one) were analyzed by adjusting simple linear models. For these models, the demographic parameters were the fixed effects and the mean calculated extrema were the predictors. The residuals of the different models were inspected for deviations from normality and homoscedasticity.

Wilcoxon signed-rank test was used to check if a group duration response was different from zero.

A p-value <0.05 was considered to be statistically significant.

6.3 Results

6.3.1 Baseline characteristics

A cohort of sixteen (n=16) subjects with high risk of severe OSA as defined in methods were recruited. All patients were diagnosed with severe OSA after being studied with a split-night PSG (n=14, 88%) or by an overnight PSG (n=2, 12%).

Table 6.1 shows the demographic, clinical and polysomnographic characteristics of the subjects. The table shows that this is a relatively homogeneous group of patients with a very severe obstructive sleep apnea syndrome, commonly associated with a high percentage of cardiovascular and metabolic comorbidity. The severity of OSA syndrome in our cohort is shown by an AHI higher than 30, and high values of CT90 and ODI4. The prevalence of hypertension in our sample was 62.3%, which is consistent with the results of other studies [92]. Four patients received beta blockers, which may cause alterations in the heart rate [177]. There was no other relevant use of medications.

6.3.2 Night sleep clinical and optical results

The time-resolution was decided during a baseline test as mentioned in methods in order to maximize the signal-to-noise ratio. The microvascular CBF during the

	OSA patients (n=16)
Age (years)	57 (52-64.5)
Males, n (%)	12 (75)
BMI (kg/cm^2)	34 (32-37.5)
Epworth	9.5 (7.5-15.5)
AHT, n (%)	10 (62.5)
Smokers, n (%)	13 (81)
Diabetes, n (%)	5 (31.25)
Dyslipidemia, n (%)	3 (18.75)
AHI (n./hours)	85 (76-94)
Mean SpO_2 (%)	92 (90.5-93.5)
CT90 (%)	23 (12-33)
ODI4 (%)	74 (65-85)
Total number of apneas detected by polysomnography n	3817
Obstructive apneas, n (%)	1365 (36)
Hypopneas, n (%)	1918 (50)
Mixed apneas, n (%)	358 (9)
Central apneas, n (%)	176 (5)

TABLE 6.1: Demographic, clinical and polysomnographic characteristics of the patient population. Values are reported in median (interquartile range) or frequency (%). OSA, obstructive sleep apnea; BMI, body mass index; AHT, arterial hypertension; AHI, apnea-hypopnea index; SpO_2, arterial oxygen saturation; CT90, % of measured night sleep time when arterial oxygen saturation is lower than 90%; ODI4, number of times where arterial oxygen saturation decreases 4% due to an apnea or hypopnea. This table is published at [170], in which I have the copyright to the published content.

whole night of sleep was continuously assessed by DCS with a range of 0.9 to 3.1 (1.5 ± 0.5, mean $\pm$ standard deviation) second time-resolution.

A total of 3817 apneic events were identified including 1365 (36%) obstructive apneic events. The DCS recording in two patients was discarded (14% of total obstructive apneic events) due to synchronization failure between the PSG and the DCS. Part of the HR of different patients was discarded due to low ECG data quality recording (15% of total obstructive apneic events). The SpO_2 recording in one patient was also discarded (9% of total obstructive apneic events) due to the detachment of the pulse oximeter during the main part of the recording. After removing the outliers, 87% obstructive apneic events were considered for the CBF, 90% events for the HR, and 88% events for the SpO_2. Table 6.2 clarifies the total of number of apneas considered for the analysis.

Step		CBF	HR	SpO_2
1	Total apneas detected by PSG, n (%)	3817 (100)	3817 (100)	3817 (100)
2	Obstructive apneas detected by PSG, n (%) of step 1	1365 (36)	1365 (36)	1365 (36)
3	Obstructive apneas, n (%) of step 2	1150 (84)	1161 (85)	1239 (91)
4	Obstructive apneas after outlier removal, n (%) of step 3	1002 (87)	1040 (90)	1088 (88)

TABLE 6.2: Total number of obstructive apneas detected by the polysomnography and the total apneas considered for the analysis for different steps. The total number of events remaining after each step and its percentage (%) are reported. Step 1, total events detected by PSG. Step 2, obstructive apneic events detected by PSG. Step 3, obstructive apneic events detected by PSG and recorded by each technique. Step 4, obstructive apneic events detected by PSG and recorded with each technique after removing the outliers. CBF, cerebral blood flow; HR, heart rate; SpO_2, arterial oxygen saturation; PSG, polysomonography. This table is published at [170], in which I have the copyright to the published content.

As an example of the apnea effect on systemic variables and cerebral blood flow, Figure 6.2 shows three minutes of continuous BFI measurement together with nasal airflow, HR and SpO_2 changes for one representative patient. BFI has been plotted here and not ΔrCBF, since ΔrCBF is calculated from a specific baseline of each individual apnea where the baseline corresponds to a pre-apnea period of thirty seconds from the start up-to a post-apnea period up-to thirty seconds from the end, as explained in methods. From the PSG recording, it can be seen that SpO_2 shows a drop with a delay relative to the apneic event. In this time period with frequent apneas, characteristic of patients with severe OSA, the SpO_2 drop of the previous apnea appears in the apnea period of the next event. Also, the HR starts to rise when the breathing restarts after a period of cessation. BFI shows a similar behavior as the HR.

ΔrCBF measurements during obstructive apneas were grouped according to their duration (as previously explained in the methods section) and averaged as shown in Figure 6.3 in order to better understand the general response of apnea-induced CBF. As it is observed, the mean of the different apnea-duration groups follows

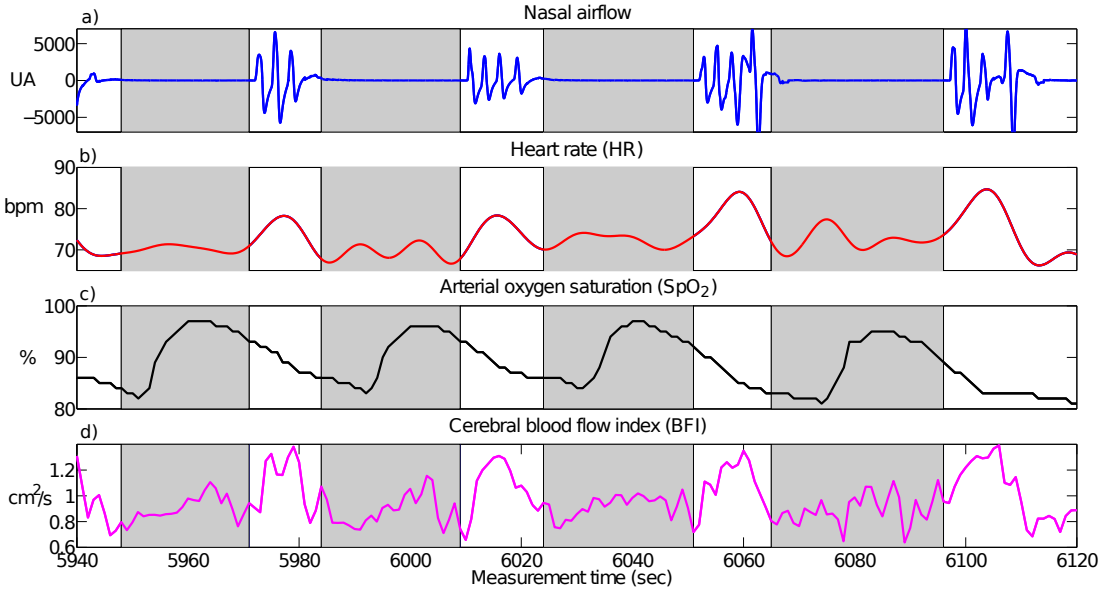

FIGURE 6.2: a) Nasal airflow, b) heart rate, c) arterial oxygen saturation, and d) cerebral blood flow index dynamics during three minutes of night sleep for one representative subject. The gray regions between two vertical lines indicate the obstructive apneic events. This figure is published at [170], in which I have the copyright to the published content.

a similar pattern with a ΔrCBF increase towards the apnea end followed by a ΔrCBF drop.

The apnea duration range from 15 up-to 30 seconds is shown here for further visualization of the data since this range includes the highest number of events. The peak observed in CBF in Figure 6.3 is also observed in the HR in Figure 6.4, whereas the SpO_2 shows a drop. Also we can observe that cerebral and systemic variables are not stable during the pre-apnea periods in Figure 6.2. This effect is evident in the peaks/drops right before or at the start of the apnea in Figure 6.3 and in Figure 6.4. Most probably this is due to the presence of a previous apnea event equal or less than thirty seconds prior to the start of the evaluated event, which was the case for 80% (n=3054) of all the events detected by the PSG, i.e. the subject's physiology was not yet stabilized. According to this, and also according to the literature, in order to characterize the response to a given apnea, we have considered the end of the apnea or the post-apnea period (as previously explained in methods section) to find the CBF peaks/drops, HR peaks, and SpO_2 drops.

Table 6.3 shows the average amounts of peaks/drops for cerebral and systemic variables grouped according to apnea duration. All peak/drop group durations

were statistically different from zero. Microvascular CBF increased by a mean of 30 ± 17 % at the end of the event followed by a drop of -20 ± 12 %. HR, as expected, increased by -11 ± 7 %. Also, SpO_2, as expected, decreased by -13 ± 4 %.

Females, in comparison to males, showed a larger CBF response (β=9.9, p=0.040). Older age was associated to a smaller SpO_2 response (β=-0.2, p=0.004). No statistically significant associations were found with the body mass index (p>0.05). When a linear model with the ΔrCBF peak or the ΔrHR peak as the dependent parameter and the apnea duration as the predictor parameter was fit, positive statistically significant associations (β=0.5 and β=0.4, respectively) were found (p<0.001) for both dependent parameters. When the dependent parameter was the ΔrCBF drop or the ΔSpO_2 drop, negative statistically significant associations (β=-0.2 and β=-0.2, respectively) were found (p<0.001) for both dependent parameters.

	ΔrCBF			ΔrHR		ΔSpO_2	
Apnea duration (sec)	n (%)	Peak (%)	Drop (%)	n (%)	Peak (%)	n (%)	Drop (%)
≤15	130 (13)	22±15	-19±16	116 (11)	8±5	126 (11)	-4±2
>15 to ≤30	618 (62)	29±18	-20±13	681 (65)	11±6	697 (64)	-6±4
>30 to ≤45	238 (24)	35±15	-21±7	236 (23)	13±8	258 (24)	-9±6
>45 to ≤60	16 (1)	45±20	-22±9	7 (1)	19±8	7 (1)	-13±4
All, 24±8	1002 (100)	30±17	-20±12	1040 (100)	11±7	1088 (100)	-6±4

TABLE 6.3: Mean ± standard deviation values for the amount of the peak or drop close to the apnea end for the different apnea duration groups considered and for all apneas. ΔrCBF, relative cerebral blood flow; ΔHR, relative heart rate; ΔSpO_2, arterial oxygen saturation change. This table is published at [170], in which I have the copyright to the published content.

6.4 Discussion

In this work, we have successfully demonstrated the assessment of microvascular CBF during individual obstructive apneic events by non-invasive, continuous cortical DCS measurements. All subjects tolerated the study during the whole-night sleep showing that DCS is suitable for bed-side continuous CBF monitoring over long periods of time and its compatibility with standard PSG monitoring in the clinics point-of-care.

The first finding to report is that DCS results had sufficient contrast-to-noise ratio to enable us to measure the microvascular CBF response to obstructive apneic events in a synchronized manner with the systemic variables from the PSG as shown in Figure 6.2. HR and SpO_2 followed the expected dynamic response to obstructive apneic events according to the literature [160, 161, 175, 178]. CBF showed a similar dynamic response behavior as HR. Only one study has also measured microvascular CBF in OSA patients continuously with diffuse correlation spectroscopy (DCS) [169] during night sleep. However, two-minute time periods with apneas and two-minute time periods with no apneas were compared in order to see differences between the microvascular cerebral hemodynamics with or without events, so, cerebral hemodynamics were not characterized.

The second finding showed a rise and a peak of microvascular ΔrCBF towards or after the end of the event, followed by a drop. Figure 6.4 illustrates that the ΔrCBF and ΔrHR dynamic responses are similar and are also in-phase. This could suggest that we are primarily measuring the extracerebral contributions instead of the cerebral contribution, since, in principle, cerebral signals are not directly driven by heart rate changes. However, DCS in adult brain with this source-detector separation has been validated against other measures of CBF in different studies where it was demonstrated that the relative changes in different challenges follow the intra-cerebral signals closely [7, 8, 24, 79]. Moreover, the literature supports this type of correlation from the cerebral signals during apnea. For instance, our measured microvascular CBF changes by DCS follow the same pattern of the changes in the middle cerebral artery (CBFV) measured by TCD as reported in the literature [113, 157, 158] showing, similarly to our measurements, a peak close to the end of the apnea. Furthermore, these ΔrCBF and CBFV peaks are in agreement quantitatively. The 14.6 $\pm$ 14 % peak change in CBFV right after the apnea end by Bålfors *et al* [113] is similar to our microvascular

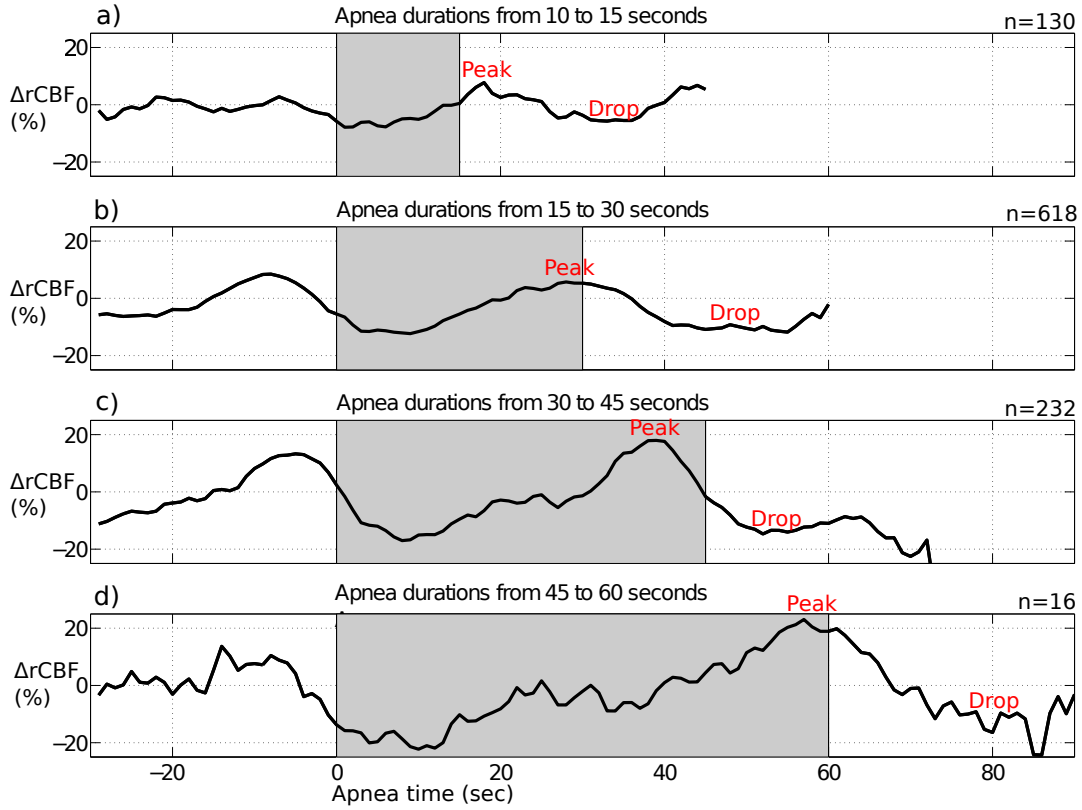

FIGURE 6.3: Mean cerebral blood flow changes (ΔrCBF) during obstructive apnea events for apnea durations of: a) 10-15 seconds; b) 15-30 seconds; c) 30-45 seconds; and d) 45-60 seconds. The gray regions between two vertical lines indicate the start of the events up-to the end of the longest events in each group. The total number of averaged apneas for each subfigure is included at the top right. The peaks and drops representative for the mean apnea hemodynamics response to obstructive apneic events for each group are labeled. See Figure 6.1 a) for the visualization of the apnea duration group before averaging. This figure is published at [170], in which I have the copyright to the published content.

ΔrCBF values of 30 ± 17 % for obstructive apnea as it can be seen in Table 6.3. Also Alex *et al* [157] found similar peaks in CBFV of 22% to 42%. However, other authors have reported larger CBFV peaks. Klingelhfer *et al* [155] found changes of CBFV of 19-219% and Siebler *et al* [158] found a mean CBFV peak during apnea of 142% compared with the baseline CBFV. The differences of these last studies with our results may be related to different normalization of the data and also to the presence of longer apnea durations. Moreover, the ΔrCBF drops after the apnea end are also in agreement with the CBFV drops found in the bibliography [113, 155]. Overall, these results tell us that there is a decrease in the cerebral perfusion due to an obstructive apneic event. If these intermittent decreases lead to ischemia, they can cause hypoxic/ischemic brain injury, especially if it is the

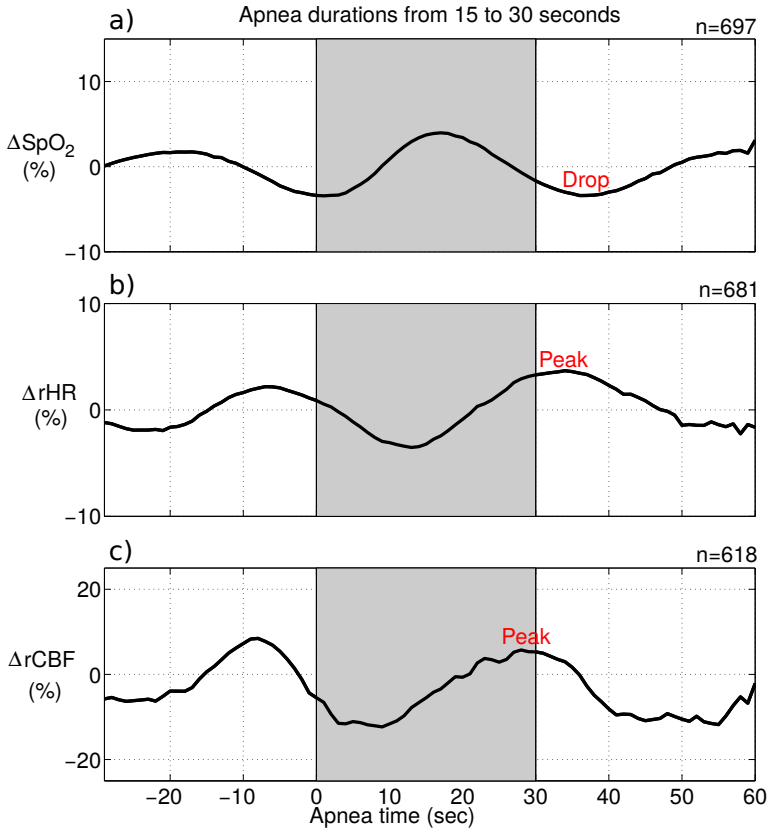

FIGURE 6.4: a) Mean change of arterial oxygen saturation (ΔSpO_2), b) mean relative heart rate (ΔrHR), and c) mean relative cerebral blood flow (ΔrCBF), for apnea durations from 15 to 30 seconds. The gray regions between two vertical lines indicate the start of the events up-to the end of the longest events of 30 seconds. The total number of averaged apneas for each subfigure is included at the top right. The peaks and drops representative for the mean ΔSpO_2, ΔrHR and ΔrCBF response to obstructive apneic events are labeled. See Figure 6.1 a) for the visualization of the apnea duration group before averaging. This figure is published at [170], in which I have the copyright to the published content.

case that cerebrovascular reactivity and/or regulation are impaired [108].

We have observed (Figure 6.2 and Figure 6.3) that cerebral hemodynamics in the pre- and during-apnea periods are not stable as it has been previously observed due to the presence and influence of the previous event [160, 161, 175, 178]. 80% (n=3054) of the total events (obstructive apneas, mixed apneas, hypopneas and central apneas are considered) are followed by the next event after 30 seconds or less, hence, we expect that the effects of the previous events will overlap with the next apnea since the rapid succession of the events do not let stabilization of the physiology. Bålfors *et al* [113] support this idea by finding that CBFV returned to baseline within 60 seconds after the apnea termination.

The CBF peak and drop amplitudes that are characteristic of each apneic event were associated with the apnea duration. This association of the peak with the apnea duration has also been observed by TCD in the middle cerebral artery [157]. About the systemic variables HR and SpO_2, several works have observed a correlation of desaturation depth with apnea duration [179, 180]. Also, Chouchou *et al* [181] found an abrupt HR increase right after obstructive apneic events, and recently, in a preliminary work, we have observed a correlation between HR excursion and the duration of apneas [172]. These findings tell us that the longer the apnea duration, the larger is its effect on HR, SpO_2, but also, on the microvascular cerebral blood flow.

About the gender effect, we observed that females showed larger CBF responses. Edlow *et al* [118] previously reported a smaller CBF response to HOB manipulation for females in the healthy population, but we hypothesize that female can have a smaller head circumference and a smaller scalp-to-brain-distance, hence, a smaller extracerebral effect. No body-mass-index effect was observed. However, Peppard *et al* [182] did observe an association between SpO_2 decreases and body mass index. The homogeneous body mass index present in our group (32-37.5) may have hidden this association. About the age effect, older age has already been previosly associated to a smaller apnea SpO_2 response as found in the literature [183].

Finally, several apneas (13% for CBF, 10% for HR and 12% for SpO_2; see Table 6.2) have been discarded as outliers. The similar percentages of apneas removed between CBF and the PSG variables (HR and SpO_2) support the idea that the DCS signal has the quality needed to be used at the poin-of-care in the clinics.

Our study has some limitations that should be taken in consideration. Our findings correspond to a group of patients with very severe OSA, which implies that these results may not be extrapolated to the different OSA severities. However, at the same time, it strengthens the validity of our results for these patients with severe OSA. Finally, two important parameters to understand CBF changes are the blood pressure and the end-tidal carbon dioxide, future studies should include their simultaneous measurement with DCS.

In summary, we have demonstrated the suitability of DCS technology for bedside and continuous monitoring of the microvascular ΔrCBF during sleep at the point-of-care in the clinics. We were able to obtain sufficient signal-to-noise ratio

for characterizing the canonical shape of the microvascular cerebral blood flow changes in patients with severe obstructive sleep apnea. We were then also able to characterize each cerebral blood flow peak and the following drop for each obstructive sleep apnea event, as well as to visualize the apnea induced cerebral and systemic hemodynamics simultaneously. This work, to the best of our knowledge, is the first characterization of the microvascular cerebral blood flow during an obstructive sleep apnea.

Chapter 7

Mild postural alterations as a challenge to evaluate cerebrovascular reactivity in carotid stenosis; a comparison to acetazolamide injection and to breath-hold challenge

Hypothesis:
The orthostatic challenge can be an alternative protocol to acetazolamide injection and breath-hold index challenges in order to derive a biomarker of cerebral vasoreactivity in evaluating the effects of internal artery carotid stenosis.

7.1 Introduction

Severe stenosis or occlusion of the internal carotid artery (ICA) causes up to 20% of all strokes [184, 185]. Older people are more likely to be affected by carotid stenosis, where men are more likely than women. Cholesterol, high blood pressure and smoking, which are conditions that are increasing in our society, are also predictors of ICA stenosis [186].

These patients with ICA stenosis are found to be at a higher risk of stroke events when cerebrovascular reactivity (CVR; the response to a stimulus that dilates or contracts the cerebral vasculature [4]) is impaired [187]. Impaired CVR was shown to have a prognostic value in future ischemic stroke risk stratification in severe extracranial internal carotid artery (ICA) stenosis patients [188]. The CVR assessment is mainly performed in asymptomatic ICA stenosis patients, since they are the population in which there is more uncertainty of the optimum treatment [189]. This assessment has been proposed to stratify ICA stenosis patients based on their assumed risk of stoke, and, therefore, to contribute in the decision of the proper treatment, such as carotid revascularization or drug therapy. To that end, it is hypothesized that a practical, point-of-care evaluation of CVR and general cerebral hemodynamics may reveal itself of clinical value in preventive interventions in this patient population.

A common way to evaluate the cerebral well-being is to measure the maximal CVR of the cerebral arterioles to a chemical stimuli using acetazolamide (ACZ), which is a selective inhibitor of the enzyme carbonic anhydrase (EC 4.2.1.1) [34, 35]. The main advantage of ACZ challenge is the lack of need of patient collaboration. However, it is minimally invasive, time-consuming and has relatively minor but relevant side-effects.

Another common challenge, relevant to this work, is the use of induced hypercapnia by carbon dioxide inhalation or a breath-hold [190–192]. However, both challenges require significant patient collaboration, controlled carbon dioxide inhalation requires specialized equipment and voluntary breath-hold is difficult to standardize.

As mentioned previously, another difficulty is that the clinically accepted methods that allow the evaluation of the status of the microvasculature (magnetic resonance imaging, perfusion computed tomography, positron emission tomography and others) are not suitable for use at the point-of-care. Transcranial Doppler ultrasound (TCD) is the only method suitable for point-of-care use but it only measures cerebral blood flow velocity in the few accessible major arteries, i.e. only the distal microcirculation is measured directly [4, 193].

In other words, two critical advances are desired for the robust, point-of-care evaluation of the CVR in these patients. Namely, a non-invasive, transcranial, portable

method that is sensitive to the local, microvascular hemodynamics and a challenge that is easy to implement with minimal patient collaboration. About the method, diffuse correlation spectroscopy (DCS) and TCD have already been utilized to compare microvascular versus macrovascular (evaluated by TCD) CVR in response to both acetazolamide [194] and hypercapnia [111, 195]. And, in another front, about the challenge, a sequence of transient alterations of the patient head-of-bed (HOB) manipulation position challenge has been considered as a stimuli as an alternative biomarker to test CVR and/or cerebral autoregulation [118–123, 127, 133, 134, 196] (also in Chapters 5, 9 and 10). Despite the complexity of its physiology and various potential confounding factors influencing the cerebral hemodynamic outcome [118, 119, 134], this challenge is attractive for many reasons because, compared to other stimuli, it is non-invasive (no need to inspire gases or inject drugs), is easy to perform and does not require subject collaboration nor special equipment. Interestingly, the cerebral hemodynamic response to HOB position manipulation as assessed by diffuse optics has been shown to be indicative of acute cerebral pathology [119–121], cerebral autoregulation [122] (Chapter 10), long term outcome [123] (Chapter 9) and secondary alterations due to chronic illness and therapeutic recovery afterwards [127] (Chapter 5) in a growing number of pilot studies.

In this work, we have used TCD and DCS on a cohort of asymptomatic ICA stenosis patients and on a cohort of healthy controls. The primary goal of the study was to compare the utility of the HOB manipulation as a challenge as evaluated by diffuse optics to the acetazolamide (ACZ) injection and to the breath-hold challenges, all for the evaluation of an alternative biomarker of CVR. We have hypothesized that HOB position challenge as a simpler, non-invasive and benign challenge, can be a good alternative to hypercapnic (breath-hold challenge) and ACZ challenges for the evaluation of CVR at the microvasculature level in patients with ICA stenosis. The results of this study are summarized in a manuscript under preparation for submission [117].

7.2 Methods

This study was conducted at the Stroke Unit of Hospital de la Santa Creu i Sant Pau, in Barcelona, Spain between February 2016 to January 2018. The study

protocol was approved by the local ethical committee (EC/15/130). The patients and volunteers gave their informed written consent.

7.2.1 Population

We have recruited patients with asymptomatic severe extracranial ICA stenosis, and also healthy volunteers.

Asymptomatic ICA stenosis refers to patients with present ICA stenosis but without a history of ischemic stroke or transient ischemic attack in the preceeding six months. The patients were diagnosed with asymptomatic severe extracranial ICA stenosis during a carotid artery ultrasound screening (multifrequency linear array transducer; Aplio-XG, Toshiba, Tochigi, Japan) due to other vascular risks factors or due to other non-related symptoms, or after an ischemic stroke related to another etiology at the Stroke Unit. The patients were asked to join the study if they had an unilateral or bilateral severe >70% stenosis or occlusion of the ICA as determined by published criteria using a carotid artery ultrasound [197]. In these patients, the ICA stenosis or occlusion was further confirmed by magnetic resonance angiography, computed tomography angiography, and/or digital subtraction angiography according to North American Symptomatic Carotid Endarterectomy Trial criteria [198]. Exclusion criteria were bilateral inadequate temporal bone windows for sufficient TCD examination or the evidence of an additional intracranial stenosis of the carotid siphon, of the middle cerebral artery, or of the anterior cerebral artery. Patients were instructed to avoid caffeine, smoking, or vasoactive medications twelve hours prior to the measurement. These substances may alter the result of any vasoreactivity test. For this reason, the cerebrovascular reactivity was measured without the effect of vasoactive substances in order to address only the effect of the ICA stenosis.

7.2.2 Challenges for testing the cerebrovascular reactivity

The study protocol consisted of a sequence of three different vasoreactivity challenges performed in the same session in each subject, as shown in Figure 7.1.

First, two breath-hold challenges were performed with a maximum duration of 30 seconds at supine (0°) position. Subjects were instructed to hold their breath

following a normal inspiration, and to avoid performing a Valsalva-maneuver. A respiratory polygraphy device was used to check for the apnea length *a posteriori*. Considering the period pre-apnea as the baseline, a relative maximum change was found during the period of apnea duration plus thirty seconds after the end of the apnea, this relative change was divided by the apnea length to obtain a breath-hold index (BHI) [192]. The two BHI calculated were averaged to obtain a general result.

The second challenge started after five minutes of resting time from the last breath-hold. The head rest of the bed was tilted from supine (0°) position up-to 30° to perform the first HOB orthostatic position challenge, and after five minutes at 30° the bed was tilted back to supine (0°) position for five more minutes. For the HOB position challenge, the first and last minutes in each position were discarded from the analysis due to possible movement artifacts and for avoiding systemic instabilities, and, a percentage change was calculated and then averaged for the position at 30° and also for the recovery back to supine (0°) respect to the initial supine position. The ΔrCBF and ΔrCBFV responses to the change from the supine position to 30° are represented as $\Delta\text{rCBF}_{\text{supine}_1 \text{ to } 30^\circ}$ and $\Delta\text{rCBFV}_{\text{supine}_1 \text{ to } 30^\circ}$, respectively; also, the ΔrCBF and ΔrCBFV responses when being tilted back to the initial supine position are represented as $\Delta\text{rCBF}_{\text{supine}_1 \text{ to supine}_2}$ and $\Delta\text{rCBFV}_{\text{supine}_1 \text{ to supine}_2}$, respectively. The mean arterial blood pressure (MAP) was measured at 2.5 minutes from the onset of each HOB position.

The HOB position challenge was followed by the acetazolamide stimulus at supine (0°) position but only the patients (not controls) were measured. We have used ACZ (1g/10ml saline) as the stimulus for CVR assessment. The hemodynamic change due to ACZ injection was calculated selecting the five-minutes maximum change during the fifth to twentieth minutes after the post-injection period and, then, this five minute period was averaged. This change was relative to the four last minutes before the start of the injection (during the last HOB back at supine (0°) position).

7.2.3 Optical methods and instrumentation

We have used the DCS unit of the hybrid device described in Section 4.1.1. Figure 5.2 in Chapter 5 shows the two optical probes placed on the forehead bilaterally on both hemispheres, as well as the TCD probes used. We have assumed that the

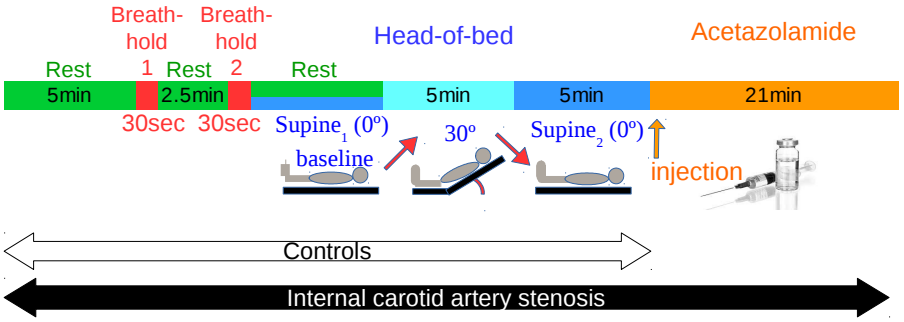

FIGURE 7.1: The timeline of the study with the different protocols depicted for both controls (white arrow) and patients (black arrow).

hemodynamic changes due to vasoreactivity stimulation are global and, therefore, for probe stability and convenience, we have placed the DCS probes on the forehead avoiding the sinus.

Simultaneously, the CBF velocity (CBFV) in both middle cerebral arteries has been measured continuously by a transcranial Doppler ultrasound (TCD) system DWL MultiDop-T digital (DWL Elektronische Systeme GmbH, Singen, Germany) with the use of a helmet to fix the probes.

The respiratory polygraphy (Embletta MPR PG, Natus Medical, Middleton, USA) included the recording of the oronasal flow (by a thermistor and a nasal cannula), the thoracic and the abdominal movements (by a respiratory inductance plethysmography band), the arterial oxygen saturation and the heart rate (both by pulse oximetry), among others. The respiratory polygraphy data was further post-processed to check for the proper performance of the breath-hold and, also, to determine its duration. We have considered that a breath-hold was performed properly if there was lack of thoracic and abdominal movements (no fluctuations in the respiratory inductance plethysmography band's signal) and lack of input or output oronasal flow (no fluctuations in the thermistor and in the nasal cannula signals) for at least 20 seconds.

The DCS data was obtained every 4 seconds during the measurement and the TCD data was obtained every 0.1 seconds.

A manual sphygmomanometer (Omron BP785 IntelliSense Automatic Blood Pressure Monitor, Omron, Osaka, Japan) was used to measure the MAP.

7.2.4 Statistical analysis

We have expressed quantitative variables as a median and an interquartile range (median (Q1, Q3)), and categorical variables as number of cases and percentages (cases (percentages)).

The Wilcoxon rank-sum test (for quantitative variables) or the chi-squared (for categorical variables) tests were used to assess the difference between two groups. The findings from two groups were considered identical (to be "on agreement") if the null hypothesis that the groups were equal was not rejected for the Wilcoxon rank-sum test. The Wilcoxon signed-rank test was used to check if a group response was different from zero. Spearman correlation was computed between the same challenge and different techniques, and *vice versa*. Levene's test was computed to assess the equality of variances of the DCS versus the TCD results.

We have categorized each cerebral hemisphere of each subject according to the degree of the ipsilesional ICA stenosis as severe ($\geq$70% or occlusion) and non-severe (stenosis<70% or absent), and, in general, the data from the ipsilesional hemisphere to a severe ICA stenosis has been used for further analysis. When both hemispheres presented the same degree of stenosis, the data of the two hemispheres was, instead, averaged. For the control subjects, the data of both hemispheres was also averaged. The two hemispheres for each patient have been used only in a substudy of patients with unilateral stenosis, where both hemispheres were compared between them.

The correlations were only accepted to be valid if and only if when extracting all patients one by one and repeating the same test (bootstrapping), every subtest (considering n-1 data points) was statistically significant.

All statistical analyses were performed with R [135]. $p < 0.05$ was considered as the threshold for rejection of the null hypothesis for all statistical tests.

7.3 Results

We have included twenty-seven (n=27) patients (67.6 $\pm$ 7.4 years, 15% female) with an asymptomatic severe ICA stenosis or occlusion (unilateral in sixteen (n=16, 59%) and bilateral in eleven (n=11, 41%)) and fifteen (n=15) healthy

controls (32.9 ± 10.2 years, 40% female). Table 7.1 shows the demographic and clinical characteristics for the patients and controls. This table shows that controls were younger than patients ($p<0.001$) and with less body mass index ($p=0.048$). No differences in gender distribution or in smoking were found between groups. As expected, patients presented more cases of diabetes, hypercholesterol and hypertension than controls ($p=0.001$).

	Patients (n=27)	Controls (n=15)	p	Total (n=42)
Age (y.)	68 (64, 62)	28 (28, 33)	<0.001*	63 (33, 69.8)
Females, n (%)	4 (15)	6 (40)	0.066	10 (24)
Body mass index (kg/cm^2)	25.2 (23.8, 26.1)	22.9 (21.5, 25.1)	0.048*	24.7 (22.7, 26.0)
Smoker, n (%)	16 (59)	5 (33)	0.107	21 (78)
Diabetes, n (%)	16 (59)	1 (7)	0.001*	17 (41)
Hypercholesterol, n (%)	26 (96)	0 (0)	<0.001*	26 (62)
Hypertension, n (%)	20 (74)	0 (0)	<0.001*	20 (48)

TABLE 7.1: Demographic and clinical variables for the patients and controls. (*) indicates a statistically significant difference between groups.

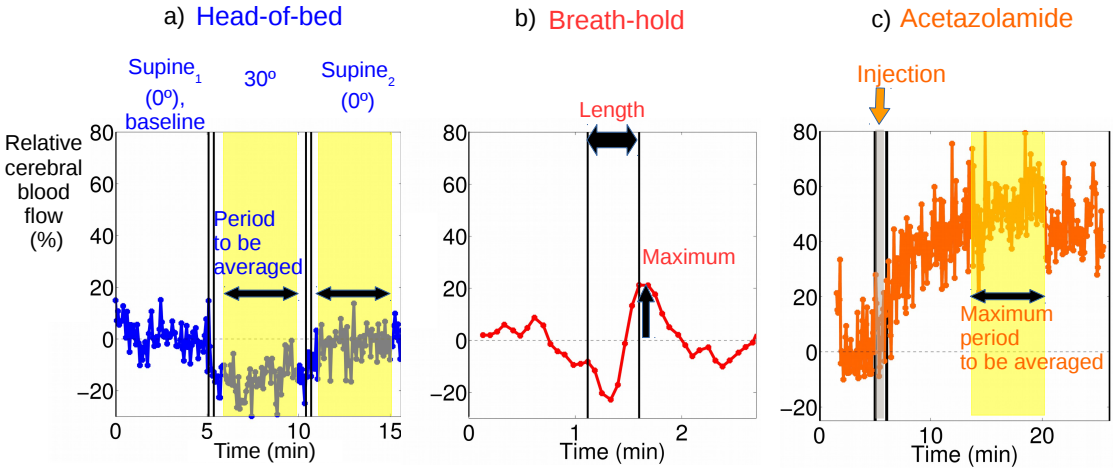

FIGURE 7.2: Representative microvascular cerebral blood flow responses to a head-of-bed position challenge, to a breath-hold challenge, and to acetazolamide injection. The data periods to be averaged for further analysis are depicted in yellow.

Table 7.2 shows the vascular variables of the patients. This table shows the high severity of the patients (>70%) as well as a heterogeneity of the lateralization of the presence of ICA stenosis.

	Patients (n=27)
Degree of ICA stenosis of the most affected hemisphere:	
0%-70%, n (%)	0 (0)
≥70%-occluded, n (%)	27 (100)
Laterality of stenosis:	
Unilateral steno-occlusion, n (%)	16 (59)
Bilateral steno-occlusion, n (%)	11 (41)
Ischemic or hemorrhagic stroke > than 6 months, n (%)	7 (35)

TABLE 7.2: Vascular variables of the patients.

ACZ was not administrated to control subjects and it was refused by two participants. Bilateral DCS probes moved during the ACZ recording of one patient due to the repositioning of the TCD helmet. The breath-hold was not properly performed in two controls and in six patients.

Figure 7.2 shows a sample of representative results for each one of the three different challenges measured by DCS.

7.3.1 The head-of-bed position manipulation challenge

The effects of head elevation: The head-of-bed position challenge from the first supine to 30°, as expected, induced changes from baseline ($p<0.001$) in the two different techniques in controls, patients and for all group. There were no statistically significant differences between controls and patients for this HOB ($p>0.05$) for the two techniques. The findings are summarized in Table 7.3 in the first column.

		Head-of-bed supine$_1$ to 30°	Head-of-bed supine$_1$ to supine$_2$	Breath-hold index (1/sec)	Acetazolamide
All	Cerebral blood flow velocity (%)	-1.2 (-5.3, 1.2)*	1.1 (-1.2, 4.8)	0.8 (0.6, 1.1)*	34.8 (19.6, 38.3)*
	Cerebral blood flow (%)	-15.3 (-22.9, -6.6)*	4.5 (-3.9, 12.4)*	0.7 (0.4, 1.0)*	18.5 (13.3, 28.9)*
Patients	Cerebral blood flow velocity (%)	-2.4 (-5.8, 2.0)*	0.9 (-3.1, 4.8)	0.6 (0.5, 0.8)*	34.8 (19.6, 38.3)*
	Cerebral blood flow (%)	-16.3 (-26.3, -6.3)*	4.5 (-2.3, 13.2)*	0.7 (0.5, 1.0)*	18.5 (13.3, 28.9)*
Controls	Cerebral blood flow velocity (%)	-1.8 (-4.4, 0.2)	1.7 (-0.1, 3.7)*	1.2 (1.0, 1.3)*	-
	Cerebral blood flow (%)	-15.0 (-19.1, -8.4)*	3.4 (-11.3, 10.1)	0.8 (0.4, 1.1)*	-

TABLE 7.3: Cerebral blood flow velocity response (ΔrCBFV) and cerebral blood flow response (ΔrCBF) for the different challenges performed, for the different study groups and for all. ($*$) indicates a statistically significant difference from baseline. Median (confidence intervals) are shown. Acetazolamide injection was not administrated to the control group.

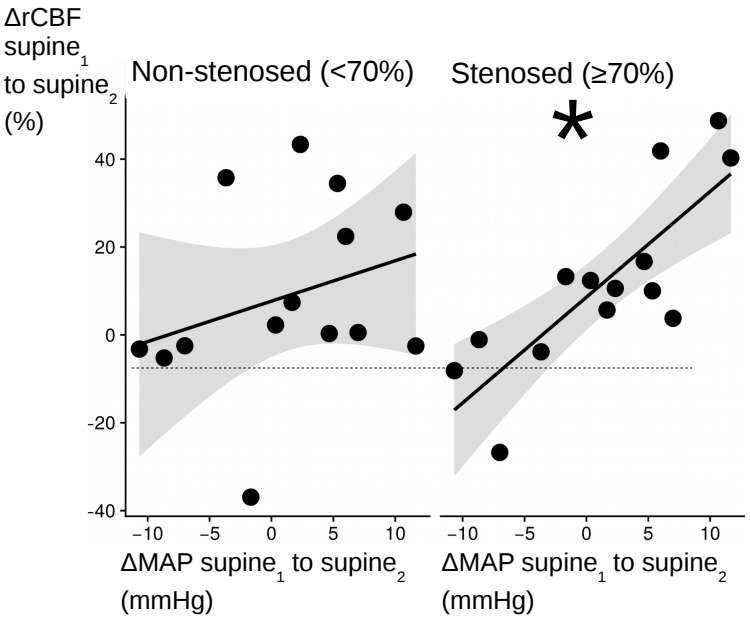

FIGURE 7.3: Cerebral blood flow response (ΔrCBF) to a head-of-bed recovery back to supine correlates to the relative mean arterial pressure change (ΔMAP) in the stenosed hemisphere (right), but not on the non-stenosed hemisphere (left). The mean $\Delta\text{rCBF}_{\text{supine}_1 \text{ to supine}_2}$ data for each patient are plotted. Linear model fit and confidence intervals (in grey) are also plotted. (*) indicates a statistically significant Spearman correlation.

The effect of returning back to the supine position: The results of the recovery (or lack thereof) of cerebral hemodynamics following the return of the HOB position back to the original supine position are shown in Table 7.3 in the second column for all the subjects. Interestingly, $\Delta\text{rCBF}_{\text{supine}_1 \text{ to supine}_2}$ on severe ICA stenosis did not recover to baseline levels after returning back to the supine position following a five minutes HOB elevation (p=0.030), but it did recover for controls (p=1). When considering all subjects measured, $\Delta\text{rCBF}_{\text{supine}_1 \text{ to supine}_2}$ did recover to baseline (p=0.056).

Head-of-bed position manipulation induced cerebral blood flow changes and their relationship to the mean arterial pressure changes: An incidental finding of this study is that the $\Delta\text{CBF}_{\text{supine}_1 \text{ to supine}_2}$ after a HOB position challenge in patients with unilateral stenosis (n=14 patients with unilateral stenosis and available MAP data) correlated to the response of ΔMAP. A statistical significant correlation has been found in the stenosed hemisphere ($\rho_{Spearman}$=0.75, p=0.002) but not in the non-stenosed hemisphere ($\rho_{Spearman}$=0.35, p=0.201) as shown in Figure 7.3.

7.3.2 Comparison of the head-of-bed manipulation position challenge with the breath-hold index and acetazolamide injection

We have studied whether there are any correlations between the responses observed in all three challenges in pairs both for the whole study population and the patient cohort, separately. However, no correlations or similarities in the amount of responses between the different challenges were found. In general, all responses to challenges were different from their baselines as shown in Table 7.3 and the amount of CBF change was different between them.

7.3.3 Comparison between techniques

ΔrCBF and ΔrCBFV results are shown in Figure 7.4. The breath-hold challenge showed an agreement between the ΔrCBFV and ΔrCBF measured ($p=0.325$), as well as the head-of-bed position challenge recovery back to supine position ($p=0.743$). The head-of-bed to 30° showed a statistical disagreement ($p<0.001$), obtaining bigger $\Delta rCBF_{supine_1 \text{ to } 30°}$ decreases than $\Delta rCBFV_{supine_1 \text{ to } 30°}$. Also, acetazolamide stimulus showed a statistical disagreement ($p<0.034$) and lower ΔrCBF increases than ΔrCBFV were obtained.

The variance of the responses was statistically significant between DCS and TCD techniques on the two head-of-bed position challenges (supine (0°) to 30°, and recovery back to supine position) ($p<0.001$), but not for the rest ($p>0.05$).

7.3.4 Effect of the degree of stenosis

When comparing the control group versus the ICA stenosis group, no differences were observed in general, except from the results presented below.

The breath-hold challenge on the ΔrCBFV response in patients with stenosis was statistically significantly lower than the controls response ($p<0.001$) (Figure 7.5), but not for ΔrCBF ($p=0.876$).

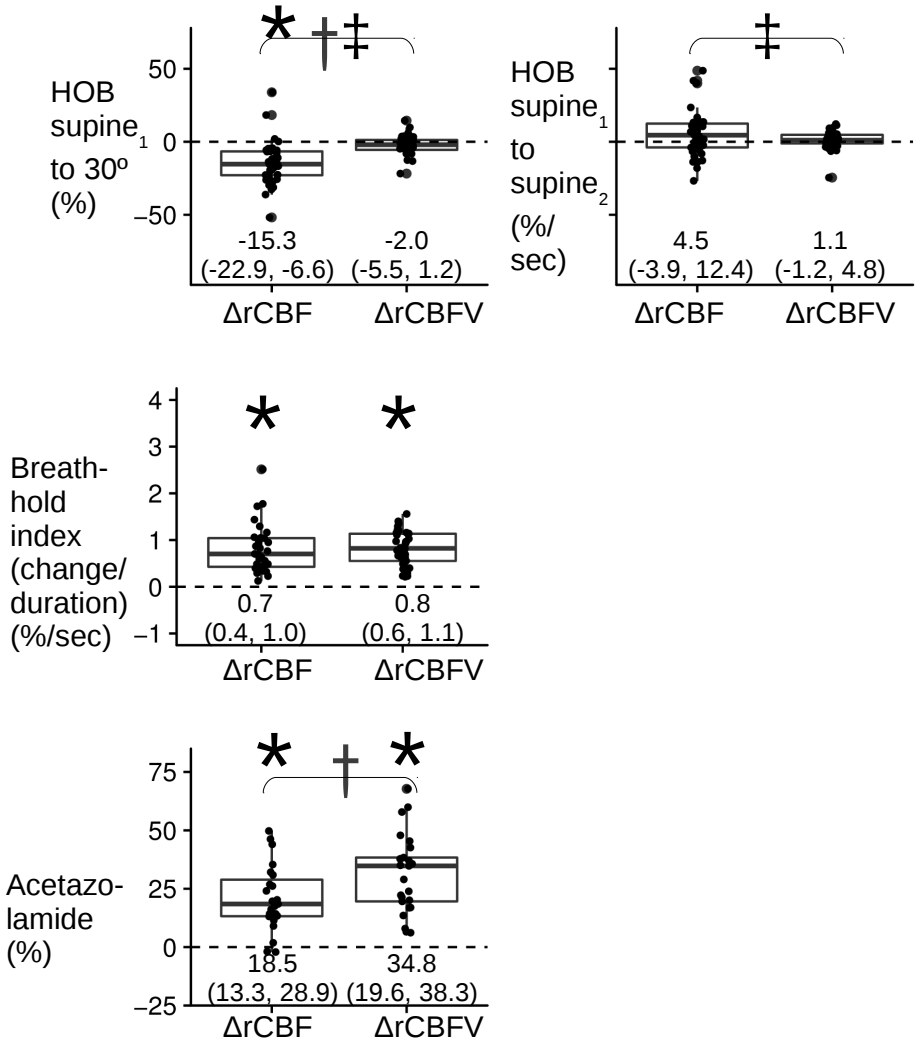

FIGURE 7.4: General ΔrCBF and ΔrCBFV respones to the different challenges for all subjects measured. Symbols indicate a statistically significant difference from baseline (∗), between ΔrCBF and ΔrCBFV (†) and between the variance of ΔrCBF and ΔrCBFV (‡).

7.4 Discussion

We wanted to study if the HOB position challenge could be a good alternative to hypercapnic (breath-hold challenge) and ACZ injection for the evaluation of the CVR at the microvasculature level in patients with ICA stenosis. Even though no correlations between the different challenges have been found, an interesting result related to the head-of-bed position challenge has been observed. Microvascular $\Delta\text{rCBF}_{\text{supine}_1 \text{ to supine}_2}$ (Table 7.3) did not recover to baseline after the first HOB position change, but did recover for controls. It is not the first time that an

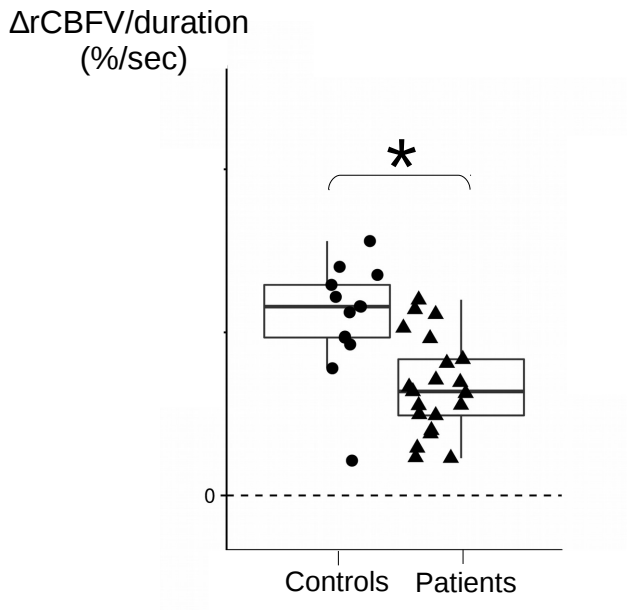

FIGURE 7.5: Breath-hold index challenge differs between controls and patients measured by TCD. (*) indicates statistically significant difference between groups.

orthostatic challenge based on mild HOB alterations led to an alteration of the supine CBF upon returning to the initial HOB supine position depending on the pathological degree. In obstructive sleep apnea (OSA) patients, we have found that this alteration was related to OSA severity. And, interestingly, that long-term treatment ameliorated this alteration [127] (Chapter 5). This result suggests that patients with OSA, or with damaged autoregulation, might need a longer time period than five minutes in each HOB position to stabilize their hemodynamic response. This is assuming that healthy cerebral auto-regulation would, given enough time, normalize the $\Delta\text{rCBF}_{\text{supine}_1 \text{ to supine}_2}$.

Moreover, we have found that the distinct response of $\Delta\text{rCBF}_{\text{supine}_1 \text{ to supine}_2}$ in the presence of a severe carotid stenosis correlated with the response of ΔMAP in the stenosed ($\rho_{Spearman}$=0.75), but not on the non-stenosed hemisphere, suggesting an impairment of cerebral autoregulation. Interestingly, this correlation was not observed by cerebral blood flow velocity by TCD in our study. This result reinforces the idea that this correlation is due to damaged CVR, and also, that DCS during a HOB position change may be superior to TCD in being able to measure the general well-being of the brain. Moreover, it is not the first time that this asymmetry between damaged and non-damaged hemispheres is observed in pathological subjects. On an unpublished study with a similar protocol but on ischemic stroke patients [122] (Chapter 10), again, $\Delta\text{rCBFV}_{\text{supine}_1 \text{ to supine}_2}$ was found to correlate

with ΔMAP only in the ipsilesional hemisphere of twenty (n=20) ischemic stroke patients, but not on the contralesional hemisphere.

When comparing the different techniques used in the three different challenges, ACZ/BHI/HOB, TCD and DCS were not correlated for any challenge. For the ACZ challenge this was already described by our group in patients with ICA stenosis [142]. The ΔrCBF response has been found to be lower than the ΔrCBFV response (Figure 7.4, third raw). According to our results, Müller *et al* [199] also found lower ΔrCBF (measured by stable xenon-enhanced computed tomography) results respect to ΔrCBFV (27 ± 24% vs 43 ± 21%), where, similarly, we have obtained changes of 20 ± 14.1% vs 31.3 ± 16.7 for CBF vs CBFV, respectively. However, in contrast, on healthy subjects, Zirak *et al* [194] found that ΔrCBFV and ΔrCBF were not correlated but were in agreement. Unfortunately, in our protocol we did not perform the ACZ challenge on the control group. For the breath-hold challenge, ΔrCBFV and ΔrCBF responses were found to be in agreement (Figure 7.4, first raw). However, no correlations were found, so the physiological meaning of this result remains unclear. About the head-of-bed position manipulation challenge, ΔrCBFV and ΔrCBF responses were not found to be in agreement (Figure 7.4, second raw) and the variance was found to be statistically different between them ($p<0.001$). These results are according to Favilla *et al* [119] study, where they also found different ΔrCBF results respect to ΔrCBFV after a HOB position change with a similar protocol.

Another interesting result of this study is that we have found differences between controls versus patients but this time with TCD technique and the breath-hold challenge. The breath-hold challenge on the CBFV response in patients with stenosis was statistically significantly lower than the controls response ($p<0.001$) (Figure 7.5), but not for the microvascular CBF. This result has already been found by Müller *et al* [199] on seventy-four (n=74) patients, considering each hemisphere as a separate unite, and using acetazolamide injection and breath-holding challenges, where both challenges similarly indicated significantly reduced vasomotor reactivity with increasing degree of internal carotid artery lesions ($p\leq0.01$). However, the acetazolamide challenge differentiated more accurately between the various groups of ICA findings. On the contrary, De Bortoli *et al* [200] found a low concordance between breath-hold and ACZ to assess CVR ($k = 0.371$). These result are in contrast to our results, where acetazolamide injection has not been able to differentiate between the different degrees of stenosis by TCD nor DCS, and breath-hold

has been shown to be superior to the ACZ injection. These discrepancies may be due to the differences in the protocols.

Table 7.1 shows that controls were younger than patients. However, aging is not expected to affect our results according to Edlow *et al* [118]. No differences in gender distribution or in smoking habits were found between groups. As expected, patients presented more cases of diabetes, hypercholesterol and hypertension than controls [186, 201].

We acknowledge that our study has several limitations. First, the lack of assessment of the baseline collateral circulation on the time of the measurement. This should be included in the protocol of future studies. Second, our findings correspond to a group of patients with asymptomatic ICA stenosis, which implies that these results are not necessarily extrapolated to the different ICA types. However, at the same time, it strengthens the validity of our results for patients with asymptomatic ICA stenosis.

The head-of-bed recovery back to the initial supine position with the measurement of microvascular ΔrCBF (by DCS) may be a new biomarker to tell us about the status of CVR in these patients. More studies are needed to understand these results.

Chapter 8

Monitoring brain reperfusion after thrombolysis for acute ischemic stroke

Hypotheses:

-Hybrid diffuse optics can reliably be employed in the emergency unit environment and utilized during treatment and intensive care.

-Hybrid diffuse optics show a change during to the restoration of the microvascular cerebral hemodynamics due to the recanalization therapy after ischemic stroke.

8.1 Background and motivation

Early reperfusion is a relevant predictor of early recovery and favorable functional outcome in acute ischemic stroke (AIS) [202, 203]. In the every day clinical practice, perfusion imaging with magnetic resonance and computed tomography (CT) are increasingly used to triage patients for reperfusion therapy. However, these methods are rarely applied to assess the reperfusion therapy success due to different associated complexities, such as the need to transport the acute patient and the expense. Because of this, the monitoring of the treatment efficacy in these patients has mainly focused on the evidence of structural damage and arterial patency rather than on perfusion (microvascular cerebral blood flow (CBF))

restoration. Partly, this is because of the unavailability of monitoring techniques suitable for repeated microvascular CBF measurement in these patients. Instead of looking at the reperfusion, it is common to look at the recanalization of the occluded artery as a surrogate [204, 205]. However, the recanalization does not necessarily lead to the reperfusion of the distal region, and, contrarily, reperfusion can sometimes occur despite the persistence of an occlusion [206]. The continuous quantification of microvascular hemodynamic changes, in particular, microvascular CBF, with a noninvasive modality, at the bed-side, during the acute period, could improve our understanding of the relationship between reperfusion, recanalization and clinical recovery. Moreover, it could allow personalized treatment and management strategies.

Previously, it has been shown in a single-case report that DCS/near-infrared diffuse optical spectroscopy (NIRS-DOS) measurements correlated with the recanalization of the middle cerebral artery (MCA) measured by transcranial Doppler ultrasound (TCD) during intravenous thrombolysis [207].

In this study, we have aimed to confirm the feasibility of using DCS/NIRS-DOS as a bedside method for real-time monitoring of local microvascular hemodynamic changes in response to intravenous recombinant tissue plasminogen activator (RtPA) treatment in a small cohort of patients with AIS, and their relationship with the recanalization and the clinical recovery. The results of this study are published in Delgado-Mederos *et al* [208].

8.2 Methods

8.2.1 Study design

We have prospectively identified acute ischemic stroke patients AIS admitted to the emergency unit before 4.5 hours from the stroke onset and that were eligible for intravenous thrombolysis treatment. The protocol was approved by the local Ethics Committee (EC/09/066/980).

The inclusion criteria for this study were: symptoms attributable to MCA territory ischemia affecting the frontal lobe (motor aphasia, contralesional motor deficit or gaze deviation), demonstration of MCA occlusion on angio-CT or TCD prior

to treatment with intravenous rtPA, and optical monitoring being able to start before or within the first fifteen minutes of the start of rtPA treatment. We note that during the study period (2011-2012), mechanical thrombectomy was not yet approved in the hospital. Written inform consent was obtained from the patients or their relatives.

As it is routinely performed in the clinics on admission, the stroke severity of these patients was assessed on admission (baseline) with the National Institute of Health Stroke Scale (NIHSS) [209]. Other baseline examinations included a medical history (demographics and vascular risk factors) and a physical examination. Clinical outcome at three months was evaluated by the modified Rankin Scale (mRS) [210]. A score > 2 has been considered indicative of an unfavorable outcome. Moreover, all patients underwent a cranial CT scan and vascular imaging either by angio-CT or TCD before rtPA treatment.

In order to know if recanalization was positive, it was assessed at 24 hours by a TCD measurement, in some cases, additionally during the rtPA perfusion.

8.2.2 Optical methods and instrumentation

Optical monitoring was performed by the hybrid DCS/continuous-wave NIRS-DOS device as described in Sections 4.1.1 and 4.1.2.

Two optical probes were made of custom built fibers consisting of a source fiber and a detector fiber bundle with four single-mode fibers with 2.5 cm source-detector separation (Figure 8.1).

For this study, the reduced scattering coefficient of the tissue at 785 nm was assumed to be constant ($\mu_s' = 8.5$ cm^{-1}) [47]. The continuous absorption coefficient (μ_a) changes at 785 nm from their baseline value ($\mu_a = 0.14$ cm^{-1}) [47] were measured by continuous-wave NIRS-DOS to improve the accuracy of the DCS measurements [7]. The percent relative CBF change (ΔrCBF) was calculated from the BFI as $\Delta\text{rCBF} = ((\text{BFI}/\text{BFI}_{baseline})\text{-}1)*100$, where $\text{BFI}_{baseline}$ was calculated from the cerebral BFI of the first five minutes of the recording.

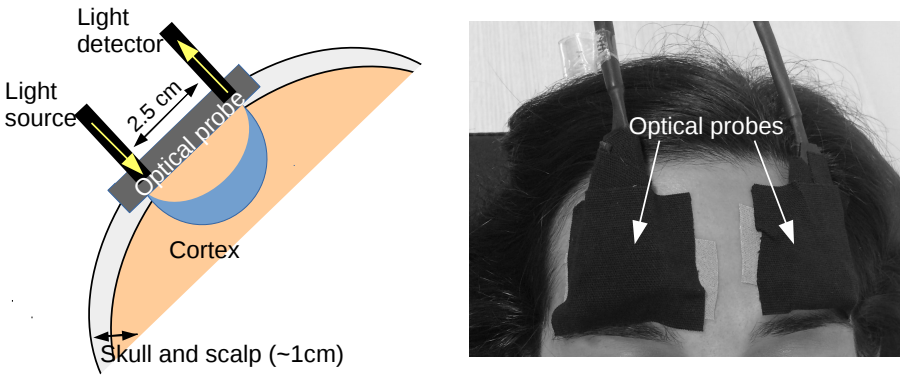

FIGURE 8.1: (Left) The schematic of the source-detector separation of the optical probe. The area in the brain of highest probability signal origin is shown in blue. (Right) The placement of the optical probes bilaterally on the frontal lobes. Figure adapted from [208].

About the continuous-wave NIRS-DOS analysis, a modified Beer-Lambert law [211] was used (as explained in Section 3.1.4.1). Furthermore, the data was corrected for pathlength and partial volume effects as explained in previous studies [211, 212]. Changes of oxy-hemoglobin concentration (ΔHbO_2) and deoxy-hemoglobin concentration (ΔHb) were calculated as $\Delta HbO_2(t)=HbO_2(t)-HbO_{2\,baseline}$ and $\Delta Hb(t)=Hb(t)-Hb_{baseline}$. Again, the baseline was calculated from the first five minutes of recording. Total hemoglobin concentration changes (ΔTHC) were then calculated as the sum of ΔHbO_2 and ΔHb. Data was collected from both hemispheres every 14.2 ± 5.7 (mean ± standard deviation) seconds. Further clarification of the protocol for each technique is shown in Figure 8.2.

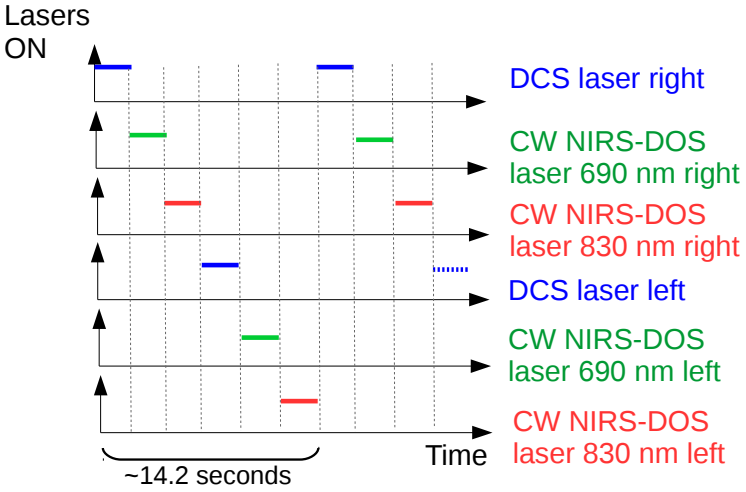

FIGURE 8.2: The protocol for the operation of the lasers of the two diffuse optical techniques.

8.2.3 Statistical analysis

The average baseline values for CBF, THC, HbO_2 and Hb were obtained by averaging the first five minutes of the data, as mentioned, after fifteen minutes from the start of rtPA. This was used to derive the changes of each variable relative to their baseline values at each time point. In this study, the time interval between fifteen minutes from rtPA bolus up to hundred and fifty minutes of monitoring (when available) has been used for analysis.

We have expressed quantitative variables as a mean and a standard deviation (mean $\pm$ standard deviation) and analyzed the data by performing linear mixed-effect models [176] for each individual patient and also for the group. Linear mixed-effect models were needed due to the longitudinal nature of the data (lack of independence of the response variable) when considering each patient independently. When analyzing the patients as a group, these models were needed due to both the longitudinal nature of the data and for correcting for the different patients in the group. The two types of analyses started with a null model that included a continuous dependent variable (CBF, THC, HbO_2 or Hb) for each hemisphere (ipsilesional and contralesional). Patients (only when modeling as a group) and time (when modeling as a group and also when considering each patient independently) were the random factors. The predictor variable time was added to the null model as a fixed effect to see whether this new model, with the predictor variable time, improved the null model. The model fit was assessed using chi-square tests on the log-likelihood values to compare the new model versus the null model. If the new model with the predictor variable time 1) improved over the null model significantly, in other words, if the p value of the chi-square test between the two models was <0.05, and 2) the null hypothesis stating that the slope of the new model was equal to zero was rejected, the slope of this model would tell us about the time evolution (rate of increase or decrease over time) of the continuous dependent variable. Residuals plots of this model were tested for the inspection of deviations from normality or homoscedasticity. Instead, if the model with the predictor variable time did not improve the null model significantly, the null hypothesis stating that the slope of the new model was equal to zero was not rejected. Then, the continuous dependent variable was considered constant over time (slope$\approx$0).

Wilcoxon rank-sum test was used to assess the difference between the slopes of

the two hemispheres with the alternative hypothesis "ipsilesional change > contralesional change".

All analyses were carried out in the R programming language and environment [135] using the "nlme" software package. A p-value <0.05 was considered to be statistically significant.

8.3 Results

Thirteen patients have been identified with the needed inclusion criteria during a 14-month period. However, six were excluded due to late onset of the optical monitoring, mainly due to logistic reasons (late arrival of trained personnel or late consent); and other two patients were also excluded due to technical problems with the optical recording. Finally, five patients (three female, mean age 81 years) were included in the study analysis (Table 8.1).

About the main clinical baseline examinations, the mean baseline NIHSS was 19 ± 3 and the MCA occlusion (four proximal, one distal) was diagnosed by angio-CT in four patients and by TCD in one patient. Also, all patients were hemodynamically stable and none received vasoactive drugs. The mean time from the stroke onset to the rtPA treatment was 144 ± 47 minutes. Relevantly, rtPA treatment administration was not delayed due to this study.

In Figure 8.3, the time course of ΔrCBF, ΔTHC, ΔHbO_2 and ΔHb can be observed in all patients from fifteen minutes of treatment onset in each hemisphere using linear mixed-effect models. The slopes of these models are shown in Table 8.2. These slopes are the change of the optical variables as a function of time in both hemispheres for each individual patient and also for the whole group. On a group basis, a statistically significant increase with time for frontal ipsilesional ($p<0.001$) and contralesional ($p=0.018$) ΔrCBF, for ipsilesional ($p<0.001$) and contralesional ($p=0.014$) ΔTHC and for ipsilesional and contralesional ΔHbO_2 (both $p<0.001$) was found. But no statistically significant change was found for ΔHb in any hemisphere. Interestingly, an asymmetrical time evolution of the optical variables between hemispheres was observed. A statistically significant faster increase (greater slope) was found in the ipsilesional hemisphere for ΔrCBF ($p=0.031$), ΔTHC ($p=0.032$) and ΔHbO_2 ($p=0.030$) compared to the contralesional hemisphere.

Case	Age (years), Sex (M/F)	MCA occlusion	NIHSS pre-rtPA	NIHSS post-rtPA	NIHSS 24h	Recanalization	mRS at 90 days
1	80, F	Left (distal)	15	-	3	Unknown	1
2	58, M	Right (proximal)	16	14	8	Yes (complete)	2
3	93, F	Left (proximal)	22	5	2	Yes (complete)	3
4	80, M	Left (proximal)	21	13	4	Yes (complete)	1
5	92, F	Right (proximal)	19	9	1	Yes (complete)	1
All	8 ± 14		19 ± 3	10 ± 4	4 ± 3		2 ± 1

TABLE 8.1: Clinical variables of each individual patient and all group. M, male; F, female; MCA, middle cerebral artery; NIHSS, National Intitute of Health Stroke Scale; rtPA, intravenous recombinant tissue plasminogen activator; mRS, modified Rankin Scale. Mean ± standard deviation. Table adapted from [208].

Case	ΔrCBF (%/min)		ΔTHC (μM/min)		ΔHbO_2 (μM/min)		ΔHb (μM/min)	
	Ipsilesional hemisphere	Contralesional hemisphere	Ipsilesional hemisphere	Contralesional hemisphere	Ipsilesional hemisphere	Contralesional hemisphere	Ipsilesional hemisphere	Contralesional hemisphere
1	0.17†	0.085	0.023†	-0.0051	0.046†	0.0006	-0.023†	-0.0057
2	0.54†	0.33†	0.035†	0.0023	0.053†	0.026†	-0.018†	-0.024†
3	0.45†	0.32†	0.063†	0.030†	0.059†	0.031†	0.0031†	-0.0015
4	0.23†	0.013	0.030†	0.029†	0.026†	0.019†	0.0042†	0.010†
5	0.023	-0.0008	0.055†	0.041†	0.050†	0.047†	0.005	-0.0063†
All	0.29† ‡	0.16†	0.041† ‡	0.019†	0.047† ‡	0.025†	-0.0056	-0.0053

TABLE 8.2: The slopes of the linear mixed models for the optical variables of each individual patient and all group. (Δ) indicates a change of each optical variable from the baseline (within fifteen minutes from rtPA bolus) to the end of the monitoring ($\sim$ 2.5 hours). (†) indicates a statistically significant slope. (‡) indicates a statistically significant difference of ipsi- over contra-lesional hemisphere as a group. rCBF, relative cerebral blood flow; THC, total hemoglobin concentration; HbO_2, oxy-hemoglobin concentration; Hb, deoxy-hemoglobin concentration. Table adapted from [208].

At 24 hours from the hospital admission, all patients improved by eight or more points in the NIHSS score. About recanalization, complete arterial recanalization was documented in all but one patient (due to insufficient acoustic window) at 24 hours. Moreover, in two patients recanalization was documented at thirty minutes and at the end of rtPA treatment by continuous TCD.

About functional outcome due to the stroke event, at three month-follow up, four out of five patients were functionally independent (mRS<3), and one had moderate disability (mRS=3).

8.4 Discussion

In this pilot study, we have found that DCS/NIRS-DOS can be used at the bedside in the emergency unit without any effects on the clinical treatment.

On a group basis, DCS/NIRS-DOS detected an increase in frontal CBF, THC, and HbO_2 in both hemispheres, which was significantly faster in the ipsilesional hemisphere in a series of AIS patients with a clinical improvement after rtPA-associated recanalization. We were able to obtain real-time optical data in five out of thirteen (38%) patients who fulfilled the clinical criteria, and the rest of the patients were excluded due to the logistics and technical reasons. Consequently, due to the small number of subjects in this proof-of-concept study, we have avoided a discussion of each individual's data.

Overall, these results support the potential role of diffuse optical technology for continuous cerebral perfusion monitoring during therapeutic interventions in patients with AIS.

Currently, TCD is the only available tool for routine clinical use for the non-invasive and real-time monitoring of cerebral hemodynamics after reperfusion therapy [193]. TCD measures blood flow velocities in the major intracranial arteries, which correlates with CBF only as long as the vessel diameter remains constant [213]. It is well-known that its main limitations are that it is operator dependent and requires training and experience to perform and interpret the results [193]. Also, an insufficient acoustic bone window limits its application in 20% to 30% of the patients [214]. Furthermore, TCD can directly insonate only proximal vascular

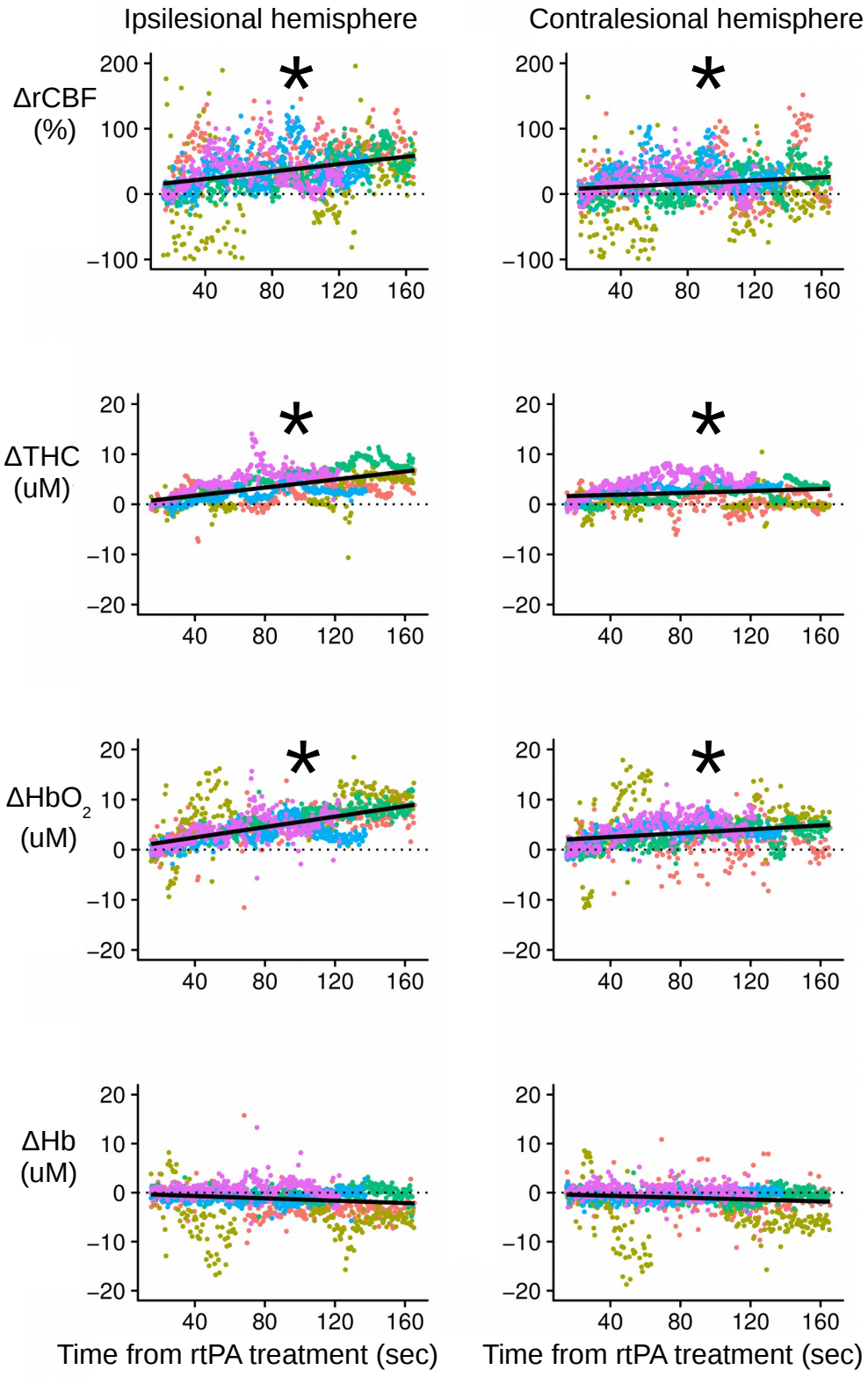

FIGURE 8.3: Frontal microvascular relative cerebral blood flow (rCBF), total hemoglobin concentration (THC), oxy-hemoglobin concentration (HbO_2), and deoxy-hemoglobin concentration (Hb) changes over time are shown for the ipsilesional hemisphere (left column) and the contralesional hemisphere (right column) for all five patients (each patient in different color). (Δ) indicates a change of the optical variable from the baseline. Black line shows the fitted linear model of all the measurement points plotted. The time, x-axis, shows the time elapsed from the rtPA (intravenous recombinant tissue plasminogen activator) treatment onset. (*) indicates a statistically significant positive slope ($p<0.05$). Figure adapted from [208].

segments of large arteries and only indirectly provides information about more distal vascularity [159]. As mentioned previously, TCD is suitable for the monitoring of the large artery recanalization, but not for the microcirculatory reperfusion as in DCS.

Previously, different studies of single case reports or small series have evaluated the potential of NIRS-DOS-based cerebral oximetry to estimate the cerebral perfusion in AIS [215–217]. Recently, Hametner *et al* reported a large cohort of sixty-three patients monitored with commercial NIRS-DOS during mechanical thrombectomy, of whom forty-three had valid data [218]. During the procedure, regional oxygen saturation peaks were observed in fourteen (32.6%) patients and a sustained increase after recanalization in only two patients (4.7%). Although some regional oxygen saturation indices were reported to be associated with the reperfusion status and clinical outcome, the authors concluded that the ability of the current commercial NIRS-DOS monitors to probe local reperfusion is limited. Others have used indocyanine green as a tracer to demonstrate CBF reductions with NIRS-DOS in patients with AIS, showing a good correlation with perfusion weighted imaging measurements [216, 219]. However, the need of an exogenous contrast agent limits their use for continuous monitoring purposes.

Relevantly, previous studies have shown that DCS can successfully track autoregulatory changes of CBF without the need of contrast agents in patients with cerebrovascular disease by using vasoactive stimuli [119, 142]. In this Chapter, we have described a real-time ΔrCBF increase measured by DCS after rtPA treatment. DCS-derived ΔrCBF measurements were in agreement with the simultaneously NIRS-DOS-measured THC and HbO_2, as previously suggested in a single case report [207]. Furthermore, DCS parameters showed a different response between the ipsilesional and contralesional hemispheres in agreement with NIRS-DOS, demonstrating the potential of DCS to detect early changes in cerebral perfusion caused by the rtPA treatment. This asymmetric response found between both hemispheres adjusts for possible systemic circulatory or respiratory disorders as potential confounders.

The main difference of DCS over NIRS-DOS is that it provides a direct measure of cerebral perfusion, which is the goal of most interventions in AIS. In contrast, NIRS-DOS is normally used as an indirect measure of cerebral perfusion based on changes in blood oxygenation or volume which has been shown to differ from CBF in brain-injured patients [121]. Furthermore, the combination of both techniques

can be used to assess the cerebral metabolic rate of oxygen extraction ($CMRO_2$) if absolute Hb and HbO_2 changes can be tracked. $CMRO_2$ is a potentially sensitive biomarker of brain injury [7, 220]. Thus, the combination of DCS and NIRS-DOS offers a more complete view of brain health than any of the techniques alone.

The increase observed in CBF during rtPA treatment may reflect the restoration of downstream flow not only by the recanalization of the occluded artery, but also by the increase of collateral circulation. We have documented arterial recanalization on TCD in four patients at 24 hours. And, in two of them, by using continuous TCD monitoring, we have showed that the arterial recanalization coincided with CBF increase during rtPA infusion. We note that leptomeningeal collateral flow may also contribute to cortical CBF changes detected by DCS, as suggested by previous studies, in which CBF variations correlated with changes in MCA velocities on TCD in healthy volunteers but diverged in patients with severe carotid artery stenosis who had activated compensatory flow sources [83, 142]. However, in order to avoid delays in the administration of intravenous rtPA, our neuroimaging protocol did not include the measurement of the collateral circulation to support this hypothesis.

In conclusion, this study shows that continuous diffuse optical monitoring of cerebral hemodynamics at the bedside in AIS patients treated with rtPA treatment is feasible. Our study supports further research in larger populations with the improved setups for the emergency unit.

8.4.1 Future work

Future work should include absolute numbers to be able to measure the $CMRO_2$ and a control group (patients with no recanalization). Instead, for this study the contralesional hemisphere has been used as control.

Chapter 9

Early microvascular cerebral blood flow response to head-of-bed elevation is related to functional outcome in acute ischemic stroke

Hypothesis:
The blood flow response to an orthostatic challenge in ischemic stroke patients correlates with the clinical outcome at three months from the stroke onset.

9.1 Introduction

There are no highly effective treatments for acute ischemic stroke (AIS) where current clinical approaches have a limited efficacy to the removal of the thrombus [221]. Therefore, it is still crucial to pick the most appropriate management strategies.

Flat head-of-bed (HOB) positioning is a management strategy that has often been used as a widely available method to promote increased cerebral perfusion in the clinics [222]. The specifics of cerebral blood flow (CBF) changes due to HOB positioning after AIS related brain injury have been studied by transcranial Doppler

ultrasound (TCD) and optical studies [119, 120, 133, 223–225]. A systematic review and meta-analysis of TCD studies found that mean cerebral blood flow velocity (CBFV) increased in the side of the affected major cerebral arteries when the patients were positioned in the lying-flat (supine) HOB position [226]. However, the clinical benefits are uncertain and contradictory [227, 228] which could be due to individual variability.

Recent research with diffuse correlation spectroscopy (DCS) has provided evidence that the cerebral hemodynamic response to HOB positioning is heterogeneous among individuals after brain injury [119–122], and is otherwise relatively homogeneous [118]. In patients with AIS, an inter-hemispheric asymmetry was observed including a paradoxical response (no change or change in the opposite expected direction) identified in $\approx 25\%$ of the cases [119, 120]. This paradoxical response was not detected in simultaneous TCD monitoring, suggesting that DCS may be superior for monitoring collateral blood flow dynamics during posture changes [119]. Similarly, the cerebral hemodynamic response to HOB position alterations was shown to be a biomarker of clinical status in obstructive sleep apnea patients [127] (Chapter 5) and in internal carotid artery stenosis patients [117] (Chapter 7).

Therefore, we have hypothesized and tested that this method may detect abnormalities in the cerebral autoregulation and its changes in response to a therapy. In particular, this method may be a biomarker of the functional outcome after AIS as the role of collateral flow is linked to the recovery of penumbra. If so, this protocol can be used for individualization of therapies including the selection of earlier optimal positioning to improve the benefits of postural and mobilization therapies on functional outcome. The results of this study have been submitted and are under review [123]. Partial results of this study are also in Igor Blanco's thesis [124]. Furthermore, they have also been utilized in the pooled data reported in Chapter 10, which is under preparation for submission [122].

9.2 Aims

In this study, we investigated the relationship between the cortical CBF response to HOB changes measured by DCS at different times after the symptom onset and the functional outcome of patients with AIS. We have hypothesized that

the cortical CBF response to HOB changes during the earlier phases of AIS is a biomarker of CBF autoregulation, and, therefore, is associated with functional outcome after stroke.

9.3 Methods

This study was conducted at the Stroke Unit of Hospital de la Santa Creu i Sant Pau (Barcelona, Spain) from 2015 to 2017, whose protocol was approved by the Ethical Committee (EC/15/130). The participants or their legal proxies gave written consent to participate.

Patients with an acute non-lacunar AIS in the anterior circulation of less than 48 hours from the symptom onset were recruited for bilateral monitoring of CBF in the frontal lobes during a HOB elevation from supine (0°) to 30°. The inclusion criteria were being older than 18 years, National Institute of Health Stroke Scale (NIHSS) [209] of more than three at admission and pre-stroke modified Rankin Scale (mRS) [210] of less than three. The exclusion criteria were resting heart rate less than 40 or greater than 110 beats per minute, peripheral arterial oxygen saturation less than 92% with supplementation, diagnosis of transient ischemic attack, minor stroke, or posterior circulation AIS.

9.3.1 Head-of-bed manipulation protocol

All patients were placed flat (HOB 0°-15°) during the first 24 hours except when being measured according to the local practice. Afterwards, mobilization was initiated according to the judgment of the clinician.

During the study, first, the patient was placed in supine position (0°) for at least thirty minutes. Afterwards, data was acquired for five minutes each at baseline supine and at 30° elevation. Finally, the patient was returned back to the flat position (0°-15°). The protocol is depicted on the top Figure 9.1. The transition between the HOB positions was recorded and lasted a maximum of thirty seconds. The protocol was repeated up-to four times at intervals of 48 hours during the first week of admission if the patient was stable.

9.3.2 Optical methods and instrumentation

We have used the DCS unit of the hybrid device described in Section 4.1.1. Two optical probes (the same as shown in Figure 8.1 in Chapter 8) were made of custom built fibers consisting of a source fiber and a detector fiber bundle with four single-mode fibers with 2.5 cm source-detector separation. Cerebral blood flow was monitored continuously every 2.5 seconds and relative CBF changes were obtained by dividing the continuous blood flow index by this mean baseline CBF. The change in CBF between 0° to 30° ($\Delta \mathrm{rCBF}_{\text{supine to } 30^\circ}$) is reported as the average of the first to four minutes at 30°.

A paradoxical response was defined as an increase of $\Delta \mathrm{rCBF}_{\text{supine to } 30^\circ} > 2\%$ or "no change", which was defined as the coefficient of variation measured in the healthy subjects of Chapter 7.

9.3.3 Clinical and imaging evaluation

Baseline examinations included the collection of demographics and vascular risk factors and a physical examination. The stroke severity was assessed with the NIHSS at admission, at the moment of the measurement, at 24 and at 48 hours from stroke onset, and at discharge. Early clinical deterioration was defined as an increase of at least four points of the 48 hour NIHSS score compared to the baseline. The etiologic stroke subtype was classified according to the modified *Trial of Org 10 172 in Acute Stroke Treatment* (TOAST) criteria [229].

At admission, a cranial computed tomography (CT) and vascular imaging with either CT-angiography or color-coded duplex sonography were performed. The extent of early ischemic changes was evaluated by the Alberta Stroke Program Early Computed Tomography Score (ASPECTS) [230].

If relevant, recanalization was assessed by transcranial duplex before our protocol. Functional outcome was evaluated at three months by the mRS. A score of >2 was considered indicative of an unfavorable functional outcome. All the neurological scales were obtained by experienced clinicians blinded to the optical information.

9.3.4 Statistical analysis

We have expressed quantitative variables as a median and an interquartile range (median (Q1, Q3)), and categorical variables as number of cases and percentages.

Wilcoxon rank-sum test was used to assess the difference of the change in cerebral blood flow between 0° to 30° ($\Delta\text{rCBF}_{\text{supine to 30°}}$) responses between with and without good functional outcome (favorable, mRS ≤ 2)) when only the first measurement for each patient was used. The Wilcoxon rank-sum test (for quantitative variables) or the chi-squared test (for categorical variables) were used to assess differences on the clinical and demographic variables between paradoxical and non-paradoxical responses; using Bonferroni correction when categorical variables presented more than two factors. The Wilcoxon signed-rank test was used to assess the $\Delta\text{rCBF}_{\text{supine to 30°}}$ response between ipsi- and contra-lesional hemispheres and to assess if the $\Delta\text{rCBF}_{\text{supine to 30°}}$ response was different from zero.

We conducted a multivariate linear mixed-effect model to assess clinical and radiological variables associated with $\Delta\text{rCBF}_{\text{supine to 30°}}$. Also, we conducted a multivariate logistic mixed-effect model to assess clinical, radiological and optical variables associated with the dichotomized mRS at three months. Only variables showing a significant trend ($p < 0.05$) in the bivariate analyses were included in the forward multivariate model. Patient identification number was considered to be a random factor for the mixed-effect models. Model fit was assessed using chi-square tests on the log-likelihood values to compare the different models. Residuals plots were tested for the inspection of deviations from normality and homoscedasticity.

All analyses were carried out in the R programming language and environment [135] and "nlme" software package was used. A p-value < 0.05 was considered to be statistically significant.

9.4 Results

9.4.1 Clinical and radiological findings

We have studied thirty-eight (n=38) patients with an AIS in the anterior circulation. Table 9.1 contains the population demographics and clinical characteristics.

The median age was 83 (68.75, 88) years. Median NIHSS score at admission was 19 (16, 21). At three months, the median mRS score was 4 (3, 6) and thirty-one patients (n=31, 82%) were disabled (mRS > 2) or had died.

Age (y)	83 (68.75, 88)
Male sex, n (%)	17 (44.7)
Hypertension, n (%)	33 (86.8)
Dyslipidemia, n (%)	19 (50)
Diabetes mellitus, n (%)	8 (26.7)
Atrial fibrilaltion, n (%)	19 (50)
Time from symptoms onset to measurement (h)	17.1 (6.7, 23.1)
Extracranial ICA stenosis > 50%, n (%)	9 (23.7)
Thrombolysis, n (%)	25 (65.8)
Thrombectomy, n (%)	3 (7.9)
Intracranial occlusion (supraclinoid ICA or MCA), n (%)	29 (76)
Recanalization, n (%)	13 (34)
Occlusion in follow-up duplex, n (%)	12 (32)
Recanalization unknown, n (%)	13 (34)
Admission ASPECTS	9 (6.25, 10)
TOAST:	
Large artery atherosclerosis, n (%)	5 (13)
Cardioembolism, n (%)	13 (34)
Other etiology, n (%)	2 (5)
Undetermined etiology, n (%)	18 (47)
NIHSS at patient admission	19 (16, 21)
NIHSS at measurement	18 (7, 20)
Early neurological deterioration, n (%)	6 (16)
mRS at three months	4 (3, 6)
Disabled at three months, n (%)	31 (82)
Death, n (%)	9 (24)

TABLE 9.1: Demographic and clinical variables of the study population (n=38). ICA, internal carotid artery; MCA, middle cerebral artery; ASPECTS, Alberta Stroke Program Early Computed Tomography Score; TOAST, Trial of Org 10 172 in Acute Stroke Treatment; NIHSS, National Institute of Health Stroke Scale; mRS, modified Rankin Scale.

9.4.2 Head-of-bed position challenge findings

Median time from the stroke onset to the first optical measurement was 17 (7, 23) hours. In one patient, the three repeated measurements performed in one hemisphere were excluded due to a frontal subcutaneous haematoma under the

optical probe. Two additional measurements in one hemisphere each were excluded due to technical reasons. All patients tolerated HOB elevation and there were no study related side effects. Finally, a total of seventy-two (n=72) measurements were analyzed.

Figure 9.1 shows representative typical and paradoxical responses of $\Delta rCBF_{\text{supine to } 30^\circ}$.

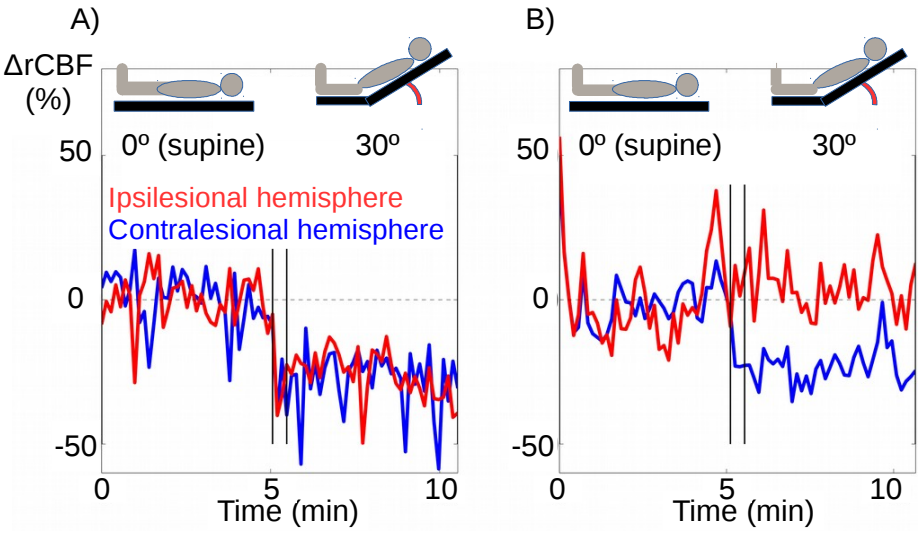

FIGURE 9.1: Continuous optical measurement showing A) an expected relative cerebral blood flow (ΔrCBF) response and B) a paradoxical response in one hemisphere (ipsilesional hemisphere) for two different patients. Vertical lines indicate the period when body position was being changed.

Overall, Table 9.2, median frontal $\Delta rCBF_{\text{supine to } 30^\circ}$ decreased significantly in both the ipsilesional (-3.1 (-10.7, 3.0)%, p=0.030) and the contralesional hemispheres (-9.5 (-15.8, -3.5)%, p=0.029) in the first measurement. There were no significant differences in $\Delta rCBF_{\text{supine to } 30^\circ}$ after HOB elevation between the ipsilesional and contralesional hemispheres (p= 0.387).

	mRS 0-2	mRS 3-6	p
ΔrCBF$_{\text{supine to } 30^\circ}$ (%), $\leq$48 hours (n=38)	n=7	n=31	
Ipsilesional	-8.8 (-13.5, -5.5)*	-2.5 (-8.5, 4.9)	0.1
Contralesional	-13.4 (-15.9, -10.5)*	-5.1 (-15.7, 4.9)	0.221
Paradoxical response	2.3, n=2	7.1 (3.0, 12.3)*, n=25	-
ΔrCBF$_{\text{supine to } 30^\circ}$ (%), $\leq$12 hours (n=17)	n=4	n=13	
Ipsilesional	-10.4 (-12.7, -7.3)	-0.9 (-4.4, 5.0)	0.032
Contralesional	-13.9 (-15.6, -7.9)	-14.0 (-17.2, 7.4)	0.878
Paradoxical response	5.6, n=1	9.1 (4.2, 27.4)*, n=12	-
ΔrCBF$_{\text{supine to } 30^\circ}$ (%), >12 hours (n=21)			
Ipsilesional	-8.3 (-11.9, -4.6), n=3	-5.2 (-23.2, 4.5), n=17	0.690
Contralesional	-13.4 (-17.1, -11.0), n=3	-3.5 (-10.3, 3.5), n=15	0.130
Paradoxical response	-1.0, n=1	5.7 (2.9, 9.5)*, n=13	-

TABLE 9.2: Median and interquartile ranges of relative cerebral blood flow responses between 0° to 30° (ΔrCBF$_{\text{supine to } 30^\circ}$) are shown grouped according to the time period of the first measurement and to the three months-modified Rankin Scale (mRS) score. ($*$) indicates a statistically significant difference from zero.

When the measurements were grouped by time of the measurement, ΔrCBF$_{\text{supine to 30°}}$ was comparable between the early ($\leq$ 12 hours) and the late ($>$ 12 hours) phase for both the ipsilesional and contralesional hemispheres (p=0.357 and p=0.510, respectively). In patients with serial measurements, there was no statistically significant difference between the first and the second measurements in the ipsilesional (p=0.190) or contralesional hemisphere (p=0.890).

In the first measurement performed, an unilateral or bilateral paradoxical response was present in twenty-one (n=21, 55%) patients (71% ipsilesional, 19% bilateral), which is further discussed in the Appendix.

There were no clinical or radiological predictors of the ΔrCBF$_{\text{supine to 30°}}$ response to HOB elevation in the early or late phase measurements or globally. For instance, the ΔrCBF$_{\text{supine to 30°}}$ response was not statistically significantly associated with either the early clinical course (deteriorated (p=0.603) or non-deteriorated (p=0.587)) or functional outcome at three months (p=0.578). An exception was the association with the mRS in the early phase, which is discussed below.

9.4.3 Relationship between ΔrCBF$_{\text{supine to 30°}}$ and functional outcome

Figure 9.2 shows ipsilesional ΔrCBF$_{\text{supine to 30°}}$ versus the modified Rankin Scale (n=38). When patients were divided according to the timing of the measurement, a statistically significant association between the ipsilesional ΔrCBF$_{\text{supine to 30°}}$ within the first 12 hours (early phase) from stroke onset and the dichotomized mRS score at three months (p=0.010) was observed (slope=1.6, see Table 9.2 and Figure 9.2 A)). Figure 9.2 B) shows that patients with a favorable functional outcome had a higher decrease of ΔrCBF$_{\text{supine to 30°}}$ in the ipsilesional hemisphere during the early phases ($\leq$ 12 hours), compared to those with an unfavorable functional outcome (-10.4 (-12.7, -7.3) and -0.9 (-4.4, 5.0) respectively, p=0.032). In contrast, the ΔrCBF$_{\text{supine to 30°}}$ response at later phases ($>$ 12 hours) was not related to functional outcome, p=0.878, as shown in Figure 9.2 D), and no linear model could be fit (Figure 9.2 C)).

Despite this association, ΔrCBF$_{\text{supine to 30°}}$ was not a predictor of functional outcome at three months of follow-up. Remarkably, NIHSS was the only predictor of functional outcome at three months ($p < 0.001$) with a slope of 1.23.

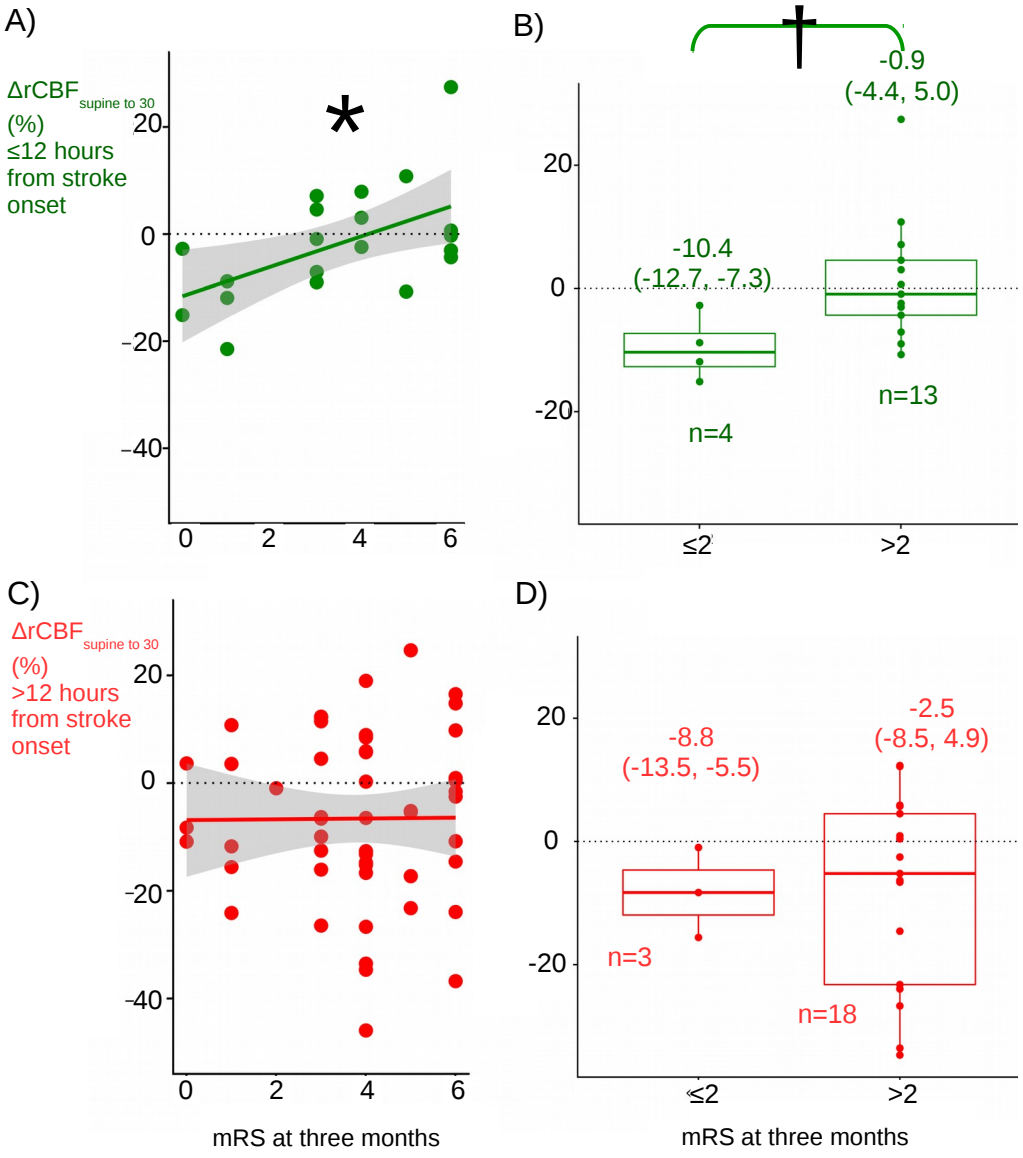

FIGURE 9.2: Ipsilesional relative cerebral blood flow responses between 0° to 30° (ΔrCBF$_{\text{supine to 30°}}$) versus modified Rankin Scale (mRS) at three months at the early phase from stroke onset (n=17) A) as a continuous variable and B) dichotomized according to functional outcome. Similarly, panels C) and D) correspond to the late phase (n=21). The shaded region shows the 95% confidence intervals. (∗) and (†) indicate a statistically significant linear model and difference between groups, respectively. Boxplots and labels show the median (interquartile range).

9.5 Discussion

The main finding of our study is the association between the early-phase, ipsilesional, microvascular CBF response to the changes of head positioning and the functional outcome in patients with anterior circulation AIS. The optical monitoring of CBF during HOB changes may, therefore, help to individualize future treatment strategies, including optimal positioning, after AIS.

Functional outcome at three months was related to the response of $\Delta\text{rCBF}_{\text{supine to }30^\circ}$ to HOB changes occurring in the early phase (<12 hours after symptom onset), but not at later time points. This is relevant since the AIS morbidity is on the restoration of the CBF in the penumbra within a time window of cellular viability that depends on duration and severity of CBF cessation. Here, cerebral collateral circulation plays a major role in the recovery, and the timing when these collaterals are activated is important for their clinical effect. Early good collateral status is a strong predictor of better clinical outcome, while delayed collateral recruitment may indicate worse outcome [231]. Therefore, it could be expected that the response to collateral-enhancing stimuli, such as HOB positioning, may differ according to the timing from stroke onset.

Unlike this study, Favilla *et al* failed to find an association between $\Delta\text{rCBF}_{\text{supine to }30^\circ}$ within the first 72 hours and stroke functional outcome [119]. This suggests that the impact of HOB positioning may be relevant during the early critical period, when potentially salvageable (penumbral) tissue is still present. Also, the higher stroke severity of our study sample may explain the difference between both studies.

Although $\Delta\text{rCBF}_{\text{supine to }30^\circ}$ did not emerge to be the best predictor of functional outcome in the multivariant logistic model in our study, its association deserves further research, as it represents a biomarker of a quantifiable effect that may enable the clinicians to personalize therapeutic strategies. Future studies could investigate whether any related management strategies may help to optimize cerebral perfusion and improve functional outcome. In fact, it has been long recognized that changes in head and body posture can worsen or improve neurological symptoms in occlusive cerebrovascular disease by inducing changes in CBF [232, 233]. The potential mechanisms include a gravitational effect in passively dilated vessels due to impaired cerebral autoregulation, the cardiovascular and respiratory effects of the upright position (including a reduction of blood pressure), increased venous

return, altered cardiac output and postural hypocapnia related to hyperventilation and improved chest wall compliance [234, 235]. Interestingly, it has been found that flat HOB positioning increases CBF possibly by improving the efficiency of passive-pressure dependent collateral flow [225, 236]. Thus, postural tilting has been proposed as a potential challenge for assessing and enhancing the functional capacity of collateral circulation [196].

The $\Delta rCBF_{\text{supine to } 30^\circ}$ was found to be paradoxical or reduced in patients with unfavorable outcome, where some patients did not respond to the HOB position change. The reason of this decreased $\Delta rCBF_{\text{supine to } 30^\circ}$ could be that these patients suffered from cerebral autoregulation impairment [30]. Recently, in non-stroke patients, Lam *et al* studied the cerebral autoregulation, the critical closing pressure, the mean arterial pressure and the CBFV during a similar protocol [134]. As hypothesized before [237], the cerebral autoregulation remained intact after the HOB position change, but the critical closing pressure, the mean arterial pressure and the CBFV were decreased. CBFV changes were -4.5 $\pm$ 3.3%, which are lower to our results of patients with a favorable outcome ($\Delta rCBF_{\text{supine to } 30^\circ}$ of -10.4 (-12.7, -7.3)% and -8.8 (-13.5, -5.5)% for early and late phases).

The HOB position change as an alternative stimuli in order to derive a biomarker for cerebrovascular reactivity/cerebral autoregulation is attractive, because, compared to other stimuli, it is non-invasive, easy to perform and does not require subject collaboration. As reported in previous studies in both brain injured and healthy subjects [118–121, 127, 133] HOB angle manipulation was well tolerated and no changes in the stroke severity were observed.

The latest advances in DCS have provided a better insight into the behavior of CBF dynamics during these mentioned HOB changes by monitoring microvascular CBF in the frontal cortex at the bedside and without the need of an exogenous contrast [7]. In agreement with previous DCS studies [117, 119–122, 127] (including Chapters 5, 7 and 10), we have observed a substantial inter-individual variation in CBF responses to HOB changes. In contrast, a more homogeneous response to HOB manipulation among individuals has been described in healthy subjects [118]. This is consistent with the presence of different degrees of collateral flow and cerebral autoregulation impairment after AIS. Unfortunately, in our study no collateral scores have been assessed.

We acknowledge that our study has several limitations. The high admission NIHSS score limited our findings to patients with large hemispheric strokes. Also, our recruitment at the early phase was limited, which should be improved in the future with the recent emergence of commercial user-friendly systems (e.g. HemoPhotonics S.L. and ISS). An intervention randomized controlled study is underway to determine whether CBF variation during position changes is a risk factor or only a biomarker of worse functional outcome.

In conclusion, microvascular CBF response to an increase of the HOB during the early phase of stroke has been related to the functional outcome. The HOB response could be related to the functional capacity of collateral circulation. However, further studies are needed to elucidate if this information could be used to individualize management for the patients in the Stroke Unit for improving the functional outcome after AIS.

9.6 Appendix

In line with prior studies [117, 119, 120, 122, 127, 133, 238] (including Chapters 5, 7 and 10), we have also observed paradoxical responses to HOB changes.

Table 9.3 shows the clinical and radiological characteristics of the study population according to the presence of an expected (non-paradoxical) or paradoxical response of CBF to the head-of-bed elevation.

	Non-paradoxical (n=12)	Paradoxical (n=26)	p
Age (y)	75.5 (65.5, 85.25)	84.5 (74.25, 88.75)	0.258
Male sex, n (%)	3 (25)	18 (69)	0.028
Hypertension, n (%)	2 (17)	3 (13)	1
Atrial fibrilaltion, n (%)	6 (50)	13 (50)	1
Extracranial ICA stenosis >50%, n (%)	4 (33)	5 (19)	0.576
Thrombolysis, n (%)	8 (67)	17 (65)	1
Thrombectomy, n (%)	2 (17)	1 (4)	0.474
Intracranial occlusion (ICA or MCA), n (%)	12 (100)	17 (65)	0.055
ASPECTS	8 (5.5, 9)	9 (7,10)	0.201
ASPECTS close to the measurement	7 (3.75, 9)	9 (2.75, 9.75)	0.713
TOAST:			0.047
Large artery atherosclerosis, n (%)	4 (33)	1 (4)	0.719
Cardioembolism, n (%)	2 (17)	11 (42)	0.049
Other etiology, n (%)	0 (0)	2 (8)	0.629
Undetermined etiology, n (%)	6 (50)	12 (46)	0.629
NIHSS at measurement	16 (6.5, 21)	18 (8.25, 20)	0.950
mRS at three months	4 (3, 5)	4 (3, 6)	0.760
Death, n (%)	6 (24)	3 (23)	1

TABLE 9.3: Demographic and clinical results for n=38 acute ischemic stroke patients divided in to non-paradoxical or paradoxical relative cerebral blood flow responders. ICA, internal carotid artery; MCA, middle cerebral artery; ASPECTS, Alberta Stroke Program Early Computed Tomography Score; TOAST, Trial of Org 10 172 in Acute Stroke Treatment; NIHSS, National Institute of Health Stroke Scale; mRS, modified Rankin Scale.

Eight (n=8, 89%) uni-/bi-lateral paradoxical responders (n=9) in the early phase (n=17) had an unfavorable functional outcome, and also in six (n=6, 67%) non-paradoxical responders (n=8). But no significant interaction was found between being or not paradoxical in the early phase and unfavorable or favorable outcome (p=1). Considering all the measurements, twenty-two (n=22, 85%) of the uni-/bi-lateral paradoxical responders (n=26) and nine (n=9, 75%) of non-paradoxical responders (n=12) had an unfavorable functional outcome. Again, no significant interaction was found (p=0.794).

In our study, 55% ((n=21) patients (71% in the ipsilesional hemisphere and 19% in both hemispheres)) of our patients showed a paradoxical response in the initial measurement. This percentage was higher (68%, n=26) during the first week after stroke onset. However, we did not find a significant change of $\Delta \text{rCBF}_{\text{supine to } 30^\circ}$ response over time. Interestingly, a gender effect was observed between patients with paradoxical and non-paradoxical $\Delta \text{rCBF}_{\text{supine to } 30^\circ}$ responses (p=0.028), with males showing a higher rate of paradoxical responses. Although the mechanism remains unclear, differences between sexes in relation to cerebral blood flow autoregulation have been previously found, suggesting that women have a stronger cerebral blood flow response than men [239]. Edlow et al. [118] previously reported a smaller CBF response to HOB manipulation for females in the healthy population, but this was not previously reported for acute ischemic stroke patients [119, 120]. Also, we found a paradoxical response more frequent in patients with cardioembolic stroke (p=0.049). In our serie, atrial fibrillation was the cardioembolic stroke subtype in all this group of patients (n=13), and, according to previous studies [240, 241], this could be linked to underdeveloped collateral circulation.

Chapter 10

A mild orthostatic challenge shows cerebral autoregulation impairment on the ipsilesional hemisphere of ischemic stroke patients

Hypothesis:
The blood flow response to an orthostatic challenge in ischemic stroke patients correlates with the mean arterial pressure response to the same orthostatic challenge.

10.1 Introduction

As presented already in the previous Chapters (5, 7 and 9), a transient alteration of the patient head-of-bed position has been considered as a stimuli to test cerebral vasoreactivity (CVR; the response to a stimulus that dilates or contracts the cerebral vasculature [4]) [117–121, 123, 127, 133, 134, 196]. I refer to this as a "head-of-bed (HOB) challenge", as in the previous Chapters 5, 7 and 9. This challenge is attractive for many reasons because, when compared to other stimuli, it is non-invasive (no need to inspire gases or inject drugs), is easy to perform and

does not require subject collaboration. As reported in previous studies in both brain injured and healthy subjects [118, 119, 121, 127, 133], HOB angle manipulation was well tolerated and did not cause any pathological alterations in the subject status.

In general, microvascular CBF has been found to be inversely correlated to the HOB angle change. In other words, it shows an increase/decrease after a decrease/increase of the HOB angle. The precise details of this hemodynamic response after a HOB positioning are complex and are believed to be a combination of cerebral autoregulation involving alterations in venous blood return to the heart, changes in intracranial pressure, in blood volume, and in mean arterial pressure (MAP), and other neuroreflex mechanisms [134, 196, 242–244][1]. Moreover, a paradoxical response (no change or change in the opposite expected direction) was observed in around a quarter of the ischemic stroke patients that were measured [119, 120], and, was routinely observed in other brain injury subjects [121]. I have also observed paradoxical response in my studies on obstructive sleep apnea and internal carotid artery stenosis patients [117, 127] (Chapters 5 and 7). Interestingly, the paradoxical response was not detected in simultaneous TCD monitoring in most cases, suggesting that DCS may provide different information over TCD for monitoring the blood flow dynamics during posture changes [119].

In general, neither the simple head-of-bed challenge going from supine (0°) to 30° nor from 30° to supine (0°), during five minutes approximately in each position, have provided a general specificity in different pathologies including ischemic stroke and obstructive sleep apnea (OSA) [119, 120, 127, 133] (also Chapters 5, 9 and 10). Only Kim *et al* [121] found a higher CBF response in controls than in brain-injured patients in a HOB from 30° to supine (0°). However, another interesting finding, and relevant to this work, is in the ability of CBF to recover back to its original levels after starting at a supine position, followed by approximately five minutes of HOB elevation, and after returning back to the original supine position. This was originally considered as a minor side-effect of the lengthier and more disruptive protocols [118, 120]. However, later on in a study on OSA patients [127] (Chapter 5), we have found that this alteration was related to OSA severity. And, interestingly, that long-term treatment ameliorated this alteration. This result suggests that patients with OSA, or with altered CVR, might need

[1]Special thanks for Dr James Munis of Mayo Clinic, Rochester, USA for his discussion on the HOB positioning

a longer time period than five minutes in each HOB position to stabilize their hemodynamic response. This is assuming that healthy cerebrovasculature, would normalize the CBF, if given enough time.

As mentioned, the microvascular cerebral blood flow response to changes in HOB position has been shown to be variably altered in acute ischemic stroke (AIS) measured by diffuse correlation spectroscopy (DCS) [119]. However, the relationship between CBF and associated systemic MAP changes has not been evaluated. After acute stroke, it has been hypothesized that the arterial hypertension that develops immediately after stroke represents a pathophysiological response to enhance perfusion of the reversible penumbra of the infarct, where the perfusion passively follows the variations in MAP since normal autoregulatory mechanisms are impaired [143, 245]. But relatively little is known about it and its measurements at early hours after stroke have been elusive.

However, it is well-known that the efficacy of reperfusion therapies is related to the time from stroke onset, since ischemia in the brain is a reversible process dependent on the restoration of the CBF in the penumbra within a time window of cellular viability that varies on duration and severity of CBF cessation [246]. Cerebral collateral circulation plays an important role in extending this time window by perfusing the penumbra [231]. Then, it could be expected that the response to collateral-enhancing stimuli, such as head-of-bed positioning, may differ according to the timing from stroke onset.

In this study, we sought to evaluate the relative cerebral blood flow (ΔrCBF) recovery back to supine position, measured by DCS, after different HOB position changes, and also to evaluate the relationship between ΔrCBF and associated systemic blood pressure changes to HOB position changes of patients with AIS. We have hypothesized that the individual profile of cortical CBF and MAP responses to HOB changes during the earlier phases of AIS may be a biomarker of CBF autoregulation. In order to achieve this, we have aggregated data from three studies from two countries.

10.2 Methods

10.2.1 Study population

For this work, data has been aggregated from three different studies. In chronological order: The first and the second studies were conducted at the Hospital of the University of Pennsylvania from 2006 to 2007 [120] and from 2009 to 2011 [119], respectively. The third study was conducted at the Stroke Unit of Hospital de la Santa Creu i Sant Pau (Barcelona, Spain) from 2015 to 2017 [123] (Chapter 9). The three protocols were approved by the corresponding local review boards, and the participants or their legal proxies gave written consent to participate.

The general inclusion criteria included patients admitted to the stroke service with radiographic evidence or clinical suspicion of anterior acute ischemic stroke and being older than 18 years. The general exclusion criteria were intracranial hemorrhage on initial computed tomography, or magnetic resonance imaging, and inability to lie supine for fifteen minutes. The specific inclusion and exclusion criteria for each study can be found on the different publications of these three studies [119, 120, 123] and are described below.

Inclusion and exclusion criteria for each study

- UPENN 2006-2007 [120] & UPENN 2009-2011 [119]:

  Inclusion: patients admitted to the stroke service with radiographic evidence or clinical suspicion of acute ischemic stroke involving the frontal lobe cortex.

  Exclusion: intracranial hemorrhage on initial computed tomography (CT) or magnetic resonance imaging (MRI) scan and inability to lie supine for 15 minutes.

- ICFO 2015-2017 [123] (Chapter 9):

  Inclusion: being older than 18 years, a National Institute of Health Stroke Scale (NIHSS) score [209] of more than three at admission, pre-stroke modified Rankin Scale (mRS) score [210] of less than three, and written informed consent.

Exclusion: resting heart rate less than 40 or greater than 110 beats per minute, peripheral arterial oxygen saturation less than 92% with supplementation, diagnosis of transient ischemic attack or minor stroke and acute ischemic stroke in the posterior territory.

10.2.2 Head-of-bed manipulation protocol

All patients were placed flat with the HOB between 0° and 20° during the first twenty-four hours (with the exception of the time where they were being measured with our protocol) according to the different local clinical practice guidelines. Afterwards, mobilization was initiated according to the judgment of the attending clinician.

The three different mild HOB orthostatic challenge protocols, one for each study, to induce CBF changes are shown in Figure 10.1. All three protocols involved orthostatic challenges in different HOB positions, including, and relevant to this work, repeated supine positions (as shown in yellow in Figure 10.1). Data was acquired for five minutes at each position. The transition between HOB positions was noted as event markers in the data.

For the UPENN studies [119, 120], the study protocol was planned for three separate days and the first measurement was performed as soon as the patient was available. For the ICFO study [123], the study protocol was initiated <48 hours after symptom onset. The protocol was repeated up-to four times at intervals of 48 hours during the first week of admission if the patient was stable.

10.2.3 Optical methods and instrumentation

For the three studies, two non-invasive, optical probes were placed on the forehead bilaterally on both hemispheres, as lateral as possible trying to avoid the sinuses. Previous studies by other methods [25] and by DCS [7] have shown that the frontal cortical area a is valid area of measurement when studying the bulk CVR at a cerebral hemisphere level. These probes consisted of a detector fibre set at a 2.5 cm from a source fibre providing mostly information about the cerebral cortex hemodynamics as previously validated [7, 8, 24].

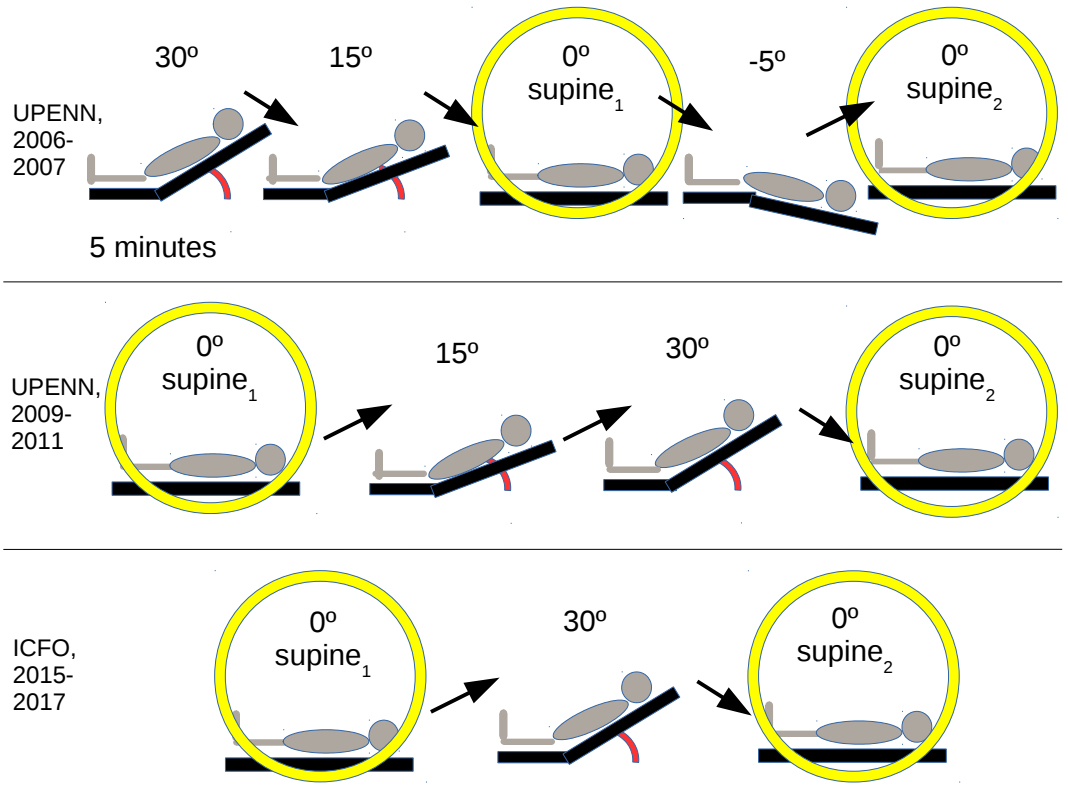

FIGURE 10.1: The three different protocols with the supine positions used for this analysis are selected with a circle.

The ΔrCBF changes considered for this work were obtained by calculating the mean blood flow index in the first supine (0°) position, and, using this mean, the continuous blood flow index was normalized for the second supine position. After explaining the general features of the devices used, the three devices for the three different protocols are explained below with more details.

For the UPENN 2006-2007 study [120], a portable custom-built instrument was employed as described in Refs. [220, 247]. Near-infrared diffuse optical spectroscopy (NIRS-DOS) was also implemented, even though this data will not be used for this analysis. The data acquisition was interleaved between NIRS-DOS and DCS. For each probe, first NIRS-DOS data was acquired for half a second on one hemisphere, then, DCS data was acquired for three seconds. This gives a total of seven seconds of measurement time per data point since one hemisphere was measured at a time. The first minute in each position was discarded from the analysis of ΔrCBF changes due to possible movement artifacts and for avoiding systemic instabilities for this dataset. No MAP measurements were acquired for this study.

For the UPENN 2009-2011 study [119], data were collected from both hemispheres every three seconds using the same instrument as in the previous study [120]. Again, the first minute in each position was discarded from the analysis of ΔrCBF changes. For the continuous MAP measurements, the first and last minutes from the analysis were discarded and the rest were used to calculate a mean of each HOB position. For this study, continuous non-invasive blood pressure monitor Finapres (Finapres Medical Systems, Arnhem, the Netherlands) device was used to measure the arterial blood pressure in a sub-set of patients.

For the ICFO 2015-2017 study [123] (Chapter 9), the custom build device used is described in Section 4.1.1. Data were collected from both hemispheres every 2.5 seconds. The first and last minutes from the analysis of ΔrCBF changes were discarded. In this study, a manual sphygmomanometer (Omron BP785 IntelliSense Automatic Blood Pressure Monitor, Omron, Osaka, Japan) at 2.5 minutes from each HOB change was used to measure the arterial blood pressure.

10.2.4 Clinical and imaging evaluation

Baseline examinations included the collection of demographics and vascular risk factors and a physical examination. The stroke severity was assessed with the NIHSS at admission.

The neurological scales were obtained by certified neurologists or senior residents under supervision blinded to the optical information.

The specific clinical and imaging evaluations for each study can be found in previous publications [119, 120, 123] and are briefly described below.

- UPENN 2006-2007 [120]:
  Baseline examinations included the collection of demographics and vascular risk factors from verbal history and available medical records. The stroke severity was assessed with the NIHSS at admission. Stroke etiology was classified according to the *Trial of ORG 10172 in Acute Stroke Treatment* (TOAST) criteria [248]. A neurologist reviewed all available head CT and brain MRI data to determine stroke (or infarct) laterality, vascular territory, and region(s) of the brain involved. The primary indicators for radiographic evidence of stroke were hypodensity on CT and/or diffusion restriction on

diffusion MRI sequences. CT and magnetic resonance angiographic data were also used to support the assessment of vascular territory involvement when being available. Vessel involvement was characterized as middle cerebral artery or anterior cerebral artery. Brain region involvement was characterized as frontal, temporal, parietal or occipital.

- UPENN 2009-2011 [119]:
  Baseline examinations included the collection of demographics and vascular risk factors. The stroke severity was assessed with the NIHSS at admission, at the moment of the measurement and at discharge. Stroke cause was recorded. The extent of early ischemic changes was evaluated on noncontrast CT by the Alberta Stroke Program Early Computed Tomography Score (ASPECTS) [230]. Functional outcome was evaluated by the mRS.

- ICFO 2015-2017 [123] (Chapter 9):
  Baseline examinations included the collection of demographics and vascular risk factors and a physical examination. The stroke severity was assessed with the NIHSS [209] at admission, at the moment of the measurement, at 24 and at 48 hours from stroke onset, and at discharge. The etiologic stroke subtype was classified according to the modified TOAST criteria [229]. At admission, a cranial CT was performed on all patients and also a vascular imaging with either CT-angiography or color-coded duplex sonography. The extent of early ischemic changes was evaluated on noncontrast CT by the ASPECTS. Recanalization was assessed by transcranial duplex before the HOB protocol. Functional outcome was evaluated at three months by the MRS.

10.2.5 Statistical analysis

We have expressed quantitative variables as a median and an interquartile range (median (Q1, Q3)), and categorical variables as number of cases and percentages (cases (percentages)). The Lilliefors test was used to assess for normality. The Kruskal-Wallis test (for quantitative dependent variables) or the chi-squared test (for categorical dependent variables) were used with three-way pairwise comparisons with a Bonferroni correction. The Wilcoxon signed-rank test was used to compare related samples or to check if a response was different from zero. The Wilcoxon rank-sum test was used to assess the differences between two groups.

Spearman correlation was used to assess the correlation between quantitative variables.

Linear models were used when the first measurement was considered, and linear mixed-effect models were used when all measurements were considered for the two different protocols (due to lack of independence of the response variable). The independent variable was the ΔMAP and the dependent variable was the ΔrCBF. Residuals plots of these models were tested for the inspection of deviations from normality or homoscedasticity. For the linear mixed-effect models, patients and databases were the random factors. The "nlme" software package was used for the linear mixed-effect models implemented by R [135].

The correlations and the linear models were accepted to be valid, if and only if, when extracting all patients one by one and repeating the same test (bootstrapping), every subtest (considering n-1 data points) was statistically significant. $p < 0.05$ was considered as the threshold for the rejection of the null hypothesis for all statistical tests. All statistical analyses were performed with R [135].

10.3 Results

Seventy-two (n=72) AIS patients from three different studies were recruited in two countries (USA, Spain) and have been aggregated in the dataset. All the three protocols involved DCS measurements during orthostatic challenges in different HOB positions, including, relevant to this work, repeated supine positions within the same series in a total of one hundred thirty-five (n=135) measurements. The mean arterial pressure (MAP) was measured continuously (n=9) or at mid-way through each HOB position (n=17) in a total of fifty-two (n=52) measurements of twenty-six (n=26) patients (see Table 10.1 for clarification).

None of the patients from any of the three studies suffered from worsening or improvement of the neurological condition of the subjects.

As shown in Table 10.2, the severity of the patients on arrival was similar (NIHSS =13.5 (6, 20), p=0.188), but ICFO 2015-2017 study patients were older than the rest (p=0.008 and p=0.045, for UPENN 2006-2007 and UPENN 2009-2011 studies, respectively). Also, UPENN 2006-2007 study patients were measured later from the stroke onset than the rest (p=0.027 and p<0.001, for UPENN 2006-2007 and

Patients considered (measurements considered)	UPENN, 2006-2007	UPENN, 2009-2011	ICFO, 2015-2017	Total
Total	17 (42)	17 (21)	38 (72)	72 (135)
$Supine_1$ to $supine_2$ CBF data	15 (35)	14 (16)	38 (72)	67 (123)
$Supine_1$ to $supine_2$ CBF ipsilesional vs contralesional hemisphere analysis	15 (35)	11 (13)	36 (65)	62 (113)
Mean arterial pressure data	0	9 (13)	17 (39)	26 (52)
Ipsilesional CBF data + MAP data	0	6 (8)	14 (35)	20 (43)
Contralesional CBF data + MAP data	0	9 (11)	13 (31)	22 (42)

TABLE 10.1: Number of patients and total number of measurements included in each analysis. CBF, cerebral blood flow; MAP, mean arterial pressure.

ICFO 2015-2017 studies, respectively). No other differences were observed between the three studies.

	UPENN, 2006-2007 (n=17)	UPENN, 2009-2011 (n=17)	ICFO, 2015-2017 (n=38)	p	Total (n=72)
Age (y.)	59 (53, 55)	62 (60, 64)	83 (68.75, 88)	0.002*	74.5 (60, 85)
Females, n (%)	10 (59)	7 (41)	21 (55)	0.94	38 (53)
NIHSS admission	15 (6, 20)	9 (5, 13)	18 (7, 20)	0.188	13.5 (6, 20)
Days from stroke onset	2 (2, 3)	1 (1, 1)	1 (0.5, 1)	<0.001†	1 (0.5, 2)

TABLE 10.2: Demographic and clinical variables available for the three datasets. NIHSS, National Institute of Health Stroke Scale. Symbols indicate a statistically significant difference between the studies versus the ICFO 2015-2017 study (∗) and between the studies versus the UPENN 2006-2007 study (†).

10.3.1 Head-of-bed challenge from the first supine position to the next supine

Some patients did not complete the protocol up-to the second supine position and, then, have been discarded for this section (see Table 10.1). For this reason and for movement artifacts, five patients (n=2, 12%, UPENN 2006-2007; n=3, 24%, UPENN 2009-2011) have been discarded. Repeated measurements have been included. For the same reasons above, twelve repeated measurements have been excluded (n=7, 17%, UPENN 2006-2007; n=5, 24%, UPENN 2009-2011).

A systematic ΔrCBF increase was observed from the first supine position to the next supine ($p<0.001$) when all patients were considered, i.e. the patients did not recover upon returning back to supine position as shown in Figure 10.2. The ΔrCBF in each hemisphere for the different studies did not recover back to supine position ($p<0.05$), except for the ipsilesional hemisphere on the UPENN 2006-2007 study ($p=0.385$).

Moreover, no ΔrCBF interhemispheric difference was observed considering the data of each study separately ($p>0.05$), or when considering the data of the three studies together ($p=0.646$). Only subjects with optical data available for both hemispheres have been included in this subanalysis (see Table 10.1).

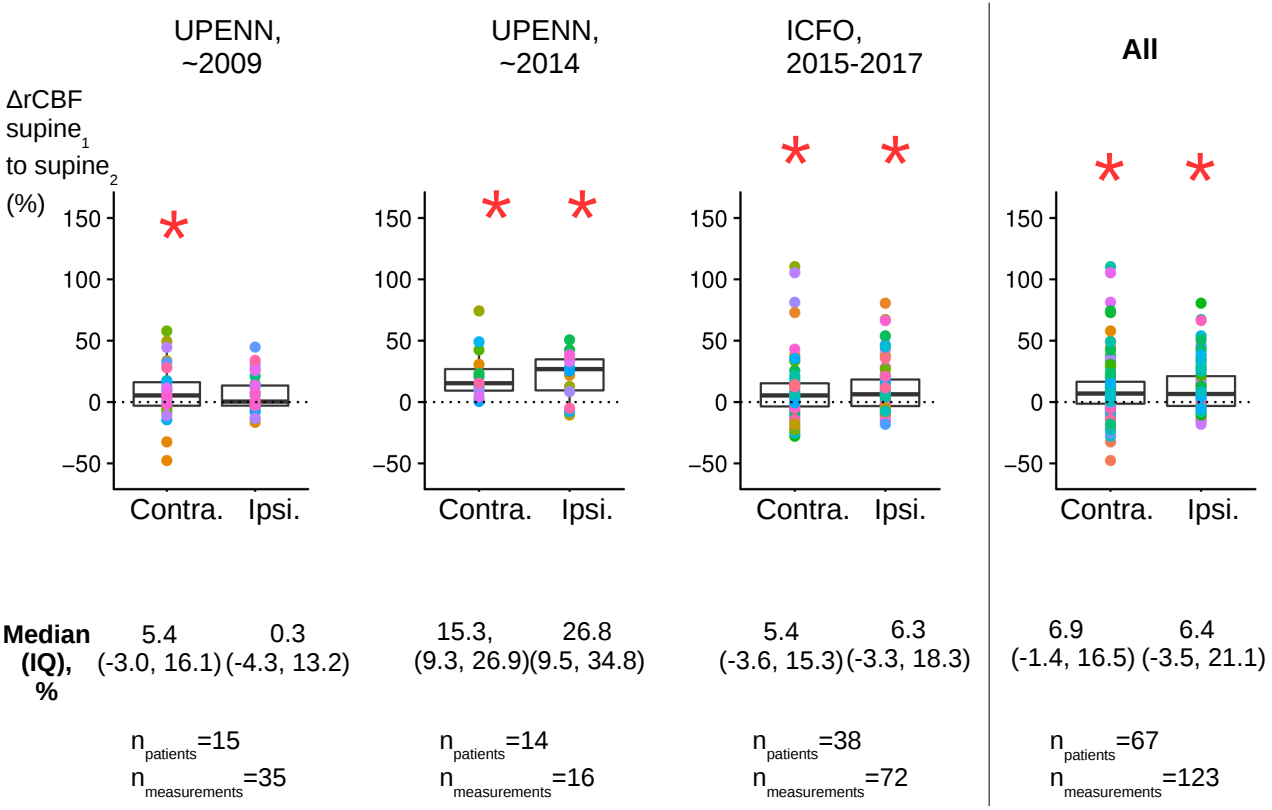

FIGURE 10.2: Cerebral blood flow response (ΔrCBF) from the first supine to the second supine for each hemisphere, for each study and for all patients is shown. Classic boxplots and the mean ΔrCBF data point color-coded for each patient are shown. Text labels below each panel show the median (interquartile range) for each hemisphere. Number of patients and total number of measurements are also shown. (*) indicates a statistically significant difference from baseline. Contra.=contralesional hemisphere. Ipsi.=ipsilesional hemisphere.

10.3.2 Relative cerebral blood flow changes versus relative mean arterial pressure changes

As mentioned, the mean arterial pressure was measured continuously (n=9, UPENN 2009-2011 study) or at mid-way through each HOB position (n=17, ICFO 2015-2017 study) in a total of twenty (n=26) patients and fifty-two (n=52) repeated measurements. Due to the artifacts either on the MAP or on the optical data during the HOB positions of interest, data has been discarded in the analysis differently between hemispheres. Table 10.1 details the total number of subjects included.

When measurements in all times from stroke onset up-to one week were considered for each hemisphere, a linear mixed model could not be fit on the contralesional hemisphere (p=0.575). For the ipsilesional hemisphere, the fit was not considered valid, even though the p value was smaller than 0.05 (p=0.022), since it failed after bootstrapping as explained in methods (see Figure 10.3).

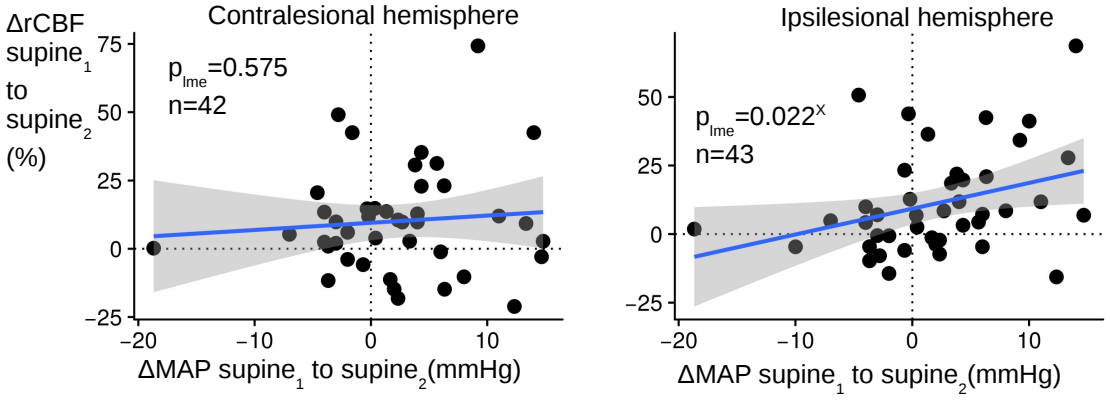

FIGURE 10.3: Cerebral blood flow response (ΔrCBF) from the first to the second supine position versus relative mean arterial pressure change (ΔMAP) in the contralesional hemisphere (left), and in the ipsilesional hemisphere (right) for all measurements performed. Linear model fit and confidence intervals (in grey) are plotted. (x) indicates that the linear mixed-effect model failed after bootstrapping.

Interestingly, in the first measurement for each patient (within 48 hours of stroke onset), a statistically significant correlation between ΔrCBF and ΔMAP from the first to the second supine position was observed in the ipsilesional hemisphere (p=0.002, $\rho_{Spearman}$=0.65, see Figure 10.4), but not on the contralesional hemisphere (p=0.976, $\rho_{Spearman}$=0.01). The ICFO 2015-2017 study alone showed

a correlation between the supine-to-supine ipsilesional ΔrCBF and ΔMAP that failed after bootstrapping for all patients (see Figure 10.5). UPENN 2009-2011 study, with less subjects available in the ipsilesional hemisphere (n=6), showed a statistically significant correlation that prevailed after bootstrapping (p=0.005, $\rho_{Spearman}$=0.94). When the same subanalysis was considered for the contralesional ΔrCBF, no statistically significant correlations were found (see Figure 10.6).

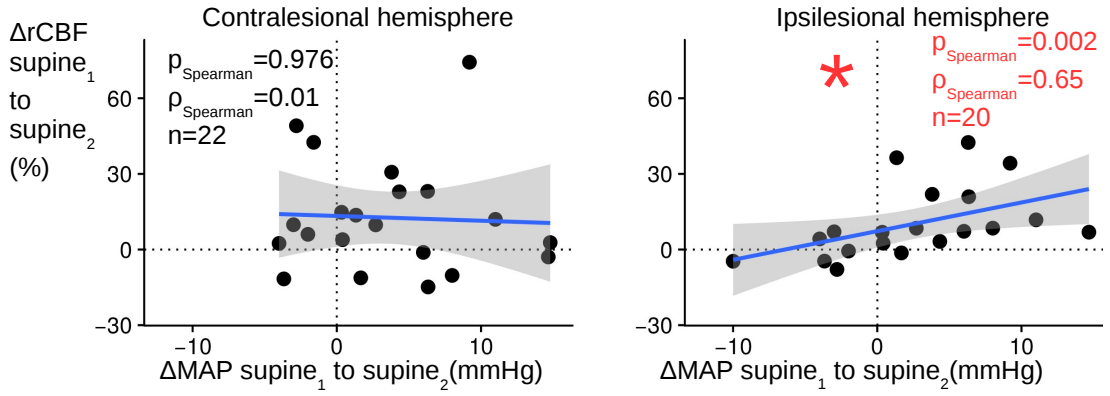

FIGURE 10.4: Cerebral blood flow response (ΔrCBF) from the first to the second supine position correlates to the relative mean arterial pressure change (ΔMAP) in the ipsilesional hemisphere (right), but not on the contralesional hemisphere (left) in the first measurement (<48 hours) for each patient. Linear model fit and confidence intervals (in grey) are plotted. (*) indicates a statistically significant Spearman correlation.

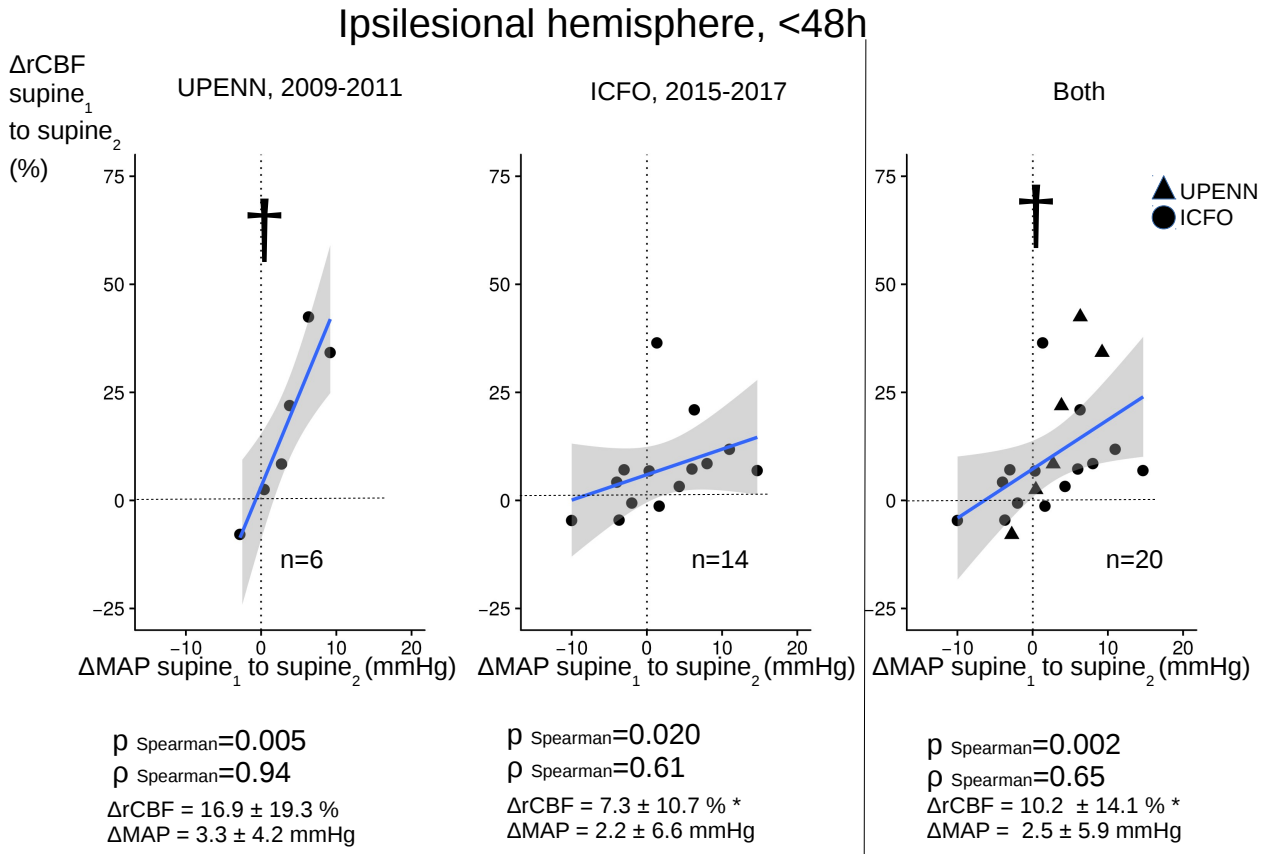

FIGURE 10.5: Cerebral blood flow response (ΔrCBF) from the first to the second supine position correlates to the relative mean arterial pressure change (ΔMAP) in the ipsilesional hemisphere for the two studies with both optical and MAP data available (n=20). Linear model fit and confidence intervals (in grey) are plotted. (*) indicates a statistically significant difference from baseline. (†) indicates a statistically significant Spearman correlation that prevails after bootstrapping.

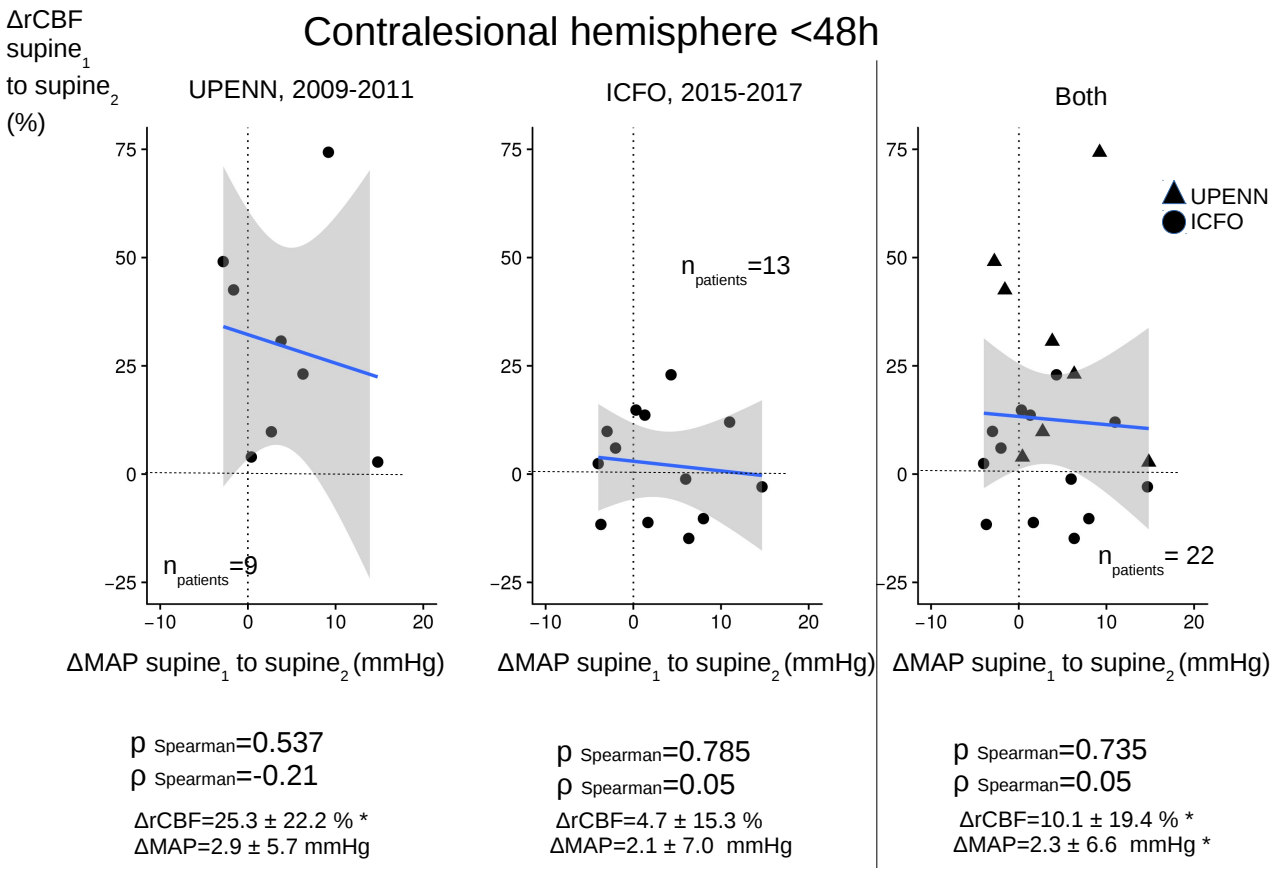

FIGURE 10.6: Cerebral blood flow response (ΔrCBF) from the first to the second supine position does not correlate to the relative mean arterial pressure change (ΔMAP) in the contralesional hemisphere for the two studies with MAP data available (n=22). Linear model fit and confidence intervals (in grey) are plotted.

10.4 Discussion

In this work, data from seventy-two AIS patients from three different studies, from two different countries, were aggregated in order to study the CBF and MAP recovery upon returning back to supine position after orthostatic challenges involving different HOB positions. Once a systematic increase of CBF was observed upon different orthostatic challenges alongside a change in mean arterial blood pressure, a further detailed analysis revealed that CBF changes in the ipsilesional hemisphere correlated with the MAP changes in less than forty-eight hours after stroke. This was a hemispheric effect, which was not detected on the contralesional hemisphere. Overall, this study suggests that AIS causes hemispheric alterations in cerebral autoregulation which disappear with time (i.e. greater than forth-eight hours after stroke onset).

This study was motivated by our previous finding, in which the CBF recovery upon returning back to supine position was a biomarker of disease severity in obstructive sleep apnea (OSA) [127] (Chapter 5).

A first result presented in this work is that a systematic ΔrCBF increase was observed from the first supine position to the next supine ($p<0.001$). As mentioned, it is not the first time that this result over a HOB protocol is reported in the literature. Patients diagnosed with moderate and severe obstructive sleep apnea (OSA) also showed an alteration (i.e., increase) of the supine CBF upon returning to the initial HOB supine position in previous studies [127] (Chapter 5). Interestingly, this alteration was related to OSA severity and long-term treatment ameliorated this alteration.

Patients with cerebral pathologies might need a longer time period than five minutes in each HOB position to stabilize their cerebral hemodynamics. Urbano *et al* [112] measured (by TCD) the effect of a strong orthostatic challenge (standing to squatting position) in twenty-six patients with moderate or severe OSA and twenty-eight control subjects. Patients with OSA had a significantly slower rate of recovery of blood pressure, cerebral blood flow velocity and cerebrovascular conductance than the control group, showing that patients with moderate or severe OSA presented an impaired compensatory response to a strong orthostatic challenge. On an unpublished study with a similar protocol but on twelve healthy subjects, we have recently measured microvascular ΔrCBF at supine position for

30 minutes, and for 30 minutes more after a HOB change from supine to 30°. Interestingly, ΔrCBF did not stabilize for any period of 30 minutes, in other words, CBF measured by DCS was found not stable over 30 minutes.

Not only CBF has been found to increase after different HOB changes in the literature, Aries *et al* [133] also found increases in MAP. In their protocol on stroke patients with different HOB angles for 3 to 5 minutes each, they found that MAP increased slightly during the course of the experiment for patients (mean 5%, 95% confindence intervals: 2% to 7%) and also for healthy controls (mean 2%, 95% confindence intervals: -1% to 6%) [133]. These changes are on the order of our ΔMAP change findings of 2.6 ± 6.9 % from the first supine to last supine with different HOB angle positions in between.

It is interesting to note here that the changes of an apparently basic parameter such as MAP are not reported in a uniform manner in the literature. Some authors have found no changes on MAP during different HOB positions on the angle ranges from supine up-to 30° in stroke patients [225, 249]. However, Aries *et al* [133] found MAP decreases due to a stronger HOB change from supine to 90° in both healthy and stroke subjects. On healthy subjects, Edlow *et al* [118] found MAP increases due to the same HOB change from supine to 90° and back to supine. And more recently, and contrary to Edlow *et al* , Lam *et al* [134] found MAP decreases with a similar protocol to the ICFO study but in healthy subjects. This may be attributed to methodological differences in measuring MAP, for example, to height reference level.

A second finding of this study related to these mentioned MAP changes is the correlation between the response of the ipsilesional microvascular CBF from supine to the next supine position and the response of the MAP to the changes of head positioning, in patients with anterior circulation AIS in less than 48 hours after stroke. Apparently, supine (0°) to a higher angle and back to supine (0°) is a more potent stimulus in eliciting hemispheric differences between MAP and CBF than just supine (0°) to a higher angle. Interestingly, this correlation was observed in the ipsilesional hemisphere (p=0.002, $\rho_{Spearman}$=0.65), but not on the contralesional hemisphere (p=0.976, $\rho_{Spearman}$=0.01).

As mentioned, ischemia in the brain is a reversible process dependent on the restoration of the CBF in the penumbra within a time window of cellular viability [246]. The timing when collaterals are activated is important for their clinical

effect on penumbra recovery, where delayed collateral recruitment can be futile or even result in worse outcome [231]. Thus, it may be expected that during the early hours after stroke, specially, the affected hemisphere may present a damaged CAR, a pathological phenomenon which has already been observed in different cardiovascular diseases, such as ischemic stroke, brain injury and trauma [4]. The asymmetry observed in this work between hemispheres during the early hours after stroke could be a biomarker of damaged autoregulation.

It is not the first time that this asymmetry between damaged and non-damaged hemispheres is observed in pathological subjects. Yew *et al* [250] estimated cerebral vasoreactivity index (CVR_i) as the ratio of mean arterial pressure to regional cerebral blood flow (measured by arterial-spin-labeling functional MRI) in amyloid-positive, amyloid-negative and Alzeimer disease subjects finding that the CVR_i was significantly elevated in amyloid-positive versus amyloid-negative cases, with additional elevation in patients with Alzheimer's disease. According to this result, another study with Alzheimer's disease, mild cognitive impairment and healthy subjects and using similar measurement techniques, found that vortical and subcortical CVR_i was more elevated in Alzheimer's disease [251].

On an unpublished study with a similar protocol but on internal carotid artery patients [117] (Chapter 7), supine-to-supine ΔrCBF was found to correlate with ΔMAP only in the stenosed ($\geq$ 70%) hemisphere of fourteen (n=14) unilateral stenosis patients, but not on the non-stenosed hemisphere. Interestingly, this correlation was not observed by cerebral blood flow velocity by TCD. This result reinforces the idea that this correlation is due to damaged cerebral autoregulation, and also, that DCS during a HOB challenge may be superior to TCD to be able to measure the general well-being of the brain.

We acknowledge that our study has several limitations. First, the different protocols for each study may have increased the variability in our results; specifically, considering that the UPENN protocols pre-selected large vessel cortical anterior circulation infarcts, while the ICFO 2015-2017 study only pre-selected large vessel anterior circulation infarct (not only cortical). Second, MAP was not assessed in one protocol, in another protocol it was assessed continuously and in the third protocol it was assessed only at mid-way through each HOB position. The fact that two different devices and methods are used to measure MAP may have increased, again, the variability of our results. Third, data from different protocols and clinical settings was gathered, but future multi-center studies with common protocols

and similar clinical management at the point-of-care should be considered for improving the reliability of the data. Finally, the time courses of these responses are longer than dynamic CVR, so it could be plausible that both cerebral and systemic mechanisms are involved. Future studies measuring cerebral hemodynamics together with systemic variables with a protocol involving different HOB angles and durations would help to understand these results.

In conclusion, microvascular CBF versus MAP responses to an increase of a brief HOB during the acute phase of stroke may provide cerebral autoregulation information in AIS. However, further studies are needed to elucidate if this information could be used to individualize management for the patients admitted to the Stroke Unit after AIS.

Chapter 11

Microvascular cerebral blood flow fluctuations in association with apneas and hypopneas in acute ischemic stroke

Hypothesis:
The unexpected cerebral hemodynamic fluctuations are associated to apneic and hypopneic events.

11.1 Introduction

Most interventions during the early hours after ischemic stroke onset aim to maximize and stabilize cerebral blood perfusion to diminish the neurological damage and improve the long-term outcome [222]. Furthermore, these patients could be at risk of possible detrimental CBF fluctuations in the case, for instance, of undiagnosed breathing disorders (BDS). Disordered breathing includes a range of respiratory disorders [252], often during sleep, characterized by repetitive reduction (hypopneas) or cessation (apneas) of airflow during sleep.

Different types of BDS with different physiological origins have been reported in association with stroke in 10% to 70% of the patients [101, 253–261]. However, it is not yet clear if the presence of a breathing disorder is associated with the

long-term outcome. While some works support the idea that BDS are associated with poor recovery from stroke [101, 262–265], one study reported that BDS in stroke patients are associated with early neurological worsening but not with long-term outcome at six months [254]. The reason for the divergence of the results of these studies could be the physiological origin of BDS (upper airway obstruction, heart failure, disease or injury involving the brain) [266] but also, the possible variable amount of detrimental impact of these events on the cerebral hemodynamics. Thus, the diagnosis and the quantification of these respiratory events, and also, the characterization of their effect on the cerebral hemodynamics may be relevant for the management of the ischemic stroke patients.

The dynamics of local, microvascular cerebral blood flow (CBF) are particularly interesting since, hypothetically, they could reveal that large, repeated changes in the cerebral perfusion could be detrimental when cerebral autoregulation is damaged in the acute stages of stroke [168]. This is relevant during the acute stages of stroke since ischemia in the brain is a potentially reversible process dependent on the restoration of the microvascular CBF in the penumbra within a time window of cellular viability that varies on duration and severity of CBF cessation [246]. However, if cerebral autoregulation is damaged, CBF can abruptly increase or decrease without following the needs of the brain and without restoring the needed CBF in the penumbra. If so, BDS treatment could be used to avoid these unwanted changes. However, there are no established methods to monitor microvascular CBF at the bed-side.

In non-stroke subjects, cerebral hemodynamic fluctuations due to apneas or hypopneas have been extensively studied and characterized previously by several groups with the measurement of the cerebral blood flow velocity (CBFV) in the middle cerebral artery by transcranial Doppler ultrasound (TCD) [113, 155–158]. However, macrovascular CBFV is only an indirect measurement of what happens in the distal microcirculation.

Fluctuations of microvascular cerebral hemodynamics have previously been observed in acute stroke patients. A study of nine patients with acute stroke [267] reported arterial oxygen desaturations from unknown origin that correlated with cerebral hemodynamics measured with near-infrared diffuse optical spectroscopy (NIRS-DOS), and showed an asymmetry of the changes in the two cerebral hemispheres. Pizza *et al* [268] observed, in seven patients, with acute/subacute middle cerebral artery stroke that obstructive and central apneas were linked to cerebral

oxygenation changes by NIRS-DOS. Asymmetrical patterns of cerebral hemodynamic changes were again found with significantly larger changes on the unaffected hemisphere compared to the affected one. However, neither NIRS-DOS nor TCD provide a direct measure of microvascular CBF.

In this pilot study, we have utilized diffuse correlation spectroscopy (DCS) to non-invasively monitor local, microvascular CBF [5, 7, 64]. In a previous study [123] (Chapter 9), we have observed unexpected fluctuations of microvascular CBF, heart rate, arterial oxygen saturation and end-tidal carbon dioxide in three (18%) of seventeen acute ischemic stroke patients during the first week from stroke onset, which has motivated the design of this study to investigate the origin of these fluctuations. Here, we have aimed to test the hypothesis that these cerebral and systemic fluctuations were associated with apneic and hypopneic events after stroke. The results of this study have been submitted and are under review [269].

11.2 Methods

This study was conducted at the Stroke Unit of Hospital de la Santa Creu i Sant Pau, in Barcelona, Spain between August 2016 to March 2017. The study protocol was approved by the local ethical committee (EC/15/130). Either the patients or their relatives gave their written informed consent.

The inclusion criteria were being older than 18 years old, confirmed ischemic stroke in the anterior circulation, measurement time less than seven days from the stroke onset, and informed written consent. The exclusion criteria were resting heart rate less than 40 or greater than 110 beats per minute, arterial oxygen saturation less than 92%, use of oxygen therapy, symptomatic lacunar stroke, previous diagnosis of breathing disorders, previous transient ischemic attack, minor stroke or intracranial hemorrhage.

The study included two different parts (see Figure 11.1 for a flow-chart of the procedure). First, patients who fit the clinical inclusion criteria were screened with a pulse oximeter for a minimum of four hours between 8 am to 2 pm. Afterwards, if the pulse oximeter showed periodic decreases of $\geq 3\%$ in arterial oxygen saturation (SpO_2), the patients were measured in the afternoon with DCS and also with a respiratory polygraphy device simultaneously for one hour in the most comfortable head-of-bed position for the patients.

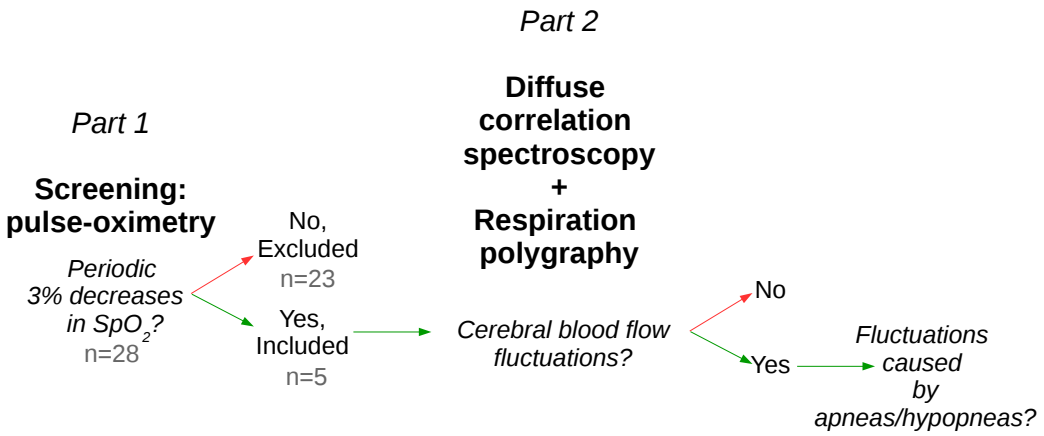

FIGURE 11.1: Methodology of the two parts of the study. The subjects included in each part are depicted in grey. SpO_2, arterial oxygen saturation.

11.2.1 Neurological evaluation

Baseline examinations included the collection of a summary of the medical history from patient records (demographics and vascular risk factors) and a clinical examination. The stroke severity was assessed with the National Institute of Health Stroke Scale (NIHSS) [209] on admission and right after the measurement. Indirect ischemic signs were evaluated by the Alberta Stroke Program Early Computed Tomography Score (ASPECTS) [230]. Long-term outcome was evaluated at three months by means of the modified Rankin Scale (mRS) [210], where a score of mRS >2 was considered indicative of an unfavorable outcome.

The extent and location of the ischemic area along with the site of arterial occlusion were evaluated on admission by a cranial computed tomography scan and vascular imaging either by angio-computed tomography or by TCD. If patients were eligible, reperfusion theraphy (thrombolysis or thrombectomy) was applied [222]. Recanalization (either spontaneous or by revascularization treatment) was assessed with TCD within 24-48 hours.

The neurological scales were scored by a neurologist or a senior neurology resident blinded to the optical information.

11.2.2 Optical methods and instrumentation

We have used the DCS unit of the hybrid device described in Section 4.1.1. Two optical probes were placed on the forehead bilaterally on both hemispheres as lateral as possible, avoiding the sinuses. These probes consisted of a bundle of four detector fibers set at 2.5 cm from a source fiber. These probes were the same as the ones presented in Figure 8.1 in Chapter 8. We have measured the blood flow index (BFI) continuously with a 2.5 second temporal resolution. The relative CBF changes were obtained by normalizing the calculated continuous BFI with the mean BFI of the first five minutes (baseline) of the measurement. Also the CBF changes per apnea/hypopnea have been calculated as explained in the statistical analysis section.

Pulse oximetry and respiratory polygraphy

A standard pulse oximeter (CMS-50D Plus, CONTEC Medical Systems CO, Qinhuangdao, China) was used for the screening of the stroke patients. If these patients were eligible, then, they were enrolled for the full study which, in addition to DCS, included a respiratory polygraphy monitoring (Embletta MPR PG, Natus Medical, Middleton, USA).

The respiratory polygraphy included the recording of the oronasal flow (by a thermistor and a nasal cannula), the thoracic and the abdominal movements (by a respiratory inductance plethysmography band), the SpO_2 and the heart rate (HR; both by pulse oximetry), among others. The respiratory polygraphy data was further post-processed by a pulmonologist to determine the following variables; the start and end time points of each event, the event type (obstructive apnea, hypopnea, mixed apnea, or central apnea), the number of times where arterial oxygen saturation decreases 3% due to an apnea or hypopnea (ODI3) and the number of apneic and hypopneic events per hour of study (AHI) [130].

11.2.3 Statistical analysis

In order to calculate the percent CBF change (ΔrCBF) due to each apneic or hypopneic event, we have estimated a basal blood flow index (BFI_{bl}) as the average of the cerebral BFI from thirty seconds before the apnea/hypopnea start up to

thirty seconds after the apnea end. This was considered to correct for slight changes in the probe position during the measurement. Afterwards, the CBF changes were calculated as $\Delta rCBF = (\frac{BFI}{BFI_{bl}} - 1) \times 100$. Similarly, ΔHR was defined as $\Delta HR = HR - HR_{bl}$ and ΔSpO_2 was defined as $\Delta SpO_2 = SpO_2 - SpO_{2bl}$. In all cases, the subscript $_{bl}$ indicates an average over the same period.

Afterwards, the events were parametrized for the characterization of the induced ΔrCBF, ΔHR or ΔSpO_2 for each event. The goal was to study if individual apneic or hypopneic events caused significant increases or decreases in these variables as it was hypothesized. This step consisted in considering each event as a function dependent on time (ΔrCBF(t), ΔHR(t) and ΔSpO_2(t)), and then, the extrema of these functions along a specific time interval were calculated. The reference time (time zero) was considered as the end of each event. The time windows to find these extrema were considered from -5 to 15 seconds for the first extrema on ΔrCBF, from 0 to 15 seconds for the ΔHR, and from 5 to 35 seconds for the ΔSpO_2. These time windows were chosen by visual observation of all the apneas and hypopneas plotted together from -30 seconds to 60 seconds and according to the literature [113, 175]. These analysis methods have been verified in nocturnal measurements of chronic obstructive sleep apnea patients [170] (Chapter 6).

Averages and standard deviations have been performed considering all apneic and hypopneic events for each patient and also for the population. The Wilcoxon signed-rank test was used to assess the difference between ipsilesional and contralesional ΔrCBF responses. The same test was used to assess if the apneic/hypopneic response of different variables was significantly different from zero. All analyses were performed with Matlab (Mathworks, MA, USA). A p-value < 0.05 was considered to be statistically significant.

11.3 Results

During the eight month period, we have screened twenty-eight ischemic stroke patients with pulse oximetry, of whom five (n=5, 18%) presented fluctuations ($\geq 3\%$) in SpO_2 and were then included in the second part of the study. Table 11.1 shows the clinical characteristics of these five patients. Four were male, had an age of 81 ± 6 years (mean ± standard deviation), an admission NIHSS of 8 (2, 16) (median

(first quartile, third quartile), and a time from stroke onset to measurement of 4 (3, 5) days.

Table 11.2 shows the results of the DCS and the respiratory polygraphy measurements. In all five patients, the respiratory polygraphy confirmed the presence of altered breathing patterns; two presented periodic breathing (clusters of breaths separated by intervals of apnea (no breathing) or near-apnea), two presented a predominance of obstructive events (the airflow is ceased or partially ceased due to upper airway obstruction) and one of central apneas (the airflow is ceased or partially ceased due to diminished or absent effort to breath).

Figure 11.2 shows a representative trace (from Case 4) of ten minutes of continuous oronasal flow, abdominal and thoracic movements, HR, SpO_2 and CBF changes. Both apneic (four obstructive apneas, green shading) and hypopneic (three, gray shading) events are visible and the simultaneous monitoring showed time correlated variation of microvascular CBF, HR and respiratory variables. From the respiratory polygraphy recording, oronasal flow is reduced during the hypopneas and ceased during the obstructive apneas, while abdominal and thoracic movements are reduced during these events. Heart rate does not follow a general pattern for this trace. SpO_2 shows a drop with a delay relative to the apneic/hypopneic event. In this time period with frequent events, as commonly observed, the SpO_2 drop of the previous event is overlapped with the next event. It can also be observed that the CBF starts to rise close to the end of an event. Finally, for this specific interval, periodic breathing is diagnosed but the rest of the acquisition is dominated by obstructive apnea events as shown in Table 11.2.

For completeness, Figure 11.3 shows ten minutes of similar traces where neither fluctuations nor apnea/hypopnea events were found. This patient (Case 3) was the only one with no apneic/hypopneic events during ten minutes.

From the five patients, two hundred and nineteen (n=219) apneic/hypopneic events were analyzed. In all patients, the CBF changes were bi-phasic. In other words, significant bilateral CBF increases of 27.1 $\pm$ 17.7% ($p<0.001$) for the ipsilesional, and, 29.0 $\pm$ 17.4% ($p<0.001$) for the contralesional hemisphere were followed by decreases of -19.3 $\pm$ 9.1% ($p<0.001$) for the ipsilesional, and, -21.0 $\pm$ 8.9% ($p<0.001$) for the contralesional hemisphere due to each apneic/hypopneic event. There were no interhemispheric differences between the maximum increases

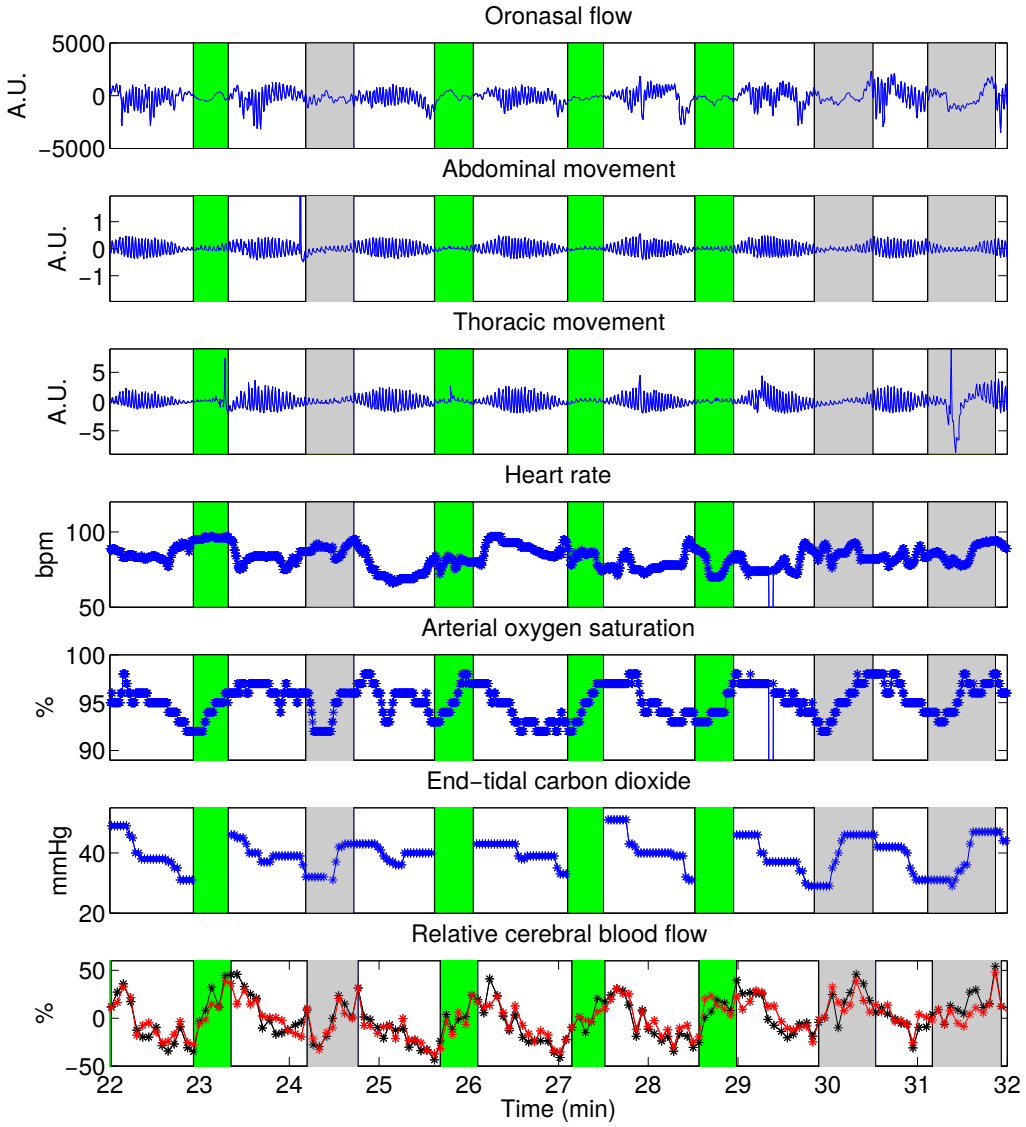

FIGURE 11.2: A ten minute trace of systemic fluctuations of physiological variables alongside fluctuations of cerebral blood flow. Hypopneas (grey) and obstructive apneas (green) are shown from the measurements of an 89 year-old male with a left middle cerebral artery ichemic stroke (Case 4). The patient presented a left middle cerebral artery stroke with insular, temporal and basal ganglia ischemic areas. The National Institute of Health Stroke Scale was 16 when measured. The patient died after 24 hours of the measurement.

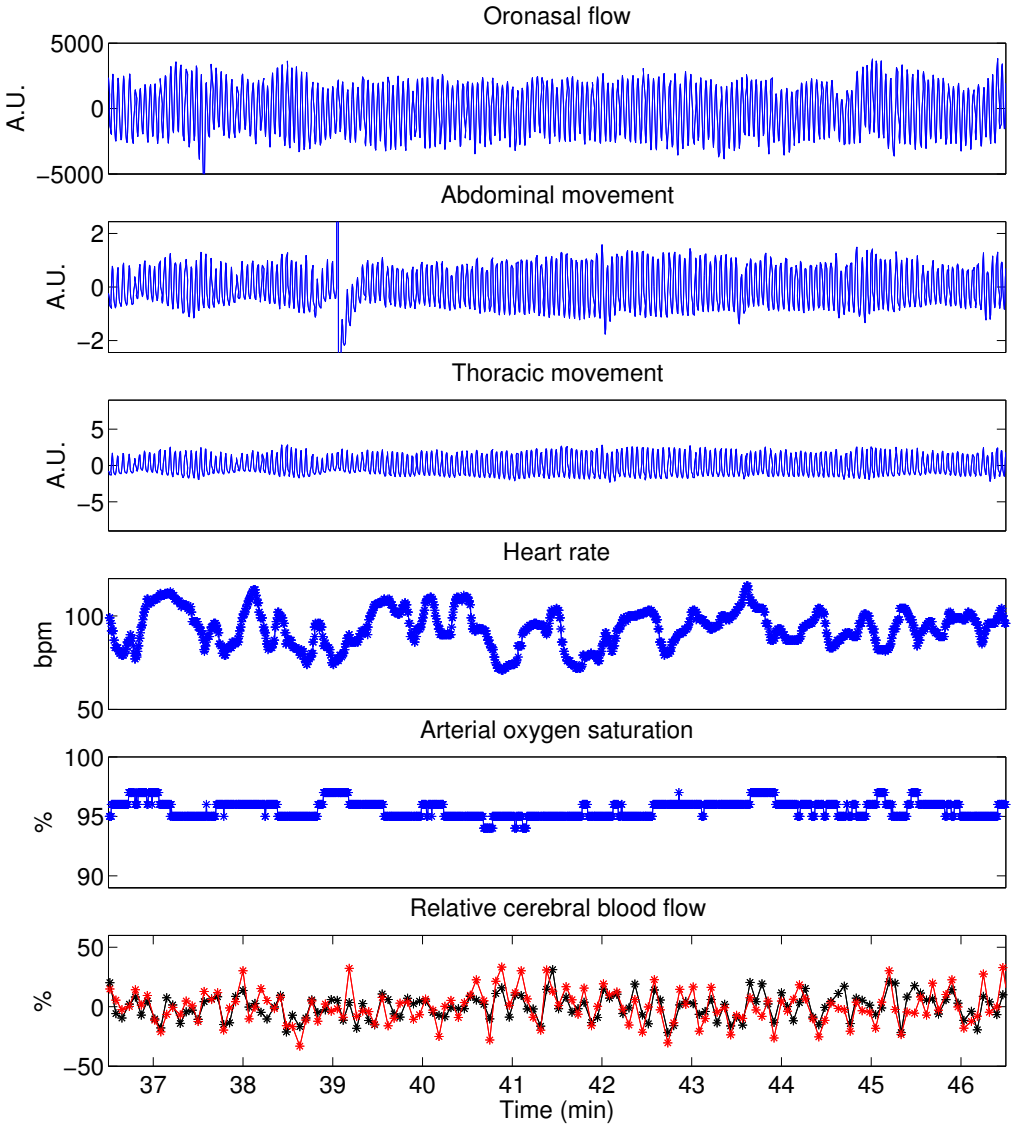

FIGURE 11.3: A ten minute trace with no typical fluctuations of cerebral blood and no apneas or hypopneas. Measurements of an 82 year-old male with a right anterior cerebral artery ichemic stroke (Case 3). The patient had a blockage of the right anterior cerebral artery with a frontal ischemic area. The National Institute of Health Stroke Scale was 8 when measured.

(p=0.189) or the maximum decreases (p=0.053). Also, as expected, HR increased (p<0.001) by 6.5 ± 6.8 bpm and SpO_2 decreased (p<0.001) by -4.9 ± 16.8%.

The two patients (Cases 4 and 5) with the highest AHI, one with predominance of an obstructive apnea pattern and the other of central apnea pattern, had the two highest NIHSS both on admission and after the measurement and the lowest ASPECTS. Unfortunately, both had an mRS of six, i.e. they have died during the three months after stroke onset. Among these two patients, the one with the highest AHI (Case 5) also presented the lowest left ventricular ejection fraction. However, none of these two patients presented the highest physiological or cerebral hemodynamic changes in response to the respiratory events. One of the characteristics of the remaining three patients (Cases 1, 2 and 3) with lower stroke severity is that they have presented mainly hypopneic events, in comparison to the obstructive and central apneas found in the two most severe patients (Cases 4 and 5). We note that given the small population, these are just anecdotal statements and should not be considered generalizable.

Case	1	2	3	4	5
Age (y), gender (M/F)	83, F	73, M	82, M	89, M	76, M
Smoking	Former	Former	Former	Former	Former
Arterial hypertension	Yes	Yes	No	No	No
Dyslipidemia	Yes	Yes	No	No	No
Diabetes	No	No	Yes	No	Yes
Ipsilesional ICA stenosis > 70%	Yes	No	No	-	No
Coronary disease	No	No	Yes	No	Yes
Atrial fibrillation	No	No	No	No	No
Left ventricular ejection fraction (%)	> 50	40-50	40	-	25
Arterial occlusion	Left MCA	Left MCA	Right ACA	Left MCA	Right MCA
NIHSS admission	7	7	3	20	21
NIHSS after the measurement	2	1	8	16	21
Reperfusion theraphy	Yes	Yes	No	No	No
Recanalization	Yes	No	Yes	No	No
Infarct location	Insular and frontal	Insular and frontal	Frontal	Insular, temporal and basal ganglia	Insular, temporal and parietal
ASPECTS	8	8	10	6	6
Days from stroke to measurement	7	4	3	5	0
mRS at 3 months	2	1	4	6	6

TABLE 11.1: Demographics, pre-stroke (top) and post-stroke clinical characteristics (bottom) of the five ischemic stroke patients. M, male; F, female; ICA, internal carotid artery; MCA, middle cerebral artery; ACA, anterior cerebral artery; NIHSS, National Institute of Health Stroke Scale; ASPECTS, Alberta Stroke Program Early Computed Tomography Score; mRS, modified Rankin Scale.

Case	1	2	3	4	5
AHI (n./hour)	45.6	13	24.8	45.8	63.8
ODI3 (%)	46.3	15.7	17.4	48.1	10
Obstructive apneas, n	0	0	1	31	1
Central apneas, n	1	0	2	0	82
Mixed apneas, n	0	0	1	0	0
Hypo-pneas, n	37	13	20	30	0
Event duration (sec)	21 ± 7	24 ± 4	27 ± 8	30 ± 11	19 ± 5
Breathing disorder	Periodic respiration	Hypopneas	Periodic respiration	Obstructive events	Central apneas
Max. increase induced ΔrCBF$_{ipsi}$ (%)	30.0 ± 12.7	37.4 ± 13.0	22.4 ± 8.9	31.0 ± 10.1	21.9 ± 23.9
Max. increase induced ΔrCBF$_{contra}$ (%)	32.9 ± 21.4	27.6 ± 11.0	29.7 ± 15	36.1 ± 11.2	21.7 ± 18.3
Max. decrease induced ΔrCBF$_{ipsi}$ (%)	-19.2 ± 7.0	-33.3 ± 12.1	-16.1 ± 8.2	-24.2 ± 6.6	-13.6 ± 5.8
Max. decrease induced ΔrCBF$_{contra}$ (%)	-17.8 ± 7.4	-25.4 ± 11.1	-19.9 ± 8.1	-28.0 ± 8.1	-16.3 ± 5.3
Max. increase induced ΔHR (bpm)	2.8 ± 1.6	14.8 ± 8.0	16.0 ± 6.8	10.6 ± 4.3	1.1 ± 0.7
Max. decrease induced ΔSpO_2 (%)	-2.2 ± 1.0	-1.6 ± 0.7	-1.5 ± 9.3	-9.9 ± 24.6	-0.9 ± 0.8

TABLE 11.2: Polygraphic characteristics (top) and maximum relative cerebral blood flow change (ΔrCBF), heart rate change (ΔHR) and arterial oxygenation saturation change (ΔSpO_2) due to each apnea/hypopnea event (bottom) of each patient. AHI, apnea-hypopnea index; ODI3, number of times where arterial oxygen saturation decreases 3% due to an apnea or hypopnea; Max., maximum; n, number of events detected; ipsi = ipsilesional hemisphere; contra = contralesional hemisphere. Mean ± standard deviation.

11.4 Discussion

In this study, we have followed up on our previous observation of unexpected bilateral fluctuations in microvascular cerebral blood flow in patients with anterior, cerebral ischemic stroke that were observed during different protocols with DCS measurements [123] (Chapter 9). We have hypothesized that these fluctuations were due to breathing disorders, in particular, due to apneic and hypopneic events. Therefore, a protocol based on pre-screening for these events with a pulse oximeter was introduced to enroll patients without a previous diagnosis of breathing disorders for a follow-up study combining respiratory polygraphy and DCS. A careful evaluation was carried out to identify the origin of these fluctuations and to characterize their details by combining this recording of different respiratory variables, arterial oxygen saturation and heart rate. Apneic and hypopneic events were determined to be the cause and their effect on cerebral hemodynamics was characterized.

By the respiratory polygraphy, HR, and SpO_2 changes were found during these events. These HR and SpO_2 changes followed the apneic/hypopneic dynamics expected by the literature in patients with BDS [160, 161, 175, 178].

In non-stroke patients with BDS, several studies have reported CBF velocity (CBFV) changes measured by TCD as showing an increase close to the end of the apnea [113, 157, 158]. Our findings are similar, we have observed a CBF increase of 27.1 ± 17.7% and 29.0 ± 17.4% for the ipsilesional and contralesional hemisphere, respectively, and a decrease of -19.3 ± 9.1% and -21.0 ± 8.9%, for the ipsilesional and contralesional hemisphere, respectively, close to end of the apneic/hypopneic events. This increase is similar to the CBF increase of 30 ± 17% and the decrease of -20 ± 12% described previously by us using DCS in obstructive sleep apnea events [170] (Chapter 6). It is also consistent with the CBFV 22% to 42% increase found by Alex *et al* [157] and also to the 14.6 ± 14% increase right after the apnea end by Bålfors *et al* [113]. However, other authors have found larger CBFV increases [155, 158]. These results show that there is a decrease in cerebral perfusion due to an apnea event. If these intermittent decreases lead to ischemia, they can cause hypoxic/ischemic brain injury, especially if cerebrovascular reactivity and regulation are impaired, which is often the case in ischemic stroke patients [30, 108]. Consequently, this could lead to a worsened prognosis, which may call for interventions such as continuous positive airway pressure (CPAP) therapy. We

note that, to date, no direct link between a degree of microvascular CBF changes, the long-term outcome, and, the use of CPAP therapy has been studied.

Several works have studied the general effect of CPAP therapy, mainly in obstructive disorders (OSA), or adaptive servoventilation (ASV) treatment for central disorders to avoid apneas and hypopneas [270–272]. In stroke patients, while some authors support the benefits of the CPAP treatment on BDS [264, 273–278], others claim that these benefits are not clear [279, 280] or that there is no benefit at all [281]. Nevertheless, as mentioned earlier, BDS diagnosis and CPAP or ASV treatment are not the common practice in the stroke units.

Future work with a larger sample size to investigate if the CPAP or ASV could be effective in those patients who show the presence and/or large fluctuations in CBF (for example above a threshold) in relation to apneic/hypopneic events is warranted. Additionally, it would be of interest to study if all ischemic stroke patients with apneic/hypopneic events show similar CBF fluctuations, or, instead, if there is an interindividual variability in the response to apneas or hypopneas, and, consequently, the response to treatment may be different.

In our cohort, the two patients (Cases 4 and 5) with the highest AHI were those with the worse stroke severity (higher NIHSS score) at the moment of the measurement. This has been previously reported in patients with stroke showing central BDS [262]. Similarly, the ASPECTS score of these two patients were the lowest of the group, which is compatible with the idea that large acute cerebral hemispheric lesions are associated to BDS [257, 282]. One of these two severe patients (Case 5; Case 4 had no information available) presented heart failure (low left ventricular ejection fraction ($< 40\%$)) and mainly central events, as it has been found in stroke patients in association with central BDS [256]. The breathing disorder present in this patient could be related to it. Insular and frontal ischemic regions were present in our cohort and, interestingly, these regions have already been associated to BDS of central origin [262, 282, 283]. However, other works support the idea of the lack of an association between the presence of BDS of central origin and the location of stroke [255, 259, 260]. Nevertheless, more patients are needed to clearly identify clinical associations.

Our proof-of-concept study has some limitations including the small number of patients included in the final analysis, the different types of possible breathing disorders with different physiological origins and the short recording time of DCS

simultaneously with respiratory polygraphy. Future studies will add more subjects, and will measure these subjects during several hours continuously in order to be able to better identify the type of breathing disorder, and moreover, to link it to the degree of the cerebral hemodynamic responses, among other previously mentioned goals.

Another limitation is that only one measurement per patient was performed for this study, so we could not track the start and cessation of the fluctuations together with the clinical stroke evolution. Anecdotally, in our previous protocols [120, 123] (Chapter 9) the physiological fluctuations observed prevailed in the different measurements performed in each patient during the first week after stroke. Accordingly, it is expected that BDS could be present during the first week after stroke in the case of patients with BDS of central origin, since BDS have been found to resolve after several weeks [283]. Future studies should include daily measurements to track when these fluctuations cease and to relate them to clinical parameters.

Due to the small number of subjects considered for this analysis, we have avoided a group analysis. Finally, two important parameters to understand CBF changes are the blood pressure and the end-tidal carbon dioxide, future studies should include their simultaneous measurement with DCS.

In conclusion, diffuse correlation spectroscopy has successfully revealed bilateral fluctuations in CBF of ischemic stroke patients with undiagnosed breathing disorders in accordance with systemic fluctuations of physiological variables. These cerebral hemodynamic fluctuations were related to apneic and hypopneic events in the five patients tested. Further studies are needed to study the possible detrimental impact of the magnitude and presence of these cerebral hemodynamic fluctuations, specially in the early hours after stroke were the interventions are more relevant to the outcome, for the recovery of stroke patients.

Part IV

Final conclusions

Chapter 12

Summary and future work

Near-infrared diffuse optical spectroscopy (NIRS-DOS) and diffuse correlation spectroscopy (DCS), the emerging techniques using near-infrared light in a non-invasive approach and employing diffuse optical concepts, have been combined for the different studies presented in this thesis.

It is well-known that our society is aging, and in Spain the Mediterranean diet is being replaced by fast food, leading to obesity; and that the stress of our daily lives reduces our quality of sleep. Considered together, all of these lead to an increased risk of cardio- and neuro-vascular diseases. Unfortunately, I am not able to radically change our society. However, during my PhD, I was lucky to have been able to contribute to the diagnosis and prognosis of the neurovascular disease in different clinical scenarios: obstructive sleep apnea, internal carotid artery stenosis, and ischemic stroke; as illustrated in Figure 12.1.

Obstructive sleep apnea (OSA) is a sleep syndrome with a frequency in stroke of 30% up-to 80% including both longer time and poorer functional outcome from rehabilitation after ischemic stroke. On a group basis, previous work from our group by Igor Blanco [124] showed that possible alterations of the cerebral vasoreactivity (CVR) on these patients could be easily measured through a simple and easy-to-do head-of-bed (HOB) position challenge. The HOB position change is presented for the first time in Chapter 5, but has been also studied in Chapters 7, 9 and 10 showing to be a potential simple and easy-to-perform challenge for testing a biomarker for the CVR in patients with neurovascular risks (i.e. internal carotid artery stenosis or stroke patients). Even more, in this thesis, on Chapter 5, I have shown that this biomarker of CVR alteration improved with treatment in

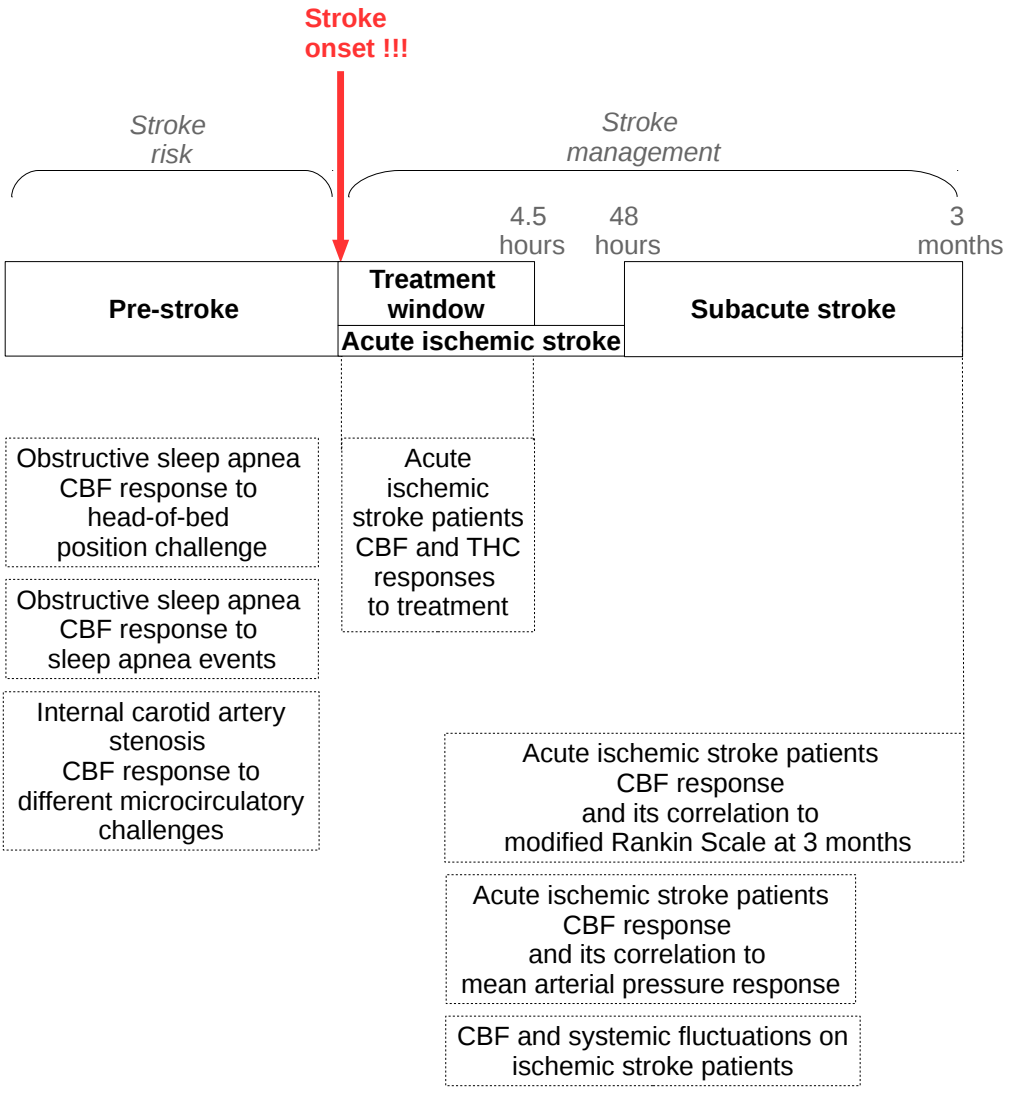

FIGURE 12.1: Schematic of the different clinical studies according the degree of risk of stroke and also to the stroke condition. CBF, cerebral blood flow.

a small group of highly compliant patients, suggesting that this impairment may be reversible, at least in part, with treatment. These results need to be confirmed in the near future in a large and clinically representative sample of patients with OSA.

At night, these OSA patients have repeated and numerous apneas. But, what exactly happens during these detrimental events, in which cerebral blood flow and oxygenation are found to change? how are these changes? are these changes the cause of the high risk of stroke and other neurovascular events? In Chapter 6, my collaborators and I were able to characterize each cerebral blood flow apneic event, by finding the peak and the following drop of the cerebral blood flow response in each obstructive sleep apnea. The hybrid device was used simultaneously with

the standard polysomnography. One of the challenges was to be able to eliminate possible confounding factors due to, for instance, probe movement and/or apneic events with a low signal quality by using outlier removing analysis. For future work, additional parameters can be considered to go deeper into the relationship between the systemic physiology and microvascular cerebral blood flow changes such as the effects of different states (i.e. arousals and leg movements).

Some patients suffer from a blockage or narrowing of a major artery, but are able to go on with their "normal" lives. What if clinicians could perform riskier interventions if they were identified to be at a higher risk of stroke event? I am talking about internal carotid artery stenosis patients, which are a well-known population at risk of damaged cerebral vasoreactivity and with high probability of neuro- and cardio-vascular risks. In Chapter 7, my collaborators and I used transcranial Doppler ultrasound (TCD) and DCS technologies on asymptomatic internal carotid artery stenosis population, and in controls, in order to compare the HOB position change to two well-known CVR challenges: the acetazolamide injection and the breath-hold challenge. Interestingly, similar to Chapter 6, the head-of-bed recovery back to the initial supine position with the measurement of microvascular relative cerebral blood flow changes (ΔrCBF) (by DCS) was found to be related to the status of CVR in these patients. However, more studies are needed to understand the cerebral hemodynamic changes due to a HOB position change and relate these changes to the clinical parameters in patients with different pathologies.

It is well-known that medicine improves our lives, but even more, it can save our lives. In this thesis, I present how technology showed us that medicine really made a difference in live, that treatment had the power to potentially reduce disability in five patients in danger of death after the most severe neurovascular condition, ischemic stroke. In Chapter 8, I showed that it is feasible to perform diffuse correlation spectroscopy measurements on the emergency department during reperfusion treatment. My collaborators and I were able to conclude that the hemodynamic parameters (total hemoglobin concentration, oxy-hemoglobin concentration and cerebral blood flow) derived from diffuse optical measurements reflected the reperfusion of the microvasculature after macrovascular recanalization in a group analysis of five patients. Further measurements adding more patients to this analysis are needed to better understand this finding.

So far, my collaborators and I have shown how the treatment could be followed-up and the effect of it could be observed in order to improve functional outcome and reduce disability of ischemic stroke patients. But, what happens to these patients once they leave the hospital and they go back to their daily lives? In another study with ischemic stroke patients (Chapter 9), my collaborators and I sought to investigate the relationship between the cortical cerebral blood flow response to HOB changes (a simple elevation from supine position to 30°) measured at different times after the symptom onset and the functional outcome (the capacity to perform basic activities during the daily living). For this study, I had to be daily in touch with the clinicians in order to be able to arrive in the hospital as soon as possible after the admission of the patient, since my collaborators and I were interested specially on the early hours after the stroke onset. In conclusion, microvascular cortical cerebral blood flow response to an increase of the HOB during the early phase of stroke was found to be related to the outcome of stoke. However, further studies are needed to elucidate if this information could be used to individualize management for the patients admitted to the Stroke Unit for improving the functional outcome after acute ischemic stroke. Part of this Chapter was also presented in the thesis of Igor Blanco [124] as a coauthor of this work.

Results of Chapter 6 showed that HOB recovery back to supine position could carry CVR information. If so, this manipulation challenge could also be used in stroke patients showing a biomarker of the severity of the CVR, which could benefit treatment and clinical management of these patients. In order to test this, I got in touch with experienced researchers from University of Pennsylvania (USA), and data from two of their studies and from Chapter 9 were aggregated, as shown in Chapter 10. DCS measurements were acquired during orthostatic challenges involving different HOB positions including repeated supine positions. As it was hypothesized, a ΔrCBF increase was observed from the first supine position to the next supine, in other words, the patients did not recover upon returning back to supine position. But a second interesting result was found, patients studied within 48 hours of stroke onset (and not later) showed a statistically significant correlation between ΔrCBF and mean arterial pressure changes from the first to the second supine position in the ipsilesional hemisphere, but not in the contralesional hemisphere. Again, the HOB position change together with DCS measurements were found to be a biomarker for the CVR/CAR, being hemispheric dependent. Further multi-center studies with the same protocol are needed to elucidate if this

information could be used to individualize management for the patients admitted to the Stroke Unit after acute ischemic stroke.

The studies during my PhD, as it is in life, were not planned and predetermined as one expects. One exciting part of research that I discovered during my PhD was to "bump into" an unexpected line of study. This was the case of the finding of unexpected fluctuations of cerebral blood flow in the acute ischemic stroke patients (Chapter 9) described in Chapter 11. Long meetings with neurologists and pneumologists resulted in a new hypothesis for this new study, suggesting that these fluctuations could be due to apneic and hypopneic events. For testing this, a new respiratory polygraphy device was bought and implemented with the diffuse optical devices. After a first screening, the patients recruited showed that these fluctuations were associated with sleep events. Further studies are needed to study the possible detrimental impact of the magnitude and presence of these cerebral hemodynamic fluctuations, specially in the early hours after stroke were the interventions are more relevant to the outcome of stroke.

Different advantages of diffuse optical techniques over the modalities that are currently present in the clinics have been presented in this thesis for the future implementation of the diffuse optical techniques in the clinics. This ranges from it being non-invasive, portable, continuous and able to measure at the point-of-care (Chapter 8) or at the bed-side (Chapters 5 to 11). However, diffuse optical techniques face different limitations. Based on my personal experience in the hospital and on long discussions with the clinicians, I have identified different suggestions towards a better implementation of the technique. First, ideally, the diffuse optical techniques should be cheaper in order to achieve continuous full access to its use for all patients in the clinics; second, these techniques should be of smaller size evolving towards becoming a "wearable" device in order to be present with the patient through out his/her stay; third, these techniques should be able to measure in multiple places of the head simultaneously; fourth, these techniques should be able to measure through hair which is often problematic and limits DCS measurements to the forehead; fifth, robust real-time data analysis and presentation are needed; and, finally, predictive cut-points in order to allow the doctors to decide on the diagnosis of the patients should be provided on-time. I will briefly speculate about these points.

About the first limitation, the recent emergence of commercial hybrid systems

(e.g. HemoPhotonics S.L. and ISS) and the results of European projects (BabyLux [284]), where user-friendly neuromonitors combining diffuse optical methods, should allow us to increase the yield of transcranial optical monitoring in the clinical settings which was lacking in our case. Second, the main goal of the new device presented in this thesis (Chapter 4) was to fit the device in the crowded-with-gadgets emergency unit of the hospital; however, the device is still not "wearable", future work needs to focus on this goal. Another diffuse optical technique, speckle contrast optical spectroscopy (SCOS) [285], is paving the way towards this end goal of becoming "wearable" with low-cost, robust and battery operated wireless device. Not only DCS has become more compact [286], but also, one of the main advances in the last years has been in improving its sample rate (from ∼1Hz to ∼100Hz) [287]. The next generation of hybrid diffuse optics for our next clinical studies will implement this advance by new hardware correlators. About the third and fourth limitations, so far, due to the cost and size of the device present in the clinics, only two specific locations of the brain have been measured in this thesis, one measurement per hemisphere, using four (out of eight) detector channels for each location obtaining an acceptable signal-to-noise ratio. Moreover, these locations have been restricted to the frontal lobes, since hair is highly light absorbing and the signal-to-noise ratio through hair is too poor for obtaining blood flow measurements. These are important drawbacks to overcome in the coming years; fast array detectors with good quantum efficiency, and probes avoiding the hair [288] could be a starting point to improve these drawbacks. Fifth, another goal of the new device presented in this thesis (Chapter 4) was to implement a real-time data analysis by a new Java based software (work of Ameer Ghouse), allowing the blood flow index to be shown on the screen on real time for each hemisphere separately. Finally, related to the predictive cut-points, an intervention randomized controlled study is underway ("Fundació La Marató de TV3" (201709.31)) to determine whether cerebral blood flow measured with diffuse optics may be used to guide a therapy decision.

There are other technical limitations from the physics/engineering point of view to overcome towards the development of diffuse optics. First, cheaper electronics (specially lasers and detectors); second, to distinguish between the skull and scalp contribution to the signals; and, third, higher depth sensitivity allowing us to measure deeper than the brain cortex. Again, I will briefly speculate about these points.

LUCA project (LUCA-project, No. 688303) [286] has been paving the way on the development of a compact hybrid TRS NIRS-DOS and DCS by implementing an ultrasound device on this hybrid system for thyroid cancer detection. About the first limitation, in the LUCA project, TRS NIRS-DOS has been advanced technologically by building cheaper correlators and DCS lasers, and being able to couple DCS technology with a cheaper TRS NIRS-DOS. About improving the DCS detection electronics, as a future work, fast array detectors with good quantum efficiency, leading to a better signal-to-noise ratio, and consequently, allowing a faster sample rate are needed. About the second limitation, an homogeneous medium has been assumed in the analysis of DCS and NIRS cerebral data, but, even though this assumption has been validated [7, 8, 24], finding that the brain-to-scalp sensitivity is of a maximum of 45% [24] for DCS, this analysis could be more precise assuming that skull and scalp present different optical properties. Different groups have tackled the problem of analytical models of different layers [23, 289–291], but none of them has been extensively applied; using high density tomography with DCS could be the next step to improve this limitation. And the third limitation mentioned is the depth sensitivity; a technical approach similar such as on time domain DCS [292]) would allow us to measure deeper than the brain cortex, even when hair is present. Evidently, a lot of work needs to be performed in the future in these directions.

Also, there are key research challenges on this field. A big research challenge is on building European Conformity (CE)/Food and Drug Administration (FDA) approved devices. These implies a lot of engineering for finding the most efficient and cheap components. It also implies big budgets for testing the different possible components, building the devices, testing them for clinical use and for obtaining CE/Food and Drug Administration approvals. And, once the devices are ready to be used for the clinical use, another research challenge is pushing diffuse optics out from the lab to the clinics. The different projects should not focus only in one hospital, multicenter studies (3-4) should be designed based on the initial results, but this is challenging since this should require careful and verified protocol design, quality control mechanisms, a lot of logistics, many clinicians interested and involved, and, again, a big budget to fulfill all this mentioned. This could be the first exercise with these systems going towards a large scale clinical trial that would last several years, since the ultimate goal is to go into routine clinical use. The European project BabyLux [284] is a good example of this first exercise, with two similar devices running in two different clinical centers, using the same

protocols for the same groups of study, and going into validation tests for CE/FDA approvals.

I imagine a near future where diffuse optical portable devices will be applied to the head of the people from the moment they enter the clinics for any standard check, obtaining a standardized biological biomarker of the cerebral well-being and of neurovascular risks. I believe that this manuscript is a contribution to this idea, by applying these techniques to new relevant biological questions at the point-of-care in the clinics in patients with neurovascular risks and stroke condition, with the main goal to get closer to this near future. Moreover, I have introduced diffuse optics together with a promising head-of-bed challenge (non-invasive (no need to inspire gases or inject drugs), easy to perform and no requirement of subject collaboration) to demonstrate that this protocol is a promising biomarker to obtain cerebral vasoreactivity information of mild-to-severe neurovascular conditioned patients.

Let's see how the future will become.

Bibliography

[1] S. S. Kety and C. F. Schmidt, "The nitrous oxide method for the quantitative determination of cerebral blood flow in man: theory, procedure and normal values," *J. Clin. Invest.* **27**(4), 476–483 (1948).

[2] W.-D. Heiss and G. Rosner, "Functional recovery of cortical neurons as related to degree and duration of ischemia," *Ann. Neurol.* **14**(3), 294–301.

[3] W. A. Pulsinelli, J. B. Brierley, and F. Plum, "Temporal profile of neuronal damage in a model of transient forebrain ischemia," *Ann. Neurol.* **11**(5), 491–498.

[4] S. Payne, *Cerebral autoregulation. Control of blood flow in the brain*, Springer Nature (2016).

[5] T. Durduran, R. Choe, W. B. Baker, *et al.*, "Diffuse optics for tissue monitoring and tomography," *Reports Prog. Phys.* **73**(7), 76701 (2010).

[6] M. Wintermark, M. Sesay, E. Barbier, *et al.*, "Comparative overview of brain perfusion imaging techniques.," *J. Neuroradiol.* **32**(5), 294–314 (2005).

[7] T. Durduran and A. G. Yodh, "Diffuse correlation spectroscopy for non-invasive, micro-vascular cerebral blood flow measurement.," *Neuroimage* **85**, 51–63 (2014).

[8] R. C. Mesquita, T. Durduran, G. Yu, *et al.*, "Direct measurement of tissue blood flow and metabolism with diffuse optics.," *Philos. Trans. A. Math. Phys. Eng. Sci.* **369**(1955), 4390–4406 (2011).

[9] M. Giovannella, B. Andresen, J. Bjerglund Andersen, *et al.*, "Validation and potential calibration of diffuse correlation spectroscopy versus (15)O-water positron emission tomography on neonatal piglets," Society for Functional Near-Infrared Spectroscopy, (Tokyo, Japan) (2018).

[10] V. Jain, E. M. Buckley, D. J. Licht, *et al.*, "Cerebral oxygen metabolism in neonates with congenital heart disease quantified by MRI and optics," *J. Cereb. Blood Flow Metab.* **34**(3), 380–388 (2014).

[11] L. He, W. Baker, D. Milej, *et al.*, "Noninvasive continuous optical monitoring of absolute cerebral blood flow in adult human subjects," **Part F91-T**, 2–3, Optics and the Brain 2018 (2018).

[12] E. M. Buckley, D. Hance, T. Pawlowski, *et al.*, "Validation of diffuse correlation spectroscopic measurement of cerebral blood flow using phase-encoded velocity mapping magnetic resonance imaging," *J. Biomed. Opt.* **17**(3), 03007 (2012).

[13] E. M. Buckley, N. Cook, T. Durduran, *et al.*, "Cerebral hemodynamics in preterm infants during positional intervention measured with diffuse correlation spectroscopy and transcranial Doppler ultrasound," *Opt. Express* **17**(15), 12571–12581 (2009).

[14] R. Arora, M. Ridha, D. S. Lee, *et al.*, "Preservation of the metabolic rate of oxygen in preterm infants during indomethacin therapy for closure of the ductus arteriosus," *Pediatr. Res.* **73**(6), 713–718 (2013).

[15] G. Yu, T. F. Floyd, T. Durduran, *et al.*, "Validation of diffuse correlation spectroscopy for muscle blood flow with concurrent arterial spin labeled perfusion MRI.," *Opt. Express* **15**(3), 1064–1075 (2007).

[16] S. A. Carp, A. Surova, M. Patel, *et al.*, "Noninvasive optical measures of CBV, StO2 , CBF Index, and rCMRO2 in human premature neonates' brains in the first six weeks of life," *Hum. Brain Mapp.* **31**, 341–352 (2010).

[17] T. Durduran, G. Yu, M. G. Burnett, *et al.*, "Diffuse optical measurement of blood flow, blood oxygenation, and metabolism in a human brain during sensorimotor cortex activation.," *Opt. Lett.* **29**(15), 1766–1768 (2004).

[18] J. P. Culver, T. Durduran, C. Cheung, *et al.*, "Diffuse optical measurement of hemoglobin and cerebral blood flow in rat brain during hypercapnia, hypoxia and cardiac arrest.," *Adv. Exp. Med. Biol.* **510**, 293–7 (2003).

[19] P. Y. Lin, K. Hagan, A. Fenoglio, *et al.*, "Reduced cerebral blood flow and oxygen metabolism in extremely preterm neonates with low-grade germinal matrix- intraventricular hemorrhage," *Sci. Rep.* **6**(November 2015), 1–8 (2016).

[20] Y. Shang, L. Chen, M. Toborek, *et al.*, "Diffuse optical monitoring of repeated cerebral ischemia in mice," *Opt. Express* **19**(21), 20301 (2011).

[21] J. Li, G. Dietsche, D. Iftime, *et al.*, "Noninvasive detection of functional brain activity with near-infrared diffusing-wave spectroscopy," *J. Biomed. Opt.* **10**(4), 44002 (2005).

[22] F. Jaillon, S. E. Skipetrov, J. Li, *et al.*, "Diffusing-wave spectroscopy from head-like tissue phantoms: influence of a non-scattering layer," *Opt. Express* **14**(22), 10181 (2006).

[23] L. Gagnon, M. Desjardins, J. Jehanne-Lacasse, *et al.*, "Investigation of diffuse correlation spectroscopy in multi-layered media including the human head.," *Opt. Express* **16**(20), 15514–15530 (2008).

[24] J. Selb, D. A. Boas, S.-T. Chan, *et al.*, "Sensitivity of near-infrared spectroscopy and diffuse correlation spectroscopy to brain hemodynamics: simulations and experimental findings during hypercapnia," *Neurophotonics* **1**, 015005 (2014).

[25] I. Hajjar, P. Zhao, D. Alsop, *et al.*, "Hypertension and cerebral vasoreactivity: A continuous arterial spin labeling magnetic resonance imaging study," *Hypertension* **56**(5), 859–864 (2010).

[26] J. Sahuquillo, M. A. Poca, A. Ausina, *et al.*, "Arterio-jugular differences of oxygen (AVDO2) for bedside assessment of CO2-reactivity and autoregulation in the acute phase of severe head injury," *Acta Neurochir. (Wien).* **138**(4), 435–444 (1996).

[27] J. D. Miller and B. A. Bell, *Cerebral blood flow*, McGraw Hill Book (1987).

[28] R. H. Wilkins and S. S. Rengachary, *Neurosurgery*, McGraw Hill Book (1985).

[29] R. B. Panerai, "System identification of human cerebral blood flow regulatory mechanisms," *Cardiovasc. Eng. An Int. J.* **4**(1), 59–60 (2004).

[30] O. B. Paulson, S. Strandgaard, and L. Edvinsson, "Cerebral autoregulation," *Cerebrovasc. Brain Metab. Rev.* **2**, 161–192 (1990).

[31] S. J. E. Lucas, Y. C. Tzeng, S. D. Galvin, *et al.*, "Influence of changes in blood pressure on cerebral perfusion and oxygenation," *Hypertension* **55**(3), 698–705 (2010).

[32] P. R. Weinstein and A. I. Faden, *Protection of the brain from ischemia*, Williams & Wilkins (1990).

[33] R. D. Miller, *Anesthesia*, Churchill Livingstone (1986).

[34] S. Vorstrup, L. Henriksen, and O. B. Paulson, "Effect of acetazolamide on cerebral blood flow and cerebral metabolic rate for oxygen.," *J. Clin. Invest.* **74**(5), 1634–9 (1984).

[35] D. Russell, S. Dybevold, O. Kjartansson, *et al.*, "Cerebral vasoreactivity and blood flow before and 3 months after carotid endarterectomy," *Stroke* **21**(7), 1029–1032 (1990).

[36] P. D. Kaplan, M. H. Kao, A. G. Yodh, *et al.*, "Geometric constraints for the design of diffusing-wave spectroscopy experiments," *Appl. Opt.* **32**(21), 3828–3836 (1993).

[37] K. Furutsu, "Diffusion equation derived from space-time transport equation," *J. Opt. Soc. Am.* **70**(4), 360 (1980).

[38] R. A. J. Groenhuis, J. J. Ten Bosch, and H. A. Ferwerda, "Scattering and absorption of turbid materials determined from reflection measurements. 2: Measuring method and calibration," *Appl. Opt.* **22**(16), 2463 (1983).

[39] A. Corlu, R. Choe, T. Durduran, *et al.*, "Diffuse optical tomography with spectral constraints and wavelength optimization," *Appl. Opt.* **44**(11), 2082 (2005).

[40] S. Susumu, T. Sumio, O. Takeo, *et al.*, "A tissue oxygenation monitor using NIR spatially resolved spectroscopy," *Proc. SPIE, Int. Soc. Opt. Eng.* **3597**(January 1999), 582–592 (199).

[41] D. M. Hueber, M. A. Franceschini, H. Y. Ma, *et al.*, "Non-invasive and quantitative near-infrared haemoglobin spectrometry in the piglet brain during

hypoxic stress, using a frequency-domain multidistance instrument.," *Phys. Med. Biol.* **46**, 41–62 (2001).

[42] S. Fantini, M. A. Franceschini-Fantini, and J. Maier, "Frequency-domain multichannel optical detector for non invasive tissue spectroscopy and oximetry," *Opt. Eng.* **34**(1), 32–42 (2005).

[43] B. Chance, M. Cope, E. Gratton, *et al.*, "Phase measurement of light absorption and scatter in human tissue," *Rev. Sci. Instrum.* **69**(10), 3457–3481 (1998).

[44] J. B. Fishkin and E. Gratton, "Propagation of photon-density waves in strongly scattering media containing an absorbing semi-infinite plane bounded by a straight edge Joshua," *J. Opt. Soc. Am. A* **10**(1), 127–140 (1993).

[45] S. L. Jacques, "Time resolved propagation of ultrashort laser pulses within turbid tissues," *Appl. Opt.* **28**(12), 2223–9 (1989).

[46] M. S. Patterson, B. Chance, and B. C. Wilson, "Time resolved reflectance and transmittance for the non- invasive measurement of tissue optical properties," *Appl. Opt.* **28**(12), 2331–2336 (1989).

[47] D. Comelli, A. Bassi, A. Pifferi, *et al.*, "In vivo time-resolved reflectance spectroscopy of the human forehead," *Appl. Opt.* **46**(10), 1717–1725 (2007).

[48] P. Taroni, A. Pifferi, A. Torricelli, *et al.*, "In vivo absorption and scattering spectroscopy of biological tissues," *Photochem. Photobiol. Sci.* **2**(2), 124 (2003).

[49] A. Torricelli, A. Pifferi, P. Taroni, *et al.*, "In vivo optical characterization of human tissues from 610 to 1010 nm by time-resolved reflectance spectroscopy," *Phys. Med. Biol.* **46**(8), 2227 (2001).

[50] M. A. O'Leary, D. A. Boas, B. Chance, *et al.*, "Refraction of diffuse photon sensity waves," *Phys. Rev. Lett.* **69**(18), 2658–2662 (1992).

[51] D. Boas, M. O'Leary, A. Yodh, *et al.*, "Scattering and wavelength transduction of diffuse photon density waves.," *Physical Review E* **47**(5), R2999–R3002 (1993).

[52] B. J. Tromberg, L. O. Svaasand, T.-t. Tsay, *et al.*, "Properties of photon density waves in multiple-scattering media," *Appl. Opt.* **32**(4), 607–616 (1993).

[53] M. N. Kim, *Applications of hybrid diffuse optics for clinical management of adults after brain injury.* PhD thesis (2013).

[54] A. Duncan, J. H. Meek, M. Clemencet, *et al.*, "Optical pathlength measurements on adult head, calf and forearm and the head of the newborn infant using phase resolved optical spectroscopy," *Phys. Med. Biol.* **40**, 295–304 (1995).

[55] A. Yodh and B. Chance, "Spectroscopy and imaging with diffusing light," *Phys. Today* **48**(3), 34 (1995).

[56] D. A. Boas and M. A. Franceschini, "Haemoglobin oxygen saturation as a biomarker: the problem and a solution," *Phylosophical Trans. R. Soc.* **369**, 4407–4424 (2011).

[57] D. T. Delpy, M. Cope, P. van der Zee, *et al.*, "Estimation of optical pathlength through tissue from direct time of flight measurement," *Phys. Med. Biol.* **33**(12), 1433–1442 (1988).

[58] G. Strangman, M. A. Franceschini, and D. A. Boas, "Factors affecting the accuracy of near-infrared spectroscopy concentration calculations for focal changes in oxygenation parameters," *Neuroimage* **18**, 865–879 (2003).

[59] D. A. Boas, G. Strangman, X. Cheng, *et al.*, "The accuracy of near infrared spectroscopy and imaging during focal changes in cerebral hemodynamics," *Neuroimage* **13**, 76–90 (2001).

[60] G. Yu, "Diffuse Correlation Spectroscopy (DCS): A diagnostic tool for assessing tissue blood flow in vascular-related diseases and therapies," *Curr. Med. Imaging Rev.* **8**, 194–210 (2012).

[61] J. W. Goodman, "Some fundamental properties of speckle," *J. Opt. Soc. Am.* **11**(66), 1145–1150 (1976).

[62] G. Cloud, "Optical methods in experimental mechanics.," *Experimental Techniques* **1**(31), 15–17 (2007).

[63] D. A. Boas and A. G. Yodh, "Spatially varying dynamical properties of turbid media probed with diffusing temporal light correlation," *J. Opt. Soc. Am.* **14**(1), 192–215 (1997).

[64] D. A. Boas, L. E. Campbell, and A. G. Yodh, "Scattering and imaging with diffusing temporal field correlations," *Phys. Rev. Lett.* **75**(9), 1855 (1995).

[65] D. J. Pine, D. A. Weitz, P. M. Chaikin, *et al.*, "Diffusing-wave spectroscopy," *Phys. Rev. Lett.* **60**(12), 1134–1137 (1988).

[66] S. A. Carp, N. Roche-Labarbe, M.-A. Franceschini, *et al.*, "Due to intravascular multiple sequential scattering, Diffuse Correlation Spectroscopy of tissue primarily measures relative red blood cell motion within vessels.," *Biomed. Opt. Express* **2**(7), 2047–2054 (2011).

[67] B. J. Berne and R. Pecora, *Dynamic light scattering with applications to chemistry, biology, and physics, year = 1990*, Krieger Malabar, FL.

[68] W. Brown, *Dynamic light scattering: the method and some applications, year = 1993*, Clarendon New York.

[69] B. Chu, *Laser light scattering, basic principles and practice, year = 1991*, Academic New York.

[70] B. Berne and R. Pecora, "Dynamic light scattering: with applications to chemistry, biology, and physics," *J. Chem. Educ.* , 430 (1976).

[71] P. A. Lemieux and D. J. Durian, "Investigating non-Gaussian scattering processes by using nth-order intensity correlation functions," *J. Opt. Soc. Am. A* **16**(7), 1651–1664 (1999).

[72] W. Zhou, O. Kholiqov, S. P. Chong, *et al.*, "Highly parallel, interferometric diffusing wave spectroscopy for monitoring cerebral blood flow dynamics," *Optica* **5**(5), 518 (2018).

[73] K. Zarychta, E. Tinet, L. Azizi, *et al.*, "Time-resolved diffusing wave spectroscopy with a CCD camera.," *Opt. Express* **18**(16), 16289–16301 (2010).

[74] G. Maret and P. Wolf, "Mutiple light scattering from disordered media. The effect of brownian motion of scatterers.," *Condens. Matter* **65**, 409–413 (1987).

[75] M. Stephen, "Temporal fluctuations in wave propagation in random media.," *Physical Review B* **37**(1), 1–5 (1988).

[76] C. Menon, G. M. Polin, I. Prabakaran, *et al.*, "An integrated approach to measuring tumor oxygen status using human melanoma xenografts as a model," *Cancer Res.* **63**, 7232–7240 (2003).

[77] G. Yu, T. Durduran, C. Zhou, *et al.*, "Noninvasive monitoring of murine tumor blood flow during and after photodynamic therapy provides early assessment of therapeutic efficacy," *Clin. Cancer Res.* **11**(9), 3543–3552 (2005).

[78] S. A. Carp, G. P. Dai, D. A. Boas, *et al.*, "Validation of diffuse correlation spectroscopy measurements of rodent cerebral blood flow with simultaneous arterial spin labeling MRI; towards MRI-optical continuous cerebral metabolic monitoring," *Biomed. Opt. Express* **1**(2), 553–565 (2010).

[79] M. N. Kim, T. Durduran, S. Frangos, *et al.*, "Noninvasive measurement of cerebral blood flow and blood oxygenation using near-infrared and diffuse correlation spectroscopies in critically brain-injured adults," *Neurocrit. Care* **12**(2), 173–180 (2010).

[80] A. Einstein, "On the motion of small particles suspended in liquids at rest required by the molecular-kinetic theory of heat," *Ann. Phys., Lpz.* **17**, 549–560 (1905).

[81] C. Zhou, S. A. Eucker, T. Durduran, *et al.*, "Diffuse optical monitoring of hemodynamic changes in piglet brain with closed head injury," **14**(3), 1–22 (2009).

[82] R. Choe, M. E. Putt, P. M. Carlile, *et al.*, "Optically measured microvascular blood flow contrast of malignant breast tumors," *PLoS One* **9**(6), 1–10 (2014).

[83] P. Zirak, R. Delgado-Mederos, J. Martí-Fàbregas, *et al.*, "Effects of acetazolamide on the micro- and macro-vascular cerebral hemodynamics: a diffuse optical and transcranial doppler ultrasound study.," *Biomed. Opt. Express* **1**(5), 1443–1459 (2010).

[84] R. C. Mesquita, N. Skuli, M. N. Kim, *et al.*, "Hemodynamic and metabolic diffuse optical monitoring in a mouse model of hindlimb ischemia," *Biomed. Opt. Express* **1**(4), 932–936 (2010).

[85] Y. Shang, L. Chen, M. Toborek, *et al.*, "Diffuse optical monitoring of repeated cerebral ischemia in mice," *Opt. Express* **19**(21), 945–949 (2011).

[86] J. Tang, S. E. Erdener, B. Li, *et al.*, "Shear-induced diffusion of red blood cells measured with dynamic light scattering-optical coherence tomography," *J. Biophotonics* **11**(2), 1–10 (2018).

[87] W. Cory, *Fan noise, Fans and Ventilation: A practical guide*, vol. 14, 215–237. Elsevier.

[88] R. H. Müller and S. Heinemann, "Fat emulsions for parenteral nutrition II: Characterisation and physical long-term stability of Lipofundin MCT LCT," *Clin. Nutr.* **12**(5), 298–309 (1993).

[89] Z. Li, W. B. Baker, A. B. Parthasarathy, *et al.*, "Calibration of diffuse correlation spectroscopy blood flow index with venous-occlusion diffuse optical spectroscopy in skeletal muscle.," *Journal of biomedical optics* **20 12**, 125005 (2015).

[90] H. Engleman and N. J. Douglas, "Sleepiness, cognitive function, and quality of life in obstructive sleep apnoea/hypopnoea syndrome," *Thorax* **59**, 618–622 (2004).

[91] J. Terán-Santos, A. Jiménez-Gómez, J. Cordero-Guevara, *et al.*, "The association between sleep apnea and the risk of traffic accidents," *N. Engl. J. Med.* **11**, 847–851 (1999).

[92] P. Peppard, T. Young, M. Palta, *et al.*, "Prospective study of the association between sleep-disordered breathing and hypertension," *N. Engl. J. Med.* **342**(19), 1378–1384 (2000).

[93] T. Young, L. Finn, P. E. Peppard, *et al.*, "Sleep disordered breathing and mortality: eighteen-year follow-up of the Wisconsin sleep cohort," *Sleep* **31**(8), 1071–1078 (2008).

[94] F. Campos-Rodriguez, M. A. Martinez-Garcia, I. de la Cruz-Moron, *et al.*, "Cardiovascular mortality in women with obstructive sleep apnea with or without continuous positive airway pressure treatment: a cohort study.," *Ann. Intern. Med.* **156**, 115–122 (2012).

[95] J. Marin, S. J. Carrizo, L. Vicente, *et al.*, "Long-term cardiovascular outcomes in men with obstructive sleep apnea-hypopnoea with or without treatment with continuous positive airway pressure: an observational study," *Lancet* **365**, 1046–1053 (2005).

[96] T. Young, L. Evans, L. Finn, *et al.*, "Estimation of the clinically diagnosed proportion of sleep apnea syndrome in middle-aged men and women," *Sleep* **20**(9), 705–706 (1997).

[97] J. Duran, S. Esnaola, R. Rubio, *et al.*, "Obstructive sleep apnea-hypopnea and related clinical features in a population-based sample of subjects aged 30 to 70 Yr," *Am. J. Respir. Crit. Care Med.* **163**, 685–689 (2001).

[98] D. S. Hui, D. K. Choy, L. K. Wong, *et al.*, "Prevalence of sleep-disordered breathing and continuous positive airway pressure compliance: Results in Chinese patients with first-ever ischemic stroke," *Chest* **122**(3), 852–860 (2002).

[99] C. Bassetti, M. S. Aldrich, R. D. Chervin, *et al.*, "Sleep apnea in patients with transient ischemic attack and stroke: a prospective study of 59 patients.," *Neurology* **47**(5), 1167–1173 (1996).

[100] M. E. Dyken, V. K. Somers, T. Yamada, *et al.*, "Investigating the relationship between stroke and obstructive sleep apnea," *Stroke* **27**(3), 401–407 (1996).

[101] D. C. Good, J. Q. Henkle, D. Gelber, *et al.*, "Sleep-disordered breathing and poor functional outcome after stroke," *Stroke* **27**(2), 252–259 (1996).

[102] Y. Kaneko, V. E. Hajek, V. Zivanovic, *et al.*, "Relationship of sleep apnea to functional capacity and length of hospitalization following stroke.," *Sleep* **26**(3), 293–297 (2003).

[103] J. A. Aaronson, C. A. M. van Bennekom, W. F. Hofman, *et al.*, "Obstructive sleep apnea affects functional and cognitive status after stroke," *Sleep* **38**(9), 1431–1437 (2015).

[104] S. Ryan, C. T. Taylor, and W. T. McNicholas, "Systemic inflammation: a key factor in the pathogenesis of cardiovascular complications in obstructive sleep apnoea syndrome?," *Thorax* **64**, 631–636 (2009).

[105] N. L. Chamberlin and L. Ling, "The effect of intermittent hypoxia on obstructive sleep apnea: beneficial or detrimental?," *J. Appl. Physiol.* **110**, 9–10 (2011).

[106] S. S. Yokhana, D. G. Gerst, D. S. Lee, *et al.*, "Impact of repeated daily exposure to intermittent hypoxia and mild sustained hypercapnia on apnea severity," *J. Appl. Physiol.* **112**, 367–377 (2012).

[107] J. T. Carlson, J. Hedner, M. Elam, *et al.*, "Augmented resting sympathetic activity in awake patients with obstructive sleep apnea," *Chest* **103**, 1763–1768 (1993).

[108] D. J. Durgan and R. M. Bryan, "Cerebrovascular consequences of obstructive sleep apnea.," *J. Am. Heart Assoc.* **1**, e000091 (2012).

[109] B. J. Morgan, K. J. Reichmuth, P. E. Peppard, *et al.*, "Effects of sleep-disordered breathing on cerebrovascular regulation: A population-based study.," *Am. J. Respir. Crit. Care Med.* **182**, 1445–52 (2010).

[110] G. E. Foster, P. J. Hanly, M. Ostrowski, *et al.*, "Effects of continuous positive airway pressure on cerebral vascular response to hypoxia in patients with obstructive sleep apnea," *Am. J. Respir. Crit. Care Med.* **175**(7), 720–725 (2007).

[111] D. R. Busch, J. M. Lynch, M. E. Winters, *et al.*, "Cerebral blood flow response to hypercapnia in children with obstructive sleep apnea syndrome.," *Sleep* **39**(1), 209–216 (2016).

[112] F. Urbano, F. Roux, J. Schindler, *et al.*, "Impaired cerebral autoregulation in obstructive sleep apnea.," *J. Appl. Physiol.* **105**, 1852–7 (2008).

[113] E. M. Bålfors and K. A. Franklin, "Impairment of cerebral perfusion during obstructive sleep apneas.," *Am. J. Respir. Crit. Care Med.* **150**, 1587–1591 (1994).

[114] R. R. Pindzola, J. R. Balzer, E. M. Nemoto, *et al.*, "Cerebrovascular reserve in patients with carotid occlusive disease assessed by stable xenon-enhanced CT cerebral blood flow and transcranial Doppler.," *Stroke* **32**(8), 1811–1817 (2001).

[115] E. L. Barbier, A. C. Silva, S. G. Kim, *et al.*, "Perfusion imaging using dynamic arterial spin labeling (DASL).," *Magn. Reson. Med.* **45**(6), 1021–1029 (2001).

[116] R. B. Workman and R. E. Coleman, *PET/CT: Essentials for clinical practice*, Springer (2007).

[117] C. Gregori-Pla, G. Cotta, G. Camps-Renom, Pol Giacalone, *et al.*, "Is the head-of-bed positioning challenge a good alternative to measure cerebrovascular reactivity? A comparison to acetazolamide injection and to breath-hold challenge by diffuse optics.," *Neurophotonics* (2018. Under preparation.).

[118] B. L. Edlow, M. N. Kim, T. Durduran, *et al.*, "The effects of healthy aging on cerebral hemodynamic responses to posture change.," *Physiol. Meas.* **31**(4), 477–495 (2010).

[119] C. G. Favilla, R. C. Mesquita, M. Mullen, *et al.*, "Optical bedside monitoring of cerebral blood flow in acute ischemic stroke patients during head-of-bed manipulation," *Stroke* **45**, 1269–1274 (2014).

[120] T. Durduran, C. Zhou, B. L. Edlow, *et al.*, "Transcranial optical monitoring of cerebrovascular hemodynamics in acute stroke patients," *Opt. Express* **17**(5), 3884–3902 (2009).

[121] M. N. Kim, B. L. Edlow, T. Durduran, *et al.*, "Continuous optical monitoring of cerebral hemodynamics during head-of-bed manipulation in brain-injured adults," *Neurocrit. Care* **20**(3), 443–453 (2014).

[122] C. Gregori-Pla, R. C. Mesquita, C. Favilla, *et al.*, "A mild orthostatic challenge shows cerebral autoregulation impairment on the ipsilesional hemisphere of ischemic stroke patients," *Journal of Cerebral Blood Flow and Metabolism* (2018. Under preparation.).

[123] C. Gregori-Pla, I. Blanco, P. Camps-Renom, *et al.*, "Early microvascular cerebral blood flow response to head-of-bed elevation is related to outcome in acute ischemic stroke," *Journal of Neurology* (2018. Under preparation.).

[124] I. Blanco, *Diffuse optical monitoring of cerebral hemodynamics in experimental and clinical neurology.* PhD thesis (2014).

[125] K. J. Reichmuth, J. M. Dopp, S. R. Barczi, *et al.*, "Impaired vascular regulation in patients with obstructive sleep apnea: effects of continuous positive airway pressure treatment.," *Am. J. Respir. Crit. Care Med.* **180**, 1143–50 (2009).

[126] O. Prilipko, N. Huynh, M. E. Thomason, *et al.*, "An fMRI study of cerebrovascular reactivity and perfusion in obstructive sleep apnea patients before and after CPAP treatment," *Sleep Med.* **15**(8), 892–898 (2014).

[127] C. Gregori-Pla, G. Cotta, I. Blanco, *et al.*, "Cerebral vasoreactivity in response to a head-of-bed position change is altered in patients with moderate and severe obstructive sleep apnea," *PLoS One* **13**(3), e0194204 (2018).

[128] G. Mancia, R. Fagard, K. Narkiewicz, *et al.*, "2013 ESH/ESC guidelines for the management of arterial hypertension: The Task Force for the management of arterial hypertension of the European Society of Hypertension (ESH) and of the European Society of Cardiology (ESC)," *Eur. Heart J.* **34**(28), 2159–2219 (2013).

[129] P. Lloberes, J. Durán-Cantolla, M. Martínez-García, *et al.*, "Diagnosis and treatment of sleep apnea-hypopnea syndrome," *Arch. Bronconeumol.* **47**(3), 143–1565 (2011).

[130] R. B. Berry, R. Budhiraja, D. J. Gottlieb, *et al.*, "Rules for scoring respiratory events in sleep: Update of the 2007 AASM manual for the scoring of sleep and associated events," *J. Clin. Sleep Med.* **8**(5), 597–619 (2012).

[131] E. Chiner, J. M. Arriero, J. Signes-Costa, *et al.*, "Validación de la versión española del test de somnolencia Epworth en pacientes con síndrome de apnea de sueño - Validation of the Spanish version of the Epworth sleepiness scale in patients with sleep apnea syndrome," *Arch. Bronconeumol.* **35**, 422–427 (1999).

[132] J. F. Masa, A. Jiménez, J. Durán, *et al.*, "Alternative methods of titrating continuous positive airway pressure: A large multicenter study," *Am. J. Respir. Crit. Care Med.* **170**(11), 1218–1224 (2004).

[133] M. J. Aries, J. W. Elting, R. Stewart, *et al.*, "Cerebral blood flow velocity changes during upright positioning in bed after acute stroke: an observational study.," *BMJ Open* **3**, 1–8 (2013).

[134] M. Y. Lam, V. J. Haunton, T. G. Robinson, *et al.*, "Does gradual change in head positioning affect cerebrovascular physiology?," *Physiol. Rep.* **6**(3), 1–12 (2018).

[135] R Core Team, *R: A language and environment for statistical computing*. R Foundation for Statistical Computing, Vienna, Austria (2015).

[136] T. Pohlert, *The Pairwise Multiple Comparison of Mean Ranks Package (PMCMR)* (2014). R package.

[137] F. Placidi, M. Diomedi, L. M. Cupini, *et al.*, "Impairment of daytime cerebrovascular reactivity in patients with obstructive sleep apnoea syndrome.," *J. Sleep Res.* **7**(4), 288–292 (1998).

[138] G. E. Foster, P. J. Hanly, M. Ostrowski, *et al.*, "Ventilatory and cerebrovascular responses to hypercapnia in patients with obstructive sleep apnoea: Effect of CPAP therapy," *Respir. Physiol. Neurobiol.* **165**, 73–81 (2009).

[139] C. M. Ryan, A. Battisti-Charbonney, O. Sobczyk, *et al.*, "Normal hypercapnic cerebrovascular conductance in obstructive sleep apnea," *Respir. Physiol. Neurobiol.* **190**(1), 47–53 (2014).

[140] N. Nasr, A. P.-L. Traon, M. Czosnyka, *et al.*, "Cerebral autoregulation in patients with obstructive sleep apnea syndrome during wakefulness.," *Eur. J. Neurol.* **16**(3), 386–391 (2009).

[141] R. B. Panerai, "Assessment of cerebral pressure autoregulation in humans - a review of measurement methods," *Physiol. Meas.* **19**(3), 305 (1998).

[142] P. Zirak, R. Delgado-Mederos, L. Dinia, *et al.*, "Microvascular versus macrovascular cerebral vasomotor reactivity in patients with severe internal carotid artery stenosis or occlusion.," *Acad. Radiol.* **21**, 168–74 (2014).

[143] J. S. Meyer, K. Shimazu, Y. Fukuuchi, *et al.*, "Impaired neurogenic cerebrovascular control and dysautoregulation after stroke.," *Stroke.* **4**(2), 169–86 (1973).

[144] S. C. Jones, C. R. Radinsky, A. J. Furlan, *et al.*, "Variability in the magnitude of the cerebral blood flow response and the shape of the cerebral blood flow-pressure autoregulation curve during hypotension in normal rats [corrected].[Erratum appears in Anesthesiology 2002 Nov;97(5):1332]," *Anesthesiology* **97**(2), 488–496 (2002).

[145] A. G. Logan, S. M. Perlikowski, A. Mente, *et al.*, "High prevalence of unrecognized sleep apnoea in drug- resistant hypertension," *J Hypertens J. Hypertens.* **19**(19), 2271–2277 (2001).

[146] L. F. Drager, L. A. Bortolotto, E. M. Krieger, *et al.*, "Additive effects of obstructive sleep apnea and hypertension on early markers of carotid atherosclerosis," *Hypertension* **53**(1), 64–69 (2009).

[147] V. K. Somers, D. P. White, R. Amin, *et al.*, "Sleep apnea and cardiovascular disease: an American Heart Association/American College of Cardiology Foundation scientific statement from the American Heart Association Council for High Blood Pressure Research Professional Education Committee, Council on Clinical Cardiology, Stroke Council, and Council on Cardiovascular Nursing," *Circulation* **118**(10), 1080–1111 (2008).

[148] D. M. Wallace, A. R. Ramos, and T. Rundek, "Sleep disorders and stroke.," *Int. J. Stroke* **7**, 231–42 (2012).

[149] S. L. Appleton, A. Vakulin, S. A. Martin, *et al.*, "Hypertension is associated with undiagnosed OSA during rapid eye movement sleep," *Chest* **150**(3), 495–505 (2016).

[150] B. G. Phillips, PharmD, V. K. Somers, *et al.*, "Hypertension and obstructive sleep apnea," *Curr. Hypertens. Rep.* **5**, 380–385 (2003).

[151] R. Mehra, E. J. Benjamin, E. Shahar, *et al.*, "Association of nocturnal arrhythmias with sleep-disordered breathing: The sleep heart health study," *Am. J. Respir. Crit. Care Med.* **173**, 910–916 (2006).

[152] M. C. Lipford, K. D. Flemming, A. D. Calvin, *et al.*, "Associations between cardioembolic stroke and obstructive sleep apnea.," *Sleep* **38**(11), 1699–1705 (2015).

[153] H. Engleman, "Neuropsychological function in obstructive sleep apnoea," *Sleep Med. Rev.* **3**(1), 59–78 (1999).

[154] E. C. Fletcher, "Effect of episodic hypoxia on sympathetic activity and blood pressure," *Respir. Physiol.* **119**, 189–197 (2000).

[155] J. Klingelhöfer, G. Hajak, D. Sander, *et al.*, "Assessment of intracranial hemodynamics in sleep apnea syndrome," *Stroke* **23**(10), 1427–1433 (1992).

[156] G. Hajak, J. Klingelhofer, M. Schulz-Varszegi, *et al.*, "Sleep apnea syndrome and cerebral hemodynamics," *Chest* **110**(3), 670–679 (1996).

[157] R. Alex, S. Manchikatla, K. Machiraju, *et al.*, "Effect of apnea duration on apnea induced variations in cerebral blood flow velocity and arterial blood pressure," *Eng. Med. Biol. Soc. (EMBC), 2014 36th Annu. Int. Conf. IEEE* , 270–273 (2014).

[158] M. Siebler and A. Nachtmann, "Cerebral hemodynamics in obstructive sleep apnea," *Chest* **103**(4), 1118–1119 (1993).

[159] M. J. H. Aries, J. W. Elting, J. De Keyser, *et al.*, "Cerebral autoregulation in stroke: A review of transcranial doppler studies," *Stroke* **41**(11), 2697–2704 (2010).

[160] T. Hayakawa, M. Terashima, Y. Kayukawa, *et al.*, "Changes in cerebral oxygenation and hemodynamics during obstructive sleep apneas.," *Chest* **109**(4), 916–921 (1996).

[161] A. D. Mcgown, H. Makker, C. Elwell, *et al.*, "Measurement of changes in cytochrome oxidase redox state during obstructive sleep apnea using near-infrared spectroscopy," *Sleep* **26**(6), 1–7 (2003).

[162] C. O. Olopade, E. Mensah, R. Gupta, *et al.*, "Noninvasive determination of brain tissue oxygenation during sleep in obstructive sleep apnea: a near-infrared spectroscopic approach.," *Sleep* **30**(12), 1747–1755 (2007).

[163] F. Pizza, M. Biallas, M. Wolf, *et al.*, "Nocturnal cerebral hemodynamics in snorers and in patients with obstructive sleep apnea: a near-infrared spectroscopy study," *Sleep* **33**(2), 205 (2010).

[164] D. B. Stanimirovic and A. Friedman, "Pathophysiology of the neurovascular unit: Disease cause or consequence," *J. Cereb. Blood Flow Metab.* **32**(7), 1207–1221 (2012).

[165] B. M. Ances, D. F. Wilson, J. H. Greenberg, *et al.*, "Dynamic changes in cerebral blood flow, O2 tension, and calculated cerebral metabolic rate of O2 during functional activation using oxygen phosphorescence quenching," *J. Cereb. Blood Flow Metab.* **21**(5), 511–516 (2001).

[166] R. Hoge, J. Atkinson, B. Gill, *et al.*, "Investigation of BOLD signal dependence on cerebral blood flow and oxygen consumption: The deoxyhemoglobin dilution model," *Magn. Reson. Med.* **863**, 849–863 (1999).

[167] F. Hyder, R. G. Shulman, and D. L. Rothman, "A model for the regulation of cerebral oxygen delivery," *J.Appl.Physiol* **85**(2), 554–564 (1998).

[168] R. Aaslid, K.-F. Lindegaard, W. Sorteberg, *et al.*, "Cerebral autoregulation dynamics in humans," *Stroke* **20**, 45–52 (1989).

[169] Y. Hou, Y. Shang, R. Cheng, *et al.*, "Obstructive sleep apnea-hypopnea results in significant variations in cerebral hemodynamics detected by diffuse optical spectroscopies.," *Physiol. Meas.* **35**, 2135–48 (2014).

[170] P. Zirak, C. Gregori-Pla, I. Blanco, *et al.*, "Characterization of the microvascular cerebral blood flow response to obstructive apneic events during night sleep," *Neurophotonics* **4**(5) (2018).

[171] S. Gyulay, L. G. Olson, M. J. Hensley, *et al.*, "A comparison of clinical assessment and home oximetry in the diagnosis of obstructive sleep apnea.," *Am Rev Respir Dis* **147**(1), 50–53 (1993).

[172] J. Solà-Soler, B. F. Giraldo, J. A. Fiz, *et al.*, "Proc. annu. int. conf. ieee eng. med. biol. soc. embs," **2017**, 1539–1542, Institute of Electrical and Electronics Engineers Inc. (2017).

[173] A. Arribas-Gil and J. Romo, "Shape outlier detection and visualization for functional data: the outliergram.," *Biostatistics* **15**(4), 603–19 (2014).

[174] M. Oviedo, "Utilities for statistical computing in functional data analysis: the package fda.usc," (2011).

[175] A. Roebuck, V. Monasterio, E. Gederi, *et al.*, "A review of signals used in sleep analysis.," *Physiol. Meas.* **35**, R1–57 (2014).

[176] J. C. Pinheiro and D. M. Bates, *Mixed-effects models in S and S-PLUS*, Springer (2000).

[177] F. McAlister, N. Wiebe, J. Ezekowitz, *et al.*, "Meta-analysis: β-blocker dose, heart rate reduction, and death in patients with heart failure," *Ann. Intern. Med.* **150**(11) (2009).

[178] A. Valipour, A. D. McGown, H. Makker, *et al.*, "Some factors affecting cerebral tissue saturation during obstructive sleep apnoea.," *Eur. Respir. J.* **20**(2), 444–450 (2002).

[179] Q. Li and X. J. Jin, "Correlations between the duration and frequency of sleep apnea episode and hypoxemia in patients with obstructive sleep apnea syndrome," *Zhonghua Er Bi Yan Hou Tou Jing Wai Ke Za Zhi* **44**(10), 825–30 (2009).

[180] A. Kulkas, B. Duce, T. Leppänen, *et al.*, "Severity of desaturation events differs between hypopnea and obstructive apnea events and is modulated by their duration in obstructive sleep apnea," *Sleep Breath.* **21**(4), 829–835 (2017).

[181] F. Chouchou, V. Pichot, J.-C. Barthélémy, *et al.*, "Cardiac sympathetic modulation in response to apneas/hypopneas through heart rate variability analysis," *PLoS One* **9**(1), e86434 (2014).

[182] P. E. Peppard, N. R. Ward, and M. J. Morrell, "The impact of obesity on oxygen desaturation during sleep-disordered breathing," *Am. J. Respir. Crit. Care Med.* **180**(8), 788–793 (2009).

[183] E. O. Bixler, A. N. Vgontzas, T. Ten Have, *et al.*, "Effects of age on sleep apnea in men," *Am. J. Respir. Crit. Care Med.* **157**(1), 144–148 (1998).

[184] H. Barnett, W. Taylor, M. Eliasziw, *et al.*, "Benefit of carotid endarterectomy in patients with symptomatic moderate or severe stenosis," *N. Engl. J. Med.* **339**, 1415–1425 (1998).

[185] B. Farrell, A. Fraser, P. Sandercock, *et al.*, "Randomised trial of endarterectomy for recently symptomatic carotid stenosis : Final results of the MRC European Carotid Surgery Trial (ECST)," *Lancet* **351**(9113), 1379–1387 (1998).

[186] J. Fine-Edelstein, P. Wolf, C. Kase, *et al.*, "Precursors of extracranial carotid atherosclerosis in the framingham study.," *Neurology* **44**(6), 1046–1050 (1994).

[187] A. Gupta, J. L. Chazen, M. Hartman, *et al.*, "Cerebrovascular reserve and stroke risk in patients with carotid stenosis or occlusion: A systematic review and meta-analysis," *Stroke* **43**(11), 2884–2891 (2012).

[188] B. Widder, B. Kleiser, and H. Krapf, "Course of cerebrovascular reactivity in patients with carotid-artery occlusions," *Stroke* **25**(10), 1963–1967 (1994).

[189] D. Inzitari, M. Eliasziw, P. Gates, *et al.*, "The causes and risk of stroke in patients with asymptomatic internal-carotid-artery stenosis," *N. Engl. J. Med.* **342**(23), 1693–1701 (2000).

[190] J. Brian, "Carbon dioxide and the cerebral circulation," *Anesthesiology* **88**, 1365–86 (1998).

[191] J. B. Fortune, D. Bock, A. M. Kupinski, *et al.*, "Human cerebrovascular response to oxygen and carbon dioxide as determined by internal carotid artery duplex scanning.," *The Journal Of Trauma* **32**(5), 618 – 627 (1992).

[192] H. S. Markus and M. J. Harrison, "Estimation of cerebrovascular reactivity using transcranial doppler, including the use of breath-holding as the vasodilatory stimulus," *Stroke* **23**(5), 668–673 (1992).

[193] M. Sloan, A. Alexandrov, C. Tegeler, *et al.*, "Assessment: transcranial Doppler ultrasonography: report of the T therapeutics and technology assessment subcommittee of the american academy of neurology," *Neurology* **62**(1526-632X (Electronic)), 1468–1481 (2004).

[194] P. Zirak, R. Delgado-Mederos, J. Martí-Fàbregas, *et al.*, "Effects of acetazolamide on the micro- and macro-vascular cerebral hemodynamics: a diffuse optical and transcranial doppler ultrasound study," *Biomed. Opt. Express* **1**(5), 1443 (2010).

[195] J. P. Culver, T. Durduran, C. Cheung, *et al.*, "Diffuse optical measurement of hemoglobin and cerebral blood flow in rat brain during hypercapnia, hypoxia and cardiac arrest.," *Advances In Experimental Medicine And Biology* **510**, 293 – 297 (2003).

[196] L. K. Ali, J. K. Weng, S. Starkman, *et al.*, "Heads up! A novel provocative maneuver to guide acute ischemic stroke management," *Interv. Neurol.* **90095**, 8–15 (2017).

[197] E. G. Grant, C. B. Benson, G. L. Moneta, *et al.*, "Carotid artery stenosis: grayscale and Doppler ultrasound diagnosis–Society of Radiologists in Ultrasound consensus conference.," *Ultrasound Q.* **19**(4), 190–198 (2003).

[198] C. of North American Symptomatic Carotid Endarterectomy Trial, "Beneficial effect of carotid endarterectomy in symptomatic patients with high-grade carotid stenosis," *N. Engl. J. Med.* **325**(7), 445–53 (1991).

[199] M. Müller, M. Voges, U. Piepgras, *et al.*, "Assessment of cerebral vasomotor reactivity by transcranial Doppler ultrasound and breath-holding. A comparison with acetazolamide as vasodilatory stimulus," *Stroke.* **26**(1), 96–100 (1995).

[200] M. De Bortoli, A. Maillet, S. Skopinski, *et al.*, "Étude de la vasoréactivité cérébrale en Doppler transcrânien: évaluation du test d'apnée comparé à l'injection d'acetazolamide en soins courants. Exploration de 20 sténoses carotidiennes asymptomatiques," *JMV-Journal Med. Vasc.* **42**(5), 272–281 (2017).

[201] P. Lacroix, V. Aboyans, M. H. Criqui, *et al.*, "Type-2 diabetes and carotid stenosis: A proposal for a screening strategy in asymptomatic patients," *Vasc. Med.* **11**(2), 93–99 (2006).

[202] D. A. De Silva, J. N. Fink, S. Christensen, *et al.*, "Assessing reperfusion and recanalization as markers of clinical outcomes after intravenous thrombolysis in the echoplanar imaging thrombolytic evaluation trial (EPITHET)," *Stroke* **40**(8), 2872–2874 (2009).

[203] T. H. Cho, N. Nighoghossian, I. K. Mikkelsen, *et al.*, "Reperfusion within 6 hours outperforms recanalization in predicting penumbra salvage, lesion growth, final infarct, and clinical outcome," *Stroke* **46**(6), 1582–1589 (2015).

[204] I. Christou, A. V. Alexandrov, W. S. Burgin, *et al.*, "Timing of recanalization after tissue plasminogen activator therapy determined by transcranial doppler correlates with clinical recovery from ischemic stroke.," *Stroke.* **31**(8), 1812–6 (2000).

[205] R. Delgado-Mederos, A. Rovira, J. Alvarez-Sabín, *et al.*, "Speed of tPA-induced clot lysis predicts DWI lesion evolution in acute stroke," *Stroke* **38**(3), 955–960 (2007).

[206] B. P. Soares, J. D. Chien, and M. Wintermark, "MR and CT monitoring of recanalization, reperfusion, and penumbra salvage: Everything that recanalizes does not necessarily reperfuse!," *Stroke* **40**(3 SUPPL. 1), 24–28 (2009).

[207] P. Zirak, R. Delgado-Mederos, L. Dinia, *et al.*, "Transcranial diffuse optical monitoring of microvascular cerebral hemodynamics after thrombolysis in ischemic stroke.," *J. Biomed. Opt.* **19**(1), 18002 (2014).

[208] R. Delgado-Mederos, C. Gregori-Pla, P. Zirak, *et al.*, "Transcranial diffuse optical assessment of the microvascular reperfusion after thrombolysis for acute ischemic stroke," *Biomed. Opt. Express* **9**(3), 1262 (2018).

[209] T. Brott, H. P. J. Adams, C. P. Olinger, *et al.*, "Measurements of acute cerebral infarction: a clinical examination scale.," *Stroke* **20**(7), 864–870 (1989).

[210] J. C. Van Swieten, P. J. Koudstaal, M. C. Visser, *et al.*, "Interobserver agreement for the assessment of handicap in stroke patients," *Stroke* **19**(5), 604–607 (1988).

[211] A. Duncan, J. H. Meek, M. Clemence, *et al.*, "Measurement of cranial optical path length as a function of age using phase resolved near infrared spectroscopy," *Pediatr. Res.* **39**(5), 889–894 (1996).

[212] S. Kohri, Y. Hoshi, M. Tamura, *et al.*, "Quantitative evaluation of the relative contribution ratio of cerebral tissue to near-infrared signals in the adult human head: a preliminary study," *Physiol. Meas.* **23**, 301–312 (2002).

[213] F. J. Kirkham, T. S. Padayachee, S. Parsons, *et al.*, "Transcranial measurement of blood velocities in the basal cerebral arteries using pulsed Doppler ultrasound: velocity as an index of flow," *Ultrasound Med Biol.* **12**(1), 15–21 (1986).

[214] G. Seidel, M. Kaps, and T. Gerriets, "Potential and limitations of transcranial color-coded sonography in stroke patients," *Stroke* **26**(11), 2061–2066 (1995).

[215] H. Nagashima, H. Okudera, S. Kobayashi, *et al.*, "Monitoring of cerebral hemodynamics using near-infrared spectroscopy during local intraarterial thrombolysis: case report.," *Surg. Neurol.* **49**, 420–4 (1998).

[216] A. Liebert, H. Wabnitz, J. Steinbrink, *et al.*, "Bed-side assessment of cerebral perfusion in stroke patients based on optical monitoring of a dye bolus by time-resolved diffuse reflectance," *Neuroimage* **24**(2), 426–435 (2005).

[217] T. Ritzenthaler, T. H. Cho, D. Luis, *et al.*, "Usefulness of near-infrared spectroscopy in thrombectomy monitoring," *J. Clin. Monit. Comput.* **29**(5), 585–589 (2015).

[218] C. Hametner, P. Stanarcevic, S. Stampfl, *et al.*, "Noninvasive cerebral oximetry during endovascular therapy for acute ischemic stroke: an observational study," *J. Cereb. Blood Flow Metab.* **35**(10), 1722–1728 (2015).

[219] C. Terborg, K. Gröschel, A. Petrovitch, *et al.*, "Noninvasive assessment of cerebral perfusion and oxygenation in acute ischemic stroke by near-infrared spectroscopy," *Eur. Neurol.* **62**(6), 338–343 (2009).

[220] C. Cheung, J. P. Culver, K. Takahashi, *et al.*, "In vivo cerebrovascular measurement combining diffuse near-infrared absorption and correlation spectroscopies," *Phys. Med. Biol.* **46**(8), 2053–2065 (2001).

[221] W. J. Powers, A. A. Rabinstein, T. Ackerson, *et al.*, "2018 Guidelines for the early management of patients with acute ischemic stroke: a guideline for healthcare professionals from the American Heart Association/American Stroke Association," *Stroke* **49**(3), e46–e110 (2018).

[222] W. J. Powers, C. P. Derdeyn, J. Biller, *et al.*, "2015 American Heart Association/American stroke association focused update of the 2013 guidelines for the early management of patients with acute ischemic stroke regarding endovascular treatment: A guideline for healthcare professionals from the American Heart Association/American Stroke Association," *Stroke* **46**(10), 3020–3035 (2015).

[223] A. J. Hunter, S. J. Snodgrass, D. Quain, *et al.*, "HOBOE (Head-of-Bed Optimization of Elevation) study: association of higher angle with reduced cerebral blood flow velocity in acute ischemic stroke," *Phys. Ther.* **91**(10), 1503–1512 (2011).

[224] V. V. Olavarría, P. M. Lavados, P. Muñoz-Venturelli, *et al.*, "Flat-head positioning increases cerebral blood flow in anterior circulation acute ischemic stroke. A cluster randomized phase IIb trial," *Int. J. Stroke* **0**(0), 174749301771194 (2017).

[225] A. W. Wojner-alexandrov, Z. Garami, O. Y. Chernyshev, *et al.*, "Heads down: Flat positioning improves blood flow velocity in acute ischemic stroke," *Neurology* **64**(8), 1354–1357 (2005).

[226] V. V. Olavarría, H. Arima, C. S. Anderson, *et al.*, "Head position and cerebral blood flow velocity in acute ischemic stroke: A systematic review and meta-analysis," *Cerebrovasc. Dis.* **37**(6), 401–408 (2014).

[227] C. S. Anderson, H. Arima, P. Lavados, *et al.*, "Cluster-randomized, crossover trial of head positioning in acute stroke," *N. Engl. J. Med.* **376**(25), 2437–2447 (2017).

[228] A. W. Alexandrov, G. Tsivgoulis, M. D. Hill, *et al.*, "HeadPoST. Rightly positioned, or flat out wrong?," *Neurology* **0**, 1–5 (2018).

[229] S. W. Han, S. H. Kim, J. Y. Lee, *et al.*, "A new subtype classification of ischemic stroke based on treatment and etiologic mechanism," *Eur. Neurol.* **57**(2), 96–102 (2007).

[230] P. A. Barber, A. M. Demchuk, J. Zhang, *et al.*, "Validity and reliability of a quantitative computed tomography score in predicting outcome of hyperacute stroke before thrombolytic therapy," *Library (Lond).* (2000).

[231] L. L. Yeo, P. Paliwal, A. F. Low, *et al.*, "How temporal evolution of intracranial collaterals in acute stroke affects clinical outcomes," *Neurology* **86**, 434–441 (2016).

[232] L. R. Caplan and S. Sergay, "Positional cerebral ischaemia 378," *J. Neurol. Neurosurg. Psychiatry* **39**, 385–391 (1976).

[233] R. J. Stark and J. Wodak, "Primary orthostatic cerebral ischaemia," *J. Neurol. Neurosurg. Psychiatry* **46**(10), 883–891 (1983).

[234] J. Toole, "Effects of change of head, limb, and body position on cephalic circulation.," *N Engl J Med* **6**, 307–311 (1968).

[235] A. Ropper, D. ORourke, and S. Kennedy, "Prevalence and risk factors associated with reversed Robin Hood syndrome in acute ischemic stroke.," *Neurology* **11**, 1288 –129 (1982).

[236] O. Y. Bang, B. Ovbiagele, and J. S. Kim, "Nontraditional risk factors for ischemic stroke: An update," *Stroke* **46**(12), 3571–3578 (2015).

[237] S. Schwarz, D. Georgiadis, A. Aschoff, *et al.*, "Effects of body position on intracranial pressure and cerebral perfusion in patients with large hemispheric stroke.," *Stroke* **33**, 497–501 (2002).

[238] D. Hargroves, R. Tallis, V. Pomeroy, *et al.*, "The influence of positioning upon cerebral oxygenation after acute stroke: a pilot study," *Age Ageing* **37**(5), 581–585. (2008).

[239] A. Kastrup, C. Thomas, C. Hartmann, *et al.*, "Sex dependency of cerebrovascular CO2 reactivity in normal subjects," *Stroke* **28**(12), 2353–2356 (1997).

[240] H. T. Tu, B. C. V. Campbell, S. M. Davis, *et al.*, "Worse stroke outcome in atrial fibrillation is explained by more severe hypoperfusion, infarct growth, and hemorrhagic transformation.," *Int. J. Stroke* **10**(4), 534–540 (2015).

[241] L. C. Rebello, M. Bouslama, D. C. Haussen, *et al.*, "Stroke etiology and collaterals: atheroembolic strokes have greater collateral recruitment than cardioembolic strokes," *Eur. J. Neurol.* **24**(6), 762–767 (2017).

[242] J. M. Valdueza, T. von Münster, O. Hoffman, *et al.*, "Postural dependency of the cerebral venous outflow.," *Lancet* **355**(9199), 200–201 (2000).

[243] F. Doepp, S. J. Schreiber, T. von Münster, *et al.*, "How does the blood leave the brain? A systematic ultrasound analysis of cerebral venous drainage patterns," *Neuroradiology* **46**(7), 565–570 (2004).

[244] S. C. Beards, S. Yule, A. Kassner, *et al.*, "Anatomical variation of cerebral venous drainage: The theoretical effect on jugular bulb blood samples," *Anaesthesia* **53**(7), 627–633 (1998).

[245] M. J. Aries, J. W. Elting, J. De Keyser, *et al.*, "Cerebral autoregulation in stroke: A review of transcranial doppler studies," *Stroke* **41**(11), 2697–2704 (2010).

[246] H. S. Markus, "Cerebral perfusion and stroke," *J. Neurol. Neurosurg. Psychiatry* **75**(3), 353–361 (2004).

[247] T. Durduran, *Non-invasive measurements of tissue hemodynamics with hybrid diffuse optical methods*. PhD thesis (2004).

[248] H. Adams, B. Bendixen, B. Bendixen, *et al.*, "Classification of subtype of acute ischemic stroke," *Stroke* **23**(1), 35–41 (1993).

[249] A. W. Wojner, A. El-Mitwalli, and A. V. Alexandrov, "Effect of head positioning on intracranial blood flow velocities in acute ischemic stroke: a pilot study," *Crit Care Nurs Q* **24**(4), 57–66 (2002).

[250] B. Yew and D. A. Nation, "Cerebrovascular resistance: effects on cognitive decline, cortical atrophy, and progression to dementia," *Brain* **140**(November), 1987–2001 (2017).

[251] D. A. Nation, C. E. Wierenga, L. R. Clark, *et al.*, "Cortical and subcortical cerebrovascular resistance index in mild cognitive impairment and Alzheimer's disease," *J Alzheimers Dis* **36**(4), 689–698 (2013).

[252] I. Darien, *International Classification of Sleep Disorders - 3rd ed. (ICSD-3)*, American Academy of Sleep Medicine.

[253] C. Bassetti and M. S. Aldrich, "Sleep apnea in acute cerebrovascular diseases: final report on 128 patients," *Sleep* **22**(0161-8105 (Print)), 217–223 (1999).

[254] A. Iranzo, J. Santamaría, J. Berenguer, *et al.*, "Prevalence and clinical importance of sleep apnea in the first night after cerebral infarction.," *Neurology* **58**(6), 911–6 (2002).

[255] A. Nachtmann, M. Siebler, G. Rose, *et al.*, "Cheyne-Stokes respiration in ischemic stroke.," *Neurology* **45**(4), 820–821 (1995).

[256] C. Nopmaneejumruslers, Y. Kaneko, V. Hajek, *et al.*, "Cheyne-stokes respiration in stroke: Relationship to hypocapnia and occult cardiac dysfunction," *Am. J. Respir. Crit. Care Med.* **171**, 1048–1052 (2005).

[257] M. Siccoli, P. O. Valko, D. M. Hermann, *et al.*, "Central periodic breathing in 74 patients with acute ischemic stroke - neurogenic versus cardiogenic," *J. Neuroimaging* **255**(11), 1687–1692 (2008).

[258] D. L. Brown, M. McDermott, A. Mowla, *et al.*, "Brainstem infarction and sleep-disordered breathing in the BASIC Sleep Apnea Study," *Sleep Med.* **18**(9), 1199–1216 (2014).

[259] C. Bassetti, M. S. Aldrich, and D. Quint, "Sleep-disordered breathing in patients with acute supra- and infratentorial strokes: a prospective study of 39 patients," *Stroke.* **28**(9), 1765–1772 (1997).

[260] O. Parra, A. Arboix, S. Bechich, *et al.*, "Time course of sleep-related breathing disorders in first-ever stroke or transient ischemic attack," *Am. J. Respir. Crit. Care Med.* **161**(2 Pt 1), 375–380 (2000).

[261] K. G. Johnson and D. C. Johnson, "Frequency of sleep apnea in stroke and TIA patients: A meta-analysis," *J. Clin. Sleep Med.* **6**(2), 131–137 (2010).

[262] A. M. Rowat, M. S. Dennis, and J. M. Wardlaw, "Central periodic breathing observed on hospital admission is associated with an adverse prognosis in conscious acute stroke patients," *Cerebrovasc. Dis.* **21**(5-6), 340–347 (2006).

[263] T. Cherkassky, A. Oksenberg, P. Froom, *et al.*, "Sleep-related breathing disorders and rehabilitation outcome of stroke patients: a prospective study.," *Am. J. Phys. Med. Rehabil. / Assoc. Acad. Physiatr.* **82**(6), 452–455 (2003).

[264] M. Á. Martínez-García, J. J. Soler-Cataluña, L. Ejarque-Martínez, *et al.*, "Continuous positive airway pressure treatment reduces mortality in patients with ischemic stroke and obstructive sleep apnea," *Am. J. Respir. Crit. Care Med.* **180**(1), 36–41 (2009).

[265] P. M. Turkington, V. Allgar, J. Bamford, *et al.*, "Effect of upper airway obstruction in acute stroke on functional outcome at 6 months," *Thorax* **59**(5), 367–371 (2004).

[266] O. C. Ioachimescu and N. A. Collop, "Sleep-disordered breathing," *Neurol Clin* **30**, 1095–1136 (2012).

[267] M. J. H. Aries, A. D. Coumou, J. W. J. Elting, *et al.*, "Near infrared spectroscopy for the detection of desaturations in vulnerable ischemic brain tissue," *Stroke* **43**(4), 1134–1136 (2012).

[268] F. Pizza, M. Biallas, U. Kallweit, *et al.*, "Cerebral hemodynamic changes in stroke during sleep-disordered breathing.," *Stroke.* **43**, 1951–3 (2012).

[269] C. Gregori-Pla, R. Delgado-Mederos, G. Cotta, *et al.*, "Microvascular cerebral blood flow fluctuations in association with apneas and hypopneas in acute ischemic stroke," *Neurophotonics* (2018. Under review.).

[270] J. Wright, R. Johns, I. Watt, *et al.*, "Health effects of obstructive sleep apnoea and the effectiveness of continuous positive airways pressure: a systematic review of the research evidence.," *BMJ* **314**(7084), 851–60 (1997).

[271] M. T. Naughton, D. C. Benard, R. Rutherford, *et al.*, "Effect of continuous positive airway pressure on central sleep apnea and nocturnal PCO2 in heart failure.," *Am. J. Respir. Crit. Care Med.* **150**(6 Pt 1), 1598–1604 (1994).

[272] W. Randerath, J. Verbraecken, S. Andreas, *et al.*, "Definition, discrimination, diagnosis and treatment of central breathing disturbances during sleep," *Eur. Respir. J.* **49**(1) (2017).

[273] C. M. Ryan, M. Bayley, R. Green, *et al.*, "Influence of continuous positive airway pressure on outcomes of rehabilitation in stroke patients with obstructive sleep apnea," *Stroke* **42**(4), 1062–1067 (2011).

[274] O. Parra, A. Sánchez-Armengol, M. Bonnin, *et al.*, "Early treatment of obstructive apnoea and stroke outcome: a randomised controlled trial.," *Eur. Respir. J. Off. J. Eur. Soc. Clin. Respir. Physiol.* **37**(5), 1128–1136 (2011).

[275] D. M. Bravata, J. Concato, T. Fried, *et al.*, "Continuous positive airway pressure: evaluation of a novel therapy for patients with acute ischemic stroke.," *Sleep* **34**(9), 1271–1277 (2011).

[276] O. Sandberg, K. A. Franklin, G. Bucht, *et al.*, "Nasal continuous positive airway pressure in stroke patients with sleep apnoea: a randomized treatment study.," *Eur. Respir. J.* **18**, 630–4 (2001).

[277] A. Gupta, G. Shukla, M. Afsar, *et al.*, "Role of positive airway pressure therapy for Obstructive sleep apnea in patients with stroke: A randomized controlled trial," *J. Clin. Sleep Med.* **14**(4), 511–521 (2018).

[278] A.-K. Brill, T. Horvath, A. Seiler, *et al.*, "CPAP as treatment of sleep apnea after stroke," *Neurology* **90**(14), e1222–e1230 (2018).

[279] L. M. Tomfohr, T. Hemmen, L. Natarajan, *et al.*, "Continuous positive airway pressure for treatment of obstructive sleep apnea in stroke survivors: what do we really know?," *Stroke.* **43**(11), 3118–3123 (2012).

[280] M. E. Dyken and K. B. Im, "Sleep-disordered breathing and stroke," *Sleep Med. Clin.* **3**(3), 361–376 (2008).

[281] C.-Y. Hsu, "Sleep-disordered breathing after stroke: a randomised controlled trial of continuous positive airway pressure," *J. Neurol. Neurosurg. Psychiatry* **77**(10), 1143–1149 (2006).

[282] A. M. Rowat, J. M. Wardlaw, and M. S. Dennis, "Abnormal breathing patterns in stroke: relationship with location of acute stroke lesion and prior cerebrovascular disease.," *J. Neurol. Neurosurg. Psychiatry* **78**(3), 277–9 (2007).

[283] D. M. Hermann, M. Siccoli, P. Kirov, *et al.*, "Central periodic breathing during sleep in acute ischemic stroke," *Stroke* **38**(3), 1082–1084 (2007).

[284] "Babylux; an optical neuro-monitor of cerebral oxygen metabolism and blood flow for neonatology." http://babylux-project.eu/.

[285] T. Dragojević, J. L. Hollmann, D. Tamborini, *et al.*, "Compact, multi-exposure speckle contrast optical spectroscopy (SCOS) device for measuring deep tissue blood flow," *Biomed. Opt. Express* **9**(1), 322 (2018).

[286] "Luca; laser and ultrasound co-analyzer for thyroid nodule." http://luca-project.eu/.

[287] D. Wang, A. B. Parthasarathy, W. B. Baker, *et al.*, "Fast blood flow monitoring in deep tissues with real-time software correlators," *Biomed. Opt. Express* **7**(3), 776–797 (2016).

[288] B. Khan, C. Wildey, R. Francis, *et al.*, "Improving optical contact for functional nearinfrared brain spectroscopy and imaging with brush optodes.," *Biomed. Opt. Express* **3**, 878–898 (2012).

[289] R. C. Mesquita, S. S. Schenkel, D. L. Minkoff, *et al.*, "Influence of probe pressure on the diffuse correlation spectroscopy blood flow signal: extracerebral contributions.," *Biomed. Opt. Express* **4**, 978–94 (2013).

[290] T. Funane, F. Homae, H. Watanabe, *et al.*, "Greater contribution of cerebral than extracerebral hemodynamics to near-infrared spectroscopy signals for functional activation and resting-state connectivity in infants," *Neurophotonics* **1**(2), 025003 (2014).

[291] J. Li, G. Dietsche, D. Iftime, *et al.*, "Noninvasive detection of functional brain activity with near-infrared diffusing-wave spectroscopy.," *J. Biomed. Opt.* **10**(4), 44002 (2014).

[292] J. Sutin, B. Zimmerman, D. Tyulmankov, *et al.*, "Time-domain diffuse correlation spectroscopy," *Optica* **3**(9), 1006–1013 (2016).